DISSERTATION

Thermally promoted cationic photopolymerization
of ring-opening monomers
for Hot Lithography

ausgeführt zum Zwecke der Erlangung des akademischen Grades eines

Doktors der technischen Wissenschaften

unter der Leitung von

Univ.-Prof. Dipl.-Ing. Dr.techn. Robert Liska

E163

Institut für Angewandte Synthesechemie

eingereicht an der Technischen Universität Wien

Fakultät für Technische Chemie

von

Dipl.-Ing. Nicolas Klikovits, BSc

01026158

Ignaz-Till-Gasse 23, 7011 Siegendorf

Wien, Juni 2020   Dipl.-Ing. Nicolas Klikovits

Danksagung

An erster Stelle bedanke ich mich bei Prof. Robert Liska für die exzellente Ausbildung, das besondere Arbeitsklima und die unvergleichlichen Erfahrungen, die ich in den vergangenen Jahren machen durfte. Unter deiner Führung konnte ich eine professionelle und persönliche Entwicklung durchlaufen, die besonders auf deinem Vertrauen und der von dir sehr geschätzten Gemeinschaftlichkeit beruht. Vielen Dank!

Meinem Betreuer Patrick danke ich, dass er mir in vielen schwierigen Situationen den Weg gewiesen hat und mir geholfen hat, in den Wirrungen der Forschungsarbeit den Blick für das Wesentliche nicht zu verlieren. Durch deine Geduld und Hilfsbereitschaft warst du mir über die Jahre hinweg ein wichtiger Mentor.

Vielen Dank an alle meine Kollegen des FBMC, welche mir mit Spaß und Teamgeist die Arbeit sehr erleichtert und erheitert haben. Neben meinen anfänglichen Begleitern Hansi, Schnölli, Hofi, Elise, Sebi, Markus, Moritz und Stefan bedanke ich mich auch bei Raffi, Kathi, Babsi, Ralle, Chris und Roli, die als neue Mitstreiter viel positive Energie innerhalb und abseits des Labors mitgebracht haben. Als Teil des neuen Teams gilt Lisa mein besonderer Dank für die großartige Unterstützung während der heiklen Phase meiner Arbeit. Ebenso bedanke ich mich bei A.D., mit dem ich nicht nur „an der Front" gedient habe, sondern von dem ich auch viel Humor und Leichtigkeit erfahren habe.

Mit Gernot, Yazgan, Sascha und Patrick verbinden mich nicht nur die vielen besonderen Erlebnisse auf dem Weg zu diesem Abschluss, sondern auch lebhafte Freundschaften, die mir viel Unterstützung geben und auch weiterhin viel Freude bereiten werden. Dafür gilt euch mein großer Dank!

Zuletzt gilt mein größter Dank meiner Familie. Durch eure bedingungslose Unterstützung habt ihr mir die Freiheit gegeben, meine Ziele zu verfolgen und eine unvergleichliche Zeit im Laufe meiner Ausbildung zu erleben. Dafür bin ich euch ewig dankbar!

<div align="center">Danke!</div>

Kurzfassung

Die kationische Photopolymerisation von ringöffnenden Monomeren bietet unübertroffene Möglichkeiten für die Herstellung von Polymermaterialien. Neben den einzigartigen Eigenschaften der lichtinduzierten kationischen Härtungsreaktion, wie Sauerstoffunempfindlichkeit und höchste Reaktionsumsätze, erzeugen kationisch ringöffnende Monomere hervorragende mechanische, chemische und elektrische Eigenschaften mit geringster Volumenschrumpfung während der Aushärtung. Von der großen Vielfalt der einsetzbaren Monomere stellen Epoxidharze die mit Abstand wichtigste Substanzklasse für die Herstellung von Polymerwerkstoffen mit einer Vielzahl von industriellen Anwendungen dar. Aufgrund dieser Vorteile ist der direkte 3D-Druck von Materialien durch kationische Photopolymerisation ein angestrebtes Ziel lithographiebasierter additiver Fertigungstechnologien (L-AMTs), leidet jedoch unter stark reduzierten Reaktionsgeschwindigkeiten im Vergleich zur vorherrschenden radikalischen Photopolymerisation von Acrylaten und Methacrylaten. Die Einführung von Hot Lithography als innovative L-AMT bei Temperaturen von bis zu 140 °C erlaubt den potentiellen Einsatz der thermisch geförderten kationischen Photopolymerisation für den direkten 3D-Druck von ringöffnenden Monomeren.

Um die Einführung der kationischen UV-Härtung in der Hot Lithography zu ermöglichen, zielt diese Arbeit auf die Untersuchung der kationischen Photopolymerisation bei erhöhten Temperaturen ab. Zunächst wurde ein Photoinitiationssystem für die Anwendung im direkten 3D-Druck von Epoxidmonomeren unter signifikanter thermischer Förderung etabliert. Darüber hinaus wurde dieses kationische Photoinitiationssystem auf die Photopolymerisation von vielbeachteten 2-Oxazolin-Monomeren angewendet, deren Verwendung für die Herstellung von strukturellen Materialien durch UV-Härtung bisher noch nicht untersucht wurde. Nach umfangreichen Untersuchungen der kationischen Photopolymerisationsreaktion von synthetisierten 2-Oxazolin-Modellverbindungen wurden die vielversprechenden thermomechanischen Eigenschaften von Poly(2-oxazolin)-Photopolymeren bestimmt. Schließlich wurde das neuartige System für den kationischen 3D-Druck von Poly(2-oxazolin)-Strukturen mit höchster Präzision und Detailauflösung in der Hot Lithography eingesetzt.

Abstract

Cationic photopolymerization of ring-opening monomers offers unmatched possibilities for the production of polymer materials. Besides the unique features of the light-induced cationic curing reaction, such as oxygen insensitivity and highest reaction conversions, cationically ring-opening monomers generate outstanding mechanical, chemical and electrical properties with lowest amounts of volumetric shrinkage upon cure. Out of the great variety of applicable monomers, epoxy resins represent by far the most important substance class for the production of polymer materials in a great number of industrial applications. Due to these benefits, the direct 3D printing of materials by cationic photopolymerization is a desired goal of lithography-based additive manufacturing technologies (L-AMTs), however, suffers from strongly reduced reaction rates in comparison to predominant free-radical photopolymerization of acrylates and methacrylates. With the introduction of Hot Lithography as an innovative L-AMT operating at temperatures up to 140 °C, the use of thermally promoted cationic photopolymerization for the direct 3D printing of ring-opening monomers is challenged.

To facilitate the implementation of cationic UV-curing in Hot Lithography, this thesis aims for the investigation of cationic photopolymerization at elevated temperatures. Firstly, a photoinitiation system for the application in unmediated 3D printing of epoxy monomers under significant thermal promotion was established. Furthermore, this cationic photoinitiation systems was applied on the photopolymerization of much-noticed 2-oxazoline monomers, which have not been investigated for the production of structural materials by UV-curing before. After extensive studies of the cationic photopolymerization reaction of synthesized 2-oxazoline model compounds, the highly promising thermomechanical properties of poly(2-oxazoline) photopolymers were evaluated. Finally, the novel system was used for cationic 3D printing of poly(2-oxazoline) structures with highest precision and detailed resolution in Hot Lithography.

Table of Contents

INTRODUCTION

Additive manufacturing technologies

Additive manufacturing technologies (AMTs) have had a great impact on industrial and private manufacturing since their first introduction in the 1980s.[1] Different terminologies of additive manufacturing (AM) are defined based on their type of application. For the additive manufacturing and production of prototypes and models, the term *rapid prototyping* is most commonly used and differentiated from *rapid tooling* as instrumentation for further manufacturing processes. Moreover, *rapid manufacturing* describes the additive manufacturing of final products.[2] Despite differentiation by specific applications, the terms *layered manufacturing* or *solid freeform fabrication* are used synonymously to *additive manufacturing and rapid prototyping* in technical literature. However, with AMTs gaining more and more attention in the private sector, the expression *3D printing* has become particularly common in popular media.[3]

The principle of AMTs is the selective *layer-by-layer* addition of material according to a computer-generated design file to form a three-dimensional object. A 3D model of the desired object is generated via computer-aided design (CAD) and virtually sliced to the processable layer thickness in AM. Subsequently, the final object is generated from the virtual dataset (Figure 1).
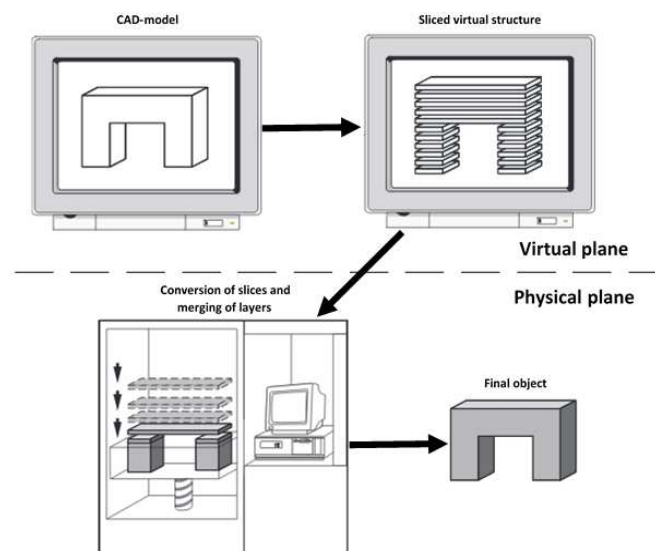
Figure 1: Principle of AMTs[2]

In contrast to conventional methods, such as subtractive and formative manufacturing technologies, AMTs differ fundamentally by the defined layer-by-layer material generation. In comparison, subtractive manufacturing is characterized by selective removal of a material e.g. by CNC milling, whereas formative manufacturing changes the geometry of a material by bending, forging or casting without changing its volume, e.g. injection molding. The advantages of AMTs are expressed by the possibility to build objects of any geometry and orientation, which allows for high flexibility in design and the possibility to easily introduce high shape complexity or even cavities to manufactured objects. Hence, in contrast to subtractive and formative manufacturing, AMTs consume fewer initial costs for the production of objects, as the process shows no need for product specific tools or tool-change. Furthermore, less material is wasted in the AM process compared to conventional manufacturing method, making it ecologically favorable.[1, 3] The general drawbacks of AMTs are the inherent limitations low throughput of 3D printing in mass production. Clearly, the greatest benefits are achieved in the production of small lot sizes, individualized products and parts of high complexity, which cannot be manufactured by conventional methods in sufficient quality or cost-efficiency.

AMTs have been introduced to a great number of industrial sectors, such as automotive, aerospace, electronics, energy, medical and dental industry. The applications in these sectors take up to three quarters of the overall AM market, in which one third of the production is covered by functional parts.[4] From an economic point of view, AMTs exhibit extraordinary growth rates with revenues from services and products estimated to 5 billion USD in 2015.[5]

The processable materials in AM are metals, ceramics and polymers and differ significantly in the type and cost of production. Due to the unique processing methods and comparably low price, the dominating materials in AMTs are polymer based and cover 50 % of the total AM material market.[4] For example, polymer-based AMTs have been implemented successfully in the production of personalized hearing aids by the company "Sonova" in order to reach the individual geometry of products in a cost-efficient process.[6] Furthermore, "Align Technology Inc." produces molds for individualized dental aligners exclusively by AM with a throughput of 17 million personalized products annually.[4] Further industrial applications in the manufacturing of functional parts are shown by the production of fuel nozzles for jet engines by "GE

Aviation".[7] However, also in the private sector, polymer-based AMTs gained great popularity for home application of low-cost desktop 3D printers for the production of individualized parts.[8]

Polymer-based AMTs are distinguished by 2 groups of material processing. On the one hand, powders or filaments from polymeric materials are processed in an layer-by-layer approach. As one of the most common and popular AMTs, Fused Deposition Modeling (FDM) is applied to extrude a thermoplastic polymer material through a heated nozzle to deposit the melt in layer-by-layer technique. Further methods include Selective Laser Sintering (SLS) to fuse a polymer powder with selective heat input by a laser beam.

A fundamentally different principle of polymer-based AM is described by methods in which a polymer is synthesized *in situ* upon irradiation by light in a photopolymerization reaction. Besides material jetting, in which droplets of photopolymerizable material are selectively deposited and subsequently cured, the most important methods are covered by *lithography-based AMTs* (L-AMTs). In L-AMTs, a vat filled with photoreactive monomer formulation is selectively photopolymerized by defined laser irradiation (Laser Stereolithography; Laser-SLA) or a digital light processor (DLP-SLA) to solidify a layer of photopolymer. As the photopolymerization occurs in thin layers only, the process is repeated in layer-by-layer technique to conduct consecutive build-up in the third dimension. Typically, high precisions are achieved in L-AMT in comparison to powder or filament precursor-based techniques. Due to the selective light-induced curing in L-AMTs, unmatched precision and surface qualities of printed parts are achieved in comparison to powder and filament-based processes. Hence, this work will exclusively focus on L-AMT utilizing photopolymerization for the 3D printing.

Lithography based additive manufacturing technologies

In lithography-based AMTs (L-AMTs) photoreactive formulations are placed inside a vat, in which selective irradiation by light solidifies thin layers of the formulation in a photopolymerization process. Therefore, L-AMTs are commonly referred to as *vat photopolymerization.* Upon continuous cross-linking of monomer in a layer-by-layer

approach, the thin photopolymer layers form a solid object in desired dimensions of the final product.[3] Although a great number of different photoreactive formulations have been introduced for vat photopolymerization in L-AMTs, the major aim to achieve comparable thermomechanical properties of conventional materials remains part of on-going research and development.[9, 10] In general, the two types of L-AMTs are defined by the type of irradiation, namely the laser-irradiated stereolithography (SLA) and the LED-irradiated digital light processing (DLP).

Stereolithography

Stereolithography (SLA) was introduced in the 1980s as the first L-AMT which found wide application in rapid prototyping.[11] SLA utilizes an ultraviolet (UV) laser to polymerize the photoreactive liquid formulation at specific locations within each layer in x-y-dimension and closely defined layer thickness. In a top-down setup, the supporting building platform is subsequently lowered into the formulation in the z-dimension to cover the cured part with uncured resin before photopolymerization of the consecutive layer on top. (Figure 2) In order to avoid environmental influences, such as oxygen inhibition, a bottom-up inverted-SLA setup with irradiation through a transparent vat bottom is applied, in which the cured part is lifted to enable photopolymerization of the consecutive layer below.[12]
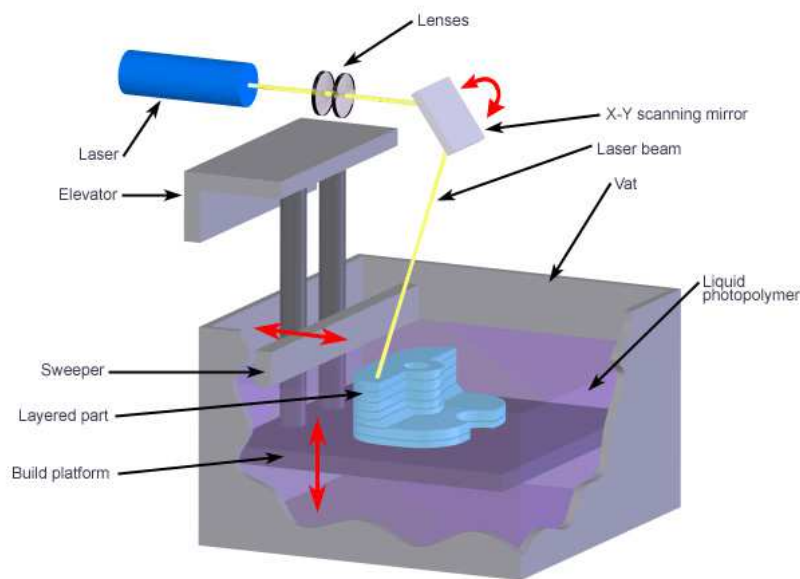
Copyright © 2008 CustomPartNet

Figure 2: Schematic setup of laser stereolithography (SLA)[13]

As the solidification occurs with highest precision provided by the accuracy of the laser, SLA is unmatched in terms of geometry and surface quality. Still problems may occur arising from the photopolymerization process due to inherent shrinkage during the selective UV-curing process and insufficient mechanical strength of photopolymer materials.[10] Furthermore, the substantial costs of advanced laser systems, and the limited variety of suitable formulations limit the applicability of SLA to epoxy or (meth)acrylate-based formulation. The formulations must comprise a sufficiently low viscosity, typically below 1 Pa s, often demanding for reactive diluents or solvents necessary for optimization of printing conditions.[3, 14] Still, SLA has been in the focus of ongoing developments and represents the most advanced AMT regarding its resolution and the surface quality of printed parts.[15]

Digital light processing

In digital light processing (DLP) the same principle is followed as in SLA, however, one layer is irradiated simultaneously using a masked LED light source which is modified at a Digital Micromirror device (DMD) chip. Comparable to SLA systems, bottom-up DPC setups are commonly applied. (Figure 3)

1. Light Source

2. DMD-chip (dynamic mask)

3. Optic

4. Material vat

5. Coating blade

6. Back light

7. Building platform

8. Load cell

9. Manufactured part
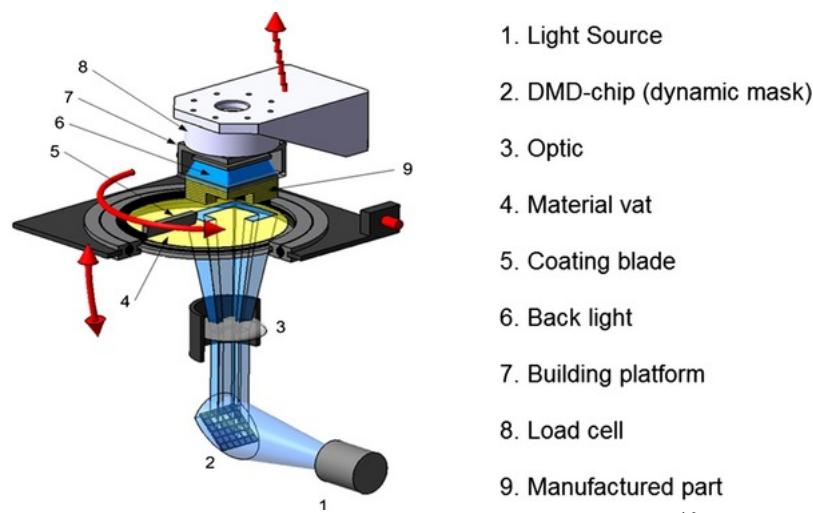
Figure 3: Schematic illustration of a DLP device[16]

As the photopolymerization occurs within one layer at a time distinctly faster solidification is achieved in the layer-by-layer technique. This significantly reduces production times in DLP. Due to the less expensive irradiation system, DLP systems are more economical, however, comprise certain drawbacks in lateral resolution (10-50 μm) depending on the resolution and size of the respective DMD chip and

corresponding pixel size on the formulation. In analogy to SLA, typical DLP is applied on low viscosity photopolymerizable formulations. However, the advantageous applicability in filled systems such as ceramic slurries has been shown by lithography-based ceramic manufacturing (LCM). By additive manufacturing of individualized high performance tools of printed ceramic parts, Lithoz GmbH applies DLP-based LCM for specialized applications.[17] Furthermore, the LCM of complex silicon oxycarbide (SiOC) microstructures with high precisions is reported by DLP methods, which show its advance utility in the fabrication of high performance ceramic materials.[18]

Radical photopolymerization

Photopolymerization describes the reaction of a formulation of liquid monomer and a photoinitiator to a solid polymer under the influence of electromagnetic irradiation. Most commonly, UV, visible or near IR radiation is used, however, also electron beam, X-rays, gamma rays, plasmas and microwaves are applicable to activate the photoinitiator and induce the polymerization reaction.[19] In contrast to thermal polymerization, photopolymerization offers distinct advantages by its rapid through cure, low energy requirements, room temperature treatment, non-polluting and solvent-free formulations and low costs of instrumentation.[20] The most dominant field of applications is the coatings industry, as the photopolymerization is limited to only thin layers due to the limited penetration depth of UV-light. By advances in photopolymerization technologies, however, the light-induced curing of layers with extended thickness was enabled and the applicability has been greatly extended to adhesives, optics, electronics, dental fillings and additive manufacturing technologies.[3]

Beyond other types of photopolymer reactions, such as photocrosslinking, photomolecular reactions, photodegradation and photo-thermal reactions, photopolymerization is defined as a chain reaction in which the initiation step is produced by a photochemical event.[19, 21] Depending on the type of radical, cationic or anionic reactive species in the chain growth reaction, the major types of photopolymerization are differentiated, with radical and cationic photopolymerization being most common.

Counted by its high abundance in industrial application the most important class is radical photopolymerization, in which a photoinitiator liberates reactive radicals upon

irradiation by light. The free radical photopolymerization is characterized by three separate steps, namely initiation, propagation and termination (Figure 4). In the initiation step the photoinitiator (PI) is cleaved by photolysis to yield radicals ($R^\bullet$) (1). Subsequently the radicals add to the reactive group of the respective monomer (M) and form a propagating species ($RM_n^\bullet$), which further adds to reactive groups of consecutive monomer molecules in a chain reaction (2). The propagation proceeds until the occurrence of termination mechanisms, either by recombination (3) or disproportionation (4) of two radicals.[19]

Initiation:
$$PI \xrightarrow{h\nu} R^\bullet \qquad (1)$$

$$R^\bullet + M \longrightarrow RM^\bullet$$

Propagation:
$$RM_n^\bullet + M \longrightarrow RM_{n+1}^\bullet \qquad (2)$$

Termination:
$$RM_n^\bullet + RM_m^\bullet \longrightarrow RM_nM_mR \qquad (3) \qquad \text{Recombination}$$

$$RM_n^\bullet + RM_m^\bullet \longrightarrow RM_n + RM_m \qquad (4) \qquad \text{Disproportionation}$$
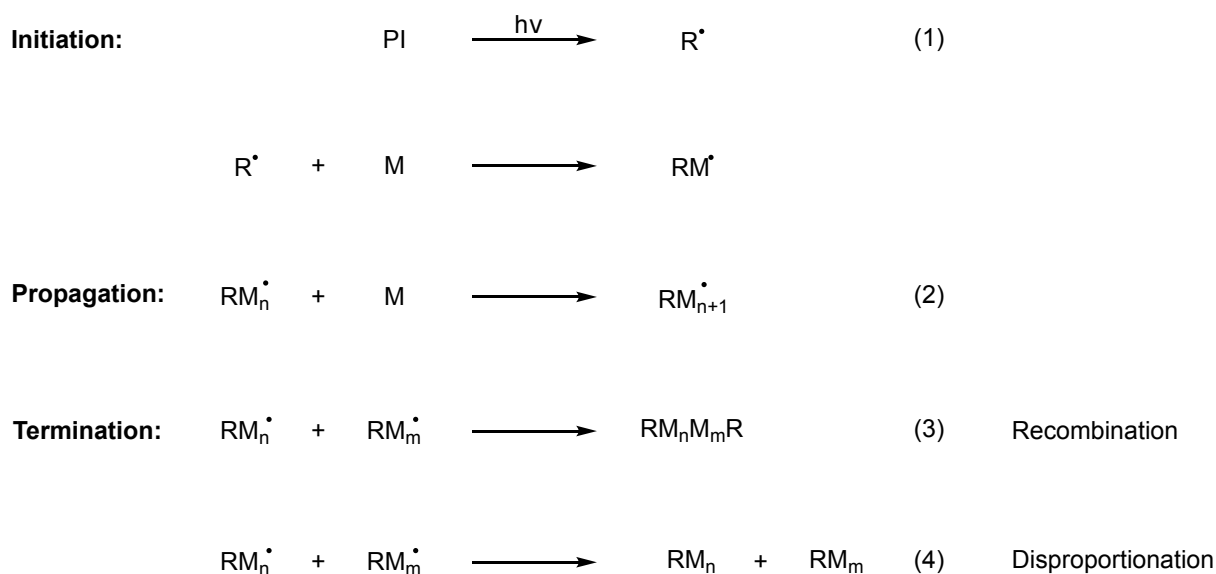
Figure 4: Reaction mechanism of radical photopolymerization

Free radical photoinitiators are generally defined by Norrish Type I and Norrish Type II photoreaction.[19] Accordingly, Type I photoinitiators undergo photo-fragmentation in a unimolecular mechanism, in which homolytic α-cleavage near an aromatic carbonyl group generates radicals, as the dissociation energy is lower than the energy of the excited state.
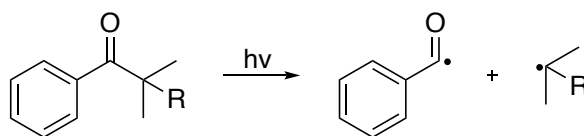
Figure 5: Photo-fragmentation of Type I photoinitiators

Compounds that follow a Type I photo-fragmentation mechanism are hydroxyacetophenones, dialkoxyacetophenones, benzil ketals or benzoyl phosphine

oxides, but also highly efficient acylgermanes. Absorption ranges up to 380 nm are typical for photoinitiators bases on benzoyl chromophores, however, in benzoyl phosphine oxides the absorptivity is significantly extended up to 420 nm, whereas aryl acylgermanes exhibit a distinct bathochromic shift up to 490 nm.[22, 23] Figure 6 depicts the prominent structures of common Type I photoinitiator classes, namely hydroxyacetophenones (Darocur 1173), bisacylphosphine oxides (BAPO) and acylgermanes (BMDG, Ivocerin).
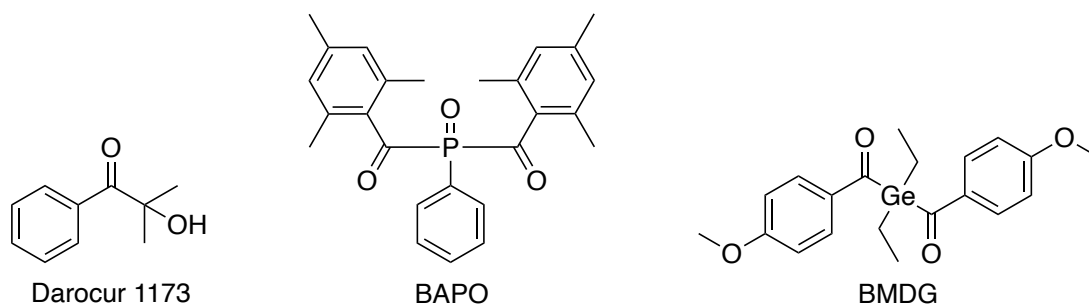
Figure 6: Type I radical photoinitiators Darocure1173, BAPO and BMDG (Ivocerin)

On the contrary, Type II photoinitiators undergo a bimolecular initiation mechanism. These compounds generate radicals without being cleaved and subsequently react with co-initiators to form initiating radicals via either H-abstraction or electron transfer. Typical Type II photoinitiators include camphorquinone, benzophenones or thioxanthones, whereas tertiary amines are used as co-initiators (Figure 7).[22]
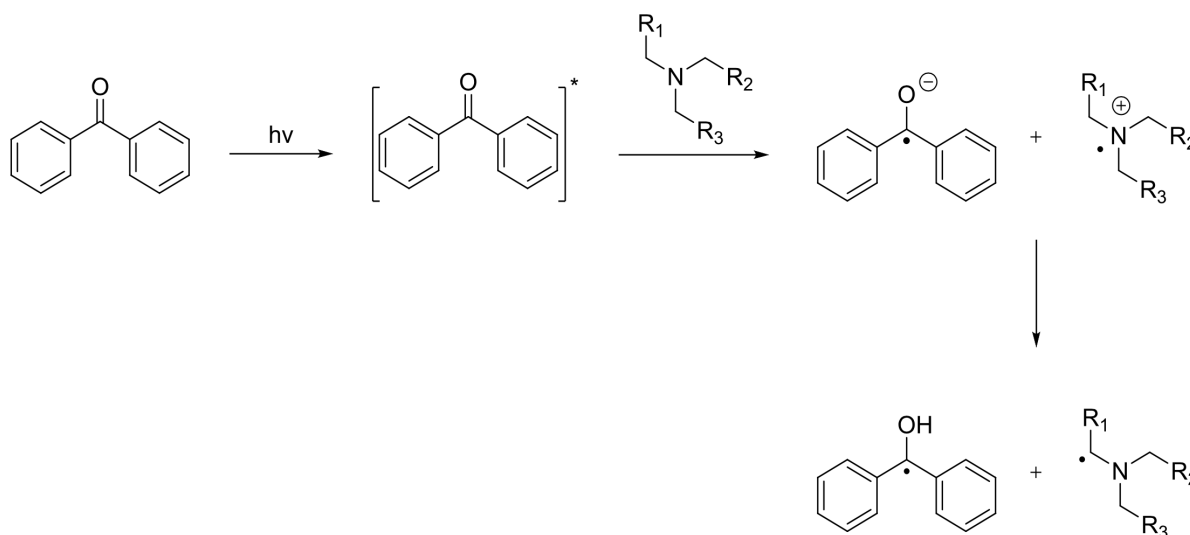
Figure 7: Photoinitiation mechanism of Type II photoinitiator benzophenone

Although Type II photoinitiators show lower initiation efficiency than Type I photoinitiators, they comprise extended absorption in the visible light range. Moreover, corresponding photoinitiation systems show significantly higher biocompatibility for utility in sensitive applications, although the applicability is highly dependent on the used monomers. [19]

The most important classes of monomers photopolymerizable by a radical mechanism are acrylates, methacrylates and vinyl monomers, of which acrylates and methacrylates are most common in applications. The radical photopolymerization of (meth)acrylate monomers exhibits explicitly high reaction rates and enables the rapid curing of photoreactive formulations. However, also considerable issues arise from the radical-induced nature of the photopolymerization reaction and the inherent limitations by (meth)acrylate monomers. As the chain reaction comprises a reactive radical initiating and propagating species, atmospheric oxygen inhibits the reaction and causes incomplete polymerization on the formulation surface. Furthermore, biradical termination reactions (Figure 4) occur with high probability which leads to inhomogeneous molecular weight distribution in the resulting polymer. Another major drawback of radical photopolymerization is the inherently high polymerization shrinkage of acrylate and methacrylate monomers upon cure. Depending on the molecular structure of the respective monomer, e.g. aromatic bisphenol-based dimethacrylate bis-GMA shrinks 5 %, aliphatic triethylene glycol dimethacrylate shrinks 12 %, whereas monofunctional methyl methacrylate exhibits shrinkage up to 21 % causing dimensional inconsistency and poor adhesion to substrates.[24][15] However, not only polymerization specific problems occur in the radical curing of acrylates and methacrylates, but also the cytotoxic behavior of these monomer classes obstructs their application in living systems. The lower toxicity of methacrylates led to their dominant application, although acrylates exhibit higher reactivity.[25] The hydrolysis of acrylates produces acrylic acid, which leads to inflammatory effects. [17] Moreover, the low biocompatibility of acrylate and methacrylate monomers is expressed as they undergo Michael addition to amino acids *in vivo*.

These intrinsic problems of radical photopolymerization reactions and respective monomers are limiting the utility in a number of applications. Therefore, many areas of industries apply cationic photopolymerization to overcome these limitations by its

fundamentally different polymerization mechanism and the particularities of cationically polymerizable monomers.

Cationic photopolymerization

As another type of photopolymerization, cationic photopolymerization represents a light-induced chain growth polymerization via cationic propagating species. The reaction system consists of a cationically polymerizable monomer and a cationic photoinitiator, which initiates the polymerization upon irradiation by light.[26]

In general, cationic polymerizations are initiated by strong Brønsted or Lewis acids. Correspondingly, the light-induced cationic polymerization is initiated by substances, which liberate strong acids upon activation by light, hence, photoacid generators (PAGs).[22] Cationically polymerizable monomers involve compounds with electron-donating groups of sufficient nucleophilicity, which are activated by electrophilic addition of an initiating proton or carbocation. In contrast to radical photopolymerization, which is limited to double bonds of acrylates, methacrylates and vinyl monomers, cationic photopolymerization is applicable to a great variety of unsaturated and heterocyclic monomers, which reflects on the outstanding versatility of resulting polymer backbone structures (Figure 8).[26]
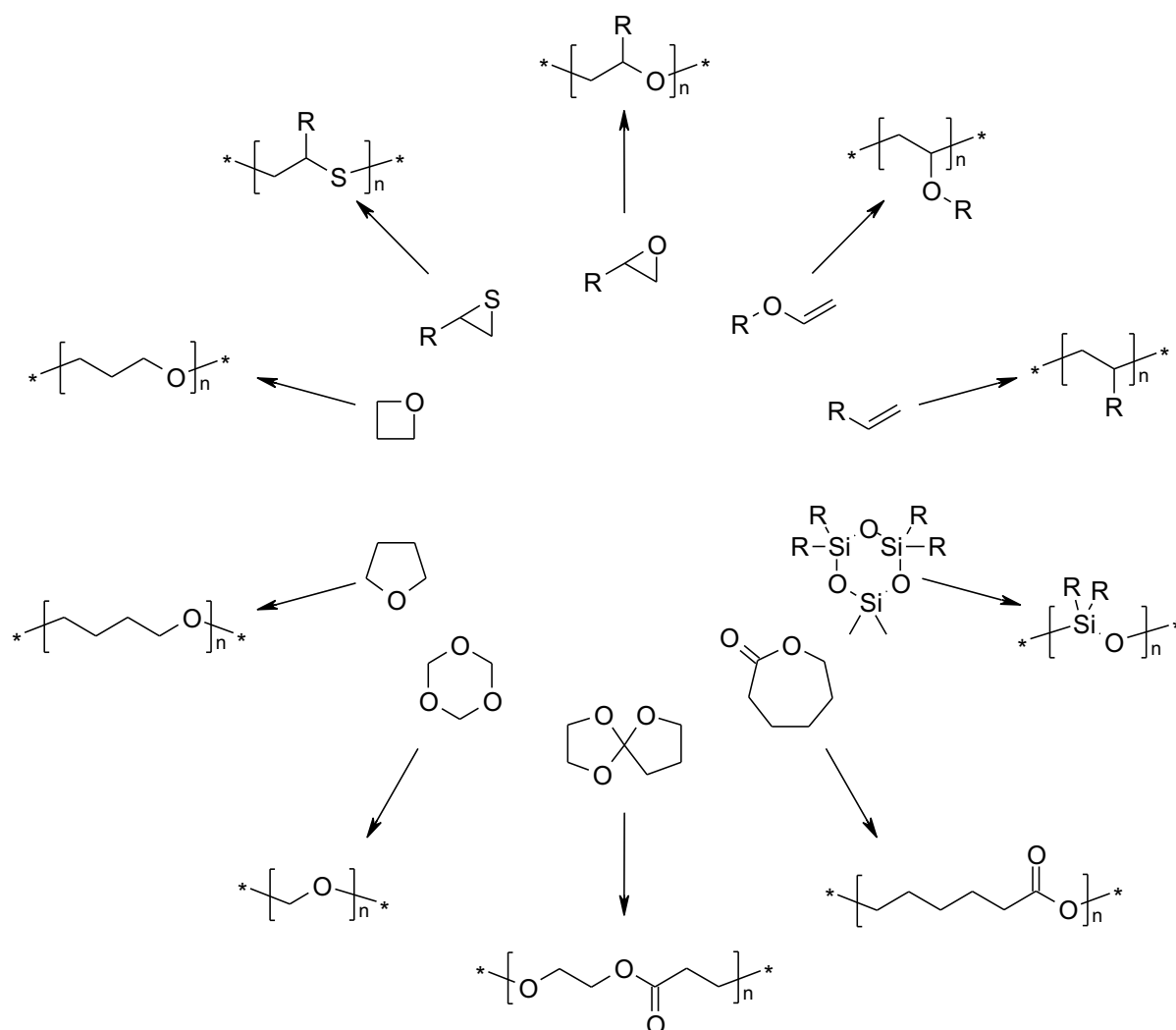
Figure 8: Variety of cationically photopolymerizable monomers

Epoxy monomers are by far the most prominent monomer class in cationic photopolymerization. In order to illustrate the mechanism of the chain growth in cationic photopolymerization, the ring-opening mechanism of an epoxy monomer is described (Figure 9). After electrophilic attack and activation by the protonic acid, a secondary oxonium ion is formed (**I**). Promoted by the inherent ring-strain and resulting instability a carbocation is produced (**II**) This highly reactive species undergoes S_N2 attack by another nucleophilic monomer to form a tertiary oxonium ion in a progressive ring-opening reaction (**III**). By consecutive nucleophilic addition of further monomer molecules to the terminal tertiary oxonium group, the chain reaction propagates to form a polymer (**IV**).[27] As the propagation in epoxy and other heterocyclic monomers involves ring-opening after the activation of the monomer, all processes in the initiation

reaction are thermally driven and kinetic rate constants are strongly influenced by temperature. [22]
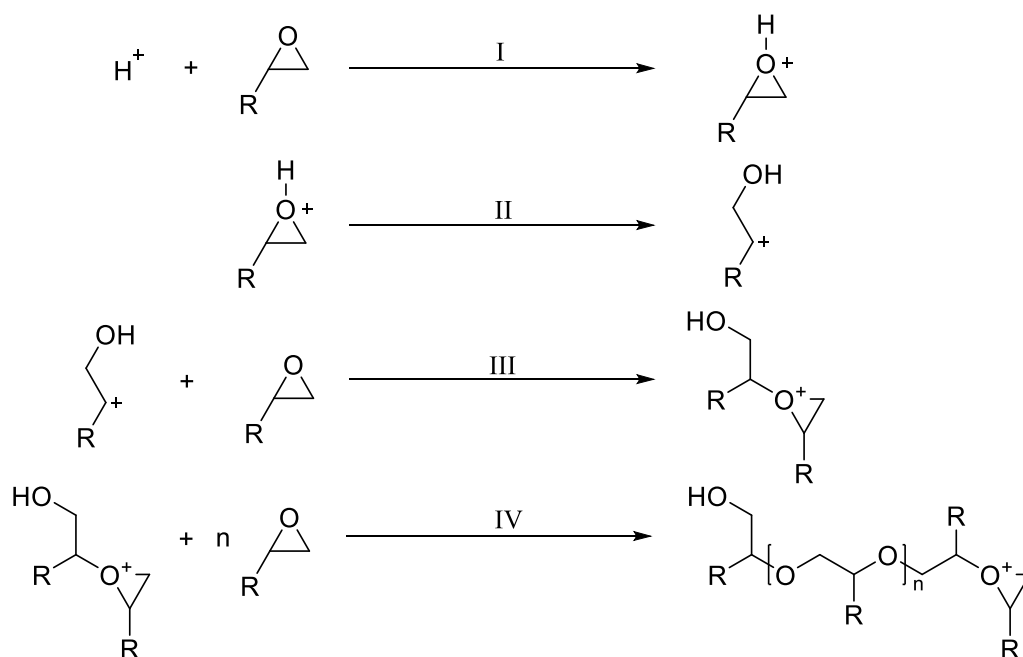
Figure 9: Cationic photopolymerization mechanism of a ring-opening epoxy monomer

Arising from the nature of the initiating species and its polymerization mechanism, cationic photopolymerization offers distinct advantages, such as its inherent oxygen insensitivity. Under ideal conditions termination reactions only arise from recombination to the anion of PAG salts, its anionic fragments after photodecomposition or by the presence of basic additives such as amines, urethanes, basic fillers, pigments or substrates, which are able to quench the cations during polymerization. By impurities of water or alcohols, the hydroxyl protons act as a chain transfer agent to transmit the positive charge onto another propagating chain, which reduces the molecular weight of the resulting polymer. Furthermore, the cationic curing reaction provides a rare feature especially beneficial for industrial curing applications, the so-called *dark curing*.[28-30] By the generation of relatively long-lived protonic acids the initiation of polymerization proceeds to highest conversions even in the absence of light. This reasoned by the thermally promoted cationic polymerization reaction and the suppression of termination reactions, which leads to the extended progress of the polymerization, once the photoacid is generated.[31] Due to short irradiation times, the dark curing facilitates the high speed production of coatings and increases yields in

industrial processes significantly.[26] In summary the cationic photopolymerization features crucial advantages over radical photopolymerization:[22, 26]

1. Insensitivity towards oxygen
2. High conversions
3. Preparation of a variety of polymers with different backbone structures
4. Cationic "dark-curing" by long-lived initiating species

High conversions, the dark curing behavior as well as the absence of inert atmosphere allows for environmentally friendly and cost-efficient UV-curing processes by cationic photopolymerization.

Although cationic photopolymerization is applicable to a great number of cationically polymerizable monomer, specific amounts of thermal energy are demanded to overcome the activation energies for efficient reaction. Hence, kinetic rate constants limit the cationic photopolymerization and only a few monomer classes meet the requirements for efficient and comparably rapid cationic photopolymerization at ambient temperature.[32]. In particular the highly exothermal polymerization of epoxy, oxetane and vinyl ether monomers is used for processes at ambient temperatures.

Monomers for cationic photopolymerization

Epoxy monomers represent the most important monomer class in cationic photopolymerization and are applied in high abundance in coatings, release coatings, automotive primers, printed circuit boards, semiconductor encapsulants, adhesives, and aerospace composites. They are characterized by a number of advantageous features, which in combination cannot be met by other photopolymer products: [33]

1. Excellent mechanical strength and toughness
2. Outstanding resistance to chemicals, moisture and corrosion
3. Good thermal, adhesive and electrical properties
4. No volatiles emission
5. Dimensional stability and low shrinkage upon cure
6. Low costs

The different classes of commercial epoxy monomers are aliphatic, cycloaliphatic and aromatic compounds. By far the most important epoxy monomer with 75% of sales

volume is the aromatic bisphenol-A diglycidyl ether (BADGE).[33] Its broad use is originated in the production of thermosetting epoxy polymers with amine hardeners and led to corresponding wide-spread application in cationic photopolymerization, especially due to their inherent mechanical strength and explicitly low shrinkage of 2-3 % in cationic ring-opening reaction.[34]

Under consideration of the increased viscosity of this aromatic epoxy monomer (11 Pa s), the main application areas found in the production of coatings, castings, tooling, flooring, adhesives and composite materials, in which the low price of about 2 $/kg provides decisive economic advantages.[33] Lately, greater attention has been paid to health and work safety concerns regarding the precursor substances, as bisphenol-A is an estrogen mimic,[35] and epichlorohydrin an orally and dermatologically active toxic agent as well as a human mutagen and carcinogen.[36] Still, BADGE remains the most applied epoxy resin in industrial applications to date.

Within the class of cycloaliphatic epoxides, foremost 3,4-epoxycyclohexylmethyl-3,4-epoxycyclohexylcarboxylate (ECC) is applied for the production of auto topcoats, weatherable high voltage insulators, UV-coatings, acid scavengers, and encapsulants for electronics. Due to their low reactivity in amine hardening of thermosets, cycloaliphatic epoxy monomers are limited to thermal and UV-curing applications. Moreover, cycloaliphatic epoxy monomers are produced at the three-fold price compared to BADGE, thus their sales volume is limited to about 25 % of the market. [33] Its advantages are represented by high oxirane content, low viscosity (0.4 Pa s), low dielectric constant and high glass transition temperatures. The structures of these most important representatives of epoxy monomers BADGE and ECC are depicted in Figure 10.
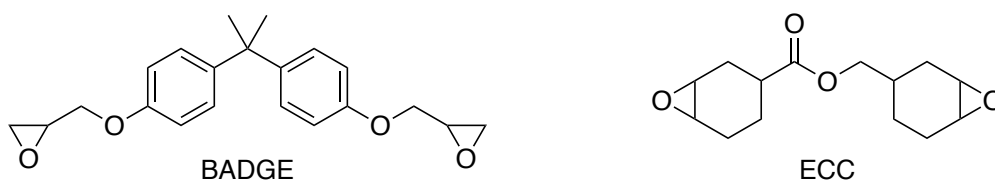
Figure 10: Structures of bisphenol-A diglycidyl ether (BADGE) and 3,4-epoxycyclohexylmethyl-3,4-epoxycyclohexylcarboxylate (ECC)

Glycidyl ethers and cycloaliphatic epoxy monomers show greatly different photopolymerization behavior.

As investigated by Crivello et al. the difference in reactivity arises from steric and electronic effects, as well as the different extent of ring-strain. [37] Cycloaliphatic ECC exhibits high ring-strains on its reactive group arising from double cyclization. Furthermore, no electronic interference stabilizes the secondary oxonium ion, hence, no induction period is exhibited in the initiation process. Once the ring-opening reaction propagates, high specific amounts of reaction heat are liberated and promote the cationic polymerization. [27]

On the contrary, glycidyl ether monomers are prone to hydrogen-bonding during the initiation process, as the neighboring ether oxygen atom provides similar basicity and proton affinity as the oxirane oxygen atom. Via a pseudo-five-membered ring, the secondary oxonium ion is stabilized and exhibits considerable induction periods.[38-40] Figure 11 shows the bidentate coordination of the two oxygen atoms with the initiating proton for an aliphatic or aromatic glycidyl ether.[41]

Figure 11: Bidentate coordination of protons in glycidyl ether monomers

For aromatic glycidyl ether monomers the formation of the metastable transition state is less pronounced, as the lower basicity of the aryl ether oxygen decreases the stability of the intermediate. Still, significant induction periods at room temperature indicated the retardation of the initiation process. Although the light-induced ring-opening polymerization of glycidyl ethers occurs in low rates at room temperatures, it is highly susceptible to promotion by thermal energy input. Once the initiation process is efficiently facilitated at increased temperatures, the polymerization shows autoaccelerated behavior under high exothermicity.[41]

In structural similarity to epoxy monomers, also oxetanes are common monomers for cationic photopolymerization. The four-membered cyclic ethers are applied in the same fields as epoxides, such as coatings, adhesives, printing inks, dental composites and 3D printing.[42] In particular their lower toxicity, lower water uptake and even lower shrinkage upon cure promotes the application of oxetanes in sensitive fields. Figure 12 depicts the disubstituted oxetane (DSO) commonly applied in additive manufacturing.[3]
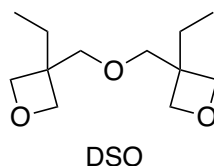
Figure 12: Disubstituted oxetane 3,3'-(oxybis(methylene))bis(3-ethyloxetane) (DSO)

Despite the slightly lower ring-strain of oxetanes (107 kJ/mol) in comparison to oxiranes (114 kJ/mol), [39] their increased basicity (pKa = 3.7) supports the initiation mechanism in comparison to oxiranes (pKa = 2.0). [43] Still, oxiranes exhibit longer induction periods as comparable cycloaliphatic epoxy monomers. [32, 44, 45] However, in analogy to ring-opening epoxy monomers, also for oxetanes a rate acceleration by increased temperatures is reported.[46]

An especially high reactive monomer class for cationic photopolymerization is represented by vinyl ethers. Vinyl ethers are among the most reactive monomers in cationic polymerization.[47] Their cure rates in cationic photopolymerization are comparable to the radical photopolymerization of acrylates.[48] In contrast to heterocyclic monomers, such as epoxides or oxetanes, vinyl ethers undergo cationic polymerization by a different mechanism, as no ring-opening reaction is involved (Figure 13).
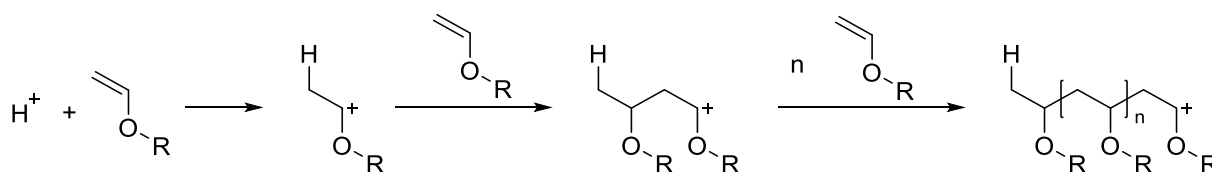
Figure 13: Cationic photopolymerization mechanism of vinyl ether monomers

The utility in cationic photopolymeiration is represented to a great extend by the high curing rates and low viscosity of vinyl ether monomers. [49, 50] Therefore, vinyl ethers are predominantly used as reactivity enhancers and viscosity modifiers in epoxy formulations, in which the ring-opening monomer serves as structural compound due to the favorable structure-property relationship of heteroatom-containing polymer backbones. As vinyl ethers show low toxicity and low odor they act as environmentally-friendly alternative for the development of non-acrylate formulations with high curing rates.[51] Due to the inherently high reactivity, the cationic photopolymerization of vinyl ethers is primarily dependent on the initiation ability of respective photoacid generators used as cationic photoinitiators.

Photoacid generators

The development of cationic photopolymerization is inevitably bound to the introduction of efficient photoacid generators (PAGs). Despite prior approaches based on organosilanes, latent sulfonic acids and non-ionic compounds for cationic initiation, the introduction of onium salt PAGs indicates the breakthrough in cationic photopolymerization. [26, 4917] The roles of cation and anion in these PAG salts are well separated regarding their influence on the cationic photopolymerization. The cation is defined as the seat of the photochemistry as it contains chromophore groups and undergoes efficient photodecomposition.[52] Furthermore, the thermal stability of the compound is solely dependent on the nature of the cation. On the contrary, the anion does not participate in the photoreaction. It solely determines the polymer chemistry by the generation of strong acids and influences the initiation, propagation and potential termination by its non-nucleophilic character. Table 1 displays the influences of cation and anion of onium salt PAGs.

Table 1: Roles of the ions of onium salt photoinitiator[52]

CATION determines photochemistry	ANION determines polymer chemistry
absorption maximum (λ_{max})	acid strength
molar absorption coefficient	nucleophilicity (ion pairing)
quantum yield	initiation efficiency
thermal stability	propagation rate constants

As most important differentiation, onium salt PAGs are characterized by the nature of photoreactive onium cations. The spectrum of investigated onium PAGs covers aryldiazonium, diaryliodonium, triarylsulfonium, triarylselenonium, dialkylphenacylsulfonium, triarylsulfoxonium, aryloxydiarylsulfoxonium and dialkylphenacylsulfoxonium salts, of which many suffered from thermal instability or gas formation upon photodecomposition.[26, 53]

With the introduction of diaryliodonium and triarylsulfonium salts by Crivello et al. in the 1970s, cationic photopolymerization became widely applicable due to facile

preparation, inherent thermal stability and highly efficient photodecomposition.[15, 16, 18] Figure 14 depicts the structures of diaryliodonium and triarylsulfonium salts.
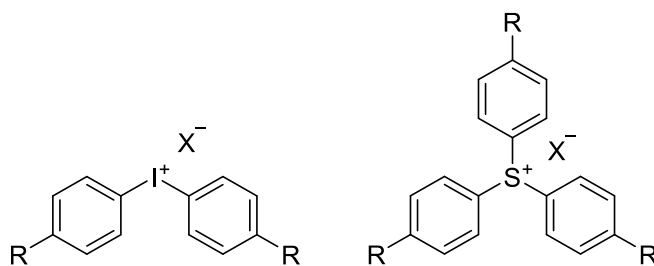
Figure 14: Diaryliodonium and triarylsulfonium salts as photoacid generators (PAG)

Typically, diaryliodonium cations, such as the unsubstituted diphenyliodonium, undergo photodecomposition at wavelengths below 320 nm and comprise an absorption maximum as low as 227 nm. Triarylsulfonium salts may absorb UV light up to 400 nm depending on their substitution pattern, whereas the unsubstituted triphenylsulfonium cation exhibit an absorption maximum of 320 nm. With extended substitution by conjugated systems, however, the triarylsulfonium cation may absorb up to 1500 times stronger at 313 nm than the unsubstituted form.[52] Moreover, extended aliphatic substitution drastically improves the solubility in organic media and reduces the toxicity of the PAG salt and corresponding decomposition products. With iodonium and sulfonium cations being strong oxidants, their ability for photosensitization to higher wavelengths is solely determined by the compatibility of redox potentials of cation and photosensitizer. Iodonium cations are easily sensitized by a number of photosensitizers (-0.2 eV), whereas the photosensitization of sulfonium cations is less favorable due to low reduction potentials (-1.2 eV).[54, 55] In correlation to their reduction potential, triarylsulfonium salts show outstandingly high thermal stability over 300 °C, whereas diaryliodonium salts decompose thermally at temperatures around 200 °C.[56, 52]

The combination of diaryliodonium and triarylsulfonium cations with non-nucleophilic anions of high acid strength give PAGs, which exhibit efficient protonation of cationically polymerizable monomers and at the same time suppress termination reactions by diminishing ion-pairing with the propagating cationic chain end. Classically used perfluorometallate anions such as SbF_6^-, AsF_6^-, PF_6^-, and BF_4^- generate super acids of Hammet acidities between -15 and -30 to efficiently initiate a cationic polymerization in high rates.[57, 58] The high fluorination of these anions reduces the

nucleophilicity and thus increases the reactivity in cationic photopolymerization in the order of $BF_4^- > PF_6^- > AsF_6^- > SbF_6^-$.[22] Despite their high reactivity, perfluorometallate anions suffer from considerable toxicity.[27] The heavy metal content of PAGs and photoreactive formulations obstructs the application in health sensitive applications, whereas low hydrolysis stability promotes the liberation of HF under aqueous conditions in final products. Still, the low price of respective PAGs promotes their wide-spread use in non-sensitive industrial applications.

Besides these classical counterions, the introduction of advanced heavy-metal free Weakly Coordinating Anions (WCAs) drastically increased acid strengths and reactivities of onium salt PAGs. Especially the perfluorinated tetrarylborates ($BAr^F_4^-$) show advantageous behavior in cationic UV-curing, however, has not been applied in broad industries due to the significantly higher price arising from challenging preparation conditions.[59, 60] The synthesis of the respective WCA precursor utilizes borontrichloride and highly reactive pentafluorophenyllithium, which cannot be up-scaled due to the explosion hazard of the intermediate.[61, 62]
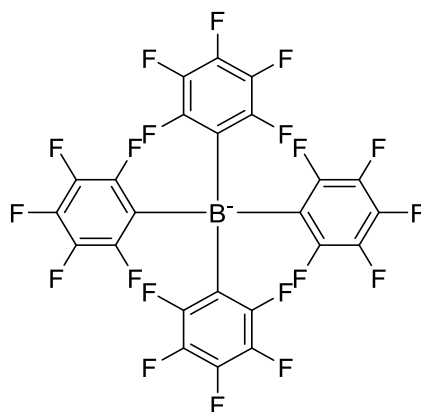
Figure 15: Weakly coordinating anion tetrakis(pentafluorophenyl)borate ($BAr^F_4^-$)

The electronic shielding of the center ion is facilitated by bulky phenyl groups which reduce strong cation-anion interactions and consequently suppress ion-pairing. Furthermore, the high fluorination of the phenyl substituents covers the ion surface with poorly polarizable atoms.[63] In result, improved solubility in even non-polar solvents facilitates the application in a great variety of organic media. Although the photochemistry is determined by the PAG's cation, the high arylation of the $BAr^F_4^-$ increases the absorption in UV of 200-240 nm and doubles the extinction coefficient of respective diaryliodonium salts.[26] In comparison to onium salts comprising the most

reactive perfluorometallate anion, SbF_6^-, the tetrakis(pentafluorophenyl)borate anion exhibits significantly higher reactivity.[59]

Besides the development of polyfluorinated tetraaryl- or tetraalkylborates $[B(R^F)_4]$, dimeric borates $[X(B(C_6F_5)_3)_2]$, tetra- or hexateflatometallates $[M(OTeF_5)_n]$, also bis(trifluoromethanesulfonyl)imides $[(RFSO_2)_2N]$ and tris(trifluoromethane-sulfonyl)methanides $[(RFSO_2)_3C]$ were introduced as WCAs with strong suppression of ion-pairing and lowest nucleophilicity.[64]

In the late 1990s, another class of WCAs based on aluminate anions with lowest nucleophilicity was introduced. Strauss and coworkers initially developed the novel alkoxyaluminates to enhance the catalytic activity of corresponding metal cations.[65, 66] In correlation with the pKa value of the corresponding alcohol, alkoxyaluminates exhibit lowest basicity, foremost the tetra-coordinated aluminum complex of perfluorinated tert-butyl alcohol, tetrakis(perfluoro-t-butyloxy)aluminate (Figure 16).[63, 67]

-Al
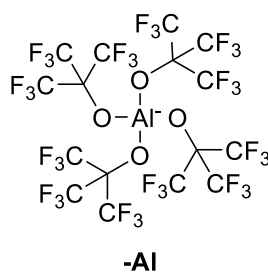
Figure 16: Alkoxyaluminate WCA tetrakis(perfluoro-t-butyloxy)aluminate

Following deep investigations by Krossing et al. novel synthesis methods led to facile preparation and better understanding of this substance class with lowest nucleophilicity known to date. [63, 68] The high number of fluorine atoms on bulky $C(CF_3)_3$ lead to outstanding electronic shielding of the most basic sites of the anion. Compared to other compounds, the alkoxyaluminate WCA exhibits outstanding stability against fluorine and ligand abstraction. In consequence, the anion exhibits stability against hydrolysis even in 6 N nitric acid.[68]

Just recently, onium salt PAGs based on alkoxyaluminate WCAs have been demonstrated as most reactive cationic photoinitiators in epoxy monomers to date.[56] Since then, the beneficial reactivity of alkoxyaluminate PAGs has led to successful application in NIR and UV-LED sensitized cationic photopolymerization,[69] sensitized

radical photopolymerization,[70] and radical induced cationic frontal polymerization (RICFP).[71, 72]

Hot Lithography

The development of SLA and DLP aim for rapid cross-linking of liquid formulations by photopolymerization. The monomers mostly applied in L-AMTs were adapted from industrial applications of coatings, where fast curing, a high degree of cross-linking, high hardness and good adhesion is demanded.[19] For application in SLA and DLP, however, their high reactivity and low viscosity is opposed by considerable drawbacks. As most commonly acrylate and methacrylate monomers are used for photopolymerization in L-AMTs, shrinkage between 5 % for cycloaliphatic and aromatic dimethacrylates and more than 10 % for aliphatic dimethacrylates is observed.[3, 24] Depending on the degree of shrinkage, deformations or curling effects of the printed parts are observed.

Moreover, the photopolymerization of low molecular weight compounds results in explicitly brittle photopolymers with low toughness, low impact resistance and low heat deflection temperatures. Structural precursors from (meth)acrylated oligomers, such as polyethers, polyesters, epoxy resins or polyurethanes are used to reduce shrinkage and improve the mechanical properties of resulting photopolymers.[73, 74] Inevitably, these monomers are highly viscous and cannot be processed in classical L-AMTs at room temperature without the addition of reactive diluents or solvents.[10]

To overcome these limitations in L-AMT and to reach desirable material properties, Hot Lithograph has recently been introduced as an innovative L-AMT technique working at elevated temperatures.[75-77] In Hot Lithography, the approaches of SLA and DLP are applied in a bottom-up 3D printer setup at temperatures up to 140 °C to process monomers with high viscosities. Hence, structural monomer resins and oligomeric precursors with viscosities up to 20 Pa s are applicable at increased temperatures, whereas classical L-AMTs are restricted to formulations below 1 Pa s.[14, 77] The SLA-based Hot Lithography approach utilizes a 375 nm laser for high-energy irradiation of the formulation through the transparent vat bottom, as depicted in Figure 17.
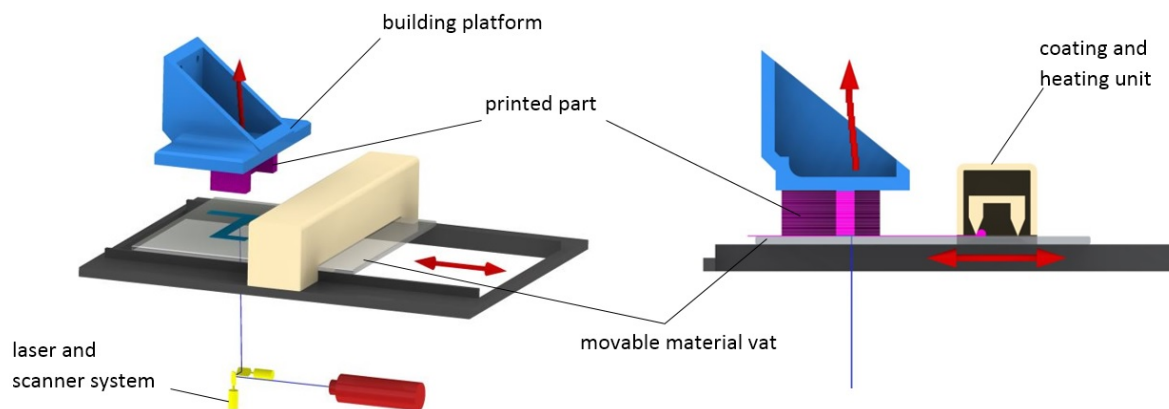
Figure 17: Heated SLA setup in Hot Lithography

As a consequence of the increased temperatures in Hot Lithography, the processing of polybutadiene-based resins, unsaturated polyester resins and thermoplast-filled formulations is reported, which crucially enhances the thermomechanical properties of printed objects. [78] Primarily, lowering the viscosity of the formulation increases the mobility of the resins and results in a distinct increase in printing speeds.

Furthermore, as shown for dimethacrylate-based formulations, the increased temperature in the Hot Lithography printing process leads to significantly increased conversions, tensile strength and storage modulus.[76] In further consideration, the general enhancement of reactivity in photopolymerization can be achieved in Hot Lithography.

OBJECTIVE

Over the last decades, lithography-based additive manufacturing technologies (L-AMTs) have marked innovative developments in a great number of industrial applications. L-AMTs demonstrate unmatched precision and surface qualities, however, face limitations arising from the photopolymerization reaction and the properties of photopolymer products. Most commonly applied acrylate and methacrylate systems suffer from high shrinkage and sensitivity towards oxygen upon radical photopolymerization, as well as poor mechanical properties and low biocompatibility. To overcome these limitations, the implementation of cationic photopolymerization of ring-opening monomers has been aspired due to inherent insensitivity towards oxygen, high conversions, low shrinkage and outstanding polymer properties. As cationic photopolymerization of ring-opening monomers occurs in low polymerization rates at room temperature, the recent introduction of Hot Lithography may crucially promote reactivities at temperatures up to 140 °C. This potentially enables the unmediated 3D printing of epoxy resins, but also the processing of low reactive monomers, such as 2-oxazolines, which have not been considered for cationic photopolymerization to date.

The first part of this thesis aims for the evaluation of efficient cationic photoinitiation systems for application in Hot Lithography. The Hot Lithography process crucially promotes the cationic ring-opening reaction, however, demands for highly reactive and thermally stable photoinitiation systems for irradiation above 375 nm for efficient and selectively light-induced cationic polymerization. Due to the predominant utility and outstanding particularities of bisphenol-A diglycidyl ether (BADGE), the investigations of cationic and free radical-promoted cationic photoinitiation systems should be conducted in formulations of this specific epoxy monomer by simultaneous thermal analysis (STA) and photo-DSC at elevated temperatures.

Using the most suitable cationic photoinitiation system, the second part of this thesis should focus on the cationic photopolymerization of 2-oxazolines. Due to unique chemical and structural characteristics of polymers cured by cationic ring-opening polymerization (CROP), 2-oxazolines have lately gained tremendous attention foremost in biomedical research. However, poly(2-oxazoline)s have been accessible

only by thermal polymerization in small scales or after long reaction times at high temperatures, hence, at excessively high costs. Despite their promising poly(amide) backbone structure, poly(2-oxazoline) have neither been considered for application in structural materials, nor for UV-curing by cationic photopolymerization. The projected investigations focus on the accessibility of poly(2-oxazoline) materials by solvent-free and rapid cationic photopolymerization at elevated temperatures, which can be evaluated by STA, photo-DSC and RT-NIR/MIR-photorheology. In consideration of the toughening of photopolymers, the 2-oxazoline-based materials should be UV-cured and analyzed by DMTA, tensile testing and impact resistance testing. Furthermore, a 2-oxazoline-based system should be applied in Hot Lithography, which provides the essential conditions for the additive manufacturing of poly(2-oxazoline)s and enables the development of novel materials by this innovative 3D printing technique.

GENERAL PART

1   Initiation systems for cationic photopolymerization in Hot Lithography

1.1   State of the art

1.1.1   Cationic photopolymerization in L-AMTs

The use of cationic photopolymerization for lithography-based additive manufacturing technologies (L-AMTs) has been considered since the introduction of efficient onium salt photoacid generators (PAGs) in the 1970s. The inherent oxygen insensitivity, advantageous polymerization behavior upon cure, as well as enhanced photopolymer properties are the driving forces behind ongoing research on the application of cationic photopolymerization in L-AMTs.

In comparison to radical photopolymerization of acrylate and methacrylate monomers, most cationic ring-opening monomers exhibit lower reaction rates upon photopolymerization at room temperatures. Therefore, first cationic systems applied in L-AMTs were based on comparably high reactive vinyl ether monomers.[79] By vinyl ether functionalization of oligomers, the application of urethane, phenol, polyester, polyether and polysiloxane precursors was reported. Due to the poor dimensional and mechanical stability of vinyl ether monomers upon cure, already in first approaches the combination of highly reactive vinyl ethers with ring-opening monomers, such as epoxy monomers, was necessary to maintain stable dimension during photopolymerization in stereolithography.[34] The rapid cross-linking of vinyl ether monomers defines the structure in stereolithography, whereas the epoxy component provides dimensional consistency, mechanical strength and reduced shrinkage during the subsequent thermal post-curing process. Despite lower reactivity of epoxy monomers, only 2-3 % shrinkage occurs during photopolymerization as a consequence of the ring-opening

reaction.[34] Hence, epoxy monomers are considered as one of the main classes of cationic monomers for L-AMTs besides their high abundance in classical UV-curing applications.[3]

By far the most commonly applied epoxy monomers in L-AMTs are diglycidyl ether derivatives of bisphenol A (such as BADGE), cycloaliphatic epoxy monomers (such as 3,4-epoxycyclohexyl-methyl-3,4-epoxycyclohexanecarboxylate; ECC), and epoxides of aliphatic alcohols.[80] Still, photoreactive systems solely based on epoxy monomers suffer from limited reactivity. Especially in the cationic photopolymerization of BADGE, long induction periods and low polymerization rates are observed.[38-40] Therefore, low molecular weight diols are added as chain transfer agents to further enhance reactivity.[22] As another effect, oligomeric diol precursors reduce the crosslink density significantly, resulting in lower brittleness of resulting photopolymers of BADGE-based systems and further enhanced mechanical strength.[81] Similar to epoxides, oxetanes are reported as ring-opening cationically photopolymerizable monomers with additional beneficial particularities such as low water uptake and comparably low shrinkage, specifically useful in dental industries.[82, 83]

Over the past years, dual cure systems of radical and cationic polymerization broadened the spectrum of applicable photopolymerization systems to combine rapid solidification with structural stability, in analogy to purely cationic vinyl ether-epoxy systems. The excessively fast polymerization of acrylates, which often causes inconsistency in structure and considerable amounts of uncontrolled shrinkage, are opposed by stable and low shrinking ring-opening compounds, such as epoxy monomers. The post-curing of the cationic system is subsequently induced either by light or heat, and is highly efficient due to the inherent dark-curing reaction.[28-30, 84] In analogy, acrylate-oxetane hybrid systems have been reported.[85] Due to the inability of copolymerization between the monomers, these hybrid systems form interpenetrating networks (IPNs).[86] Besides the structural enforcement, a major advantage of these is the inherently lower oxygen sensitivity provided by the cationic portion of the dual cure system. However, also incompatibility between the monomer systems may occur as reported for urethane-macromer components of acrylates and epoxides.[87]

Apart from these approaches, the factual 3D printing of pure epoxy systems has remained inaccessible due to the strongly limited reactivity of most ring-opening monomers at room temperature. By the introduction of Hot Lithography, however, the

cationic photopolymerization may be strongly promoted by the input of thermal energy to support the cationic ring-opening polymerization of epoxy monomers.[41] Foregoing investigations on the monomer BADGE support this approach, as they showed the distinct promotion of the cationic photopolymerization at elevated temperatures.[88]

Besides the increase of temperature to facilitate the cationic photopolymerization, the use of photosensitizers and radical photoinitiators to promote the photoreactivity of onium salt PAGs and extend their absorption spectrum to higher wavelengths is considered.

1.1.2 Photosensitized and radical-promoted cationic photoinitiation systems

Since the inception of cationic photopolymerization by Crivello and al. in the 1970s, ongoing developments have led to great improvement of cationic photoinitiation systems to meet the demands of growing industrial applications and innovative technologies. As common diaryliodonium and triarylsulfonium salts absorb light mostly below 350 nm, one major aim was the modification of the photoinitiation mechanism to enable cationic photopolymerization at higher wavelengths and increase the polymerization rates.[20, 89] With the advance of photopolymerization industries to fabricate pigmented or filled photopolymers, the use of longer wavelengths is desired to enhance penetration depth into the formulations.

The trend towards higher wavelength irradiation in UV-curing processes is accompanied by the development of progressive light-sources. In contrast to common medium and high pressure mercury arc lamps, which provide broadband irradiation with strong emission at 313 and 366 nm, modern LED light sources emit at narrowly defined wavelengths between 360 and 460 nm with greatly reduced energy demand and lower UV exposure to the surrounding.[26] The change to higher wavelengths thus not only improves penetration depth in the photo-curing processes, but also promotes the cost-efficiency and work safety in applications of photopolymerization.

Therefore, great effort has been spent on the alteration of spectral sensitivity in photoinitiation systems based on onium salt PAGs. The approaches aim for the direct manipulation of the photodecomposition of the onium cation to generate a reactive species.

In the classical photodecomposition mechanism, the cation is excited to a singlet state, from which a homolytic or heterolytic cleavage occurs.[90] In the example of a diphenyliodonium cation, the cleavage of the halogen-carbon bond leads to the generation of radical-cations, radicals, cations and arylhalides following homolytic and heterolytic cleavage (Figure 18). In the homolytic decomposition pathway, the intermediate radicals conduct hydrogen abstraction from either monomer or potentially present solvent to form neutral aromatic species and the Brønsted acid of the corresponding counterion present in the system. In the heterolytic decomposition pathway, the intermediate phenyl cations undergo electrophilic attack on the monomer or solvent to give the neutral photolysis products including the corresponding Brønsted acid. By electron transfer, the homolytic decomposition products are convertible to corresponding heterolytic products.[26, 52]
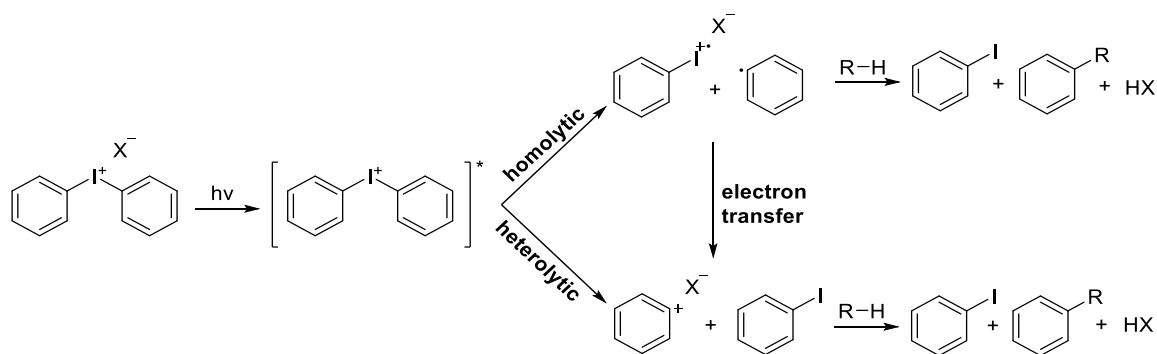
Figure 18: Photodecomposition pathways of diphenyliodonium salts in homolytic and heterolytic decay

The given photolysis mechanism is analogously valid for triarylsulfonium cations, whereas the heterolytic decomposition predominates in these compounds. Upon irradiation with adequate wavelengths, the photolysis of diaryliodonium salts occurs in high quantum yields of 0.7-0.9, whereas triarylsulfonium exhibit quantum yields of typically 0.7.[26, 52]

The described *direct photolysis* of covalent bonds from the excited singlet state demands for high energy input by UV irradiation, which provides energies of 70 kcal/mol and higher. As a reference carbon-carbon bond comprises 83 kcal/mol, the use of UV-light is inevitable to break corresponding bonds in the photodecomposition of diphenyliodonium or triarylsulfonium cations.[26] By substituents on the aromatic chromophores the absorption can only be shifted marginally towards

higher wavelengths, whereas the extinction coefficient is significantly enhanced with highly conjugated systems in triarylsulfonium cations.[26]

Thus, in order to distinctly extend the absorption range of photoinitiation systems for cationic photopolymerization, the use of photosensitizers to interact with onium salt PAG has been shown as a viable approach towards visible light photoinitiation. Due to high singlet and triplet energies of onium salt PAGs, a photosensitization by energy transfer, as applicable on radical photoinitiators, is highly improbable. Hence, onium salt PAGs undergo *electron transfer photosensitization* with photosensitizers of suitable oxidation potentials. Figure 19 illustrates the photosensitization mechanism of a diphenyliodonium salt by an electron transfer photosensitizer.
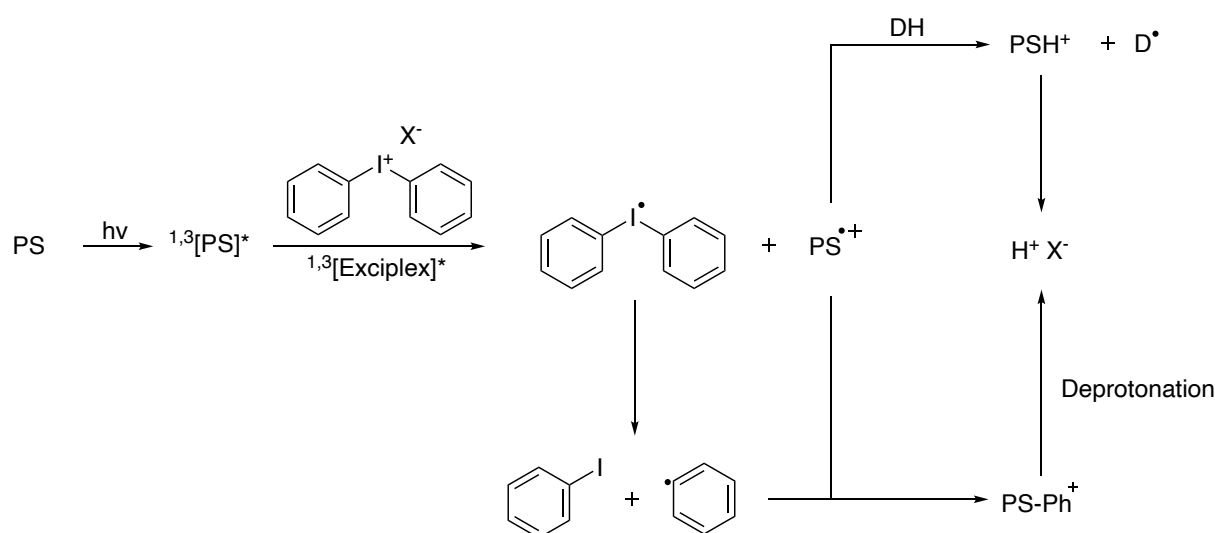
Figure 19: Photosensitization mechanism of a diphenyliodonium salt[89]

By irradiation with compound-specific wavelength, the photosensitizer (PS) is promoted to the excited singlet or triplet state (^{1,3}[PS]*). During the formation of an *exciplex* transition state, the diphenyliodonium salt is reduced in an electron transfer reaction to form the corresponding diphenyliodine radical, whereas the PS is oxidized to the corresponding cation radical PS$^{\bullet+}$. As reported, the initiation of cationic polymerization by direct protonation from intermediate PS$^{\bullet+}$ is negligible.[89] Subsequently, the formation of the initiating species may occur in two dominating pathways. Via hydrogen abstraction from a hydrogen donor DH, the intermediate PSH$^+$ forms the protonated cation, from which the protonic acid is generated, and the PS is recovered. In the alternative, less favored pathway, the PS$^{\bullet+}$ is arylated by the phenyl

radical, which is provided by the rapid decomposition of highly unstable diphenyliodine radicals. The arylated PS-Ph$^+$ subsequently undergoes deprotonation to form the protonic acid, whereas the arylated PS-Ph may further act as photosensitizer in subsequent electron transfer reactions. [22, 26, 89]

The compatibility of photosensitizer and onium salt is determined by the redox potentials of the compounds. Triarylsulfonium salts exhibit low reduction potentials (-1.2 eV), thus, undergo less effective photosensitization due to the thermodynamically unfavored electron transfer.[55] Thus, only photosensitizers with high singlet energies are applicable for sulfonium salts, as the free energy change of electron transfer (ΔG_{et}) for the electron transfer is sufficiently negative.[26, 91] In contrast, diaryliodonium salts are easily sensitized according to their redox potential of -0.2 eV.[54] Table 2 lists the absorption maxima of common photosensitizers and the resulting ΔG_{et} in electron transfer reactions with diphenyliodonium or triarylsulfonium cations.

Table 2: Free energy change in electron transfer photosensitization (ΔG_{et}) for several photosensitizers in combination with diphenyliodonium and triphenylsulfonium salts[89]

	λ_{max} [nm]	Ph$_2$I$^+$ ΔG_{et} [kJ/mol]	Ph$_3$S$^+$ ΔG_{et} [kJ/mol]
Anthracene	374	-193	-89
Perylene	435	-170	-66
Phenothiazine	318	-161	-58
Thioxanthone	383	-93	11
Benzophenone	333	-9	95
Acetophenone	382	-7	96

As seen from the magnitude of ΔG_{et}, diphenyliodonium salts are efficiently sensitized by a number of photosensitizers, whereas triphenylsulfonium salts may only be sensitized by anthracene, perylene and phenothiazine.[89] As reported, electron-donating aliphatic substituents on the anthracene derivatives further promote the reactivity and solubility of resulting photosensitized initiation systems as shown for 9,10-dibutoxyanthracene.[92]

Besides the photosensitization and resulting increase of reactivity in visible light, the favorable reduction potential of iodonium salts enables another highly efficient way to promote the cationic photopolymerization. Free radical promoted cationic polymerization (FRPCP) describes the efficient decomposition of onium salt PAGs by suitable free radical photoinitiators. After the discovery of the favorable interaction of certain radicals and onium salts,[93] Yagci and coworkers examined a number of free radical photoinitiators such as benzoin derivatives, acylphosphine oxides,[94] o-phtalaldehyde,[95] vinyl halides,[96] and polysilanes,[97] benzophenones and phenylazotriphenylmethane derivatives[98] for the applicability in the promotion of cationic photopolymerization. As found, most carbon-centered radical systems are inefficient without the addition of hydrogen donating agents, such as cyclic ether monomers, aromatic amines, benzyl alcohols or silanes, thus representing bimolecular initiation systems.[99, 100, 89] As an example, the unmediated reduction of diphenyliodonium salts by acylphosphine oxides occurs via the phosphinoyl-based radical, since the benzoyl radical does not undergo oxidation reactions even with strong oxidants, such as iodonium cations, corresponding to its redox potential.[101] By oxidation of phosphinoyl radicals the resulting phosphonium ions act as initiating species for the cationic polymerization, successfully extending the absorption of the radical promoted photoinitiation system to visible region.[102]

This discovery gave rise to the investigation of further heteroatom-based free radical photoinitiators for advantageous reactivity in FRPCP. Advanced Type I radical photoinitiators such as acylgermanes were applied and compared to photoinitiation systems of acylphosphine oxides and a bimolecular benzophenone system, showing the high potential of acylgermane derivatives to undergo FRPCP in correlation to their oxidation rate constants.[103, 104] Same as phosphinoyl radicals, the resulting germyl radicals react most efficiently with diaryliodonium salts to form germyl cations for initiation of the cationic polymerization.

Figure 20 shows the FRPCP mechanism after α-cleavage of a bisacylgermane-based free radical photoinitiator bis(4-methoxybenzoyl)diethylgermanium (BMDG) with a diphenyliodonium salt PAG.
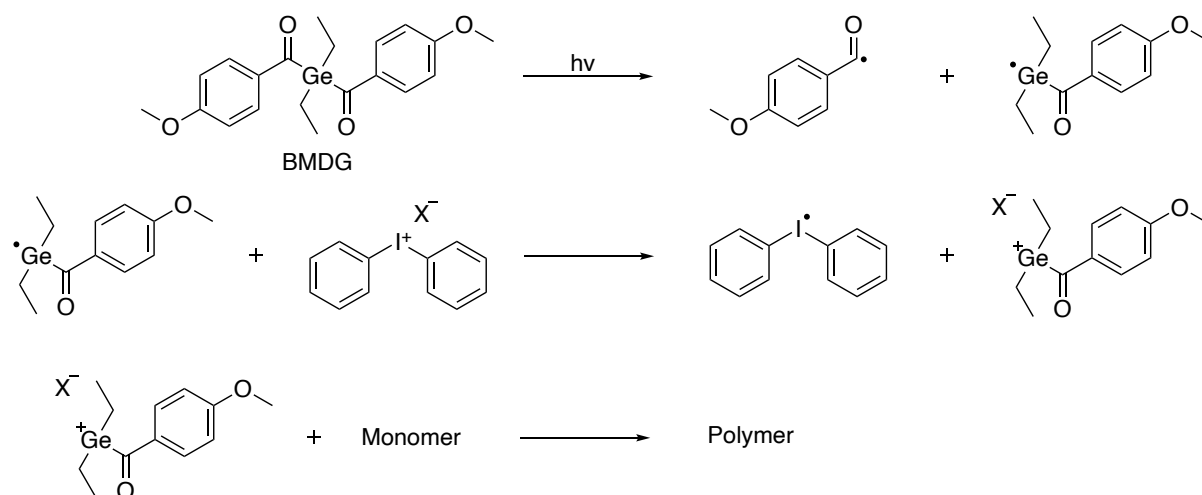
Figure 20: FRPCP mechanism of bis(4-methoxybenzoyl)diethylgermanium (BMDG) with a
diphenyliodonium salt PAG

Mono- and bisacylgermanes undergo α-cleavage in significant bathochromic shift up to 490 nm, whereas the absorption maximum of BMDG is at λ_{max} = 420 nm.[23] The explicitly high quantum yield of decomposition (0.8-0.9) indicates the highly efficient photochemistry of this advanced free radical photoinitiator. A further important feature of acylgermane derivatives for high curing depths is the efficient photobleaching behavior due to the low absorption of photolysis products.[105]

Most significantly, the highly efficient promotion of cationic photopolymerization and extension of the absorption range to the UV-Vis region reflects on the potentially advantageous applicability to increase the polymerization rates of epoxy monomers in UV-curing and further photopolymerization technologies, such as Hot Lithography.

1.2 Synthesis of alkoxyaluminate-based PAGs

The aim to promote the cationic photopolymerization of epoxy monomers for applicability in Hot Lithography is followed by optimization of the photoinitiation system and the applied conditions of photopolymerization. Therefore, the major aspect lay on the implementation of a highly reactive cationic photoinitiator for application in direct cationic photopolymerization, as well as free radical promoted-cationic polymerization (FRPCP) by a radical photoinitiator. As described, the promotion of onium salt PAGs by radicals is limited to iodonium salts, as sulfonium salts exhibit unsuitable reduction

potentials. Therefore, only diphenyliodonium PAGs were considered for FRPCP at elevated temperatures.

Furthermore, the nature of the onium salt PAG is one limiting factor for obtaining highest reactivity of cationic photopolymerization in general. Within the class onium salt PAGs based on advanced weakly coordinating anion (WCAs), the promising features of perfluoroalkoxyaluminates have been reported.[56] Especially in application for the cationic photopolymerization of bisphenol-A diglycidyl ether (BADGE) the diphenyliodonium tetrakis(perfluoro-t-butyloxy)aluminate (I-Al) provides highest reactivity in comparison to benchmark PAGs comprising borate-based $BAr^F_4{}^-$ or the classical perfluorometallate anion $SbF_6{}^-$.

The advantageous alkoxyaluminate PAG is accessible starting from purified lithium aluminum hydride and the corresponding fluorinated alcohol. Subsequently, the produced lithium alkoxyaluminate salt is converted to the PAG by straight-forward salt metathesis reaction using the onium chloride under cleavage of lithium chloride. The synthesis route of alkoxyaluminate PAGs is depicted in Figure 21.
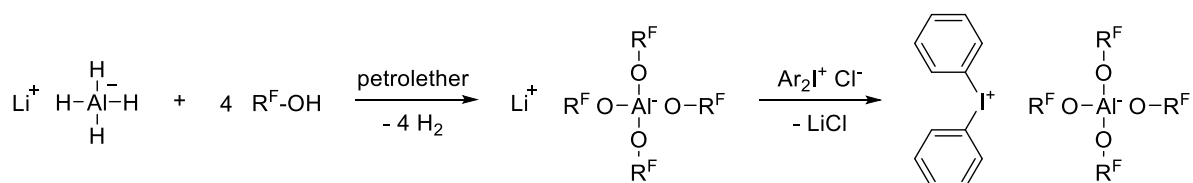
Figure 21: Synthesis route towards onium alkoxyaluminate PAGs

1.2.1 Synthesis of diphenyliodonium tetrakis(perfluoro-t-butyloxy)aluminate (I-Al)

As the starting material $LiAlH_4$ in commonly available quality contains up to 30 % of impurities (Al, Al oxides and Li_3AlH_6) it was purified by extraction with diethyl ether, followed by evaporation of solvent and fine grinding in a glove box to maximize the surface area of the solid for subsequent synthesis of the desired WCA.
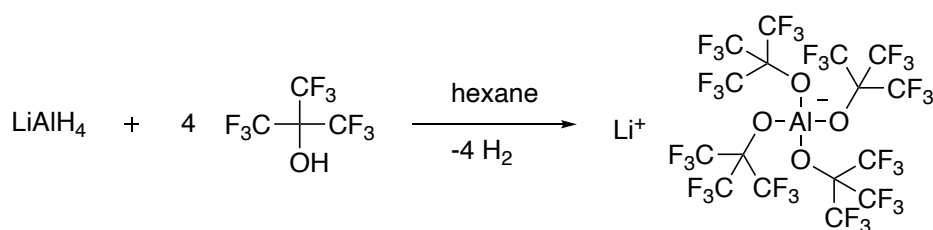
The reaction was performed under argon protective atmosphere to ensure moisture-free environment (LiAlH$_4$).

1.0 equivalents (eq) of purified lithium aluminum hydride were mixed with 50 mL hexane (abs.) in a 2-necked Schlenk flask. The flask was connected an intensive cooler (reflux condenser) and closed by a septum. The intensive cooler was cooled to -25 °C using a cryostat. After dropwise addition of 4.1 eq of perfluoro-t-butanol the reaction mixture was heated to reflux for 3 hours. The flask was then cooled down to -25 °C to allow complete precipitation of the product. The supernatant solvent was decanted off and the product was dried under high vacuum until constant weight resulting in a white solid in a yield of 70 % of theory.

The subsequent conversion to the PAG diphenyliodonium tetrakis(perfluor-t-butyloxy)aluminate (I-Al) was conducted in a straight-forward metathesis reactions according to a reported procedure.[56] The ion exchange was performed using the respective diphenyliodonium chloride as the cation source, and the prepared lithium tetrakis(perfluor-t-butyloxy)aluminate as the anion source.
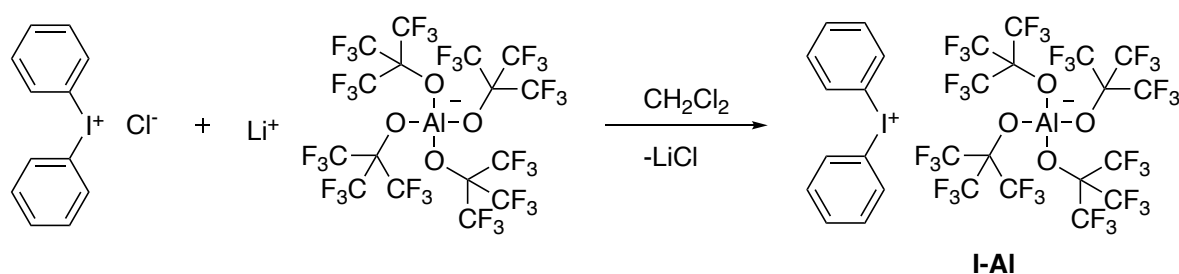
The synthesis was conducted in the orange light room under argon atmosphere conditions by adding diphenyliodonium chloride to lithium tetrakis(perfluoro-t-butyloxy)aluminate in dichloromethane solution. The reaction mixture was stirred at room temperature for 24 hours. After aqueous extraction and removal of the solvent the product was dried in high vacuum. I-Al was obtained as white powder in a yield of 82 % of theory. The purity was confirmed by TLC and elementary analysis.

As reported, the high electronic shielding and hydrolysis stability of the tetrakis(perfluoro-t-butyloxy)aluminate WCA makes it highly suitable for the cationic photopolymerization of epoxy monomers.[56] Still, the poor availability and high-priced production of the starting material perfluoro-t-butanol increases the costs of the resulting cationic photoinitiator for demanding applications. In an approach towards a cationic photoinitiator with only insignificantly lower reactivity and stability, however, improved cost-efficiency, the synthesis of the corresponding hexafluoroisopropanol-substituted alkoxyaluminate PAG was conducted.

1.2.2 Synthesis of diphenyliodonium tetrakis(hexafluoroisopropoxy)aluminate

Similar to the highly efficient tetrakis(perfluoro-t-butyloxy)aluminate-based PAG I-Al, the potentially more cost-efficient PAG diphenyliodonium tetrakis(hexafluoroisopropoxy)aluminate should be prepared. Based on a literature-known synthesis procedure the product should be obtained in the analogous way.[68] In comparison to the above preparation of lithium tetrakis(perfluoro-t-butyloxy)aluminate, the inherently lower pKa of hexafluoroisopropanol and the lower hydrolysis stability of the respective product demanded for elaborate synthesis conditions using Schlenk technique and the absolute exclusion of moisture throughout the whole preparation procedure.

Hence, hexafluoroisopropanol (HFIP) was distilled prior usage, reaching a water content below 20 ppm. The water content of absolute n-heptane was confirmed to amount below 20 ppm. All handling of starting materials was performed in a glove box to prevent contamination with moisture. Following the reaction, all work-up procedures were performed under argon protection.
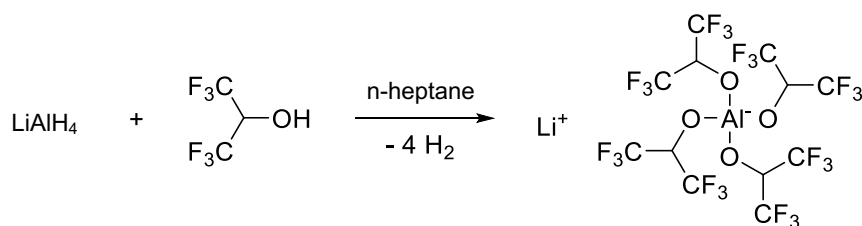
The purified and finely ground LiAlH$_4$ and absolute n-heptane were placed in a Schlenk tube fitted with a magnetic stirring bar, an intensive reflux condenser and a dropping funnel. The reflux condenser was cooled to -25 °C using a cryostat throughout the

synthesis. 10 eq hexafluoroisopropanol (HFIP) were added dropwise to give a vigorous reaction with formation of a white precipitate. After reaction at 80 °C overnight and complete precipitation at -20 °C, all liquids were removed by decantation and evaporation. The product was purified by sublimation resulting in a white solid in a yield of 90 % of theory.

The subsequent conversion of the lithium salt to the diphenyliodonium PAG was intended in a metathesis reaction according to a previously reported method.[56]
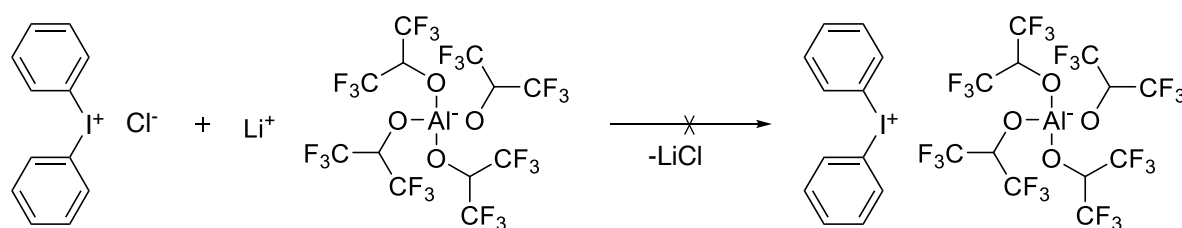
Several metathesis approaches in different solvents including absolute dichloromethane, absolute methanol and dimethylsulfoxide were conducted in the orange light room under argon atmosphere, as well as in the glove box. After addition of a solution of diphenyliodonium to the lithium alkoxyaluminate salt, the reaction mixtures were stirred at room temperature for 24 hours. No precipitation was observed and reaction control by TLC and NMR did not indicate conversion. It is assumed that the stronger ion pairing, lower electronic shielding and most probably the reported lower stability of the hexafluoroisopropanol-substituted WCA impedes the metathesis to the corresponding onium salt, resulting in no product.[63]

Following the successful preparation of the tetrakis(perfluoro-t-butyloxy)aluminate PAG I-Al, however, the suitability of this most reactive cationic photoinitiator for application in an epoxy monomer at elevated temperatures was investigated.

1.3 Thermal stability of cationic photoinitiation systems in BADGE

The investigations on cationic photopolymerization at elevated temperatures for Hot Lithography was conducted using three cationic photoinitiation systems. In order to reach highest reactivities, the WCA-based diphenyliodonium alkoxyaluminate PAG I-Al was used in formulation with epoxy monomer BADGE. Furthermore, the combination

of I-Al with the bisacylgermane-based free radical photoinitiator bis(4-methoxybenzoyl)diethylgermanium (BMDG) was considered as highly suitable system for free radical promoted cationic polymerization (FRPCP).

Based on the reported high reactivity in epoxy monomer BADGE, the commercially available tris(4-((4-acetylphenyl)thio)phenyl)sulfonium tetrakis(pentafluorophenyl)-borate (S-B) was included in these studies to serve as a benchmark for a highly reactive triarylsulfonium PAG with outstanding thermal stability in comparison to diphenyliodonium-based compounds.[56] The components of the respective photoinitiation systems are depicted in Figure 22.

BADGE

I-Al   **BMDG**

S-B
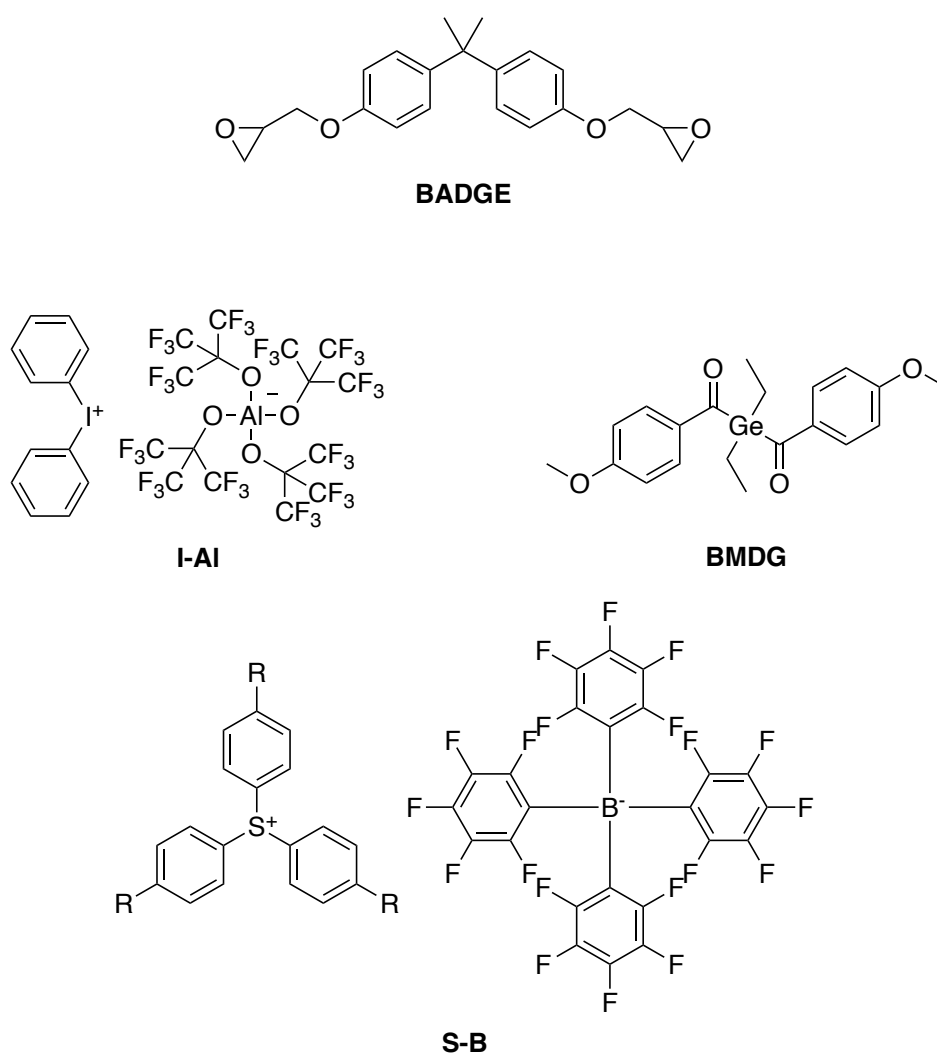
Figure 22: Structures of photoinitiation systems for cationic photopolymerization of bisphenol-A diglycidyl ether (BADGE): Diphenyliodonium tetrakis(perfluoro-t-butyloxy)aluminate (I-Al), bis(4-methoxybenzoyl)diethylgermanium (BMDG) and tris(4-((4-acetylphenyl)thio)phenyl)sulfonium tetrakis(pentafluorophenyl)borate (S-B; R = -S-Ph-COCH$_3$)

Based on the nature of the cation the diphenyliodonium PAG I-Al absorbs UV-light below 350 nm (λ_{max} = 227 nm) and withstands temperatures up to 210 °C as an isolated salt before thermal degradation. The triarylsulfonium PAG S-B is known for absorption up to 400 nm (λ_{max} = 318 nm) and shows thermal stability over 300 °C. The free radical photoinitiator bis(4-methoxybenzoyl)diethylgermanium (BMDG) has an absorption maximum of 420 nm and may be used to promote the cationic photopolymerization with a diaryliodonium PAG under visible light irradiation up to 490 nm. The general suitability of germy radicals for FRPCP has been described in literature, however, never under the aspect of cationic photopolymerization at elevated temperatures.[103]

The demands for a cationic photoinitiation system for Hot Lithography not only rely on the photochemistry of the PAG, but also on its inherent thermal stability for selective photopolymerization of the irradiated areas of the formulation. Therefore, the thermal stability was examined by simultaneous thermal analysis (STA), which combines differential scanning calorimetry (DSC) and a thermo-gravimetric analysis (TGA). By heating photoreactive formulations with a gradient of 10 K/min to temperatures of 300 °C, the thermal onset of polymerization indicating the thermal stability limit can be determined in the absence of light. Furthermore, the mass loss by evaporation and degradation of the formulation can be evaluated from the same measurement. In further investigations of photoinitiation systems in BADGE, the thermal resistance over a period of time at constant temperatures has been examined.

1.3.1 STA of cationic photoinitiation systems in BADGE

The selected photoinitiation systems based on a diphenyliodonium PAG (I-Al), a triarylsulfonium PAG (S-B) and an acylgermane-based FRPCP system (I-Al + BMDG) were firstly examined for their thermal stability in BADGE formulations. Therefore, STA measurements were conducted to examine the temperature range for subsequent cationic photopolymerizations at elevated temperatures.

The BADGE formulations contained 1 mol% S-B, 1 mol% I-Al, or 1 mol% I-Al in combination with 0.1 mol% BMDG, respectively. The analysis was conducted by heating the samples to 300 °C under nitrogen atmosphere using a heating rate of 10 K/min. Figure 23 shows the analysis of the three examined formulations in comparative display.

Figure 23: STA with temperature gradient of photoinitiation systems in BADGE formulations: 1 mol% I-Al in BADGE, 1 mol% I-Al and 0.1 mol% BMDG in BADGE, and 1 mol% S-B in BADGE; TGA dashed

In comparison to the pristine photoinitiators, the measurements show lower thermal stability when applied in formulations with reactive monomer BADGE. The diphenyliodonium PAG I-Al induced cationic polymerization upon thermal cleavage at temperatures above 137 °C, whereas the FRPCP formulation with free radical photoinitiator BMDG shows even lower thermal stability, with polymerization occurring exothermally at 121 °C. Only the triarylsulfonium PAG S-B shows inherently high thermal stability above 200 °C in BADGE formulations. The thermal onsets of polymerization are displayed in Table 3.

Table 3: Thermal onset of polymerization from STA measurements of I-Al, I-Al + BMDG and S-B in BADGE formulations

Photoinitiation system	Thermal onset of polymerization [°C]
I-Al	137
I-Al + BMDG	121
S-B	215

As seen from the onset temperatures, formulations of BADGE containing S-B can be photopolymerized selectively at high temperatures without interference by thermal

polymerization. However, photoinitiation systems based on diaryliodonium salts do not withstand temperature exceeding 120 °C, especially in combination with the free radical photoinitiator BMDG, which reduces the thermal stability significantly.

It is expected that the FRPCP photoinitiation system would not withstand temperatures of 120 °C over time. To still determine the thermal stability of respective systems over a period of time and to simulate the conditions of a print job in Hot Lithography, the formulations were investigated by STA at constant temperatures.

1.3.2 STA of cationic photoinitiation systems in BADGE at constant temperature

Following the determination of thermal stability limits in STA measurements with a temperature gradient, the evaluation of thermal stability over a period of time was conducted. These measurements should provide more information about the possibility for cationic UV-curing applications at elevated temperatures, such as Hot Lithography, in which the formulations need to be heated throughout the print job.

Based on the foregoing measurements, the formulations containing diphenyliodonium PAGs cannot be applied at temperatures above 120 °C without thermally induced cleavage of the photoinitiators. Therefore, their thermal stability at 100 °C was examined over 2 hours. In contrast, the thermally stable formulation of triarylsulfonium PAG S-B in BADGE was measured at a temperature of 140 °C, as this temperature represents the maximum designated working temperature in Hot Lithography.

The samples were prepared in analogy to formerly conducted STA analyses of photoreactive formulations. Using a heating rate of 10 K/min the samples were heated under nitrogen atmosphere to the designated temperature and kept for 120 min at 100 or 140 °C, respectively. The analyses are depicted in Figure 24.
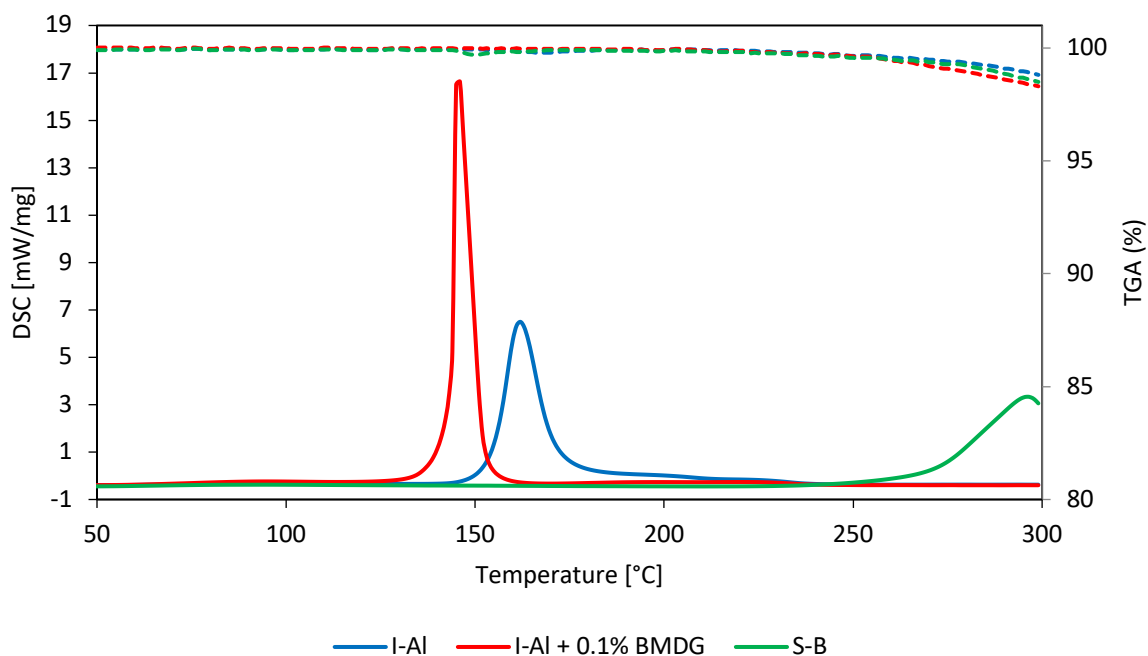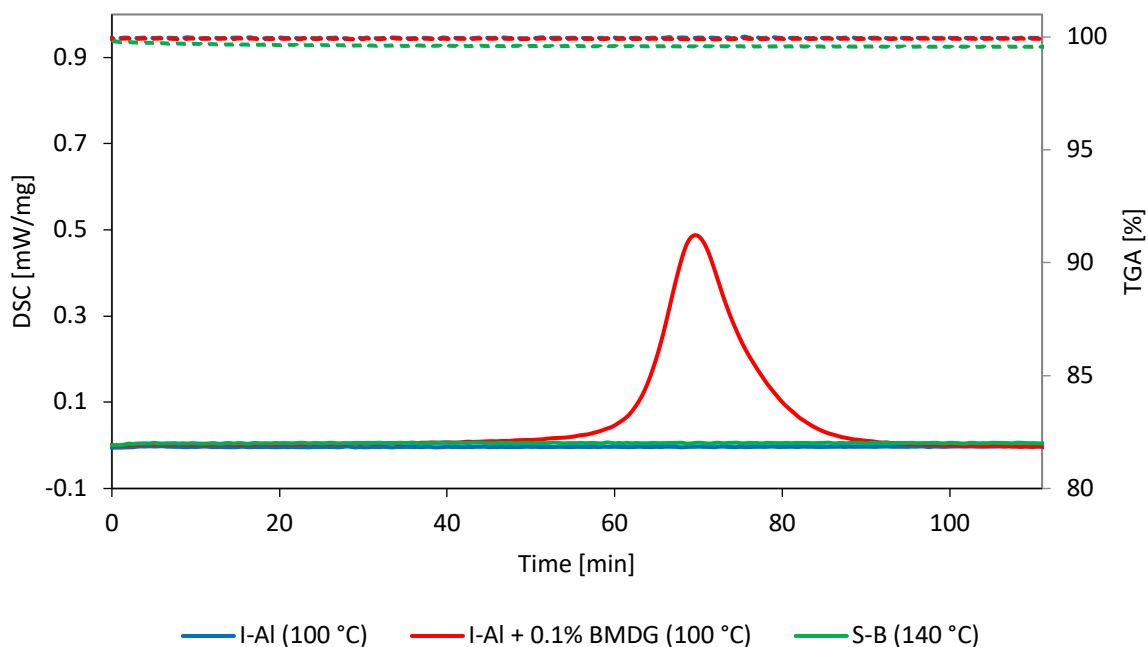
Figure 24: STA at constant temperatures of photoinitiation systems in BADGE formulations: 1mol% I-Al in BADGE, 1mol% I-Al and 0.1 mol% BMDG in BADGE, and 1 mol% S-B in BADGE; TGA dashed

The resulting DSC curves show the resistance to thermal polymerization for the formulations containing I-Al and S-B at the designated measurement temperatures. However, the FRPCP system containing I-Al and 0.1 mol% BMDG polymerized exothermally after 30 min at 100 °C.

The lower thermal stability is attributed to the readily occurring FRPCP reaction of BMDG with the iodonium salt I-Al. It is assumed that the decreased thermal stability correlates with increased reactivity of the FRPCP initiation system. To confirm this assumption and moreover investigate the reactivity in light-induced curing reactions, further examinations of the comparative systems were conducted by photo-DSC. Under variation of temperature and different light sources the applicability of these systems in conditions of Hot Lithography was investigated.

1.4   Photo-DSC studies of cationic photoinitiation systems in BADGE at elevated temperatures

The reactivity of comparative photoinitiation systems was investigated in photo-DSC analyses. The main focus of these measurements lay on the general enhancement of

reactivity in the cationic photopolymerization of BADGE at elevated temperatures. Moreover, the use of different sources of irradiation should allow the evaluation of the reactivity of the photoinitiation systems based on their selective absorption behavior. The diphenyliodonium PAG may only be directly activated at wavelengths below 350 nm, the triarylsulfonium PAG up to 400 nm, whereas the FRPCP system containing bisacylgermane-based BMDG absorbs up to 490 nm. Therefore, photo-DSC studies were conducted using broadband irradiation (320-500 nm) to activate all photoinitiators, 385 nm to activate only BMDG and S-B, as well as 400 nm to limit the absorption to BMDG only. The wavelengths of 385 and 400 nm furthermore correspond to the light-sources predominantly used in Hot Lithography applications, thus giving an application-near analysis of potentially suitable cationic photoinitiation systems.

For these measurements, the formulations of comparative photoinitiation systems were used and weighed into DSC crucibles analogously to foregoing STA measurements. According to the STA results, the measurements were conducted at 80, 100 and 120 °C. The irradiation intensity within all measurements was set to 3 W/cm^2 at the tip of the light-guide, corresponding to 130 mW/cm^2 on the sample.

In order to quantify the photo-DSC measurements by representative measures, several result parameters are extracted from the measurements after evaluation. The most significant results in consideration of the initiation ability and reactivity of a system are the heat of polymerization (by area), the time to reach the peak maximum (t_{max}), the peak height (h), which is in direct relation to the rate of polymerization (R_P), and the time to reach 95 % of the final conversion (t_{95}).

The conversion (C) is directly related to the detected heat of polymerization (area) and can be calculated via the heat of polymerization of BADGE monomer (80.6 kJ/mol per reactive group) using Equation 1.[56]

Equation 1: Calculation of the conversion by photo-DSC

$$C = \frac{\Delta H * M}{\frac{m}{m_{tot}} * \Delta H_0}$$

C   Conversion by photo-DSC [%]

ΔH Heat of polymerization by photo-DSC (area) [J/g]

M   Molecular weight of monomer [g/mol]

$\dfrac{m}{m_{tot}}$ Ratio of monomer mass to total mass [ ]

ΔH_0 Theoretical heat of polymerization of monomer [J/mol]

Furthermore, the rate of polymerization R_p is in direct relation to the obtained peak height considering the density and the theoretical polymerization heat of the monomer. It is calculated following Equation 2.

Equation 2: Calculation of the rate of polymerization

$$R_p = \frac{h * \rho}{\Delta H_0}$$

R_p Rate of polymerization [mol L^{-1} s^{-1}]

h Height of photo-DSC peak [W/g]

ρ Density of monomer [g/L]

ΔH_0 Theoretical heat of polymerization of monomer [J/mol]

Using this analytic setup, photo-DSC measurements were conducted with different sources of irradiation, namely broadband irradiation (320-500 nm), 385 nm LED and 400 nm LED at temperatures of 80, 100 and 120 °C.

1.4.1 Photo-DSC studies using broadband irradiation

In photo-DSC measurements using broadband irradiation (320-500 nm), the photoinitiation ability of the three systems should be evaluated at temperatures of 80, 100 and 120 °C. With this wavelength range, all photoinitiators in the formulations are cleaved by irradiation and allow for a general comparison of photoreactivity in high temperature photopolymerization. The photolysis of diphenyliodonium PAG I-Al and triarylsulfonium S-B is equally triggered under these conditions as the photolysis of the acylgermane-based free radical photoinitiator BMDG, giving a simultaneous direct and free radical-promoted cationic photopolymerization of BADGE.

Figure 25, Figure 26 and Figure 27 show the photo-DSC analyses at 80, 100 and 120 °C, respectively.
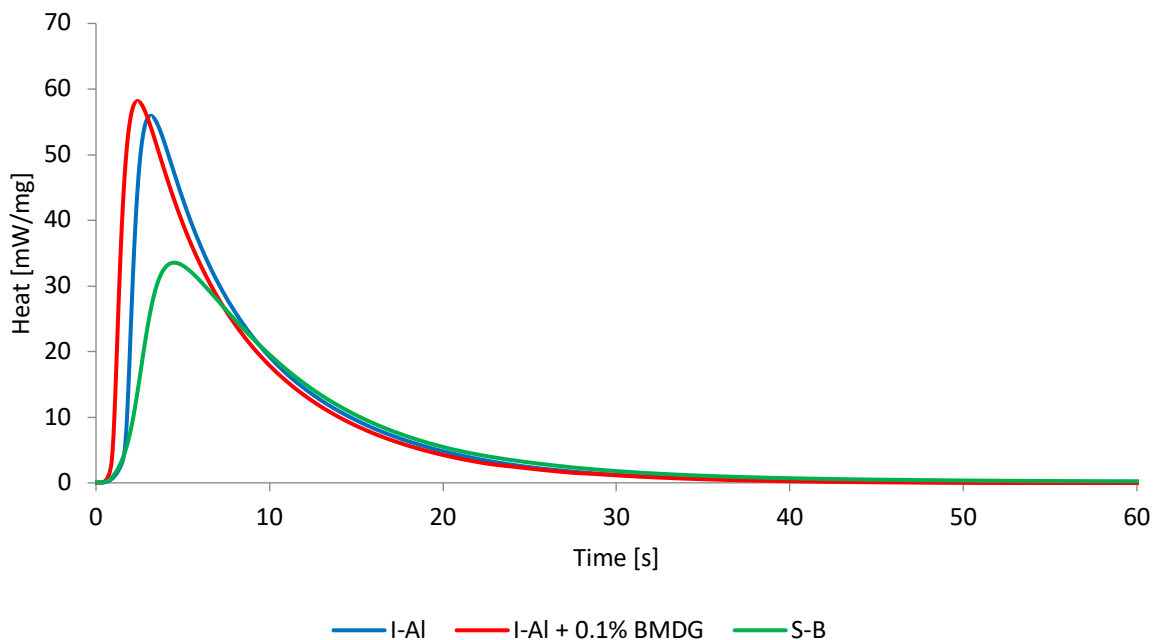
Figure 25: Photo-DSC analysis of photoinitiation systems in BADGE formulations at 80 °C using broadband irradiation (320 – 500 nm)
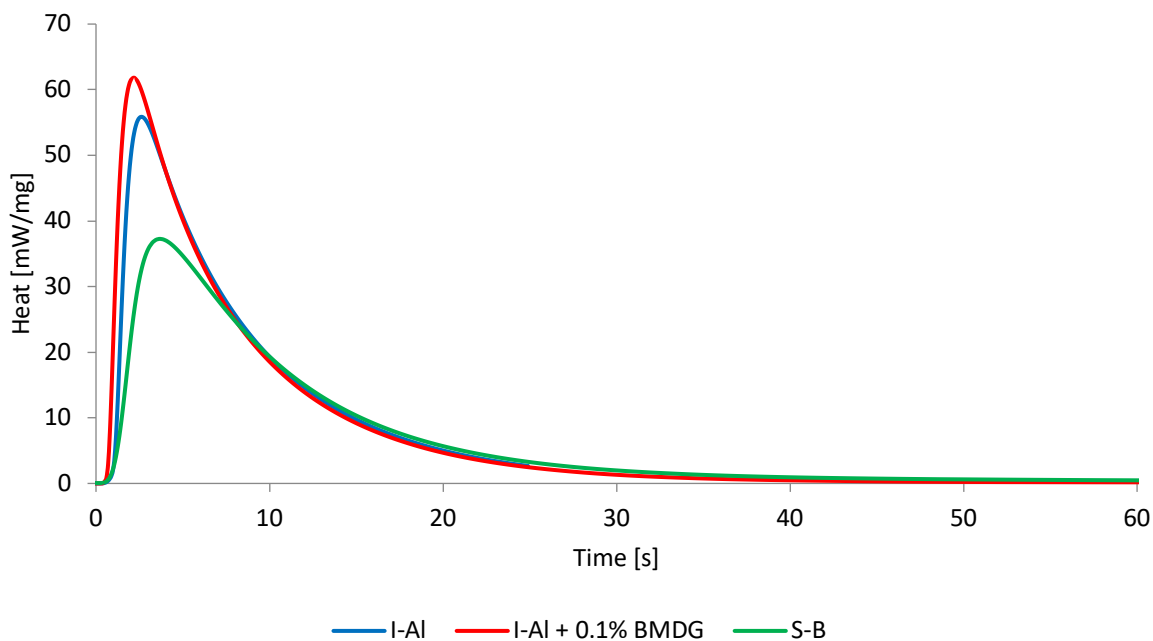
Figure 26: Photo-DSC analysis of photoinitiation systems in BADGE formulations at 100 °C using broadband irradiation (320 – 500 nm)
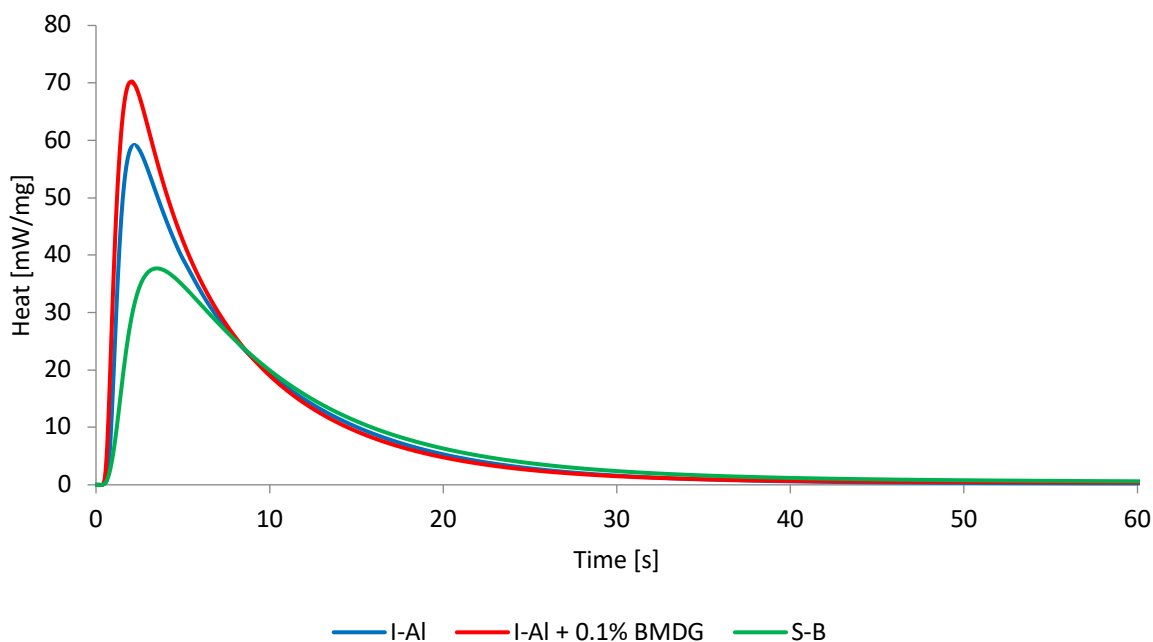
Figure 27 Photo-DSC analysis of photoinitiation systems in BADGE formulations at 120 °C using broadband irradiation (320 – 500 nm)

From the comparative display in above figures, the distinctly increased reactivity of the applied BADGE systems in comparison to photopolymerizations at room temperature is apparent. Although the monomer BADGE exhibits a low polymerization rate at ambient temperatures, the exothermicity of the cationic photopolymerizations above 80 °C reaches t_{max} below 5 seconds for each photoinitiation system. The promotion of the reaction using BMDG as bisacylgermane-based free radical photoinitiator is observed and leads to highest reactivities at all applied temperatures. The higher reactivities of both diphenyliodonium-based systems (I-Al and I-Al + BMDG) are represented by low t_{max}-values and high rates of polymerization R_p. The triarylsulfonium PAG S-B expectedly exhibits lower photoreactivity in reduced rates R_p and with higher t_{max}. The results of comparative photo-DSC analyses are displayed in Table 4.

Table 4: Photo-DSC results of photoinitiation systems in BADGE at elevated temperatures using broadband irradiation (320 – 500 nm)

Temperature (°C)	Formulation	C [%]	t_{max} [s]	R_P [mmol L^{-1} s^{-1}]	t_{95} [s]
80	I-Al	95	3.1	403	23
	I-Al + BMDG	>99	2.4	420	23
	S-B	87	4.5	242	48
100	I-Al	>99	2.6	402	25
	I-Al + BMDG	>99	2.2	444	25
	S-B	94	3.7	267	48
120	I-Al	>99	2.2	425	27
	I-Al + BMDG	>99	2.0	504	27
	S-B	>99	3.5	270	54

As seen from result parameters, the increased temperatures lead to rapid photopolymerizations with t_{max} values below 3 s using diphenyliodonium PAG photoinitiation systems. Furthermore, the photopolymerizations generate full conversion and high polymerization rates of up to 504 mmol L^{-1} s^{-1} at temperatures above 80 °C. The triarylsulfonium PAG S-B causes lower reactivity with t_{max} values above 3.5 s and distinctly lower polymerization rates. Still, conversions between 87 % at 100 °C and over 99% conversion at 120 °C are reached.

With these results of photo-DSC using broadband irradiation, the general reactivity difference of diphenyliodonium and triarylsulfonium PAGs at elevated temperatures is seen. Moreover, the efficient increase of reactivity using FRPCP by BMDG is evident.

Still, the comparative analyses do not consider the different absorption properties of these applied systems. To reflect on the light sources applied in modern LED-based systems and in SLA-based Hot Lithography, the photoinitiation systems were examined in photo-DSC using selective LED irradiation at 385 and 400 nm.

1.4.2 Photo-DSC studies using LED irradiation

Further studies by photo-DSC were conducted using not only elevated temperatures in cationic photopolymerization of BADGE, but also selective sources of irradiation, which are considered for the application of these photoinitiation system in Hot Lithography. As described earlier, Hot Lithography is applicable in an SLA-based system with 375 nm laser irradiation, or in a DLP setup with 405 nm LED irradiation. In order to examine the photoinitiation systems in a more representative way for application in Hot Lithography, photo-DSC analyses were conducted using LED light sources with narrow wavelength distribution. For the here performed studies using photo-DSC, LEDs with 385 and 400 nm were applicable. It must be considered that these LEDs not only provide narrow distributed irradiation wavelength, but also strongly decreased irradiation intensity of 16 mW/cm^2 (385 nm) and 9 mW/cm^2 (400 nm). Although a lower overall photoreactivity was expected, the photoinitiation systems were tested in comparative manner to evaluate the reactivity in dependence of the respective irradiation.

Furthermore, these studies aim for applicability and feasibility of cationic photopolymerization in Hot Lithography. Therefore, the diphenyliodonium alkoxyaluminate PAG I-Al was replaced by the abundantly applied hexafluoroantimonate-based PAG I-Sb ((p-octyloxyphenyl)phenyliodonium hexafluoroantimonate) comprising a diaryliodonium cation with equal thermal stability, absorption properties and reduction potential for FRPCP reactions, however, a significantly lower price.

I-Sb
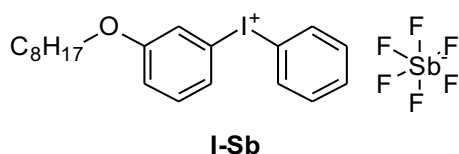
Within these comparative measurements using LED irradiation, a formulation containing solely diphenyliodonium PAG was excluded, as both LEDs of 385 and 400 nm exceed the absorption range of the onium cation and result in no photopolymerization.[56] Furthermore, the FRPCP system containing acylgermane-based free radical photoinitiator BMDG was also analyzed using a concentration of 1 mol% BMDG. As at higher wavelengths only the free radical photoinitiator is activated

and initiates the cationic polymerization via a redox reaction mechanism with the onium salt, equimolar concentrations of BMDG and I-Sb are expected to generate distinctly increased reactivity. Thus, the three comparative photoinitiation systems in monomer BADGE for photo-DSC analysis using LED irradiation consisted of 1 mol% I-Sb with 0.1 mol% BMDG, 1 mol% I-Sb with 1 mol% BMDG and the unchanged formulation of 1 mol% S-B.

1.4.2.1 Photo-DSC studies using 385 nm LED irradiation

The SLA system applied in Hot Lithography utilizes laser irradiation with 375 nm wavelength. To simulate the narrow wavelength distribution in photo-DSC measurements, a commercial 385 nm LED spotlight system with 16 mW/cm^2 peak output power was coupled with the photo-DSC system. In analogy to previous analyses, photo-DSC measurements at 80, 100 and 120 °C were conducted. BADGE formulations containing three photoinitiation systems of 1 mol% I-Sb with 0.1 mol% BMDG, 1 mol% I-Sb with 1 mol% BMDG, and 1 mol% S-B, respectively, were applied.

The photo-DSC analysis at 80, 100 and 120 °C are depicted in Figure 28, Figure 29 and Figure 30.
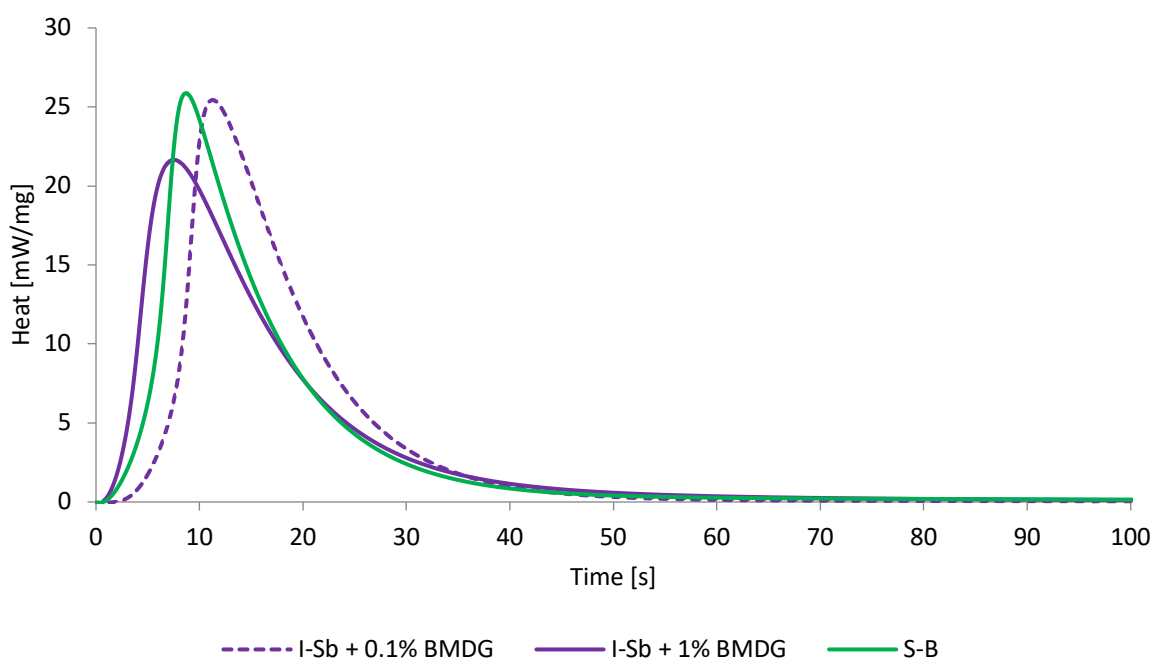
Figure 28: Photo-DSC analysis of photoinitiation systems in BADGE formulations at 80 °C using 385 nm LED irradiation
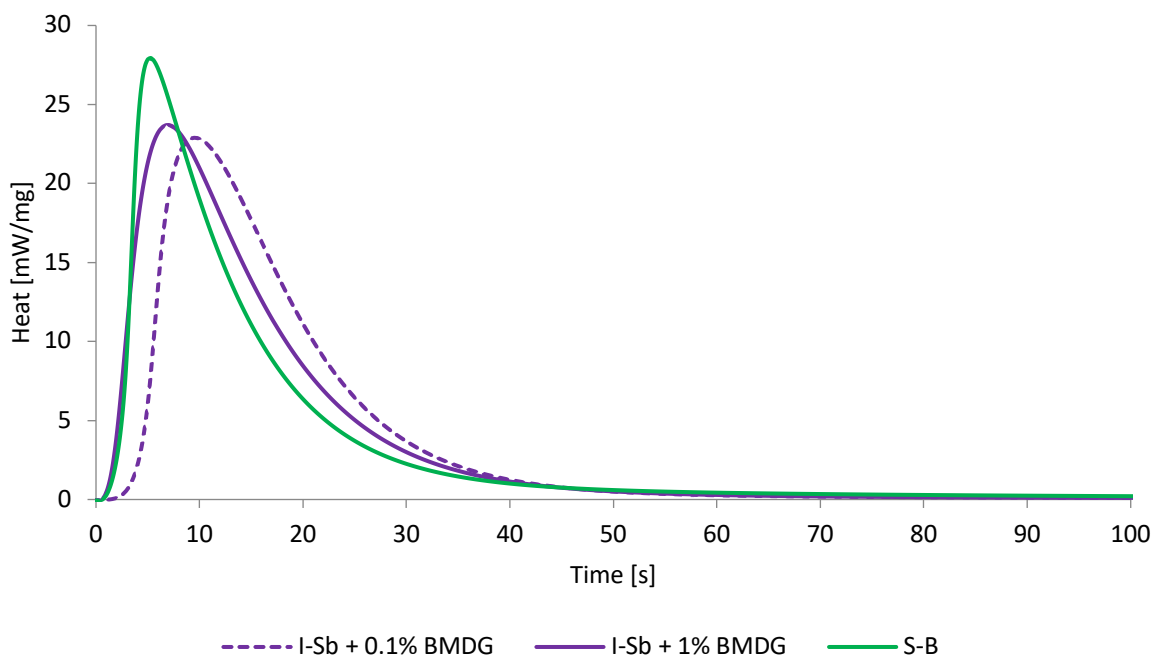
Figure 29: Photo-DSC analysis of photoinitiation systems in BADGE formulations at 100 °C using 385 nm LED irradiation
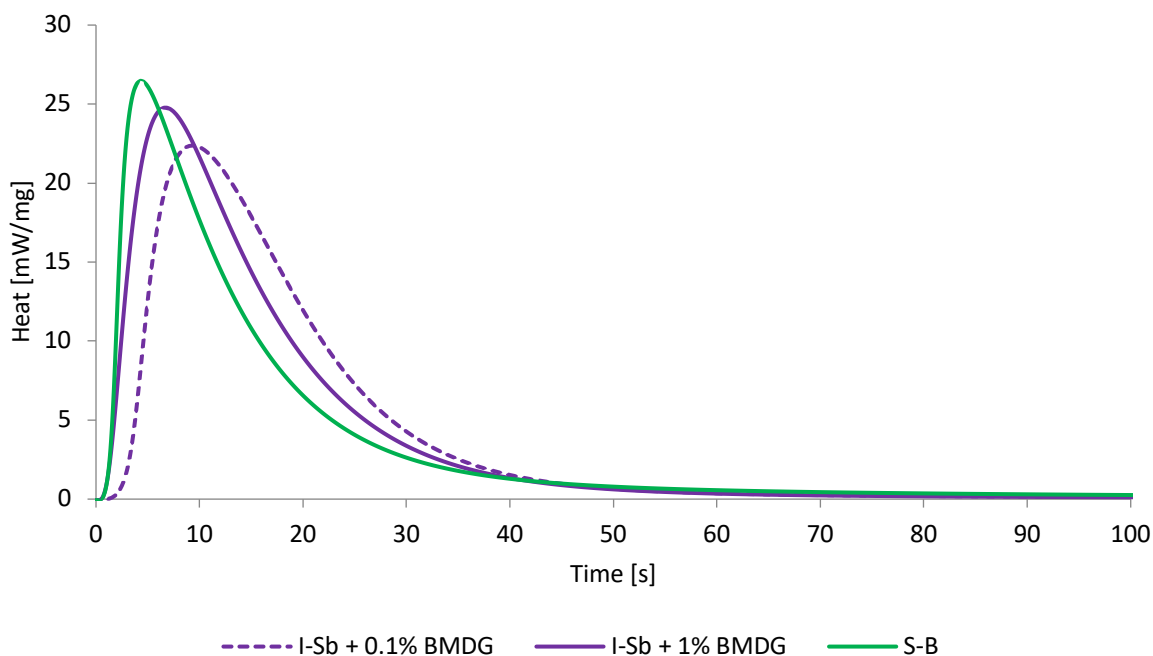
Figure 30: Photo-DSC analysis of photoinitiation systems in BADGE formulations at 120 °C using 385 nm LED irradiation

An overall decrease of photoreactivity was observed, which is attributed to the reduced irradiation intensity provided by the LED light source and the reduced reactivity arising from the limiting rates of the redox mechanism in FRPCP with iodonium PAG I-Sb. A

clear change in trends is observed in comparison to the photo-DSC analysis with broadband irradiation before. This is seen from the reactivity of the triarylsulfonium PAG S-B being in a comparable range as the FRPCP system based on I-Sb and BMDG at 80 °C. Expectedly, the absorption characteristics of the photoinitiators become more expressed with 385 nm irradiation. Although the higher irradiation wavelength exceeds the absorption maximum of S-B (λ_{max} = 318 nm), increasing the temperature to 100 and 120 °C overcomes the inadequate absorptivity and indicates the advantageous initiation potential of S-B, as photopolymerization occurs faster and in higher rates.

The numeric results of photo-DSC analyses using 385 nm LED irradiation are depicted in Table 5.

Table 5: Photo-DSC results of photoinitiation systems in BADGE at elevated temperatures using 385 nm LED irradiation

Initiator	T (°C)	t_{max} (s)	C (%)	R_p (mmol L^{-1} s^{-1})	t_{95} (s)
I-Sb + 0.1% BMDG	80	11.3	73	183	36
	100	9.6	83	165	43
	120	9.3	91	161	47
I-Sb + 1% BMDG	80	7.5	75	156	41
	100	6.9	84	171	42
	120	6.7	91	178	44
S-B	80	8.7	73	186	51
	100	5.2	82	201	65
	120	4.3	87	190	73

Despite the efficient FRPCP using BMDG with iodonium salts at higher wavelengths, the lowest t_{max} are observed using the triarylsulfonium PAG S-B in direct cationic photopolymerization at increased temperatures. The conversions of the photoinitiation systems are comparable and increase from 70 to 90 % with raised temperatures. As S-B also generates highest R_p values over 200 mmol L^{-1} s^{-1}, it is considered as a suitable photoinitiator for photopolymerizations using 385 nm irradiation.

1.4.2.2 Photo-DSC studies using 400 nm LED irradiation

In analogy to above photo-DSC studies at 385 nm LED irradiation, the measurements were conducted using 400 nm LED irradiation. Equally, elevated temperatures of 80, 100 and 120 °C were applied. It was expected that a wavelength of 400 nm would exceed the absorption range of triarylsulfonium PAGs, such as S-B, whereas the FRPCP system containing the free radical photoinitiator BMDG can still be initiated, as it absorbs up to visible light regions (λ_{max} = 420 nm).

The resulting photo-DSC plots of measurements at 80, 100 and 120 °C are displayed in Figure 31, Figure 32 and Figure 33.
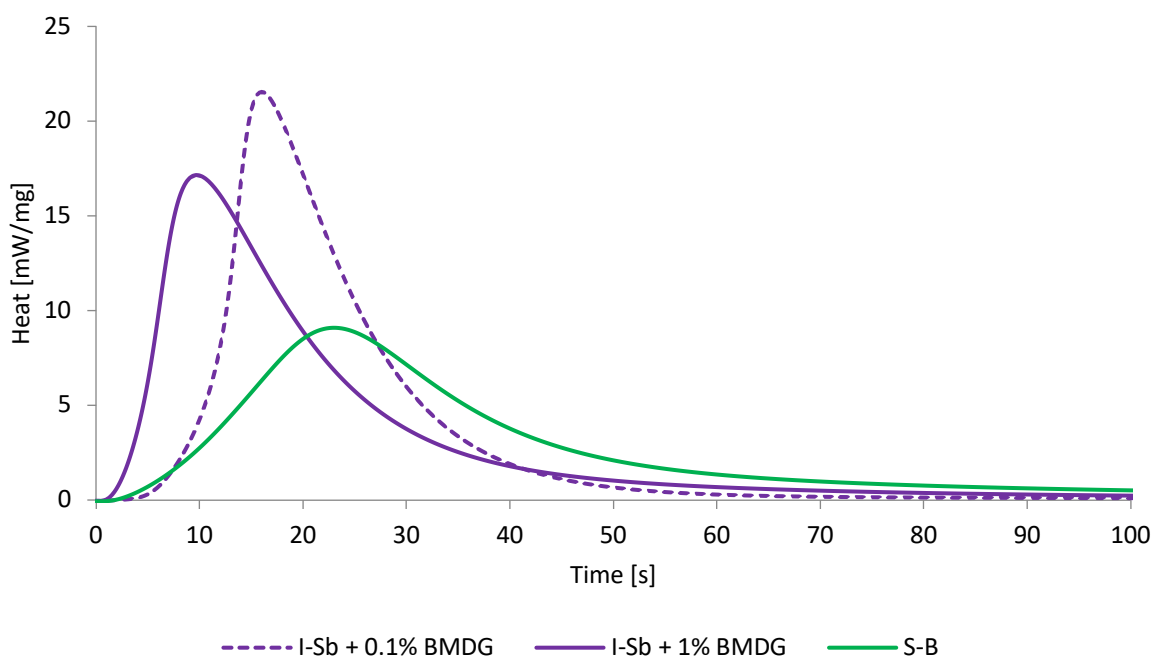
Figure 31: Photo-DSC analysis of photoinitiation systems in BADGE formulations at 80 °C using 400 nm LED irradiation
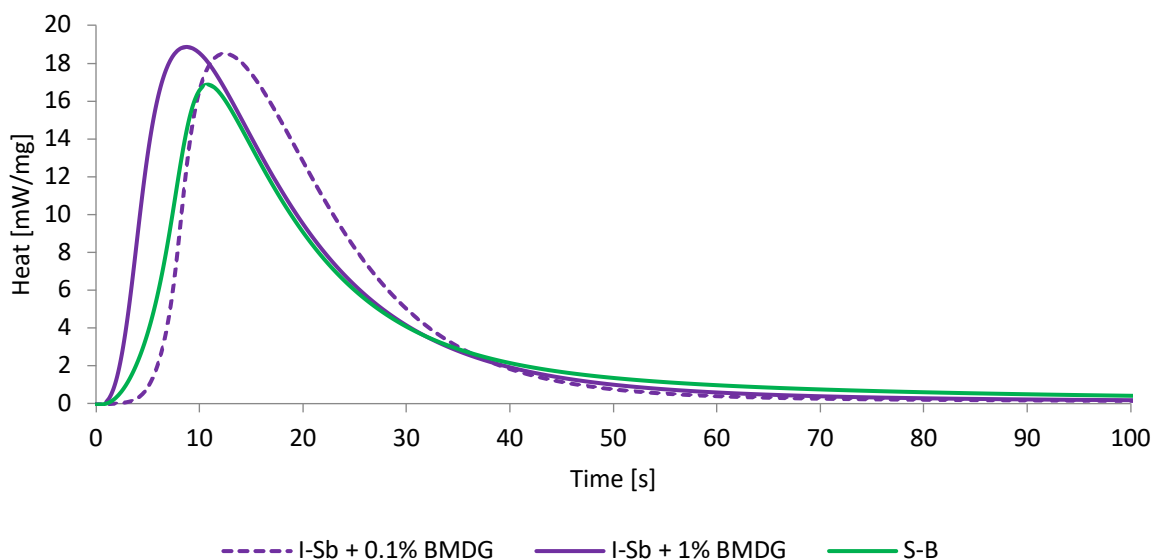
Figure 32: Photo-DSC analysis of photoinitiation systems in BADGE formulations at 100 °C using 400 nm LED irradiation
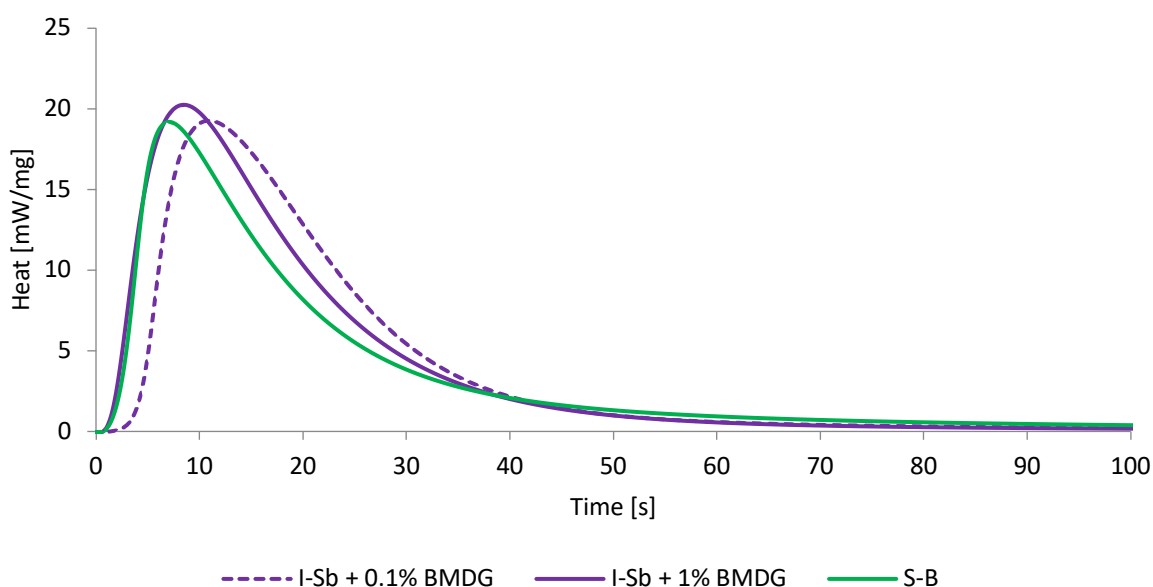
Figure 33: Photo-DSC analysis of photoinitiation systems in BADGE formulations at 120 °C using 400 nm LED irradiation

As seen from the analysis at 80 °C, the higher wavelength irradiation causes a distinct decrease in reactivity of the triarylsulfonium-based photoinitiator S-B in BADGE. In comparison to the FRPCP system, a low rate of polymerization R_p and a strong increase in t_{max} is observed. With increasing temperature to 100 and 120 °C, however, the loss in reactivity is compensated by thermal energy input. At 120 °C S-B induces the photopolymerization with lowest t_{max} and reaches overall conversion of 90 %.

The result parameters are displayed in Table 6.

Table 6: Photo-DSC results of photoinitiation systems in BADGE at elevated temperatures using 400 nm LED irradiation

Initiator	T (°C)	t_{max} (s)	C (%)	R_p (mmol L^{-1} s^{-1})	t_{95} (s)
	80	16.0	74	155	53
I-Sb + 0.1% BMDG	100	12.4	76	133	53
	120	10.9	90	138	65
	80	9.7	77	123	117
I-Sb + 1% BMDG	100	8.8	86	136	96
	120	8.5	93	146	76
	80	23.0	71	65	193
S-B	100	10.8	81	121	161
	120	7.1	90	138	154

From the above results it can be concluded that the photoinitiation system based on solely S-B shows beneficial reactivity behavior, given that sufficient thermal energy is provided to the cationic photopolymerization of BADGE. Although the FRPCP system gives greater reactivity at lower temperatures using 400 nm irradiation, the lack of polymerization rate can be made up for by thermally promoting the cationic photopolymerization at temperatures of 120 °C and higher.

From the conducted photo-DSC studies using 320-500 nm, 385 nm and 400 nm irradiation at elevated temperatures, the reactivity of photoinitiation systems for Hot Lithography was analyzed in the commonly applied epoxy monomer BADGE. Using broadband irradiation, the general temperature sensitivity of the cationic photopolymerization and photoinitiated free radical promoted cationic polymerization was evaluated. The photo-DSC studies with 385 and 400 nm irradiation were conducted as application-near photopolymerizations to test the selectivity of the investigated photoinitiation systems using comparable light sources as applied in Hot Lithography.

The generally high reactivity using the acyl-germane free radical photoinitiator BMDG in combination with a diphenyliodonium salt is seen. However, considering its low

thermal stability, the applicability in Hot Lithography is expected to be severely limited. Furthermore, when changing to LED light sources with narrow wavelength distribution, the advantageous reactivity of the FRPCP system becomes less distinct. In fact, at temperatures of 120 °C the triarylsulfonium PAG S-B exhibits equal or higher reactivity in 385 nm as well as 400 nm irradiation. With respect to its outstanding thermal stability even in presence of reactive monomer, the triarylsulfonium salt PAG investigated here shows clear benefits in cationic photopolymerization applications at elevated temperatures, which cannot be met by other cationic photoinitiation systems within these comparative studies. Clearly, a photoreactive system of BADGE containing S-B can be applied in Hot Lithography within the full working range up to 140 °C without undesired thermal polymerization, in order to further increase the reactivity.

In conclusion, cationic photopolymerization at elevated temperatures is best initiated using triarylsulfonium PAGs, given their inherent thermal stability, extended absorption range, high absorption coefficients and efficient photodecomposition. In combination with a weakly coordinating anion, the generation of strong acids with non-nucleophilic counterions provides sufficient reactivity for application in Hot Lithography of cationically polymerizable monomers.

Furthermore, this photoinitiation system for elevated temperatures sets the limits for investigation of cationic photopolymerization using monomers, which do not meet the requirements of fast propagation at room temperature and require extensive thermal input as a precondition for effective polymerization. Of the many classes of cationically polymerizable monomers, especially ring-opening reactive moieties provide unique characteristics and are often restricted by insufficient polymerization rates at room temperature. To address one of the most promising monomer classes of recent developments, the following part of this thesis will exclusively focus on the cationic ring-opening polymerization of 2-oxazoline monomers and the potential cationic photopolymerization thereof, which has not been investigated before.

2 Cationic photopolymerization of 2-oxazolines

2.1 State of the art

2.1.1 Applications of poly(2-oxazoline)s

The introduction of 2-oxazolines as monomers for thermally initiated cationic ring-opening polymerization (CROP) dates back to the 1960s, when first homopolymerization of 2-alkyl- and 2-aryl-2-oxazolines were reported.[106-110] Since then, the potential of the polymers arising from CROP of 2-oxazolines have been thoroughly investigated, especially due to their great versatility in polymer architecture. The ring-opening mechanism of a 2-substituted 2-oxazoline is depicted in Figure 34.
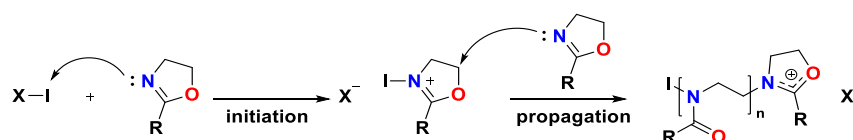
Figure 34. CROP mechanism of 2-oxazolines

The polymers resulting from CROP of 2-oxazolines are synthetic polyamides with facile accessibility to a broad range of polymer structures given by the 2-oxazoline substituent on the one hand, and their ability for copolymerization in a living cationic polymerization mechanism on the other.[111] Depending on the substituent, poly(2-oxazoline)s with hydrophilic, hydrophobic or fluorophilic side groups are obtained. Hence, the living cationic polymerization mechanism offers facile access to copolymers by sequential addition of respective monomers to yield well-defined block, gradient, and statistical copolymers.[112]

Over the past decades, poly(2-alkyl/aryl-2-oxazoline)s (PAOx) have gained significant attention for their promising application in various fields. Soon after their discovery, PAOx have been applied in coatings and coating-related applications, e.g. pigment dispersants in inks. However, as batch polymerization of PAOx by thermal polymerization methods takes from hours to days, they did not find widespread application in the industrial sector.[113] More prominently, PAOx have been deeply investigated for advanced surface modification, as addressed by Kobayashi et al. in

many different applications. One basic application is given by copolymer surfactants, in which a hydrophilic block based on 2-methyl-2-oxazoline (MeOx) or 2-ethyl-2-oxazoline (EtOx) is copolymerized with hydrophobic blocks of higher 2-oxazoline monomers.[114] Further applications of polymer surfactants cover block copolymer microligands for micellar catalysts,[115], emulsifiers for styrene-water polymerization,[116] as well as surface modification of poly(methacrylate) and poly(styrene) films.[117] Moreover, 2-oxazoline-based copolymers were used for hydrophilic backbones of non-ionic hydrogels, for organic-inorganic polymer hybrid particles, polymeric compatibilizers and for the investigation of self-assembling supramolecular structures.[109]

Mostly due to the introduction of microwave-assisted high temperature and high pressure preparation methods in the early 2000s, the synthesis was accelerated by a factor up to 350.[118] Hence, the inherently low rate polymerization of 2-oxazoline monomers became accessible for broader utility, especially in biomedical research.[113, 119-121] The one-pot synthetic procedures enabled accurate control over a wide range of polymer architectures, monomer compositions and distribution, as well as polymer properties such as the hydrophilic/hydrophobic ratios.[111] Especially hydrophilic polymers of MeOx and EtOx show high biocompatibility and no bioaccumulation, as well as inherent "stealth" behavior *in vivo*, which confirms the absence of immunologic adverse effects in living systems.[122, 123] The inherent biocompatibility is reasoned by the structural similarity to poly(amino acids) and led to the perception of PAOx as "pseudo-peptides".[111]
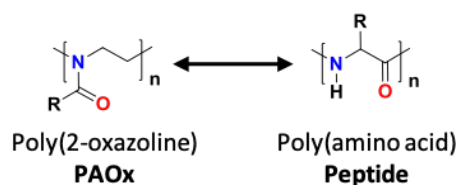
Figure 35: Poly(2-alkyl/aryl-2-oxazoline)s (PAOx) as "pseudo-peptides" [111]

Despite poly(ethylene oxide) (PEO) being the "gold-standard" for application in biomaterials, PAOx systems provide higher versatility and tunability for non-fouling and non-adhesive surfaces, biomedical analysis methods, protein and drug conjugation and polymer-based drug delivery.[124-127] In comparative studies with PEO-based biomaterials, the blood compatibility, adsorption of proteins and bacteria, cell viability

as well as the biocompatibility of corresponding hydrogels was found equal or better for poly(MeOx) and poly(EtOx).[111] Especially due to the significant efforts on drug delivery systems in oncological research, much effort has been spent on the development of 2-oxazoline-based systems to date.

Another completely new research field emerged with the discovery that PAOx copolymers exhibit more tunable lower critical solution temperatures (LCST) than comparable systems, which opened the gate to thermoresponsive polymers in hydrogels and in solution.[111]

Despite the enhanced accessibility by microwave-assisted methods and promising structural characteristics arising from their polyamide backbones, PAOx polymers have not been considered for materials to a great extent. The limitations of PAOx for their utility as structural polymers are given by their high costs in comparison to commodity polymers. Most reported applications in structural materials are restricted to modifiers and functional poly(2-oxazoline) precursors that do not yield polymer networks via a cationic polymerization mechanism. Primarily due to beneficial miscibility, the use of various linear PAOx homo- and copolymers as compatibilizers and surface modifiers in composites with commodity polymers such as polyamide (Nylon 6), poly(vinyl alcohol) (PVA), poly(vinyl chloride) (PVC), poly(vinylidene fluoride), polystyrene, poly(acrylonitrile), poly(acrylic acid), poly(α-hydroxystyrene) and poly(ethylene-co-methacrylic acid) has been shown.[110]

However, as reported by Mülhaupt et al., the CROP of α,ω-bis(2-oxazolinyl)-substituted oligo(tetrafluoroethylene)s shows promising physical properties of corresponding PAOx thermosets. The resulting polymers give glass transition temperatures between 72 and 95 °C and shrinkage extents between 7 and 8 % after CROP of low molecular difunctional 2-oxazolines. Resulting from the polyamide backbone, thermal stabilities up to 350 °C are reported for these cross-linked polymers.[128] Moreover, linear PAOx with hydrocarbon side chains show inherent thermal stability of at least 300 °C.[129, 130] In correlation with the length of alkyl substituent, linear PAOx polymers give respective glass transition temperatures between 80 °C for poly(MeOx) and 10 °C for poly(HexOx), due to increasing flexibility of polymer side chains. In polymers of 2-butyl-2-oxazoline and higher derivatives, increasing degrees of crystallinity generate melting points around 150 °C.[131] Although

only few investigations on the mechanical properties have been conducted, the elastic modulus of monofunctional homologues showed the decreasing mechanical strength with increasing alkyl chain length of PAOx homopolymers.

2.1.2 Cationic ring-opening polymerization of 2-oxazolines

As described, the introduction of microwave (MW)-assisted CROP of 2-oxazolines greatly enhanced the preparation of PAOx. Consequently, investigations of polymerization kinetics and rate-defining effects of both monomers and initiators led to better understanding of the CROP reaction.[118, 132]

2-Oxazoline CROP is initiated by exothermal nucleophilic attack of the cyclic imino ether to strong electrophiles. Besides organic and inorganic Lewis acids,[106-108] acid halides,[133, 134] silyl halides,[135, 136] chloroformates,[137] iodine[138, 139] and supercritical CO_2,[140, 141] most importantly tosylates,[142] nosylates[143] and triflates[144] are used as extremely electrophilic initiators.[145] At room temperature, initiation occurs only with most electrophilic initiators, such as methyl triflate (MeOTf), which reasons their predominant use as thermal initiators.[146] Figure 36 depicts the structures in order of reactivity in the initiation of CROP of 2-oxazoline monomers. (MeOTs < MeONs < MeOTf).
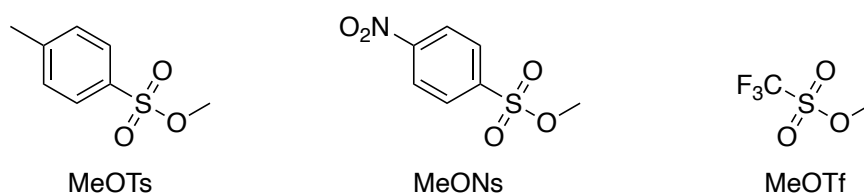
Figure 36: Thermal initiators for CROP of 2-oxazolines

Despite being a ring-opening reaction, the CROP of 2-oxazolines is thermodynamically driven by the isomerization of the cyclic imino ether into a more stable tertiary amide, whereas the release of ring-strain has a negligible effect on the polymerization.[145] After activation of the 2-oxazoline nitrogen atom by alkylation, the liberated counterion determines the rate of propagation by an equilibrium of the active cationic oxazolinium species and the dormant covalent species (Figure 37).[146, 147] Upon further addition of monomer molecules to the active cationic initiating species, propagation of the chain growth occurs. In analogy to the initiation, the equilibrium of active cationic and

dormant covalent species decisively influences the propagation rate, which is determined by the non-nucleophilicity of the counterion (tosylate < nosylate < triflate) and the nucleophilicity of the respective 2-oxazoline monomer.[145] The degree of non-nucleophilicity of the counterion reduces the recombination with the propagating chain end and shifts the equilibrium towards the active cationic species, whereas a high nucleophilicity of the monomer enhances the propagation by attack to the cationic chain end and facilitates propagation. Figure 37 illustrates the CROP mechanism of a 2-oxazoline initiated by methyl tosylate with indicated cationic-covalent equilibria of initiating and propagating species.
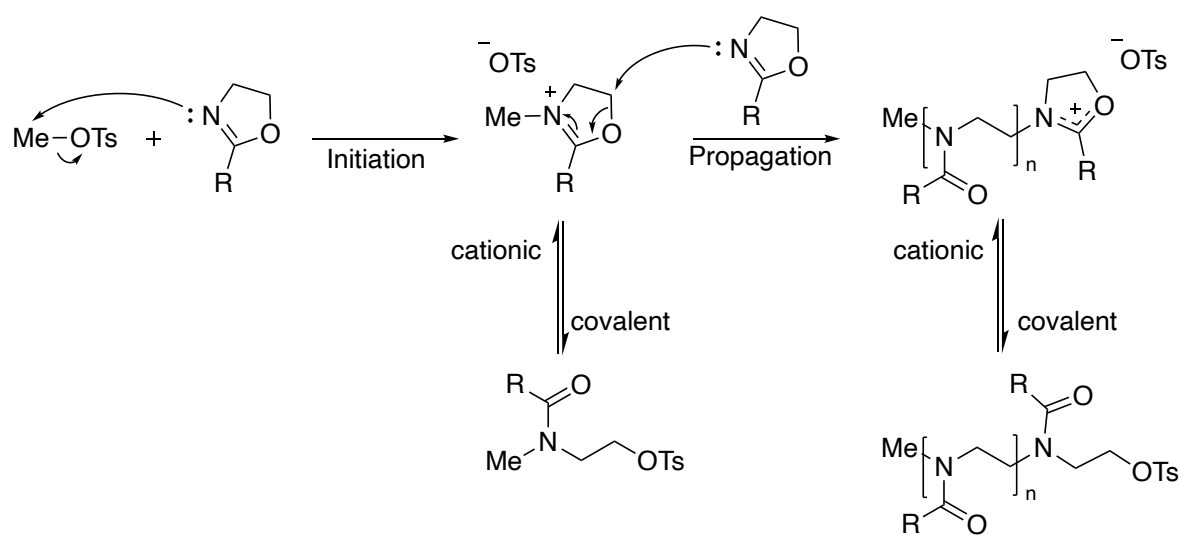
Figure 37: CROP mechanism of 2-oxazolines with cationic-covalent equilibrium[145]

Due to the steric and electronic interaction with the reactive moiety, the substituents have a complex influence on the initiation and propagation rates. Due to the steric hindrance of propagation, 2-oxazolines with substituents in 4- and 5-position exhibit significantly lower reactivities. Thus, the most common method for preparing a whole variety of different poly(2-oxazoline)s is based on substitution in 2-position, as it is easily accessible. However, the substituent in 2-position has a strong impact on the reactivity during polymerization, which is dependent on two effects: The extent of nucleophilicity on the 2-oxazoline nitrogen atom on the one hand (for initiation), and the influence on the partial positive charge of the oxygen-neighbored carbon atom in 5-position (for propagation). Electron-donating substituents provide high electron density on the nitrogen-atom, which enhances the nucleophilicity of the imine functionality and increases the initiation rate constant k_i. At the same time, high

electron density on the oxygen atom reduces the cationic character of the oxygen-neighbored carbon atom in 5-position, decreasing the propagation rate constant k_p for subsequent nucleophilic attack. Provided that highly electrophilic initiators are used, the overall polymerization rate is dominantly governed by the propagation rate constant k_p, as reflected in the polymerizability of respective 2-oxazoline monomers.[145, 148]

Within the class of alkyl-substituted monomers the decrease of k_p from methyl- to ethyl- to iso-propyl-substituted 2-oxazolines is observed due to increasing inductive electron-donating character (MeOx (146) > EtOx (105) > iPrOx (47.8) [x 10^{-3} L mol^{-1} s^{-1}]).[145] For linear alkyl substituents ranging from ethyl to n-nonyl it was found that the side-chain length has only minimal influence on k_p. However, to indicate the complexity of the electronic interaction it is noted that perfluoroalkyl substituents show a reduction of overall reactivity, as the excessive electron withdrawing effect leads to diminished nucleophilicity on the reactive moiety and obstructs efficient polymerization due to crucially suppressed k_i.[149]

In comparison to 2-alkyl-2-oxazolines, aryl-substituted 2-oxazolines generally show three-times lower k_p (PhOx 35.8 x 10^{-3} L mol^{-1} s^{-1}).[150, 151] The stabilization of the oxazolinium species by the aromatic system leads to partial compensation of the positive charge by the exhibited +M effect.[118, 152] Furthermore, the addition of electron-withdrawing or electron-donating para-substituents further influences the k_p accordingly, in the order Cl > H > OMe. The electron-withdrawing chlorine atom in para-position promotes the cationic character of the propagating species, whereas the electron-donating methoxy group further reduces k_p.[148]

The reactivity of a 2-oxazoline-based system is, thus, confined by the low propagation rates of the monomers at room temperature. Therefore, procedures in MW-assisted syntheses of PAOx are based on the thermal initiation of the CROP reaction at temperatures between 100 and 140 °C.[94, 98] It was shown that exclusively the increased thermal energy input is decisive for significantly reduced reaction times and high efficiency in MW-assisted polymerizations.[153] Furthermore, the propagation in high temperature and high pressure synthesis is supported by the use of solvents such as acetonitrile, dimethylacetamide, chlorobenzene and sulfolane, which not only provide good solubility but also stabilize the cationic propagating chain-end.[154 145]

In summary, the efficient propagation of the CROP reaction is determined by the suppression of termination processes and the stabilization of the living cationic species. Hence, also the use of weakly coordinating anions (WCAs) to suppress termination reactions and to shift the equilibrium to the cationic species have emerged lately. Different to former systems for alkylation, acylation and silylation of the 2-oxazoline-based nitrogen atom, the initiating species of WCA-based initiators aim for the initiation of CROP by direct protonation. The direct protonation by the free para-toluenesulfonic acid,[155] or by undesired side products of established initiation systems was shown.[156] Moreover, Wu et al. reported the direct protonation of the nucleophilic nitrogen atom by the mild Brønsted acid diphenylphosphate (DPP).[157] Spectroscopic investigations confirmed that the initiation of the polymerization of 2-ethyl-2-oxazoline (EtOx) is taking place via direct protonation of the nitrogen atom.

Based on early reports of the use of superacid esters as potent initiators for the CROP of tetrahydrofuran,[158] Krossing et al. evaluated the strong Brønsted acid $[H(OEt_2)_2]$-$[Al(OC(CF_3)_3)_4]$ for efficient initiation of 2-oxazolines and showed its advantageous initiation ability in comparison to methyl tosylate.[159] The reported method utilizes the direct protonation by the oxonium acid $[H(OEt_2)_2]^+$ to polymerize EtOx, tButOx and copolymers thereof at 140 °C in solution. Clearly, the alkoxyaluminate WCA supports the suppression of covalent mechanisms during the reaction.

The approach of direct protonation and WCA-based enhancement of the CROP of 2-oxazolines gives rise to the assumption that cationic photopolymerization is possible by direct protonation from onium salt PAGs. The hypothetical cationic photopolymerization of 2-oxazolines may give access to the fast polymerization of 2-oxazoline monomers in formerly reported applications and desirable bulk curing of PAOx materials upon activation by light. Given that sufficient thermal energy input is provided to the inherently low reactive 2-oxazoline monomers, the CROP can be decisively promoted to enable direct cationic photopolymerization.

In consideration of foregoing investigations of photoinitiation systems for cationic photopolymerization at elevated temperatures, the use of thermally stable triarylsulfonium PAGs may enable the UV-curing of 2-oxazolines, as well as potential application in Hot Lithography at temperatures up to 140 °C.

2.2 Synthesis of a triarylsulfonium alkoxyaluminate PAG

The foregoing studies on initiation systems for cationic photopolymerization in Hot Lithography showed the general advantages of triarylsulfonium PAGs in comparison to diphenyliodonium PAGs, as well as free radical promoted cationic polymerization (FRPCP) systems in combination with a bisacylgermane photoinitiator. The requirements of cationic photopolymerization at high irradiation wavelengths and elevated temperatures can only be met by the use of triarylsulfonium PAGs, which comprise inherent thermal stability, extended absorption range, high absorption coefficients and efficient photodecomposition. The reference triarylsulfonium PAG S-B showed promising polymerization behavior in epoxy monomer BADGE at elevated temperatures. However, the aimed cationic photopolymerization of 2-oxazolines was expected to show high temperature sensitivity, as the polymerizability at room temperature is obstructed by low propagation rates in comparison to epoxy monomers. Therefore, an alkoxyaluminate-based triarylsulfonium PAG should provide the lowest possible nucleophilicity for investigations of UV-induced CROP of 2-oxazolines at elevated temperatures.

The preparation of lithium tetrakis(perfluoro-t-butyloxy)aluminate starting from purified lithium aluminum hydride and the corresponding fluorinated alcohol was conducted according to the synthesis methods described in section 1.2.1 The synthesis of the alkoxyaluminate PAG tris(4-((4-acetylphenyl)thio)phenyl)sulfonium tetrakis(perfluor-t-butyloxy)aluminate (S-Al) was conducted in a straight-forward metathesis reactions according to a reported procedure. [56]

In analogy to the preparation of the respective diphenyliodonium PAG (I-Al), S-Al was synthesized from the corresponding triarylsulfonium chloride and lithium tetrakis(perfluoro-t-butyloxy)aluminate.
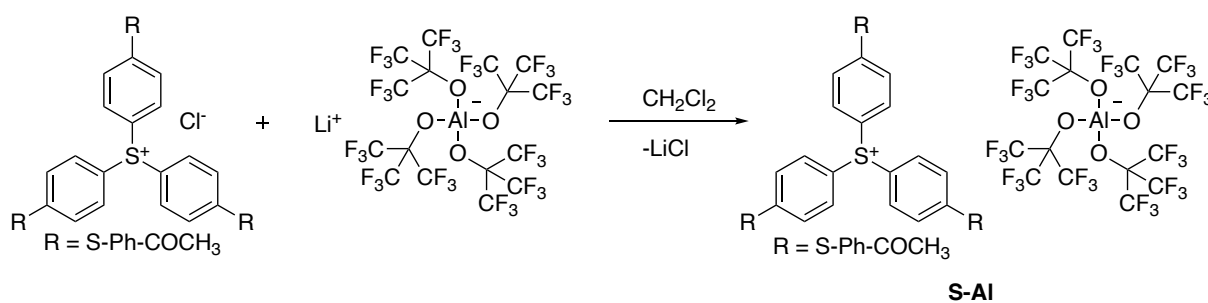
S-Al

The synthesis was conducted in the orange light room and under argon atmosphere conditions by adding a solution of tris(4-((4-acetylphenyl)thio)phenyl)sulfonium chloride in dichloromethane to a solution of lithium tetrakis(perfluoro-t-butyloxy)aluminate in dichloromethane. The reaction mixture was stirred at room temperature for 24 hours. Subsequently the reaction mixture was extracted with water and the organic phase filtered over silica. After removal of the solvent the product was dried in high vacuum at room temperature. S-Al was obtained as white powder in a yield of 80 % of theory. The purity was confirmed by TLC and elementary analysis.

2.3 Preceding investigations of photoinitiation systems for CROP of 2-oxazolines

The UV-initiated CROP of 2-oxazolines by direct protonation from onium salt PAGs was firstly tested in preceding investigations using conditions, which are based on reported microwave-assisted procedures.[118, 129, 132, 150, 153] As 2-oxazoline monomers suffer from poor reactivity at room temperature, polymerizations using thermal initiators are commonly applied at elevated temperatures of 140 to 160 °C. It was expected that 2-oxazolines would react in very low rates also in a light-induced polymerization using onium salt PAGs at room temperature, thus, making equally high temperature necessary for efficient photopolymerization. Furthermore, most described microwave-assisted syntheses are conducted in solvents that support the cationic character of the propagating species. Also the low solubility of e.g. polyMeOx in the monomer MeOx itself is reported.[154] However, as a solvent-free process represents a key benefit of photopolymerization reactions and UV-curing applications, the here reported studies were conducted using bulk formulations.

In correlation to the investigations of initiation systems for cationic photopolymerization at elevated temperatures described in section 1, a suitable photoinitiation system had to be established for the examination of a photoacid-initiated CROP of 2-oxazolines using a set of diphenyliodonium and triarylsulfonium PAGs by STA and photo-DSC. As most commercially available 2-alkyl-2-oxazoline monomers are low molecular weight compounds with high volatility, aromatic 2-phenyl-2-oxazoline (PhOx) was selected for preceding investigations regarding the cationic photopolymerization of 2-oxazolines in general.

As seen with epoxy monomer BADGE before, photoreactive mixtures exhibit individual thermal stability limits depending on the type of onium salt and the nature of the respective monomer. Therefore, STA measurements were conducted with a set of diaryliodonium and triarylsulfonium PAGs in PhOx to evaluate the applicable temperatures for selective cationic photopolymerization.

2.3.1 STA of diaryliodonium and triarylsulfonium PAGs in PhOx

In foregoing STA studies, the thermal stability of diphenyliodonium and triarylsulfonium PAGs was investigated in the monomer BADGE, as described in section 1.3. In analogy to these determinations, the thermal stability of a set of diphenyliodonium and triarylsulfonium PAGs was investigated in the cationically polymerizable monomer 2-phenyl-2-oxazoline (PhOx). The monomer-to-initiator ratio was chosen as [M]/[I] = 60 based on thermal CROP procedures described in literature aiming for a corresponding degree of polymerization of 60 in microwave-assisted preparations.[152, 153, 160, 161] Consequently, a concentration of 1.67 mol% was used in the bulk formulations of PhOx for the conducted studies.

The STA analyses included two diaryliodonium PAGs, namely the synthesized diphenyliodonium tetrakis(perfluoro-t-butyloxy)aluminate (I-Al) and the commercially available (p-octyloxyphenyl)phenyliodonium hexafluoroantimonate (I-Sb). Furthermore, the synthesized tris(4-((4-acetylphenyl)thio)phenyl)sulfonium tetrakis(perfluoro-t-butyloxy)aluminate (S-Al), as well as the commercially available tris(4-((4-acetylphenyl)thio)phenyl)sulfonium salts of the WCAs tetrakis(pentafluorophenyl)borate (S-B) and tris((trifluoromethyl)sulfonyl)methanide (S-C) were included in this analysis. It is mentioned that the three triarylsulfonium PAG S-Al, S-B and S-C comprise the same cation, which exclusively determines their thermal stability. The substances are depicted in Figure 38.

Figure 38. Diaryliodonium (I-Al, I-Sb) and triarylsulfonium (S-Al, S-B, S-C; R = -S-Ph-COCH$_3$) salt PAGs for cationic photopolymerization at elevated temperatures

To measure the thermal stability of diaryliodonium and triarylsulfonium PAGs in monomer solution, STA was designated to provide information about the onset of polymerization (by DSC) as well as the thermogravimetric mass loss (by TGA) due to evaporation of monomer. Analyses were performed in a range of 25 to 300 °C using a ramp of 10 K/min. In comparative display Figure 39 shows the measurements of formulations of the PAGs I-Al, I-Sb, S-Al, S-B and S-C in PhOx.

Figure 39. STA analysis of 2-phenyl-2-oxazoline with I-Al, I-Sb, S-Al, S-B and S-C (TGA dashed)

The analysis clearly shows the onset of polymerization by thermal cleavage of the PAGs at 120 °C for I-Al, and 130 °C for the antimonate-based I-Sb. Starting from 120 °C also a distinctive thermogravimetric loss by evaporation of the monomer is observed, which occurs increasingly with the thermal onset of polymerization. By the exothermicity of cationic ring-opening polymerization (CROP) the evaporation seems further induced. This assumption is supported as the weight loss occurs at the same temperature as the onset of polymerization occurs. Due to the earlier onset of polymerization for I-Al, the weight loss reaches a plateau at 6 % when sufficient conversion is achieved, whereas for I-Sb a weight loss of up to 11 % is reached until the completion of polymerization.

The STA analysis of three triarylsulfonium PAGs S-Al, S-B and S-C resulted in equal thermal stabilities in PhOx formulations. It can be seen from the DSC curve that no polymerization occurs below 200 °C. Starting at 210 °C all triarylsulfonium PAGs exhibit CROP by thermal cleavage of the cation. Considering the TGA, significant evaporation of monomer occurs above 160 °C. The evaporation before and during polymerization leads to a weight loss of almost 50 % for all three formulations.

It is concluded that selective cationic photopolymerization of PhOx by triarylsulfonium PAGs can be conducted up to 200 °C without any thermal polymerization occurring.

However, diaryliodonium PAGs, which exhibit significantly lower thermal stability, show thermal polymerization already at temperatures as low as 120 °C. Hence, triarylsulfonium PAGs are considered as better suitable for the here presented purpose.

2.3.2 Photo-DSC of triarylsulfonium PAG S-B in PhOx at elevated temperatures

Subsequent to the determination of thermal stability limits of onium salt PAGs in PhOx, photo-DSC analysis was conducted as a first confirmation for the hypothesis of cationic photopolymerization of 2-oxazolines. Temperatures below 140 °C were selected, as both polymerization by thermal cleavage of PAG and evaporation of monomer are avoided within this range. Thus, the reactivity of a formulation containing PhOx and triarylsulfonium PAG S-B in the ratio of [M]/[I] = 60 was examined at 120, 130 and 140 °C. The measurements were performed using an irradiation intensity of 3 W/cm² at the tip of the light guide, corresponding to 130 mW/cm² at sample position within the photo-DSC chamber. Two-fold irradiation of 900 s was applied to ensure full conversion within the first irradiation period. The results of photo-DSC measurements are depicted in Table 7.

Table 7: Photo-DSC results of PhOx containing 1.67 mol% S-B at 120, 130 and 140 °C; mass loss by evaporation during analysis

Temperature (°C)	t_{max} (s)	Area (J/g)	h (W/g)	t_{95} (s)	mass loss (%)	C_{NMR} [%]
120	113	174	0.71	572	4.5	70
130	106	247	1.13	561	5.7	-*
140	90	231	1.41	416	7.2	-*

* no residual monomer detected

The results achieved by photo-DSC analysis show that PhOx photopolymerizes with significant exothermicity in this temperature range using the triarylsulfonium PAG S-B. Although slower polymerization is observed in comparison to diglycidyl ether BADGE (section 1.4), distinct exothermicity shows the photoacid-initiated cationic polymerization upon irradiation. The strong dependence on thermal energy input is expressed by increasing reaction heat (area) indicating promoted conversion of polymerization. As the theoretical heat of polymerization of 2-oxazolines was not given

within these preceding studies, the conversion was measured in ^{1}H-NMR spectroscopy from residual amounts of unreacted monomer (C_{NMR}). However, the results for C_{NMR} are strongly affected by the potential undetected post-curing within the second irradiation period and the evaporation of unreacted monomer between 5 and 7 %, resulting in no residual monomer traces after measurements at 130 and 140 °C. Hence, the accurate evaluation of conversions from photo-DSC measurements demands for further analytical studies on the theoretical polymerization heat of 2-oxazoline monomers.

As expected, the t_{95} of over 400 s indicates the low propagation rates of the 2-oxazoline monomer. Especially the peak heights h, which directly correspond to the rate of polymerization R_p according to Equation 2, show the linear increase of R_p with raised temperatures. In conclusion it was shown that triarylsulfonium PAG S-B effectively enables the photopolymerization of PhOx at temperatures above 120 °C, and subsequent ^{1}H-NMR analyses confirm the conversion of monomer.

In order to extend the investigations on cationic photopolymerization of 2-oxazolines regarding reactivity of different monomers, structural analysis of resulting photopolymers as well as thermomechanical studies of poly(2-oxazolines), mono- and difunctional 2-oxazoline model compounds were synthesized.

2.4 Synthesis of 2-oxazoline monomers for cationic photopolymerization

After successful analyses confirming the cationic photopolymerization of 2-phenyl-2-oxazoline (PhOx) at elevated temperatures, a set of 2-oxazoline model compounds was synthesized. Especially the reactivity of 2-alkyl-2-oxazolines should be examined in photopolymerization studies, as increased reactivity is reported for monomers with alkyl substituents in comparison to aromatic monomers, which retard the propagation by stabilizing the cationic propagating species. However, only 2-methyl-, 2-ethyl- and 2-isopropyl-2-oxazoline are commercially available.[113] Due to the high volatility of these low molecular 2-n-alkyl-2-oxazoline derivatives, the synthesis of sufficiently nonvolatile compounds was conducted. Most commonly, the routes depicted in Figure 40 are applied for the preparation of 2-oxazoline monomers.
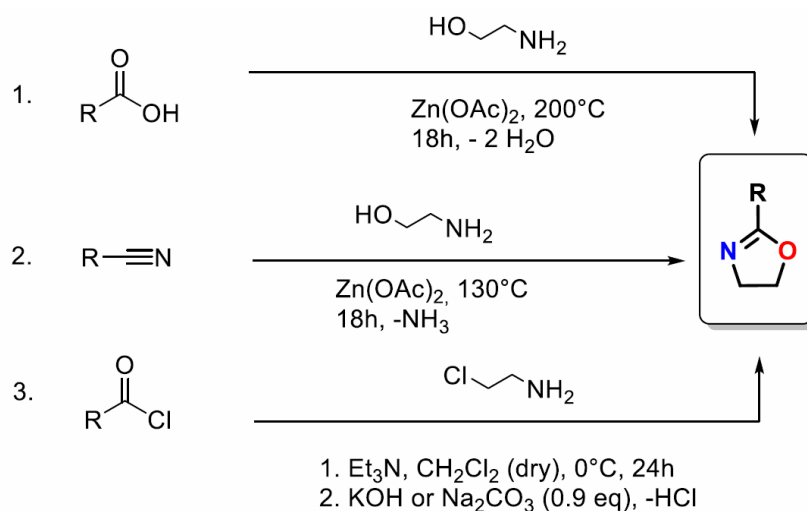
Figure 40: Synthesis routes for the preparation of 2-oxazolines[131]

Although many 2-oxazolines based on natural fatty acids are accessible following synthesis route 1, the cyclization of N-(2-hydroxyethyl)alkylamide at high reaction temperatures (170-230 °C) represents an impracticable method in laboratory instrumentation.[162] Under milder conditions, the cyclization of acid chlorides described by the two-step synthesis in route 3 is applicable. As most versatile approach, the direct conversion of nitriles via ethanolamine leads to the respective 2-oxazoline products (route 2). Under the aspect of facile availability of a great variety of applicable nitriles and low costs, route 2 was considered as a straight-forward method, which is highly common in prior reports on CROP of 2-oxazolines.[150, 163] The one-step synthesis is conducted in a solvent-free reaction and further purification by distillation.[164] Following this preparation method, 2-oxazoline model compounds potentially suitable for cationic photopolymerization at elevated temperatures were prepared. Besides the preparation of aliphatic 2-octyl-2-oxazoline (OctOx), the synthesis of a difunctional aliphatic 2-oxazoline (BisOx) was conducted to obtain a cross-linking monomer for the UV-curing of thermosetting 2-oxazoline-based materials in further investigations.

2.4.1 Synthesis of 2-octyl-2-oxazoline (OctOx)

In order to obtain 2-alkyl-2-oxazoline monomers with low volatility and sufficiently high reactivity in cationic photopolymerization, 2-octyl-2-oxazoline (OctOx) was prepared according to literature starting from the respective nitrile.[164] [156]
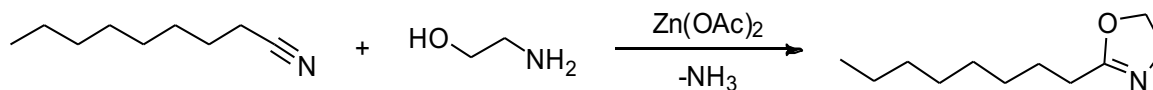
Under nitrogen atmosphere dry ethanolamine (1.1 eq) was added to n-nonanenitrile (1 eq) in the presence of zinc acetate catalyst at 130 °C. A low stream of nitrogen was maintained to remove the produced ammonia from the reaction. The mixture was stirred at 130 °C overnight. After extraction and evaporation of solvent the product was isolated by distillation in vacuum. Significant amounts of N-(2-hydroxyethyl)nonanamide were obtained as a side product. The synthesis yielded a colorless liquid in a yield of 45% of theory, in accordance to literature.[156] The purity was confirmed by ^{1}H-NMR and GC-MS.

2.4.2 Synthesis of 1,6-bis(4,5-dihydrooxazol-2-yl)hexane (BisOx)

The difunctional 2-oxazoline monomer 1,6-bis(4,5-dihydrooxazol-2-yl)hexane (BisOx) was prepared according to literature starting from the respective dinitrile under zinc acetate catalysis in bulk.[163, 164]
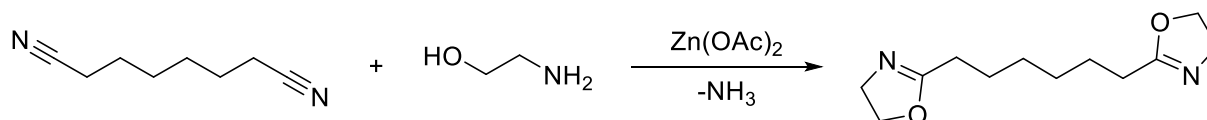
Figure 41: Synthesis route for difunctional 2-oxazoline 1,6-bis(4,5-dihydrooxazol-2-yl)hexane (BisOx)

Under nitrogen atmosphere ethanolamine (3 eq) was added dropwise to a mixture of 1,6-dicyanohexane (1 eq) and zinc acetate dihydrate (0.05 eq) at 100 °C. The reaction mixture was stirred for 48 hours and subsequently extracted with water and dichloromethane. The crude product was purified by high-vacuum distillation, after which a colorless solid crystallized at room temperature. A yield of 54 % of theory was obtained. The product 1,6-bis(4,5-dihydrooxazol-2-yl)hexane was identified by ^{1}H-NMR and GC-MS.

2.4.3 Synthesis of hydroxyl-terminated 2-alkyl-2-oxazolines

As many photopolymers based on low-molecular weight monomers suffer from high brittleness and low toughness due to high cross-link densities, a common approach to reach desired thermomechanical properties is end group functionalization of precursors as building blocks with photopolymerizable moieties. Therefore, further syntheses of 2-hydroxyalkyl-2-oxazoline monomers were designated for the addition to diisocyanate precursors.

The synthesis routes taken into consideration followed literature-known methods from corresponding nitriles, as well as patent literature starting from cyclic lactones in a two-step procedure. [165, 166]

The target molecules HO-PentOx and HO-EtOx are depicted in Figure 42.
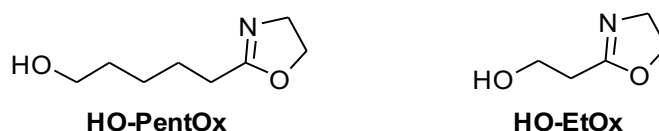
HO-PentOx   **HO-EtOx**

Figure 42: ε-hydroxypentyl-2-oxazoline (HO-PentOx) and β-hydroxyethyl-2-oxazoline (HO-EtOx)

Due to the great variety of cyclic lactone starting materials and high versatility in hydroxyalkyl chain length, the latter synthesis route was considered for the preparation of ε-hydroxypentyl-2-oxazoline (HO-PentOx). The chain length of this hydroxyalkyl substituent was chosen in order to avoid the stabilizing effect of six-membered cyclization via proton bridging with the hydroxyl oxygen atom, as observed for glycidyl ether monomers. [38-40] Furthermore, the synthesis of β-hydroxyethyl-2-oxazoline (HO-EtOx) was considered by the common synthesis procedure starting from propionitrile.

2.4.3.1 Synthesis of ε-hydroxypentyl-2-oxazoline
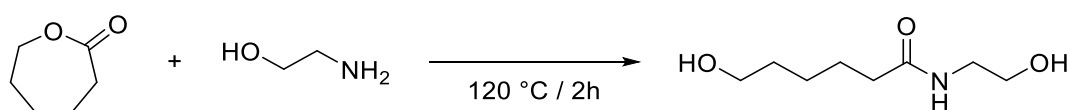
Under nitrogen atmosphere dry ethanolamine (1 eq) was added to ε-caprolactone (1 eq) and heated to 120 °C for 3 hours. The product precipitated at room temperature overnight and crystallization was completed at -20 °C. The crude product was purified

by recrystallization from acetone. The synthesis gave 7.3 g of white waxy solid in a yield of 42% of theory. The product was identified by ^{1}H-NMR and GC-MS.

The intermediate was subsequently used for the preparation of ε-hydroxypentyl-2-oxazoline.
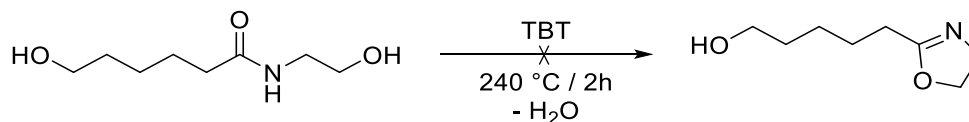
Under Schlenk conditions tetra-n-butyl titanate (TBT, 0.005 eq) was added to the intermediate ε-hydroxy-(N-ethyl-2-hydroxy)-caproamide (1 eq) and heated to 240 °C on a metal bath for 2 hours. The condensation of significant amounts of water was apparent and the occurrence of 2-oxazoline signals was detected in ^{1}H-NMR analysis of the reaction mixture. At the high reaction temperature significant degree of degradation was observed by strong discoloration. The reaction mixture was purified by extraction (ethylacetate/H_2O). The reaction showed very low conversion (below 20%), whereas literature describes the procedure with 77% of theory. No product could be obtained after purification by column chromatography.

The use of a water-sensitive catalyst in a condensation reaction is considered as another reason of insufficient conversion. In presence of moisture, the catalyst tetra-n-butyl titanate (TBT) hydrolyses to n-butanol and TiO_2. Thus, the catalyst is assumed to be inactivated in course of the reaction, especially with progressing conversion.

2.4.3.2 Synthesis of β-hydroxyethyl-2-oxazoline (HO-EtOx)

As the preparation of ε-hydroxy-(N-ethyl-2-hydroxy)-caproamide according to patent literature was unsuccessful, the preparation of a hydroxy-terminated 2-oxazoline by the priorly applied method starting from the corresponding nitrile was conducted. Starting from 3-hydroxypropionitrile, the conversion to the corresponding β-hydroxyethyl-2-oxazoline (HO-EtOx) via cyclization by ethanolamine was intended.
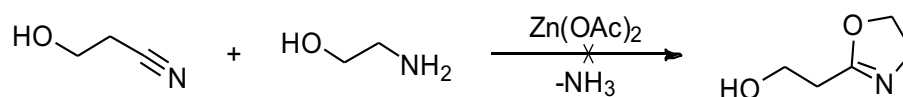
Under nitrogen atmosphere dry ethanolamine (1.2 eq) was added to 3-hydroxypropionitrile (1 eq) in the presence of zinc acetate catalyst at 130 °C.

Throughout the reaction no evolution of ammonia gas was observed. The mixture was stirred at this temperature overnight. Reaction control by ^{1}H-NMR did not show product in the reaction mixture. It is assumed that the given preparation method is not applicable to hydroxy-functionalized nitriles as catalytic conversion shows insufficient selectivity between the hydroxy groups of ethanolamine and 3-hydroxypropionitrile.

2.5 STA of photoreactive formulations of PhOx, OctOx and BisOx with S-B

The investigations of cationic photoinitiation systems for Hot Lithography of epoxy monomers in section 1 showed the advantageous properties of a triarylsulfonium PAG over other photoinitiators based on diphenyliodonium salts and a photoinitiation system for free radical promoted cationic polymerization. Besides the inherently efficient initiation arising from strong WCA-based protonic acids, triarylsulfonium PAGs exhibit outstandingly high thermal stability given by the nature of the cation. Clearly, triarylsulfonium PAGs in combination with a non-nucleophilic anion present a viable approach for the cationic photopolymerization at elevated temperatures in order to polymerize low reactive monomers, such as 2-oxazolines.

Subsequent to preceding investigations in the commercially available monomer 2-phenyl-2-oxazoline (PhOx) and the syntheses of two aliphatic model compounds 2-octyl-2-oxazoline (OctOx) and 1,6-bis(4,5-dihydrooxazol-2-yl)hexane (BisOx), analyses of the thermal stability of photoreactive 2-oxazoline-based formulations were conducted. Figure 43 shows the molecular structures of PhOx, OctOx and BisOx.
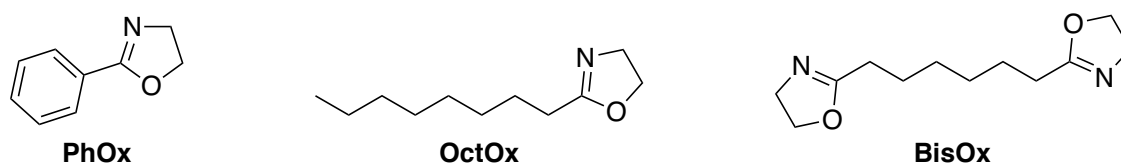
Figure 43: 2-oxazoline model compounds 2-phenyl-2-oxazoline (PhOx), 2-octyl-2-oxazoline (OctOx) and 1,6-bis(4,5-dihydrooxazol-2-yl)hexane (BisOx)

The thermal stability of photosensitive formulations differs in dependence of both the nature of the PAG and the cationically polymerizable monomer. Although the PAG S-B is reported to be stable at temperatures up to 300 °C, a reactive formulation exhibits

intrinsic stability limits, as seen in section 1.3 with epoxy monomer BADGE.[56] This is reasoned by the nucleophilicity of the monomer, which increases the tendency to electrophilic attack of a cationic species during initiation and propagation. Furthermore, ring-strain of the reactive moiety may promote the thermally driven ring-opening reaction upon initiation of the monomer.

Therefore, the thermal stability of formulations of PhOx, OctOx and BisOx containing 0.5 mol% of S-B per reactive group (corresponding to 1 mol% in difunctional monomer BisOx) were evaluated by simultaneous thermal analysis (STA). The combination of thermogravimetric analysis (TGA) and differential scanning calorimetry (DSC) was used to determine the highest applicable temperature for photopolymerization. 14 ± 1 mg of the formulations was weighed into a DSC crucible, which was closed using a pierced lid. In case of solid BisOx, the melted formulation was stirred at 80 °C and the resulting clear solution was weighed into DSC crucibles before solidification. The measurements were conducted by heating the samples to 300 °C under nitrogen atmosphere using a heating rate of 10 K/min. The measurements of PhOx, OctOx and BisOx are depicted in Figure 44 in comparative display.
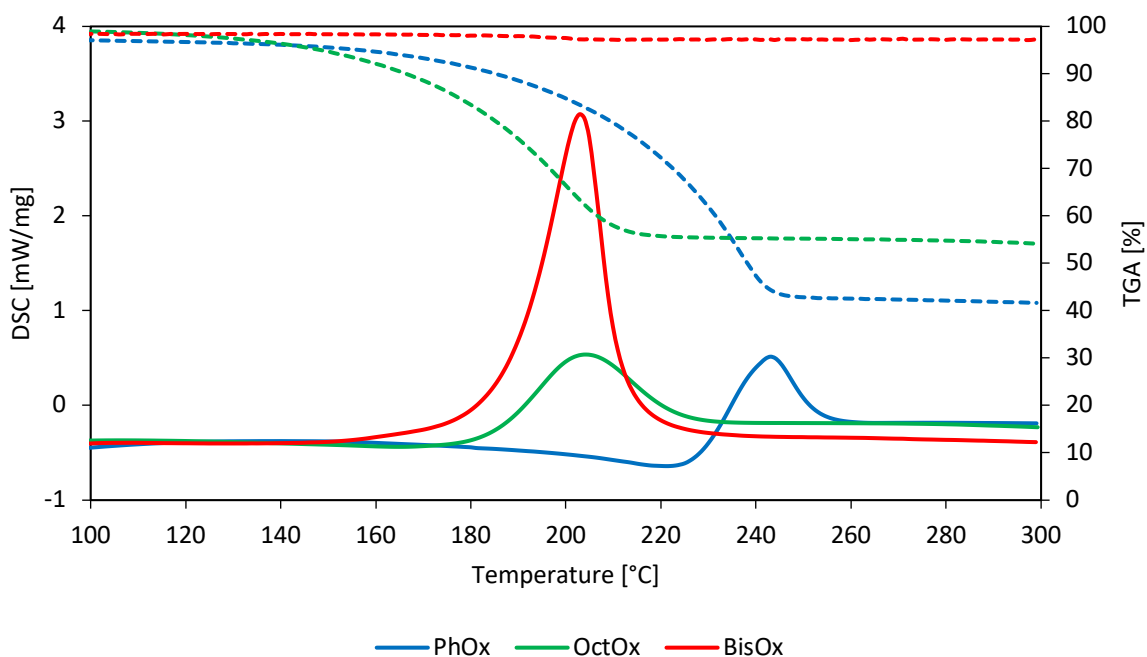
Figure 44: STA analyses of BisOx with 1 mol% PAG (S-Al, S-B, S-C); TGA dashed

From the STA analyses it is concluded that the 2-oxazoline formulations are generally stable below 140 °C. This is represented by the onset temperatures of thermal polymerization, displayed in Table 8.

Table 8: Thermal onset of polymerization from STA measurements of BisOx, OctOx and PhOx containing 0.5 mol% S-B per reactive group

Monomer	Thermal onset of polymerization [°C]
BisOx	148
OctOx	167
PhOx	222

The TGA curves show the significant mass loss by evaporation of volatile 2-oxazoline monomers at increased temperatures, such as for PhOx and OctOx. These monomers show evaporation throughout the heating process until polymerization occurs. For OctOx, weight loss is more significant and ceases at about 210 °C once full conversion is reached. Until reaching the exothermal peak of polymerization, the monofunctional 2-oxazoline monomers evaporate to an extent of about 50 %. In comparison, PhOx is less prone to thermal polymerization and polymerizes at much higher temperatures. Hence, higher evaporation is observed before polymerization (endothermal, negative DSC) up to 220 °C. The formulation of difunctional 2-oxazoline monomer BisOx shows no evaporation throughout the analysis and thermal stability up to 148 °C. It is assumed that the thermal onset of polymerization serves as an indicator for the different reactivity of monomers, which is influenced by the nucleophilicity of the monomer and the substituent effect on the ring-opening reaction.

It is concluded that within the designated working temperature in Hot Lithography up to 140 °C no premature thermal polymerization is expected according to STA analysis.

2.6 Photo-DSC studies of 2-oxazolines at elevated temperatures

Subsequent to the syntheses of model compounds and STA analysis of PhOx, OctOx and BisOx formulations, photo-DSC studies were conducted to evaluate their reactivity. These analyses aim for the comparative investigation of the influence of

aromatic and aliphatic substituents of 2-oxazoline monomers in cationic photopolymerization, as well as the influence of different WCAs in triarylsulfonium PAGs.

In analogy to photo-DSC studies of the cationic photopolymerization of epoxy monomers at elevated temperature in section 1.4, the investigations of 2-oxazolines were conducted using a similar analytic setup. To enable the comparison of different photopolymerizable 2-oxazoline systems by representative result parameters, the determination of the theoretical polymerization enthalpy of 2-oxazoline reactive groups was conducted.

2.6.1 Theoretical polymerization enthalpy of 2-oxazolines in photo-DSC

The determination of the theoretical heat of polymerization ΔH_0 in cationic photopolymerization of 2-oxazolines was performed based on the synthesized monofunctional model compound OctOx. The analyses were conducted by photo-DSC and subsequent ^{1}H-NMR measurements of the incompletely cured photopolymers. Therefore, formulations of OctOx with 0.5 mol% of the PAG S-B were prepared. Due to the limited solubility of the triarylsulfonium salt S-B in OctOx, the PAG was firstly mixed with propylene carbonate (50:50 wt%) before adding the monomer to the mixture.

All samples were weighed before and after the high-temperature photo-DSC measurement to determine the mass loss by evaporation of monomer. The measurements were performed using an irradiation intensity of 3 W/cm² at the tip of the light guide, corresponding to 130 mW/cm² in sample position. Only one irradiation period of 900 s was applied to avoid deviations by thermal post-curing in the second irradiation period at temperatures of 120 and 140 °C. Although no exothermicity is expected during the second irradiation period, the conversion at high temperatures could still proceed below the sensitivity limit of the instrument once the polymerization is initiated by light. After the single irradiation segment the measurement ended and the sample was immediately dissolved in deuterated chloroform. The potentially proceeding cationic polymerization was quenched with one drop of pyridine. After full dissolution, the sample was transferred to a brown glass NMR tube and measured by ^{1}H-NMR spectroscopy.

The conversion (C_{NMR}) was determined from resulting ^{1}H-NMR spectra, in which the residual 2-oxazoline monomer signals were set in relation to the methyl protons signals of the octyl substituent as internal standard, as those are not changing throughout the polymerization. The pristine, unreacted formulation served as a blank.

The heat detected in photo-DSC analysis was set in relation to the conversion according to the following Equation 3.

Equation 3: Calculation of Theoretical Heat of Polymerization ΔH_0

$$\Delta H_0 = \frac{\Delta H * M}{\frac{m}{m_{tot}}} * C_{NMR}$$

ΔH_0	Theoretical heat of polymerization of monofunctional monomer [J/mol]
ΔH	Heat of polymerization by photo-DSC (Area) [J/g]
M	Molecular weight of monomer [g/mol]
$\frac{m}{m_{tot}}$	Ratio of monomer mass to total mass of formulation []
C_{NMR}	Conversion measured by ^{1}H-NMR [%]

The results arising from triplicate photo-DSC measurements are summarized in Table 9.

Table 9: Results of the determination of theoretical polymerization enthalpy using OctOx with 0.5 mol% S-B

T [°C]	C_{NMR} [%]	ΔH [J/g]	ΔH_0 [kJ/mol]	Mass loss [%]	$\Delta H_{0,corr}$ [kJ/mol]]
120	88.7 ± 0.4	305 ± 2.4	68.3 ± 0.4	7.0 ± 0.7	73.1 ± 0.9
140	100	324 ± 35	64.4 ± 7.0	9.0 ± 5.1	69.8 ± 4.6

The results in Table 9 show the detected polymerization heat ΔH, from which ΔH_0 is derived for OctOx. The results for 120 °C show good reproducibility and low standard deviation. The overall mass loss by evaporation is considered and corrected by calculation of $\Delta H_{0,corr}$, giving reproducible results within a low error margin. By this correction of the overall mass loss, a result of $\Delta H_{0,corr}$ = 73.1 kJ/mol is obtained.

The results at 140 °C, however, show critical deviations. As no residual monomer is detected in ^{1}H-NMR analysis, it cannot be ensured whether total conversion occurred within these measurements or evaporation at the increased temperature led to the loss of unreacted monomer. The detected polymerization heat as well as the overall mass loss shows great deviations, reducing the reliability of the results at 140 °C. For this reason, the theoretical heat of polymerization determined at 140 °C was not considered, however, supports the correctness of the results at 120 °C.

2.6.2 Photo-DSC of PhOx, OctOx and BisOx

Based on reports of thermally induced CROP of 2-oxazolines, it was expected that 2-alkyl-substituted derivatives generally show higher reactivity than 2-aryl-substituted monomers as PhOx.[118, 150, 151] Due to formerly described influences on the reactivity, a basic setup for comparison of reactivity at temperatures above 100 °C was defined. The standard conditions of 130 mW/cm² irradiation intensity at sample position and 320-500 nm wavelength were applied. The measurement was conducted using irradiation periods of two-times 900 s. Formulations of the 2-oxazoline monomers PhOx, OctOx and difunctional BisOx containing 0.5 mol% S-B per reactive group of the monomer (1 mol% for difunctional BisOx) were thus measured by photo-DSC at 100, 120 and 140 °C. Figure 45, Figure 46 and Figure 47 show the measurements of 2-oxazoline monomers at 100, 120 and 140 °C.
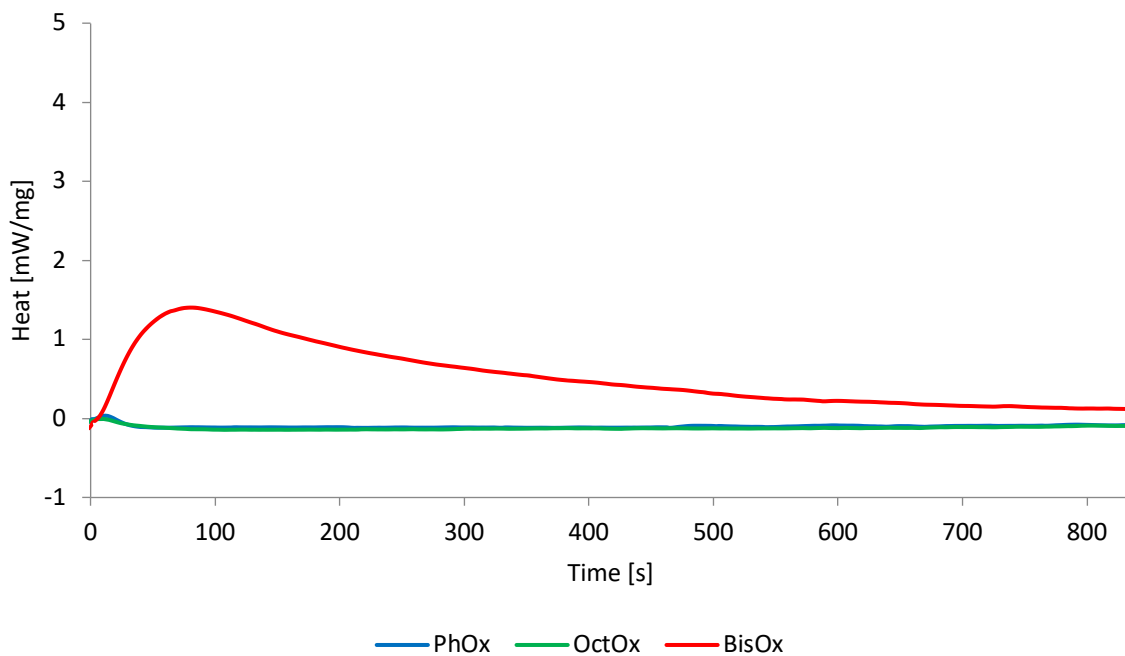
Figure 45: Comparative photo-DSC analysis 2-oxazolines at 100 °C
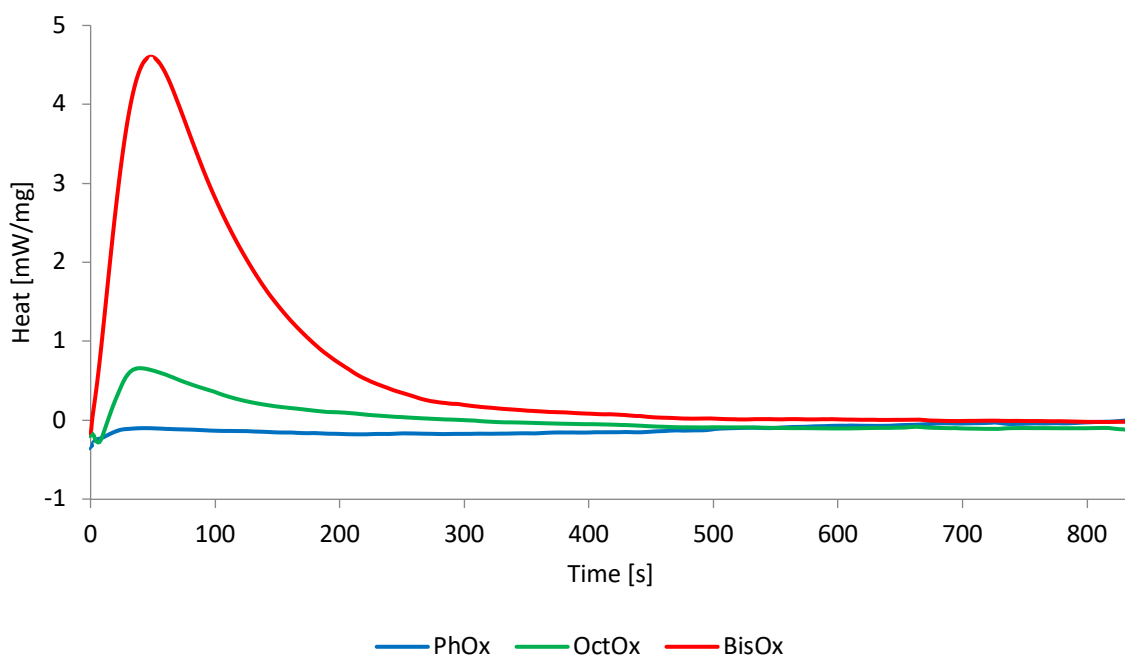
Figure 46: Comparative photo-DSC analysis 2-oxazolines at 120 °C
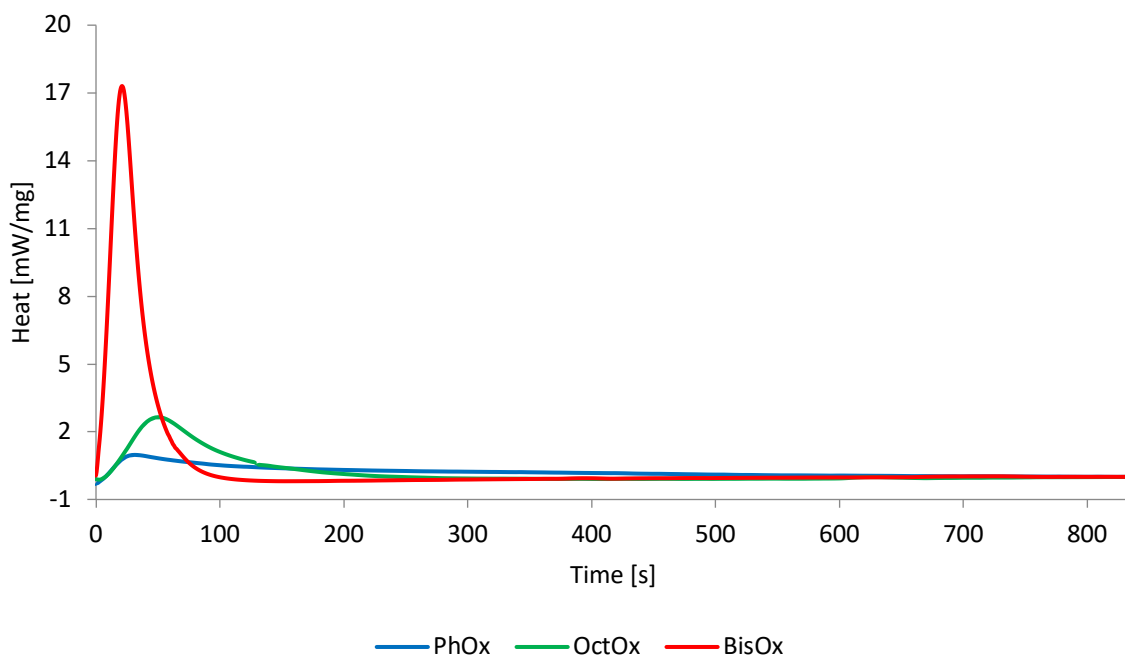
Figure 47: Comparative photo-DSC analysis 2-oxazolines at 140 °C

Evidently, the difunctional monomer BisOx exhibits photopolymerization even at 100 °C, which is insufficient for the monofunctional monomers PhOx and OctOx as no exothermicity is detected. No gelation or solidification was observed in the monofunctional samples, whereas the difunctional monomer polymerized and gave a glassy photopolymer. However, also BisOx shows low reaction rates at 100 °C as the polymerization reaction does not cease within one irradiation period of 900 s.

With an increase of the temperature to 120 °C, the difunctional monomer BisOx shows a distinctive increase in reactivity. The photopolymerization has clearly ceased within the irradiation period and shows a t_{95}-value of 299 s. A significant exothermicity in photopolymerizations of monofunctional 2-oxazolines is only observed for OctOx. Aromatic PhOx does not show a distinctive exothermal peak in the photo-DSC curve.

At 140 °C an unexpectedly high increase in reactivity of difunctional monomer BisOx is observed. The great ascent of reactivity confirms to the assumption that the ring-opening polymerization is highly dependent on external heat. Its sensitivity to thermal energy input accelerates the photopolymerization supposedly by its impact on the ring-opening reaction, which is driven by heat. Also, both monofunctional monomers show a photopolymerization reaction at a temperature of 140 °C, whereas the photopolymerization of aliphatic OctOx occurs at distinctly higher rates. This confirms

the higher reactivity of aliphatic 2-oxazolines in comparison to aromatic 2-oxazolines, as expected from reported propagation rate constants of OctOx (k_p = 122 x 10^{-3} L mol^{-1} s^{-1}) and PhOx (k_p = 35.8 x 10^{-3} L mol^{-1} s^{-1}) in MW-assisted CROP at 140 °C.[152, 156] The reactivity in photopolymerization is evaluated by the photo-DSC results displayed in Table 10.

Table 10: Photo-DSC results of BisOx, OctOx and PhOx containing 0.5 mol% S-B per reactive group at 100, 120 and 140 °C

Temperature (°C)	Formulation	C [%]	t_{max} [s]	R_P [mmol L^{-1} s^{-1}]	t_{95} [s]
100	BisOx	56	80.2	9	535
	OctOx	-*	-*	-*	-*
	PhOx	-*	-*	-*	-*
120	BisOx	91	48.2	32	299
	OctOx	27	39.1	9	322
	PhOx	-*	-*	-*	-*
140	BisOx	99	26	118	93
	OctOx	69	50.5	35	211
	PhOx	38	31.4	15	558

* no exothermicity detected in DSC

As seen from the results above, conversions up to 99 % are reached in BisOx at 140 °C, whereas the monofunctional monomers reach significantly lower conversions. Moreover, inherently high polymerization rates R_p are observed with increasing temperature using the difunctional 2-oxazoline monomer. It has to be considered that the difunctional BisOx and the monofunctional OctOx both bear a comparable long-chained aliphatic substituent. Hence, their reactive moieties should not differ significantly in reactivity. However, the polymerization kinetics of difunctional monomers deviate from monofunctional monomers due to the cross-linking mechanism. Still these photo-DSC results represent the different UV-curing behavior of 2-oxazolines depending on the rate-determining effect of the substituent in 2-position.

In consideration of the strong discoloration observed in many polymers following cationic photopolymerization, Figure 48 shows the resulting photopolymers of BisOx formulation containing 1 mol% S-B after photopolymerization at 140 °C.

Figure 48: Poly(BisOx) photopolymerized with 1 mol% S-B at 140 °C

It is noted that the difunctional 2-oxazoline BisOx gives glassy, transparent photopolymers with low discoloration and high rigidity after photopolymerization at 140 °C.

2.6.3 Photo-DSC of triarylsulfonium PAGs in BisOx

The significantly increased reactivity of difunctional BisOx in cationic photopolymerization is considered for the efficient cross-linking of 2-oxazoline-based photopolymers. Moreover, the rapid solidification upon irradiation at elevated temperatures further promotes the potential application of 2-oxazolines in Hot Lithography. In order to evaluate the reactivity arising from the use of advanced WCA-based PAGs, the triarylsulfonium PAGs used in foregoing STA studies were analyzed by photo-DSC in comparably high-reactive difunctional BisOx. Three PAG salts of the same tris(4-((4-acetylphenyl)thio)phenyl)sulfonium cation, namely tetrakis(perfluoro-t-butyloxy)aluminate (S-Al), tetrakis(pentafluorophenyl)borate (S-B) and tris((trifluoromethyl)sulfonyl)methanide (S-C) were used in a concentration of 1 mol% (0.5 mol% per reactive group of monomer), respectively. The structures of the triarylsulfonium PAGs S-Al, S-B and S-C are depicted in Figure 49.
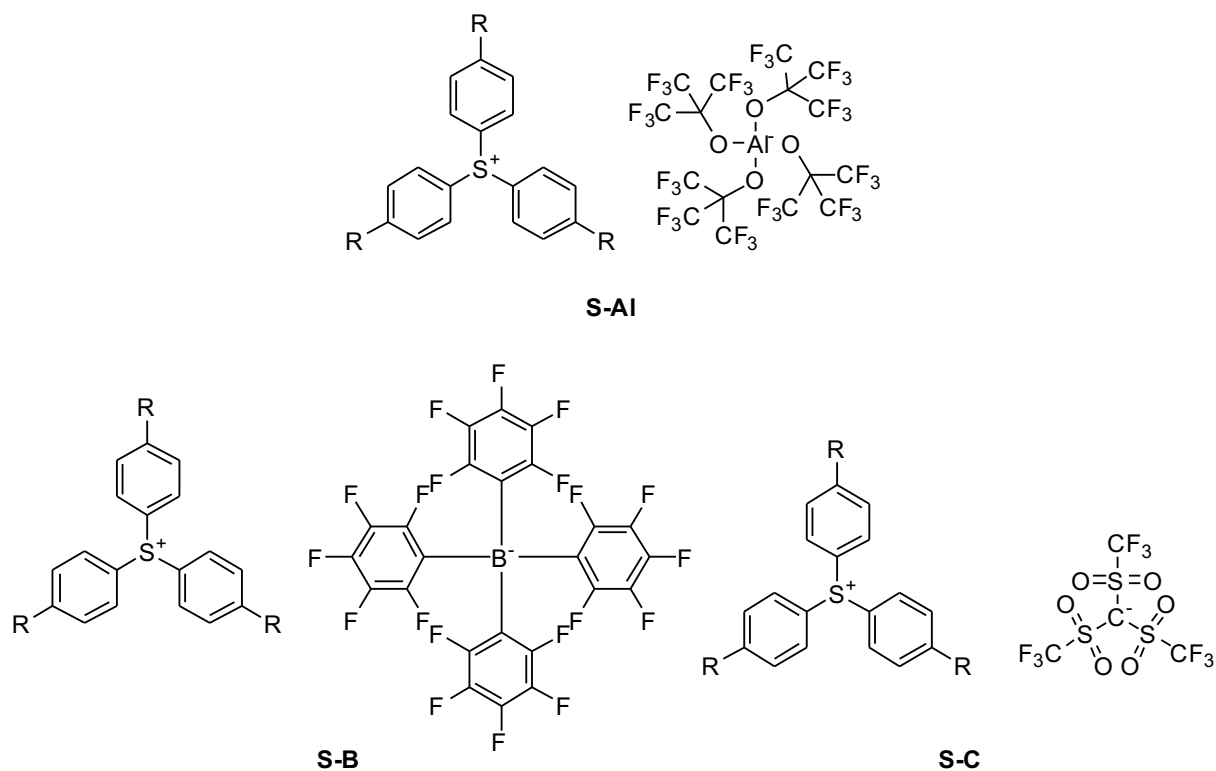
Figure 49: Triarylsulfonium PAGs for cationic photopolymerization of 2-oxazolines at elevated temperatures (R = S-Ph-COCH₃)

As the thermal stability of PAG salts is determined by the cation, the triarylsulfonium PAGs S-Al, S-B and S-C exhibit equal resistance against thermally induced cleavage at elevated temperatures. Thus, photo-DSC analyses were conducted at formerly applied temperatures of 100, 120 and 140 °C to investigate the differences in initiation ability and reactivity. The reactivity in photopolymerization is strongly influenced by the nature of the WCA-based counterion in cationic photopolymerization. Equal measurement conditions as in foregoing photo-DSC analyses of 2-oxazoline monomers were applied. Figure 50, Figure 51 and Figure 52 show the comparative photo-DSC curves of the three formulations at 100, 120 and 140 °C, respectively.
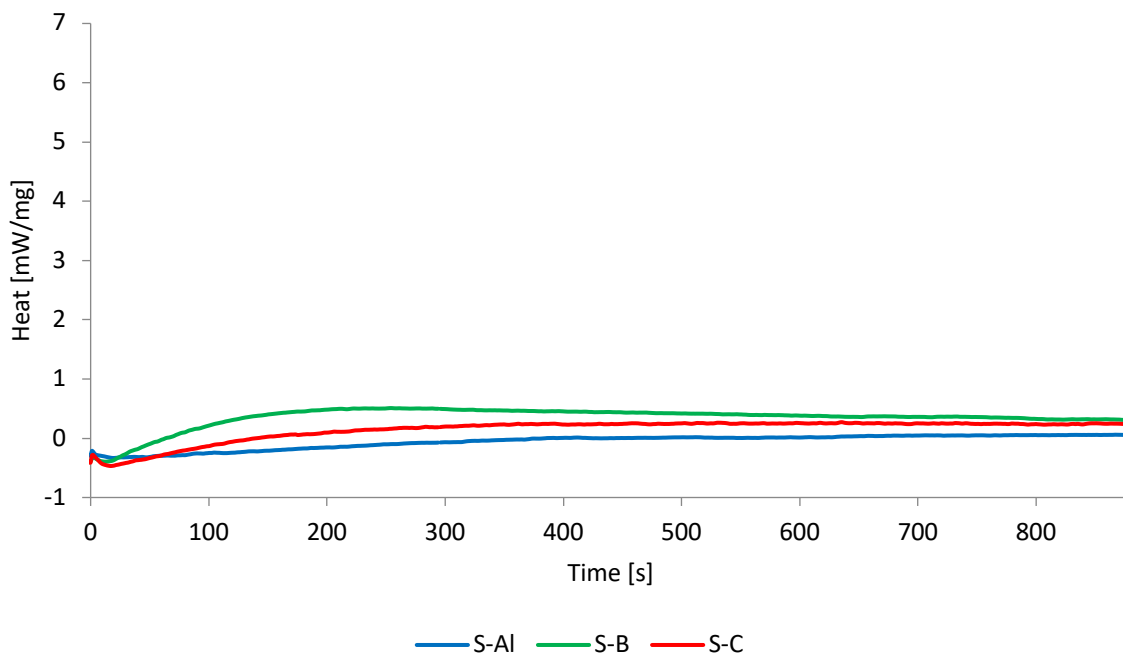
Figure 50: Photo-DSC curves of BisOx formulations containing 1 mol% of S-Al, S-B or S-C, respectively, at 100 °C
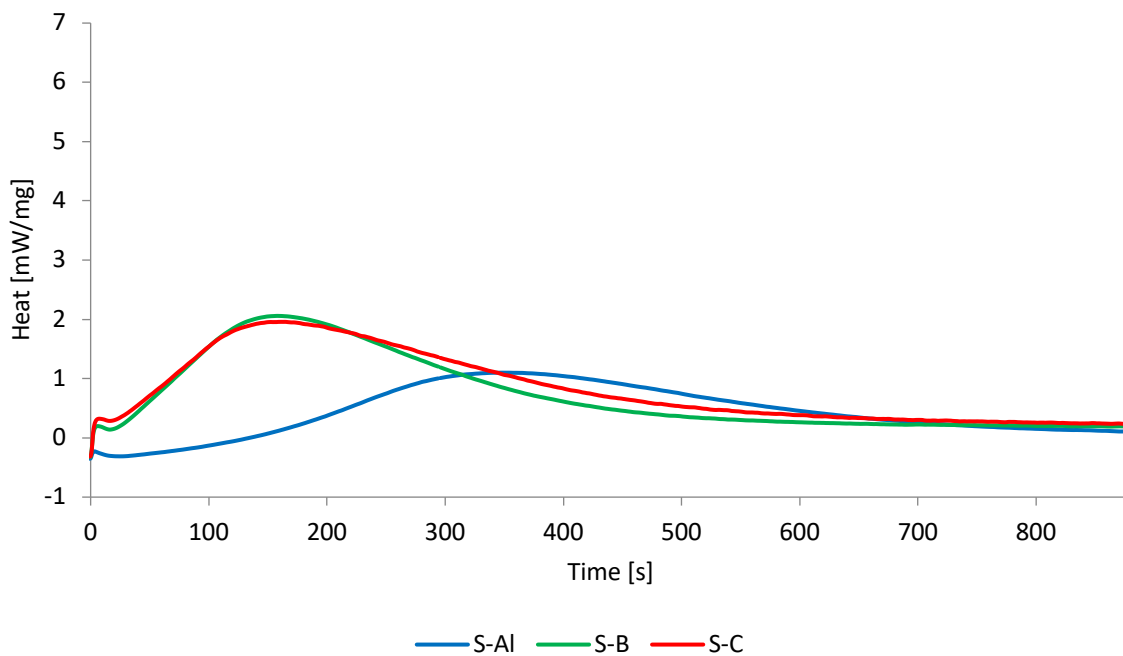
Figure 51: Photo-DSC curves of BisOx formulations containing 1 mol% of S-Al, S-B or S-C, respectively, at 120 °C
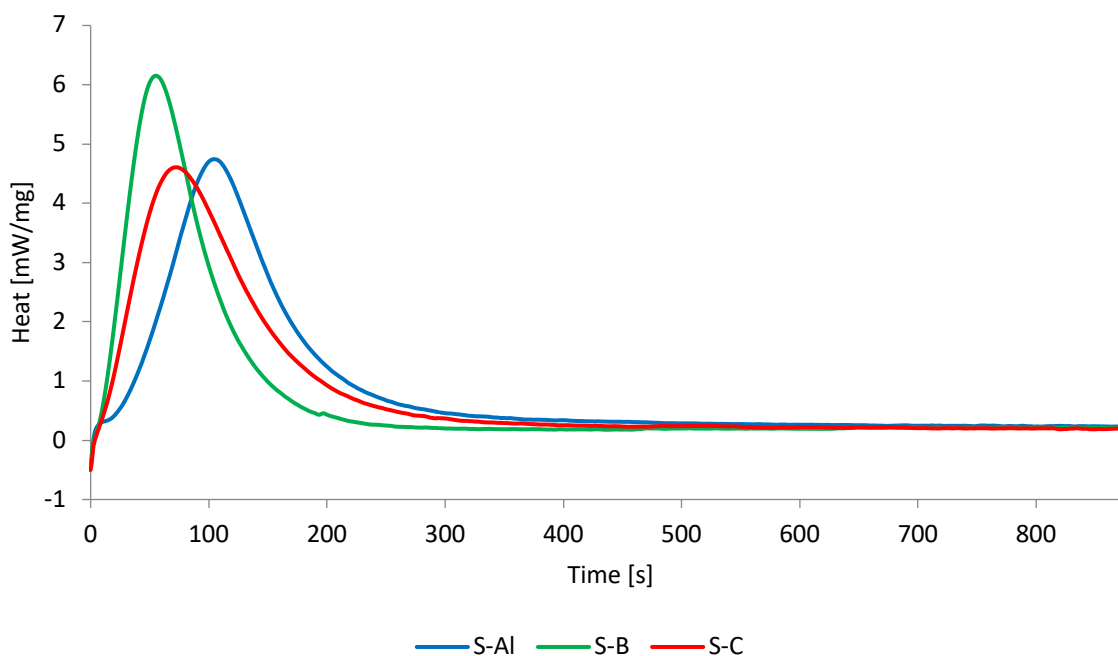
Figure 52: Photo-DSC curves of BisOx formulations containing 1 mol% PAG (S-Al, S-B, S-C) at 140 °C

The advantageous curing behavior of the commercial triarylsulfonium PAG S-B in comparison to S-C and S-Al is evident. At a temperature of 100 °C all PAGs generate incomplete polymerization reactions within 900 s, however, reactivities are increasing from S-Al to S-C to S-B. Raising the temperature to 120 °C leads to significant reactivity advantages using S-B and S-C in comparison to the unexpectedly less reactive S-Al. At a temperature of 140 °C, the clearly most reactive PAG S-B shows fastest photopolymerization reaction, whereas S-Al shows retarded reactivity.

The result parameters are displayed in Table 11.

Table 11: Photo-DSC results of BisOx formulations containing 1 mol% PAG (S-Al, S-B, S-C) at 100, 120 and 140 °C

Temperature (°C)	Formulation	C [%]	t_{max} [s]	R_P [mmol L^{-1} s^{-1}]	t_{95} [s]
100	S-Al	-*	-*	-*	-*
	S-B	57	215	5	-
	S-C	33	288	3	-
120	S-Al	85	340	9	717
	S-B	77	158	13	476
	S-C	84	164	12	547
140	S-Al	88	109	31	322
	S-B	76	60	41	145
	S-C	87	77	30	30

Although tetrakis(perfluoro-t-butyloxy)aluminate represents the lowest nucleophilic WCA and showed beneficial curing behavior in glycidyl ether BADGE,[56] the advantageous reactivity is not reflected in the cationic photopolymerization of a 2-oxazoline monomer at elevated temperatures. As seen, the borate-based PAG S-B exhibits highest reactivities in BisOx formulation, indicating its excellent suitability for the investigated purpose. As derived from these experimental results, S-B was further used as efficient PAG for the investigations of cationic photopolymerization of 2-oxazoline monomers at elevated temperatures.

2.6.4 Variation of PAG concentration in PhOx, OctOx and BisOx

Experience of preliminary examinations of the cationic photopolymerization of 2-oxazolines showed that the PAG concentration also has a crucial impact on the reactivity of this low reactive monomer class. A greater number of activated monomers and propagating polymer chains may autoaccelerate the polymerization by the liberated enthalpy of the ring-opening reaction, as reported for other heterocyclic monomers.[41 27, 42, 46, 167]

Therefore, the influence of PAG concentration was investigated in photoreactive systems of the model compounds BisOx, OctOx and PhOx. The photopolymerizations were followed by photo-DSC measurements at 120 °C, as highest reproducibility was observed in photopolymerizations with only low evaporation of monomers at this temperature. The photo-DSC analyses of BisOx, OctOx and PhOx were conducted using the PAG S-B in concentrations of 0.5, 1.0 and 1.5 mol% per reactive group of the respective monomer. Accordingly, the difunctional BisOx was measured in formulations containing 1, 2 and 3 mol% of S-B. The standard measurement conditions were applied in these analyses at 120 °C. Figure 53, Figure 54 and Figure 55 illustrate the photo-DSC curves of each monomer in formulations with varied concentrations of S-B.
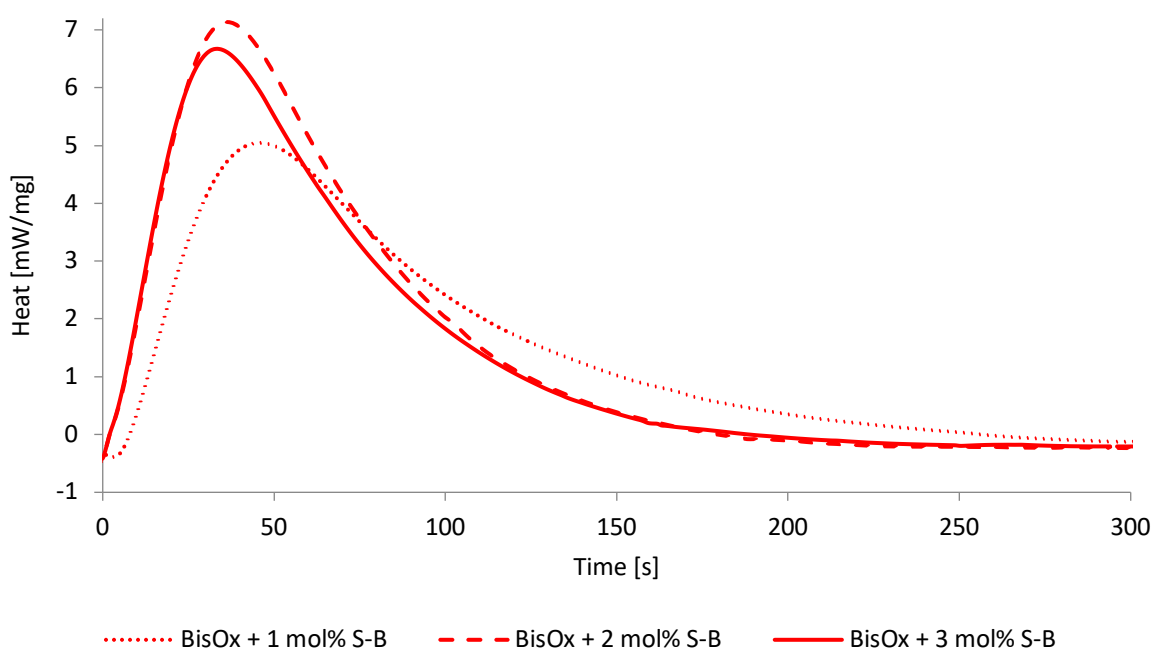
Figure 53: Photo-DSC analysis of BisOx at 120 °C with varied PAG concentration (0.5, 1.0 and 1.5 mol% S-B per reactive group of monomer)
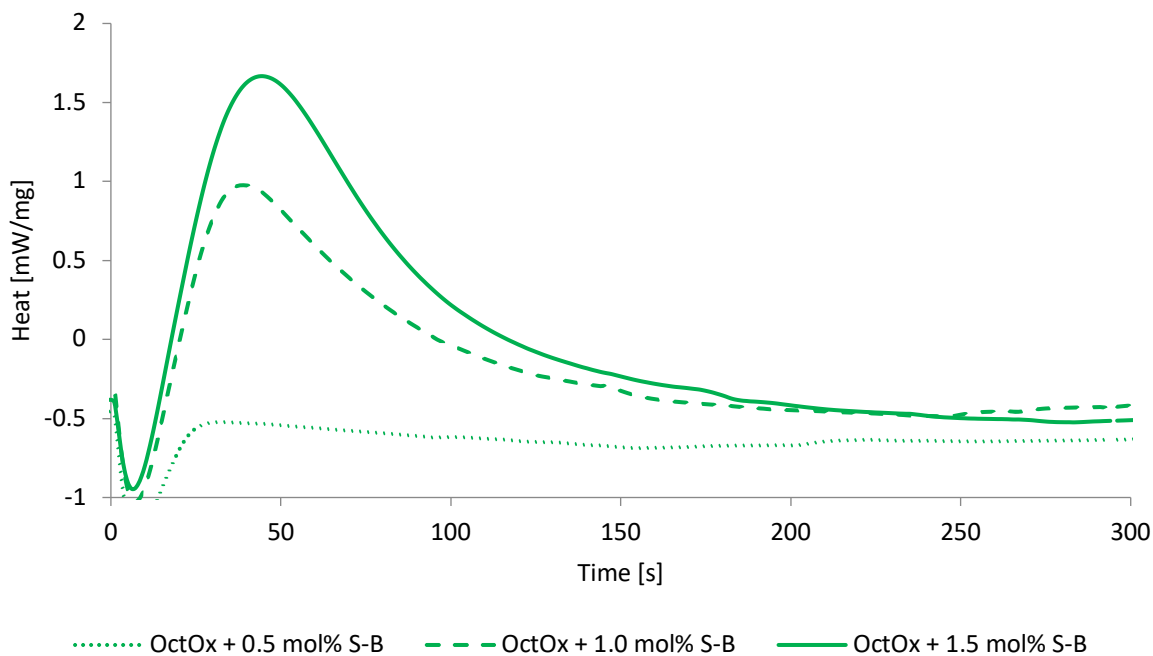
Figure 54: Photo-DSC analysis of OctOx at 120 °C with varied PAG concentration (0.5, 1.0 and 1.5 mol% S-B per reactive group of monomer)
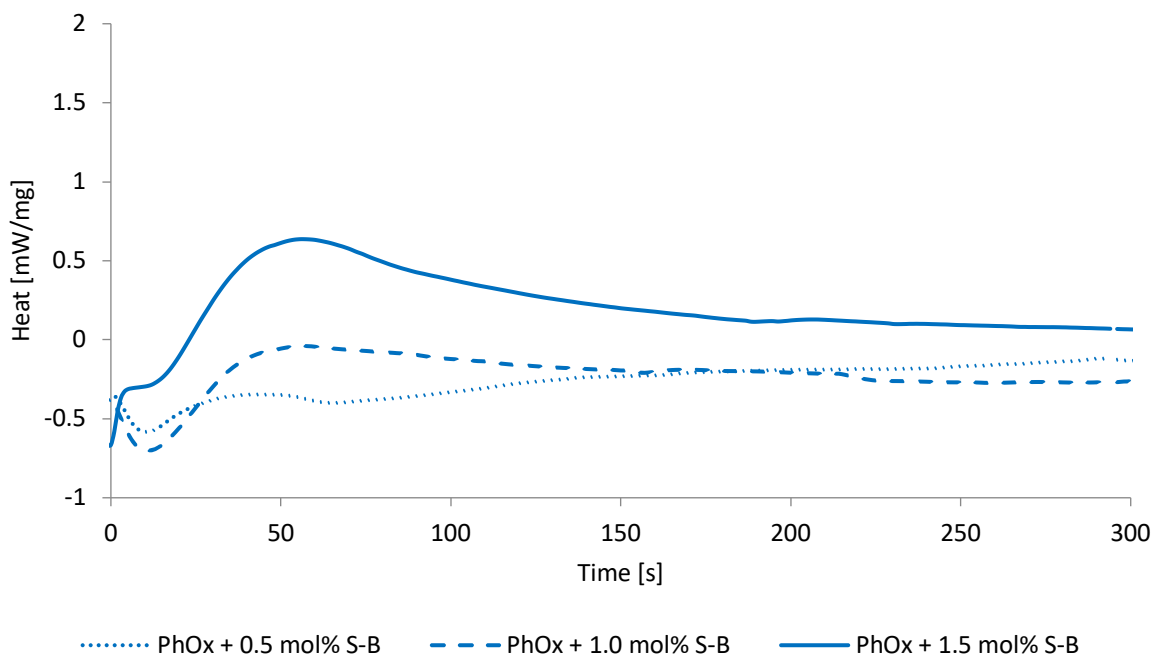
Figure 55: Photo-DSC analysis of PhOx at 120 °C with varied PAG concentration (0.5, 1.0 and 1.5 mol% S-B per reactive group of monomer)

As seen from above analyses, the PAG concentration has a significant influence on the reactivity of 2-oxazoline monomers BisOx, OctOx and PhOx. Whereas the increase from 0.5 to 1 mol% S-B per reactive group gives a great increase in overall reactivity, further increase to 1.5 mol% does not result in reactivity increase in the same extent. Especially in the difunctional monomer BisOx, high amounts of PAG do not lead to significantly higher reactivity. The evaluated photo-DSC results are displayed in Table 12.

Table 12: Results of photo-DSC of BisOx, OctOx and PhOx including 0.5, 1.0 or 1.5 mol% of S-B per reactive group at 120 °C

Monomer	PAG conc. [mol%]	C [%]	t_{max} [s]	R_p [x 10^{-3} mol·L^{-1}·s^{-1}]	t_{95} [s]
BisOx	1	86	48	36.5	247
	2	91	43	49.2	159
	3	91	39	46.0	158
OctOx	0.5	3	38	2.0	130
	1.0	27	42	17.3	171
	1.5	45	49	26.9	207
PhOx	0.5	-*	-*	-*	-*
	1.0	5	65	2.2	280
	1.5	19	57	9.5	543

* no exothermicity detected in DSC

Evidently, increased amounts of S-B lead to higher conversions foremost in monofunctional monomer formulations, as the conversion of monofunctional monomers increases significantly. Furthermore, the polymerization rate increases significantly with increased PAG concentration in monofunctional OctOx and PhOx. In BisOx, however, the reactivity is not increased using higher amounts than 2 mol% S-B, as it reaches a plateau in polymerization rates and conversion.

As the PAG concentration also has a fundamental influence on the molecular weight in cationic polymerizations, more detailed studies were conducted by

photopolymerization of OctOx and subsequent characterization of photopolymers by GPC.

2.7 GPC studies of poly(OctOx)

In contrast to free radical photopolymerization, no chain transfer, recombination or other termination processes occur during the propagation of the cationic chain growth reaction, unless the system is not free of nucleophilic impurities. Therefore, the concentration of initiating species within the system has a direct influence on the number of growing chains and the resulting chain length in the polymer.

By gel permeation chromatography (GPC) the analysis of poly(OctOx) was conducted for samples photopolymerized in two series, namely at temperatures of 100, 120 and 140 °C with 1 mol% PAG, as well as with varied PAG concentrations of 0.5, 1.0 and 1.5 mol% S-B in photopolymerizations at 120 °C. The photopolymerizations were conducted by photo-DSC using equal conditions as in prior photo-DSC studies. Subsequently, the polymers were dissolved in dry THF to give solutions of 3 mg/mL concentration. The measurements by GPC gave the molecular weights M_n and M_w, as well as the polydispersity Đ, which are displayed in Table 13.

Table 13: Results of GPC of poly(OctOx) photopolymerized at temperatures of 100, 120 and 140 °C, and with 0.5, 1.0 and 1.5 mol% S-B at 120 °C

T [°C]	c(PAG) [mol%]	$C_{photo-DSC}$ [%]	M_n [Da]	M_w [Da]	Đ
100		-*	7700	16800	2.2
120	1.0	40	8500	16800	2.0
140		49	9200	19100	2.1
120	0.5	3	9600	21100	2.2
	1.0	40	8500	16800	2.0
	1.5	47	8000	14300	1.8

* no exothermicity detected in DSC

From the GPC results of poly(OctOx) in Table 13 the influence of temperature and PAG concentration during photopolymerization is seen. Using a formulation of OctOx containing 1 mol% S-B, the molecular weights increase with higher temperatures in

photopolymerization. This is reasoned by the enhanced propagation which is strongly influenced by thermal energy input to the photopolymerization. By the increase of PAG concentration in photopolymerizations at 120 °C the expected reduction of molecular weights is observed. The increase of PAG concentration in the cationic photopolymerization of OctOx generates shorter polymer chains in the resulting poly(OctOx). The polydispersity Đ is not significantly influenced by the variation of temperature, however, decreases with increasing PAG concentration presumably due to lower molecular weights and more homogenous molecular weight distribution.

2.8 Photoreactivity studies of 2-oxazoline, epoxy and methacrylate formulations

The cationic photopolymerization of 2-oxazolines enables the production of a new class of photopolymers with promising polymer characteristics. In order to evaluate the properties of 2-oxazoline photopolymers representatively, the direct comparison with photopolymers comprising other reactive moieties was conducted. The focus of these studies was the testing of difunctional 2-oxazoline-, epoxy- and methacrylate-based systems with aliphatic substitution patterns.

Clearly, 2-oxazoline and epoxy monomers can be subjected to direct and analogous comparison in cationic photopolymerization. The aliphatic butanediol diglycidyl ether (BDDGE) is commonly used as a highly reactive and low viscous difunctional reactive diluent in various applications of epoxy resins and served as a suitable reference monomer for the comparison in cationic photopolymerization.

The dimethacrylate butanediol dimethacrylate (BDDMA) was included as a benchmark for reactivity and polymer properties of a system based on free radical photopolymerization, as aliphatic dimethacrylates are highly abundant in UV-curing applications. Also in stereolithography, such as Hot Lithography, aliphatic dimethacrylates are commonly used, yet in formulations containing further modifiers to overcome the high brittleness and to adjust the mechanical properties of the photopolymer material.[3]

Figure 56 shows the synthesized monomer BisOx with the reference monomers BDDGE and BDDMA and their corresponding polymer structures.
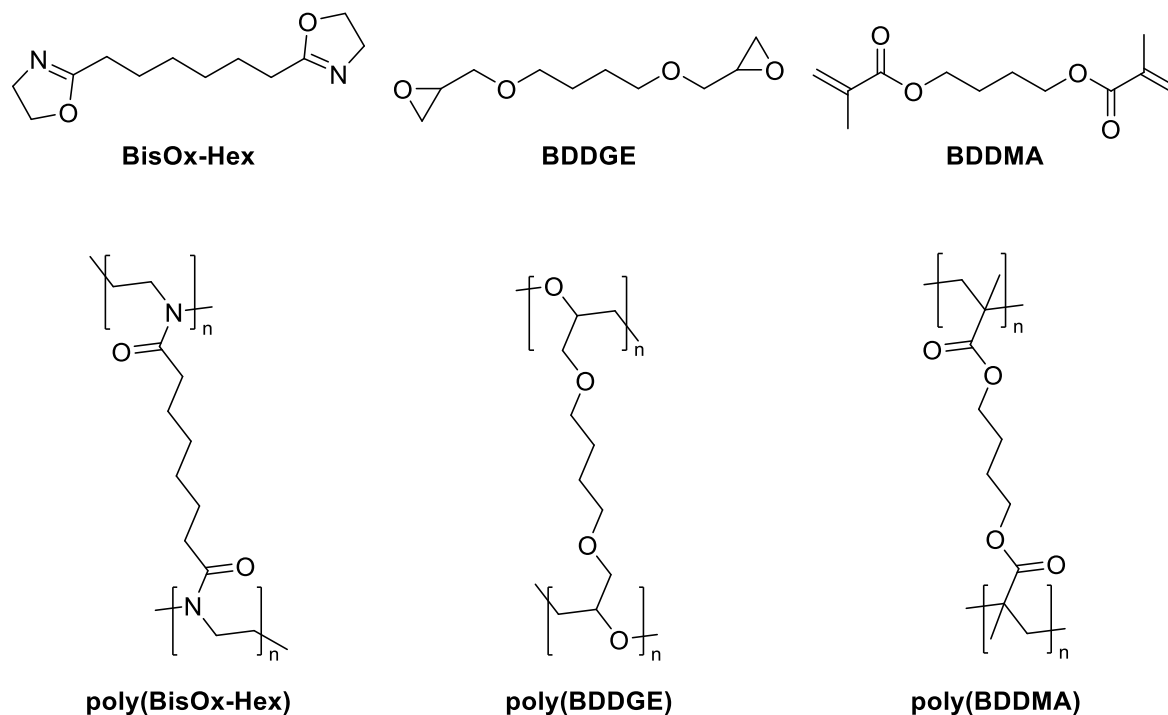
Figure 56: Comparison of 1,6-bis(4,5-dihydrooxazol-2-yl)hexane (BisOx) with reference monomers butanediol diglycidyl ether (BDDGE) and butanediol dimethacrylate (BDDMA); illustration of spacer length within polymer network of poly(BisOx), poly(BDDGE) and poly(BDDMA)

The monomers provide the same spacer length of 8 atoms in crosslinked polymer networks. Thus, expected differences in polymer characteristics are attributed to the influence of the reactive moiety, the corresponding polymerization mechanisms and the resulting polymer backbone structure. As 2-oxazolines generate poly(amide) structures, significantly different properties are expected in comparison to the poly(ether) structures generated in cationic polymerization of epoxy monomers, such as BDDGE. A fundamentally different physical behavior is expected from the polymers arising from free radical photopolymerization of dimethacrylate BDDMA, due to the radical-mediated chain growth and the lack of heteroatoms in the polymer backbone, which diminishes molecular interactions within the network.

In first considerations, the comparative formulations of BisOx, BDDGE and BDDMA with respective cationic and radical photoinitiators were examined for their photoreactivity by photo-DSC and RT-NIR/MIR-photorheology. The formulations consisted of BisOx or BDDGE containing triarylsulfonium PAG S-B, as well as BDDMA containing the highly reactive acylgermane-based free radical photoinitiator BMDG. The structure of BMDG is depicted in Figure 57.
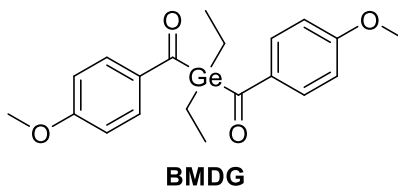
Figure 57: Free radical photoinitiator bis(4-methoxybenzoyl)diethylgermanium (BMDG)

As the 2-oxazoline BisOx only reacts at temperatures beyond 100 °C in sufficient rates, the studies of all formulations were conducted at elevated temperatures to ensure comparable conditions. Temperature screenings by STA showed the thermal stability of respective formulations when heated to elevated temperatures.

Generally, the characterization of purely difunctional monomer formulations throughout and after photopolymerization causes problems due to the insolubility and high brittleness of the photopolymers. An analysis method that allows for detailed monitoring and controlled photopolymerization is provided by RT-NIR/MIR-photorheology. Photorheology displays the change in rheological parameters throughout the photopolymerization process in combination with the reactive group conversion monitoring in real-time NIR/MIR.

In addition to the photorheological measurement, the resulting polymer films were recovered from the thin-layer analysis and submitted to polymer characterizations in DSC and DMTA.

2.8.1 STA of photoreactive formulations of BisOx, BDDGE and BDDMA

In analogy to 2-oxazoline model compounds in section 2.5, the thermal stability limits of photoreactive formulations of BisOx, BDDGE and BDDMA were compared in STA analyses. Thus, the measurements of BDDGE with 1 mol% S-B and BDDMA with 1 mol% BMDG were conducted and evaluated in relation to the foregoing STA analysis of BisOx with 1 mol% S-B. Analyses were performed in a range of 25 to 300 °C using a ramp of 10 K/min. A sample mass of 14 ± 1 mg was used for all measurements. The STA measurements are depicted in Figure 58 in comparative display.
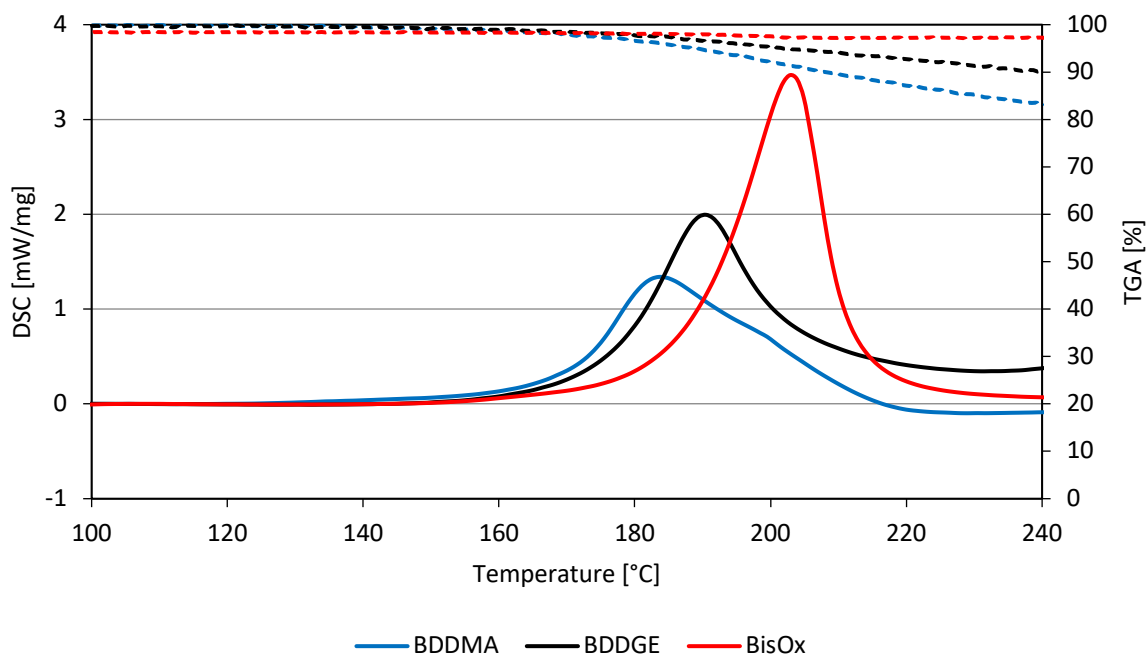
Figure 58: STA analyses of BisOx with 1 mol% PAG (S-Al, S-B, S-C); TGA dashed

As seen from above analyses, the formulations of BDDGE and BDDMA expectedly show reduced thermal stability. Dimethacrylates tend to polymerize at temperatures of around 120 °C, whereas the thermal polymerization of BDDGE is caused by thermal cleavage of S-B in the formulation. The thermal onsets of polymerization are displayed in Table 14.

Table 14: Thermal onset of polymerization from STA measurements of photoreactive formulations of BisOx, BDDGE and BDDMA

Monomer	Thermal onset of polymerization [°C]
BisOx	148
BDDGE	151
BDDMA	129

As seen from the thermal onset temperatures, the thermal polymerization of BDDMA formulations starts at temperatures as low as 129 °C. This limitation expresses the temperature range for applications of photopolymerization at elevated temperatures, such as methacrylate-based systems in Hot Lithography.

Although high thermal stabilities over 200 °C were observed for formulations of S-B in low reactive aromatic diglycidyl ether BADGE (section 1.3), the formulation of highly reactive aliphatic diglycidyl ether BDDGE polymerizes at lower temperatures of 151 °C. Clearly, the greater induction periods of aliphatic glycidyl ethers at low temperatures are not pronounced at elevated temperatures. In comparison, also the low rate propagation of BisOx is facilitated above 148 °C, once initiating species are liberated by thermal decomposition of S-B.

2.8.2 RT-NIR/MIR-Photorheology of BisOx, BDDGE and BDDMA formulations at 100 °C

The analysis via RT-NIR/MIR photorheology is a powerful tool to follow the progression of the photopolymerization by *in situ* rheologic measurement and real-time reactive group conversion. Based on a reported method by Gorsche et al., the cationic photopolymerization of BADGE can be followed by RT-NIR-analysis, as the glycidyl moiety gives a distinct signal around 4530 cm^{-1} and decreases to baseline level in course of the progressing polymerization.[88] This method was used to follow the conversion of BDDGE, as the epoxy vibration band appears at the same frequency. The decreasing double bond signal in RT-NIR measurements of BDDMA formulations was followed by the band around 6160 cm^{-1}.

The measurements were conducted at the maximum applicable temperature of 100 °C. The rheologic plate-to-plate setup comprised a gap size of 200 µm between the stainless-steel upper plate and a quartz glass lower plate covered with PE tape. The photopolymerization was initiated using 320-500 nm broadband irradiation with a maximum applicable intensity of 80 mW/cm^2 in sample position. Due to the reduced irradiation intensity and temperature in comparison to photo-DSC analyses, 2 mol% of respective photoinitiators were used in the formulations to obtain fully cured samples within the set irradiation period of 900 s. Hence, formulations of BisOx with 2 mol% S-B, BDDGE with 2 mol% S-B and BDDMA with 2 mol% BMDG were used. For each measurement, 150 µL of formulation were applied.

In the photorheological measurement, the gel point is indicated by the cross-section of storage and loss modulus, G' and G'', following the abrupt solidification of difunctional monomers. As most representative parameters, the time to reach the gel point (t_g), the

conversion at gel point (C_g), the time of 95 % conversion (t_{95}) and the final conversion (C_{final}) are defined and were accessible by evaluation using the corresponding analytic software.

Figure 59 shows the conducted comparative analysis of BisOx, BDDGE and BDDMA formulations at 100 °C.
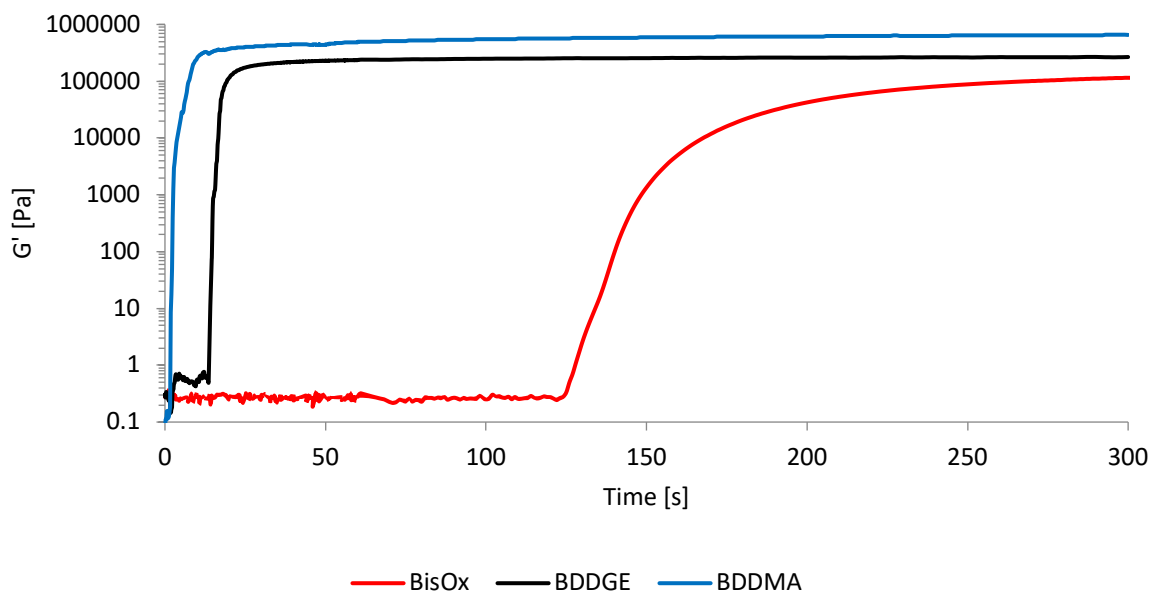
Figure 59: Storage moduli over time in the photorheology measurements of formulations of BisOx, BDDGE and BDDMA at 100 °C

The distinct reactivity difference of the systems is primarily expressed by the gel points t_g. The dimethacrylate BDDMA and the diglycidyl ether BDDGE show fast photopolymerization with t_g of 1.7 s and 14.4 s, whereas the gel point of low reactive BisOx occurs at 125 s. The conversion was monitored by the NIR signal of reactive groups in the course of the photopolymerization. The conversions were determined for the epoxy signal of BDDGE and the double-bond signals of BDDMA, however, no representative signals could be evaluated in the spectra for BisOx throughout the polymerization. Figure 60 shows the NIR spectra of BisOx formulation at the beginning (t_0), the gel point (t_g) and the end (t_{final}) of the RT-NIR-photorheology measurement.
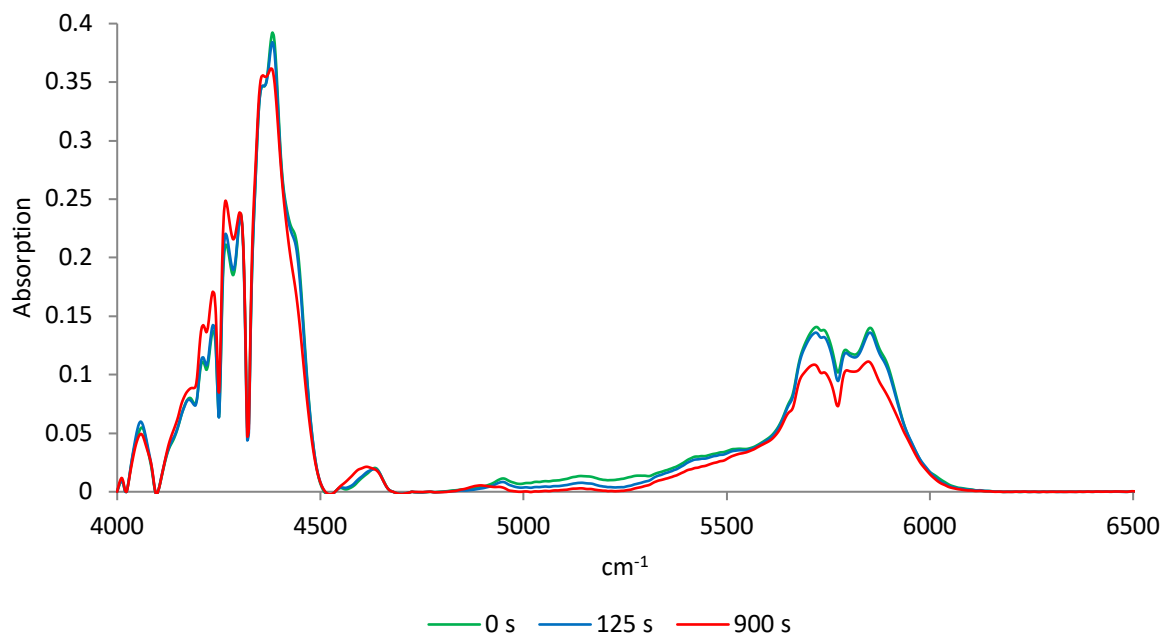
Figure 60: NIR spectra at times of 0 seconds, 125 s (t$_g$; gel point) and 900 s of the photorheology measurement of BisOx formulation (200 µm, 100 °C)

Evidently, the NIR spectra does not give signals, which exhibit significant change in course of cationic photopolymerization. Therefore, MIR-photorheology analysis was considered to follow the conversion of 2-oxazoline monomers. It was assumed that the diminishing signal of the 2-oxazoline C=N vibration (1667 cm^{-1}), or the increase of the intense carbonyl C=O signal (1634 cm^{-1}) could be followed in MIR. RT-MIR-photorheology measurements were conducted using a calcium fluoride lower plate to allow for transmission of MIR radiation. Furthermore, due to the high intensity of signals in MIR, the gap size was reduced to the minimum applicable distance of 50 µm. The IR spectra resolved at the beginning, the gel point and the end of the RT-NIR-photorheology measurement of BisOx formulation are depicted in Figure 61.
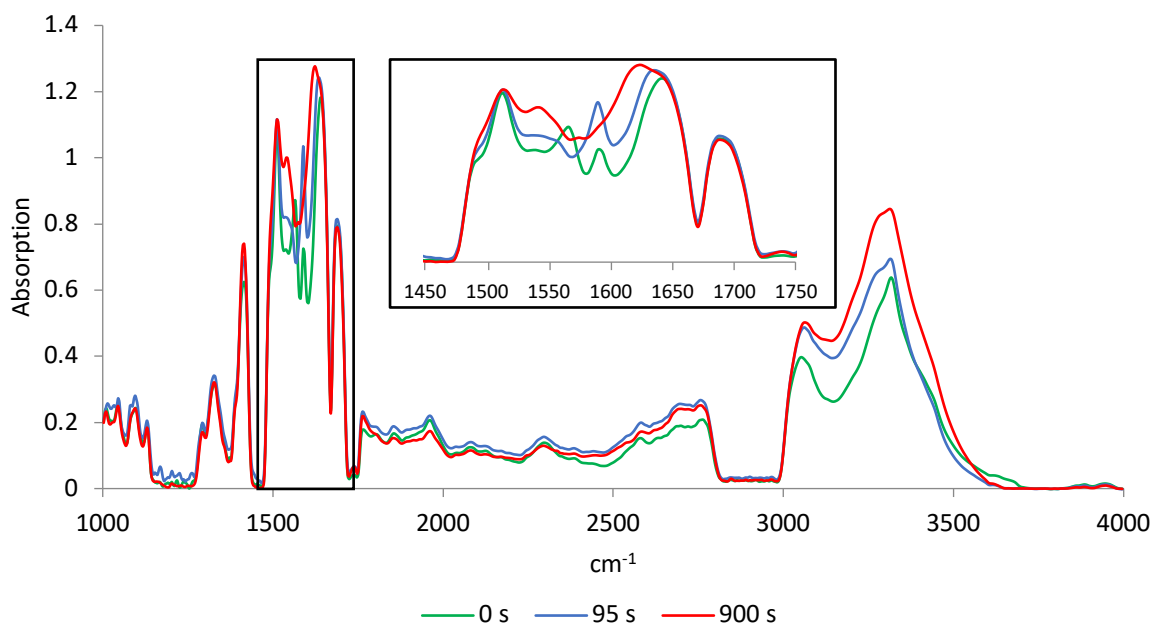
Figure 61: MIR spectra at times of 0 seconds, 95 s (t$_g$; gel point) and 900 s of the photorheology measurement of BisOx formulation (50 µm, 100 °C)

The high intensity of the observed signal generally interferes with correct evaluation, as they leave the range of linearity according to Lambert-Beer's law. Besides this, the signals do not show selective change and could not be correlated to the conversion of the photopolymerization. As 50 µm of gap size was the minimum which could be applied (using PE-tape and 100 °C), no increase in resolution or correction of signals was possible. The strong intensity and poor deconvolution of vibrational signals in the considered range inhibits the evaluation of conversion in RT-MIR-photorheology measurements of BisOx monomer.

From the applicable evaluation of formulations of BDDGE and BDDMA in NIR, the results were correlated to the photorheologic measurement and visualized as epoxy conversion (EC) for BDDGE and double bond conversion (DBC) for BDDMA. Figure 62 shows the RT-NIR-photorheology analysis of BDDGE and BDDMA formulations including conversion curves.
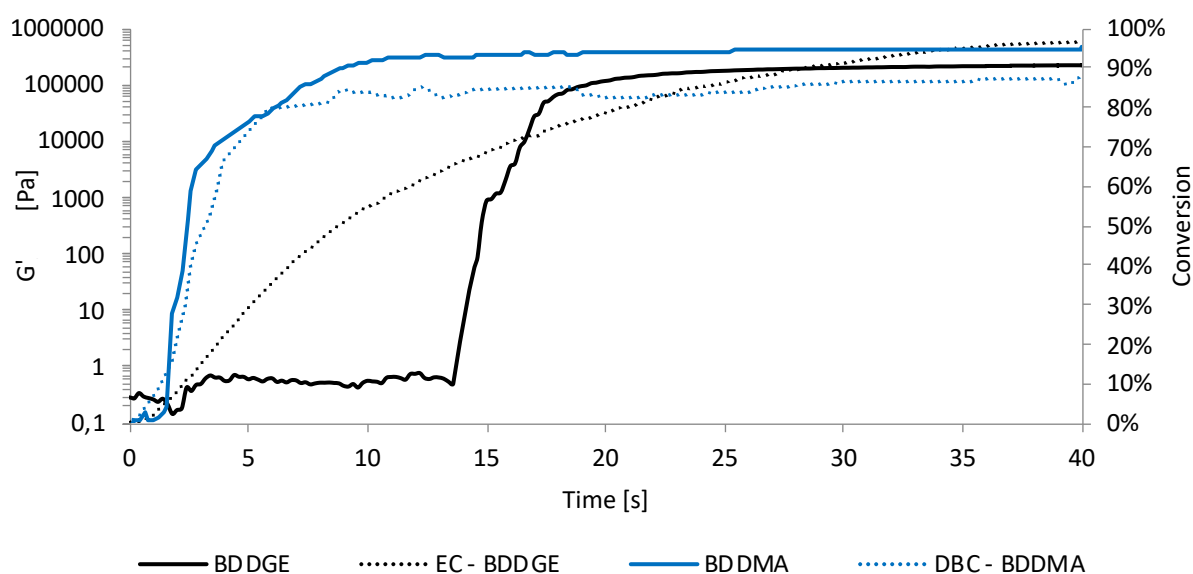
Figure 62: RT-NIR-photorheology of BDDGE and BDDMA formulations with NIR conversion curves

One can see that the conversion curve of BDDMA shows much faster increase due to the generally higher reactivity of the system in comparison to the cationically photopolymerized epoxy monomer BDDGE. A conversion at gel point C_g of 24% is observed, whereas the final conversion C_{final} reaches 89%.

Table 15: RT-NIR-photorheology results of formulations of BDDGE and BDDMA at 100 °C

	t_g [s]	C_g [%]	t_{95} [s]	C_{final} [%]
BDDGE*	14.4	67	35	99
BDDMA	1.7	24	11	87

*strong discoloration

As observed during the measurement of BDDGE, intense discoloration occurred in the epoxy polymer. The lower reactivity of BDDGE was related to the increasingly limited penetration depth of UV irradiation into a dark polymer layer of 200 µm thickness. This explains the delayed t_g of 14 s, and the excessively high C_g of 70 %, whereas BDDMA shows a rapid gel point and C_g of 24 %. Still, the cationic photopolymerization of BDDGE reaches t_{95} after 35 s and a high C_{final} of 99 %. The inhibited polymerization

behavior of BDDGE formulation was subsequently further examined in studies with variation of layer thickness in photorheology.

Moreover, the comparative measurements of BisOx, BDDGE and BDDMA gave polymer films with suitable thickness of 200 µm for subsequent thermal characterization of the photopolymers. Poly(BisOx) and poly(BDDGE) could be recovered as stable and homogeneously cured discs with a diameter of 25 mm, whereas poly(BDDMA) was too brittle to give a complete polymer disc from photorheology. In consequence, all three polymer samples where investigated by differential scanning calorimetry (DSC), however, only poly(BisOx) and poly(BDDGE) were additionally examined by dynamic-mechanical thermal analysis (DMTA) in tension mode.

2.8.2.1 Influence of gap size and discoloration on the photorheology analysis of BDDGE

Although the photorheology setup allows for accurate control over dimension and light distribution on the sample, the foregoing analyses of BDDGE formulations showed unreliable results of conversion and rheological parameters. It was observed that the conversion had already reached around 70 % as soon as the gel point occurred. This, however, seems rather unreliable in this highly cross-linked polymer network. Comparative literature values of the monomer BADGE at 70 °C show C_g values of around 25 % at a time of t_g = 90 s.[88] The results reached within the presented analysis are highly questionable, as the gel point was expected to occur at much lower conversions. The source of error that seems most probable under these circumstances is the discoloration of the sample during the measurement. The samples of BDDGE turn dark brown during polymerization and presumably shield the irradiation from penetrating the whole sample simultaneously. The UV-light may firstly induce photopolymerization in the bottom-most layer of the sample and generate a polymerization gradient within the thickness of the layer. By this, high conversion is detected in the overall transmission IR-spectrum, although the irradiation did not yet polymerize the upper layer of the material, where the stainless-steel plate instrument is in contact. This may cause a shift of the gel point to much higher overall conversions than in samples, which are cured simultaneously in the whole layer, such as free radical photopolymerization using photo-bleaching BMDG.

Therefore, the intrinsic discoloration in the photopolymerization of the diglycidyl ether BDDGE was investigated in detail within further measurements. To overcome the potential build-up of a gradient within the sample, analysis with lower gap size 100 µm or 50 µm should be performed to rule out this source of deviation without affecting the rheological measurements significantly. It was assumed a conversion gradient occurred within the thickness of the sample and that a reduction of gap size would shift the gel point to occur earlier and at lower conversions. Comparative measurements with 50, 100 and 200 µm gap size were performed and displayed in Figure 63.
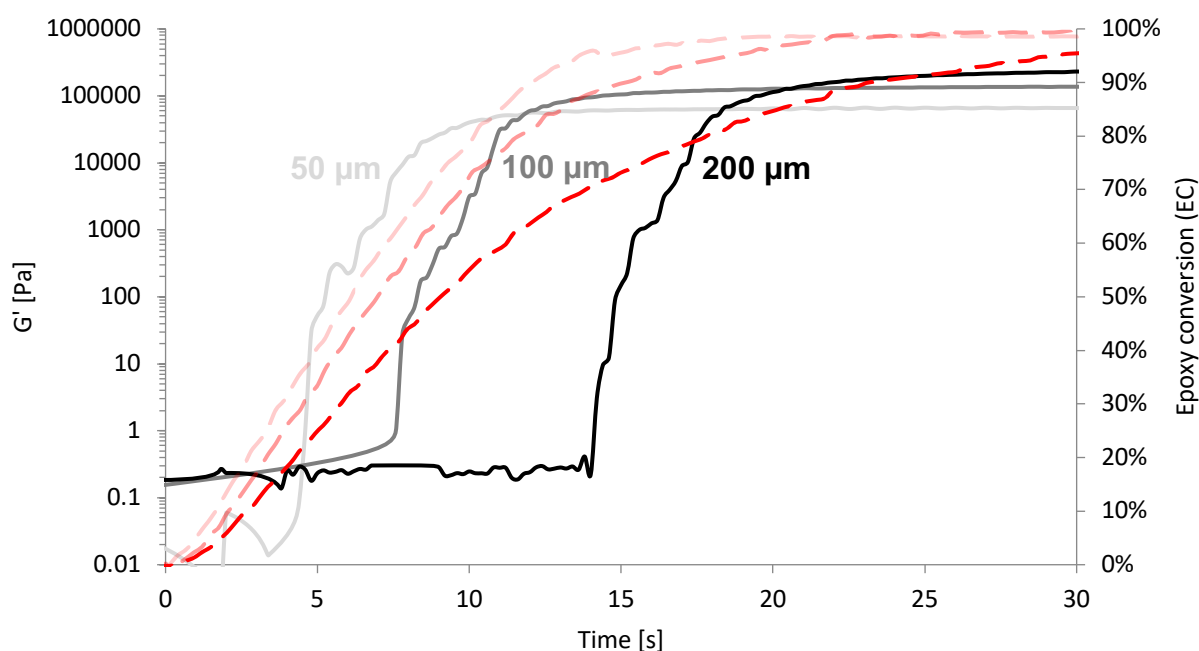
Figure 63: Influence of gap size on photorheology measurement of BDDGE; 50 µm (G ' — , EC —); 100 µm (G ' — , EC —), 200 µm (G ' — , EC —)

The curves show the general trend of the t_g shifting not only to earlier times (14.4 s → 7.6 s → 4.7 s), but also to much lower C_g with decreased gap size (70 % → 54 % → 37 %). Also, the slope of conversion throughout the sample thickness is significantly faster with decreased gap size, which confirms the assumption of a conversion gradient arising from inhibited light penetration into the depth of the sample due to dark discoloration. Clearly, a strong discoloration has a crucial impact on photorheology analysis in cationic photopolymerization.

2.8.2.2 DSC of poly(BisOx), poly(BDDGE) and poly(BDDMA)

The thin film polymer samples of poly(BisOx), poly(BDDGE) and poly(BDDMA) were obtained from photorheology measurements and investigated in polymer analysis by DSC and DMTA. DSC analysis shows the glass transition temperature by a change in heat capacity of the polymer. By a significant endothermal shift the DSC signal indicates the phase transition in the inflection point of the curve. As reported, thermally polymerized monofunctional 2-oxazoline show a range of glass transitions for amorphous linear PAOx between 80 °C for poly(MeOx) and 10 °C for poly(HexOx), whereas higher derivatives give semi-crystalline and crystalline polymers. [131] However, only limited data is reported for thermosetting difunctional 2-oxazolines, such as α,ω-bis(2-oxazolinyl)-substituted oligo(tetrafluoroethylene)s, which give thermally cured polymers with glass transition temperatures between 72 and 95 °C.[128]

For the analyses of poly(BisOx), poly(BDDGE) and poly(BDDMA) a broad phase transition was expected. DSC samples were analyzed in 2 cycles in a range from -80 to 250 °C to ensure full thermal post-curing of the polymers. The second cycle gives the glass transition temperatures of the fully polymerized samples. Figure 64 shows the thermal behavior of the photopolymers from photorheology measurements by DSC curves in the first heating cycle.
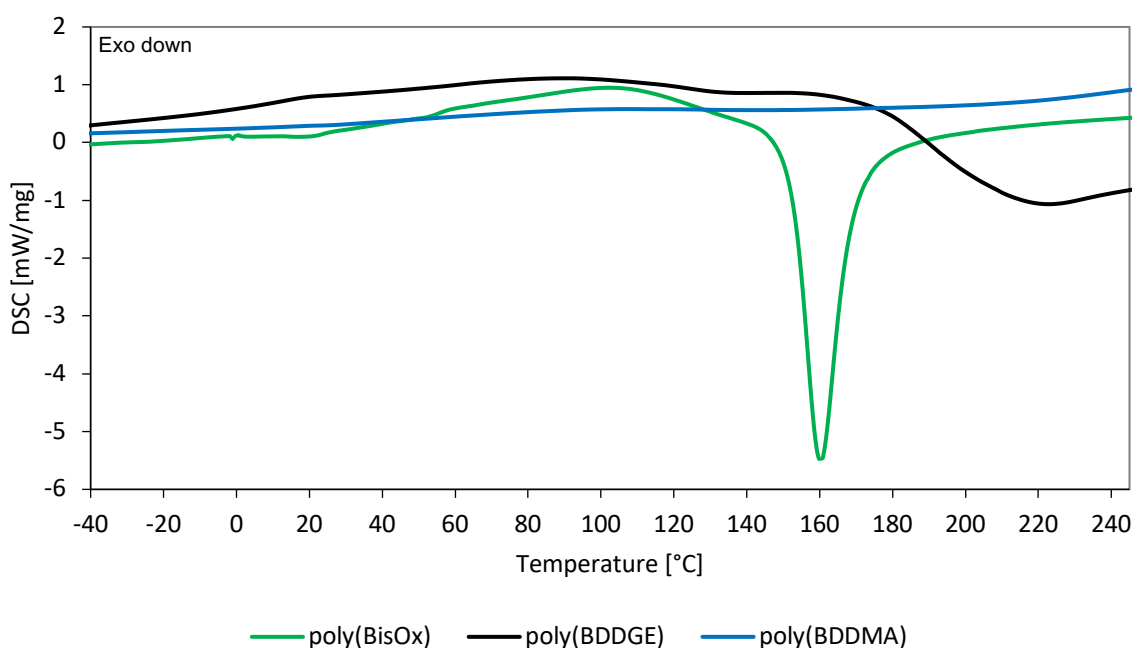
Figure 64: Thermal analysis of photopolymers by DSC (1st heating cycle)

As seen from the thermal post-curing of poly(BisOx) by distinct exothermicity, full conversion was not reached in photorheology measurements at 100 °C. Also the epoxy polymer poly(BDDGE) shows exothermicity at temperatures above 150 °C arising from thermal polymerization in agreement to prior STA analyses (2.8.1).

In the second heating cycle the effects of changed thermal properties are considered, as all polymers were post-cured at temperatures distinctly above their intrinsic T_g after photopolymerization. The DSC curves of the second heating cycle and the indicated glass transition temperatures are shown in Figure 65.
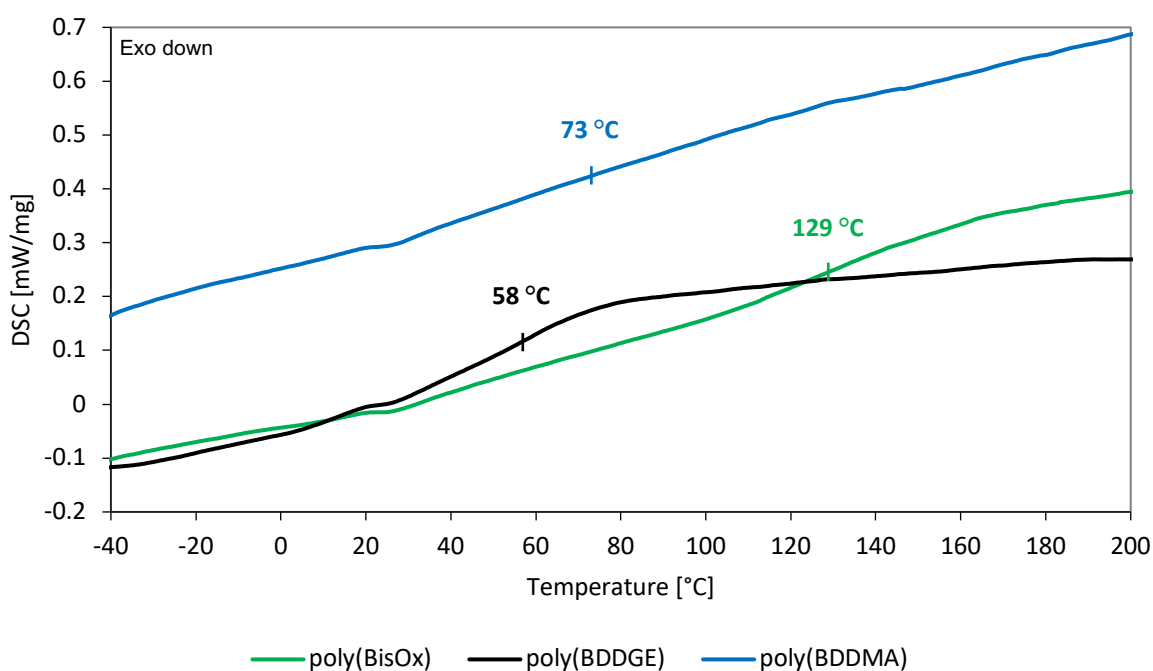
Figure 65: Thermal analysis of photopolymers by DSC (2nd heating cycle)

The comparative analysis of the three polymer samples show the glass transitions at maximal conversion of the polymers. As expected, the epoxy reference poly(BDDGE) shows a low T_g of 58 °C, which is in good correlation with literature data of 55 °C to 75 °C.[168] In comparison, the equally treated poly(BisOx) shows very high T_g of 129 °C within this analysis. Although a very broad phase transition is observed, a high T_g is observed and attributed to the resulting poly(amide) backbone structure, as all other parameters, such as molecular structure, type and concentration of photoacid generator as well as photopolymerization conditions were comparable to the epoxy reference BDDGE.

The reference poly(BDDMA) was photopolymerized by free radical photopolymerization mechanism under equal conditions as poly(BDDGE) and poly(BisOx). It shows an indistinct phase transition with very low shift of heat capacity throughout the heating process. Using the instruments calculative tool for indication of the inflection point, a T_g of 73 °C was detected. The broad glass transition is given by the high crosslink density arising from the uncontrolled free radical polymerization with inhomogeneous polymer network formation and high probability of chain transfer reactions.

In conclusion, the 2-oxazoline monomer BisOx gives photopolymers with significantly higher glass transition temperatures than comparable reference monomers BDDGE and BDDMA, which were photopolymerized under equal conditions. The polymer backbone structure with higher intermolecular interactions is interpreted as the reason for this difference. Especially the direct comparison of the cationically polymerizable monomers BisOx and BDDGE shows a great difference of T_g. The photopolymers of these cationically polymerizable monomers were subsequently examined by thin film DMTA measurements in tension mode to investigate their thermomechanical properties.

2.8.2.3 DMTA of poly(BisOx) and poly(BDDGE)

Only the samples poly(BisOx) and poly(BDDGE) were recovered as sufficiently loadable polymers after photopolymerization in photorheology. Therefore, these two specimens were additionally analyzed by thin layer DMTA in tension mode, to investigate the change of storage modulus over temperature and reconfirm the T_g. For anhydride-cured BDDGE a storage modulus at 0 °C between 2100 and 2800 MPa, and T_g of 45 °C is reported for DMA analyses.[168] In contrast to DSC measurements, the destructive tension mode DMTA analysis was conducted in one heating cycle only, hence, showing the properties of purely light-cured polymers without thermal post-curing. In DMTA measurements, the peak of loss factor tanδ, which is derived as the quotient of storage modulus G' and loss modulus G'', indicates the glass transition temperature T_g.

Figure 66 shows the DMTA analysis of poly(BisOx) and poly(BDDGE) in tension mode.
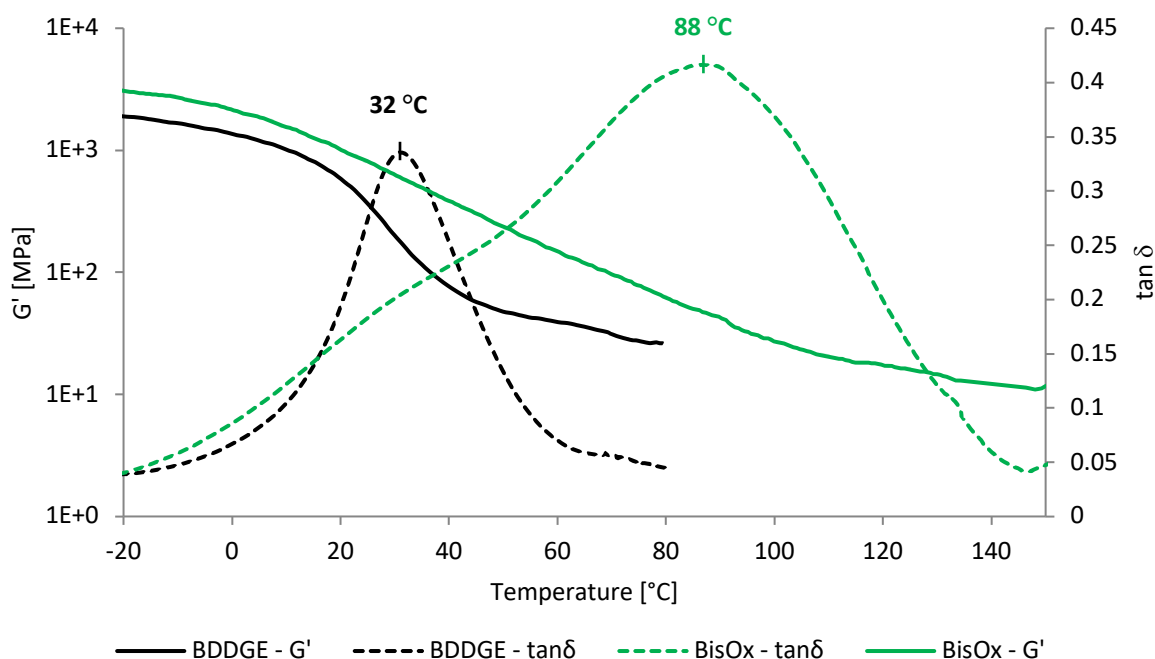
Figure 66: DMTA measurements of poly(BisOx) and poly(BDDGE) in tension mode

In comparison to the T_g values of post-cured polymers in previous DSC measurements, the results of DMTA measurement give lower T_g values. The T_g of poly(BDDGE) deviates by 15 °C, whereas the T_g of poly(BisOx) deviates by 40 °C due to the incomplete curing reaction at 100 °C. Nevertheless, poly(BisOx) shows a higher storage modulus than poly(BDDGE). Same as the comparably higher glass transition temperature, this property is attributed to the inherently stronger interactions within the network, arising from the poly(amide) backbone structure of the polymer.

2.8.3 Shrinkage of BisOx, BDDGE and BDDMA formulations in photorheology

Further NIR-photorheology studies were conducted with formulations of BDDGE and BDDMA at 25 °C and compared to the formulation of BisOx at 100 °C. The photorheology measurements below respective glass transition temperatures allowed for the investigation of shrinkage during photopolymerization, as it correlates with the normal force (F_N) applied on the rheometer tool in photorheology measurements. Cationic photopolymerization of ring-opening monomers reportedly exhibits distinctly lower shrinkage upon cure than free radical photopolymerizations of methacrylate monomers.[3, 34] For low molecular weight bis(2-oxazoline)s shrinkage of 7-8 % is

reported, whereas other low-molecular weight difunctional monomers reach shrinkages typically over 10%.[128]

Corresponding to prior photorheology studies, the formulation of BisOx including 2 mol% S-B was measured at the maximum applicable temperature of 100 °C, whereas BDDGE (+ 2 mol% S-B) and BDDMA (+ 2 mol% BMDG) were measured at 25 °C. All parameters except the temperature were kept equal to formerly conducted analyses. The onset of solidification is depicted in the time-resolved plot of storage moduli G' throughout the photorheology measurements in Figure 67.
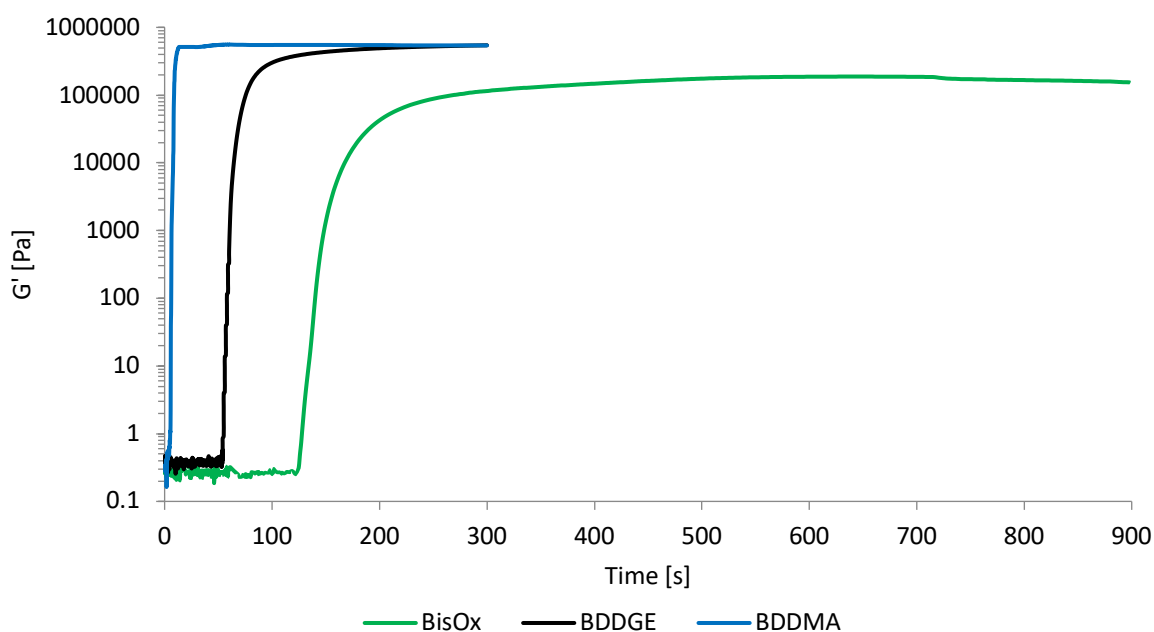
Figure 67: Photorheology measurements of BisOx (100 °C), BDDGE (25 °C) and BDDMA (25 °C) formulations

The gel points were detected at t_g = 6s (BDDMA), t_g = 56 s (BDDGE) and t_g = 125 s (BisOx). Lowering the temperature in photorheology analysis of BDDGE and BDDMA formulations to 25 °C has a significant effect on the curing behavior. Whereas the dimethacrylate BDDMA shows only low delay in t_g, the diglycidyl ether BDDGE exhibits a great retardation of t_g in comparison to the analysis at 100 °C. As the ring-opening polymerization of the epoxy monomer BDDGE is thermally driven, it is crucially influenced by the lowered temperature. The rapid propagation of radically polymerizing BDDMA is clearly less influenced by the temperature decrease to 25 °C.

In correlation to the storage modulus, the magnitude of normal force increases abruptly for the rapidly polymerizing monomers BDDGE and BDDMA, whereas the low reactive BisOx formulation shows slow increase of normal force. The plot in Figure 68 depicts the evolution of normal force (F_N) on the rheometer tool throughout the measurements.
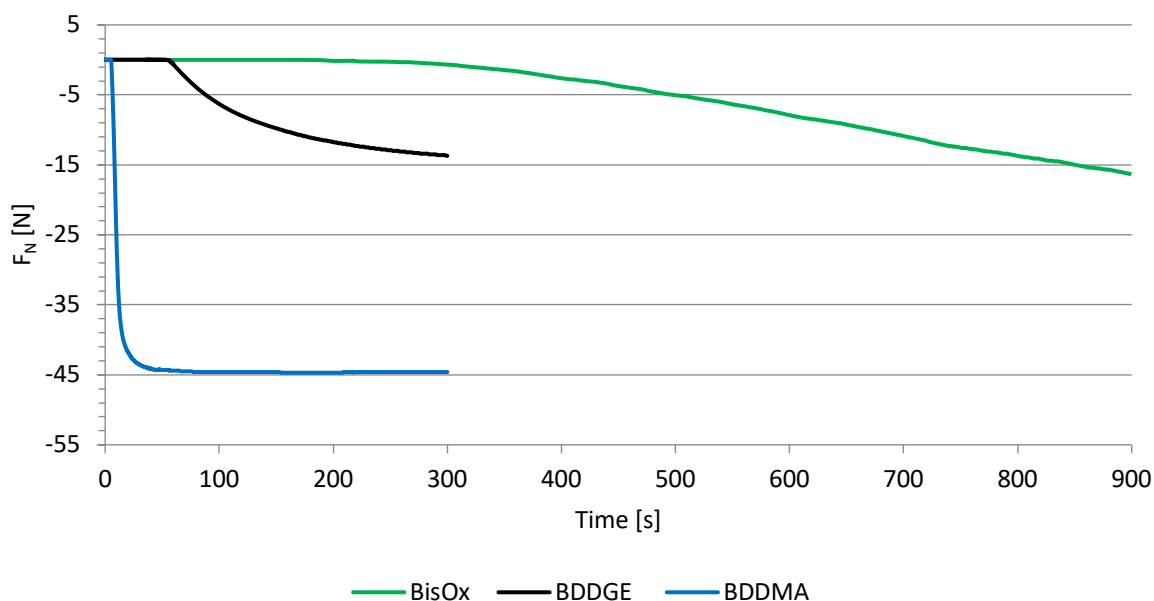
Figure 68: Normal force F_N in the photorheology measurements of BisOx (100 °C), BDDGE (25 °C) and BDDMA (25 °C) formulations

The rise in shrinkage stress, displayed by abruptly increasing normal force pulling on the rheometer tool, occurs at the same time as the gel point. The extent of shrinkage can be quantified and compared by the maximum normal force. The methacrylate formulation of BDDMA shows distinctly higher shrinkage force of -45 N compared to BDDGE and BisOx, which reach maximum values of about -15 N within the measuring time. However, according to the real time NIR conversion measurement it was seen, that BDDMA and BDDGE reach their maximum conversion within 300s causing the evolution of shrinkage to cease, whereas the cationically photopolymerized BisOx does not reach its maximum shrinkage with the respective irradiation times of 900 s. No trend of approximation towards a final shrinkage is observed in the curve, which indicated further shrinkage to occur with proceeding polymerization at 100 °C. According to the comparison between the epoxy monomer BDDGE and the 2-oxazoline BisOx, it can be summarized that the 2-oxazoline does not show advantageous shrinkage behavior over the epoxy monomer upon

photopolymerization, however, greatly enhanced shrinkage properties in comparison to low molecular weight dimethacrylate BDDMA.

2.9 Thermomechanical properties of poly(2-oxazoline)s

Besides the beneficial reaction characteristics of cationic photopolymerization, the major driving force for novel approaches at elevated temperatures is to obtain photopolymer materials with improved mechanical strength and toughness. Following the investigation of reactivity of different 2-oxazoline monomers in foregoing studies, the analysis of material properties was conducted. To test stressable materials solely based on 2-oxazoline monomers, the 2-oxazoline model compounds 2-phenyl-2-oxazoline (PhOx), 2-octyl-2-oxazoline (OctOx) and 1,6-bis(4,5-dihydrooxazol-2-yl)hexane (BisOx) were used in photoreactive formulations of different compositions. The molecular structures of these 2-oxazoline model compounds are depicted in Figure 69.
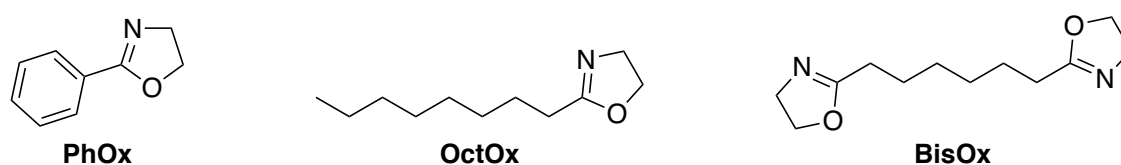
Figure 69: 2-phenyl-2-oxazoline (PhOx), 2-octyl-2-oxazoline (OctOx) and 1,6-bis(4,5-dihydrooxazol-2-yl)hexane (BisOx)

For the preparation of suitable specimen based on 2-oxazoline formulations, a setup for UV-curing at elevated temperatures was established to produce 2-oxazoline materials by cationic photopolymerization.

2.9.1 UV-Curing of 2-oxazoline-based photopolymers at elevated temperatures

In foregoing photo-DSC analyses it was found that a temperature between 100 and 140 °C provides sufficient thermal energy for the UV-induced cationic ring-opening polymerization in reasonable periods of time and without thermally induced polymerization. Also, for the investigation of material properties, a "hot UV-curing" process was necessary to ensure sufficient curing efficiency in the production of specimen for thermomechanical testing.

The UV-curing process was conducted by adhering a preheated silicon mold to a custom-made heating plate with temperature control. The heating plate and silicon mold was conditioned to 140 °C inside a UV floodlight oven and subsequently filled with photopolymerizable formulation. The setup was irradiated for 900 s, the sample was turned upside-down, and irradiated from the bottom side for another 900 s.

Using this UV-curing procedure at elevated temperatures, 2-oxazoline-based formulations of any composition could be photopolymerized in the desired dimensions. Thus, specimen for thermomechanical testing by DMTA, tensile testing, Dynstat impact resistance and thermal analysis were prepared for the following investigations.

2.9.2 DMTA screening of 2-oxazoline-based photopolymers

The 2-oxazoline-based photopolymers were analyzed by thermomechanical methods, such as DMTA, tensile testing, DynStat impact resistance testing and STA. Different compositions of the components PhOx, OctOx and BisOx were prepared containing 1 mol% S-B per reactive group of respective monomers.

The materials produced in the above described manner were primarily tested in DMTA to determine the correlation of monomer composition and the properties of resulting photopolymers. Firstly, a composition of 10 mol% crosslinker BisOx and 90 mol% monofunctional 2-oxazoline PhOx was tested. The photopolymer specimen was prepared in above described UV-curing procedure at 140 °C. The analysis of the specimen was performed in two runs up to 250 °C in order to investigate a thermal post-curing effect and the change of the polymer network when exceeding the glass transition temperature T_g. The repeatedly conducted analysis of a photopolymer of BisOx/PhOx 10:90 is depicted in Figure 70 and shows the influence of the thermal post-curing.
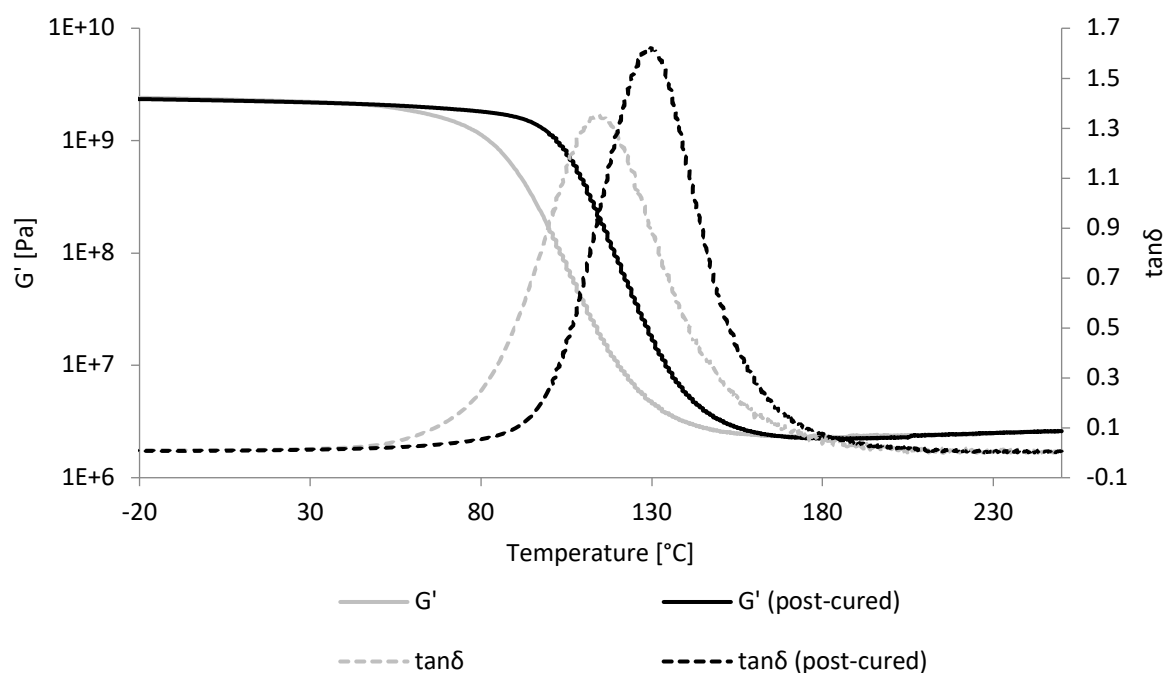
Figure 70: DMTA analysis of a photoreactive formulation of BisOx/PhOx 10:90 in two consecutive heating cycles

Evidently, a distinct post-curing effect is observed in the comparative display. The PhOx-based formulation exhibits a high T_g of 111 and 131 °C, respectively. The thermal properties in literature indicate T_g values of thermally cured poly(PhOx) of 103 °C to 107 °C, which shows good agreement.[129, 162] As further parameters, the storage modulus at 20 °C (G'_{20}) and the storage modulus in the rubbery region (G'_r; measured at $T_g + 30$ °C) were accessible, giving values of $G'_{20} = 2200$ MPa and $G'_r = 2.6$ MPa.

This formulation based on aromatic PhOx gave photopolymers, which could not be tested under mechanical stress due to its high brittleness. Therefore, mixtures additionally containing aliphatic OctOx were photopolymerized at 140 °C to increase the toughness of resulting materials. A DMTA screening should provide significant information about which formulations give suitable mechanical properties for subsequent tensile testing and impact resistance testing. It was expected that the different monofunctional monomers in the compositions have a significant influence on the glass transition temperature T_g of the polymer. The aromatic PhOx should generate a very rigid polymer with high T_g values, whereas the flexible aliphatic n-octyl substituent of OctOx should enhance the ductility of the material and give a lower T_g.

Also, the increase of the concentration of crosslinker BisOx in the formulation was considered in order to investigate the impact on the mechanical strength of the material. This gave two comparative DMTA measurement series.

The first series showed the influence of the ratio of aliphatic (OctOx) and aromatic monofunctional monomer (PhOx) with fixed crosslinker concentration (10 mol% BisOx). Herein, molar ratios of OctOx/PhOx 2:1, 1:1 and 1:2 were used, giving corresponding compositions of BisOx/OctOx/PhOx in molar ratios of 10:60:30, 10:45:45 and 10:30:60. The photopolymers of different formulations should express the influence of aliphatic and aromatic side groups on the mechanical properties of 2-oxazoline-based materials. Figure 71 shows the obtained DMTA measurement curves with the OctOx/PhOx ratios described above.
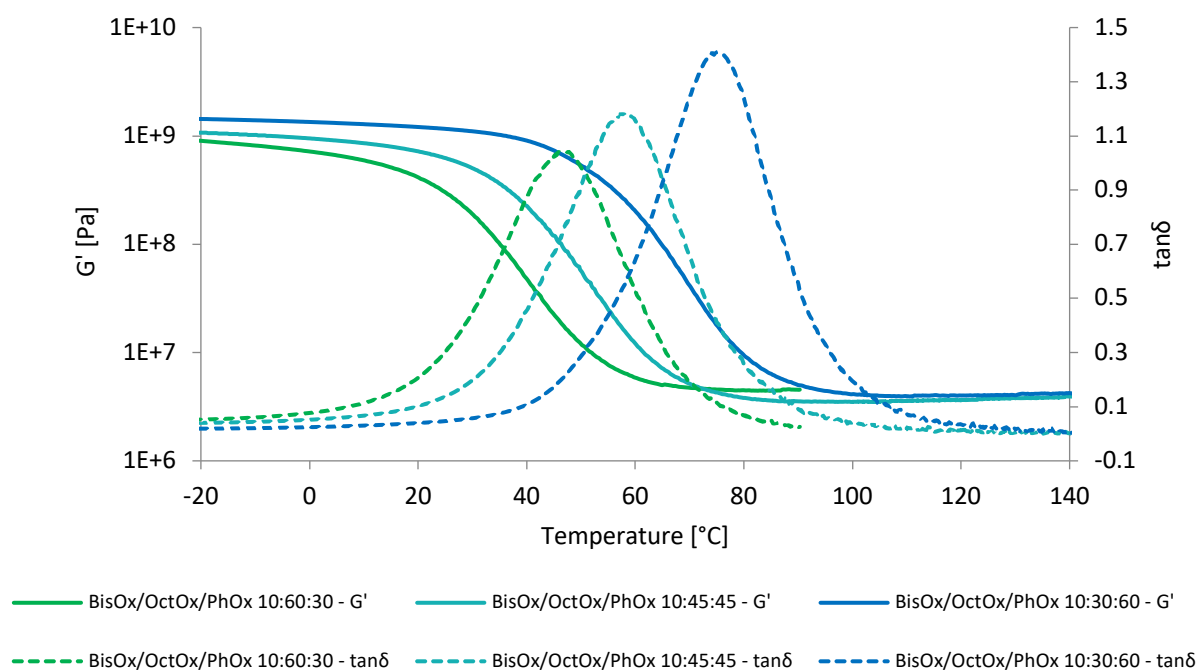
Figure 71: DMTA analysis with variation of monofunctional ratio (OctOx/PhOx 2:1, 1:1, 1:2)

As expected, a general trend towards higher storage moduli G' and higher T_g is observed with the use of greater amounts of aromatic monomer PhOx. In dependence of the monofunctional ratio, the formulations showed results displayed in Table 16.

Table 16: Glass transition temperatures (T_g) and storage moduli (G'_{20} and G'_r) of 2-oxazoline-based materials with variation of monofunctional ratio (OctOx/PhOx 2:1, 1:1 and 1:2)

BisOx/OctOx/PhOx	T_g [°C]	G'_{20} [MPa]	G'_r [MPa]
10:60:30	48	400	4.5
10:45:45	59	700	3.5
10:30:60	76	1200	4.0

All three photopolymers of these compositions exhibit lower T_g and G'_{20} than the photopolymer of BisOx/PhOx 10:90. In fact, the sample BisOx/OctOx/PhOx 10:60:30 exhibits a low T_g of 48 °C, thus, an already distinctly reduced storage modulus at 20 °C. With increased ratio of aromatic PhOx in the sample BisOx/OctOx/PhOx 10:60:30 an increase of T_g is observed from the analysis, however, a loss of ductility was observed upon handling of the photopolymer. Therefore, the equimolar ratio of OctOx/PhOx 1:1 is considered as the best option to achieve suitable properties for further material testing.

In the second measurement series, the variation of crosslinker concentration was investigated with fixed monofunctional ratio (OctOx/PhOx 1:1). The concentration of BisOx was changed from 10 to 20 to 30 mol%, respectively. In analogy to earlier preparations, the formulations were UV-cured at 140 °C. The materials were examined by DMTA and the analysis resulted in the plots depicted in Figure 72.
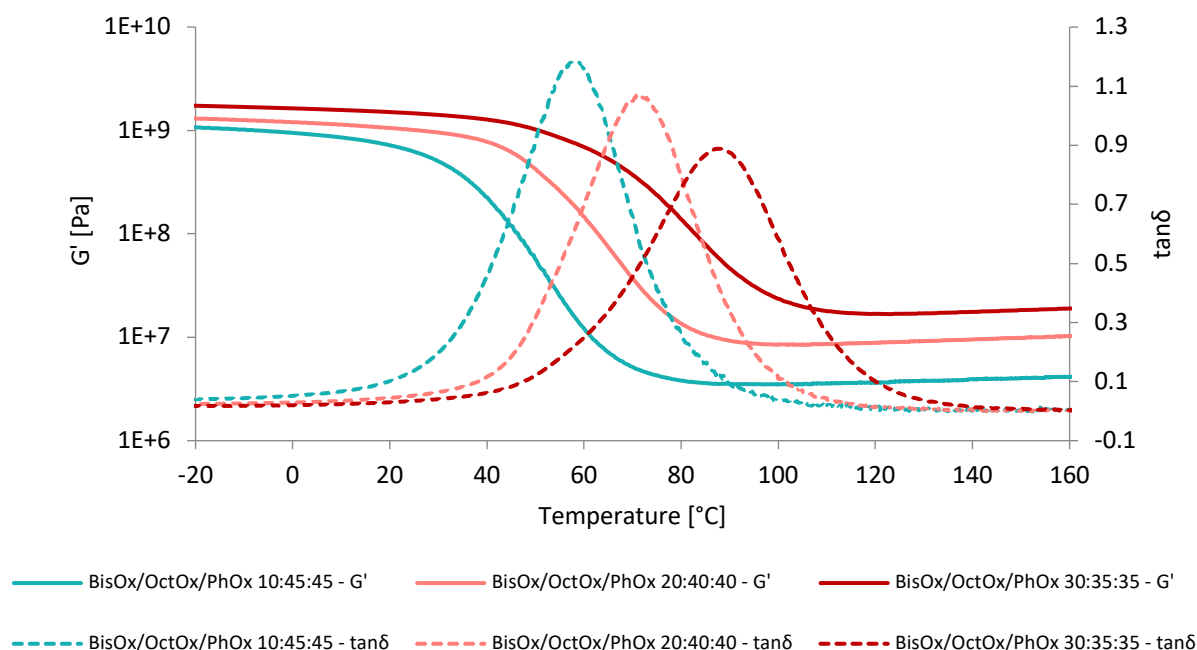
Figure 72: DMTA analysis with variation of crosslinker concentration (10, 20, 30 mol% BisOx)

The plot in Figure 72 shows the influence of increased crosslinker concentration on storage moduli and T_g. Expectedly a significant shift of T_g towards higher temperatures is observed in the resulting photopolymer. Moreover, the increased crosslink density results in a higher storage modulus in the rubbery region above glass transition. The results of T_g, G'_{20} and G'_r are displayed in Table 17.

Table 17: Glass transition temperatures (T_g) and storage moduli (G'_{20} and G'_r) of 2-oxazoline-based materials with variation of crosslinker concentration (BisOx 10, 20, 30 mol%)

BisOx/OctOx/PhOx	T_g [°C]	G'_{20} [MPa]	G'_r [MPa]
10:45:45	59	700	3.5
20:40:40	73	1000	8.5
30:35:35	88	1500	16.8

As seen from above results, the T_g shifts to 88 °C using a crosslinker concentration of 30 % BisOx in the formulation. Moreover, the higher crosslink density causes a distinct increase of G'_{20} and most significantly of G'_r in the resulting photopolymer.

In conclusion, formulations with equimolar ratio of OctOx and PhOx with 20 or 30 mol% crosslinker BisOx, give 2-oxazoline-based photopolymers with suitable T_g and storage moduli for mechanical testing. Excessive ratios of PhOx and BisOx, however, lead to brittle polymers with glassy behavior that do not withstand high mechanical load. Therefore, a formulation of BisOx/OctOx/PhOx in a molar ratio of 20:40:40 was considered as optimum for further examination of photopolymer characteristics in mechanical testing.

2.9.3   Photo-DSC of a formulation for 2-oxazoline-based photopolymers

The formulation designated for the photopolymerization of mechanical testing specimens by tensile testing and impact resistance testing was investigated in photo-DSC measurements to analyze its polymerization behavior and final conversion. The formulation BisOx/OctOx/PhOx in a molar ratio of 20:40:40 including 0.5 mol% PAG S-B per reactive group was measured at temperatures of 100, 120 and 140 °C. The corresponding photo-DSC analysis is depicted in Figure 73.
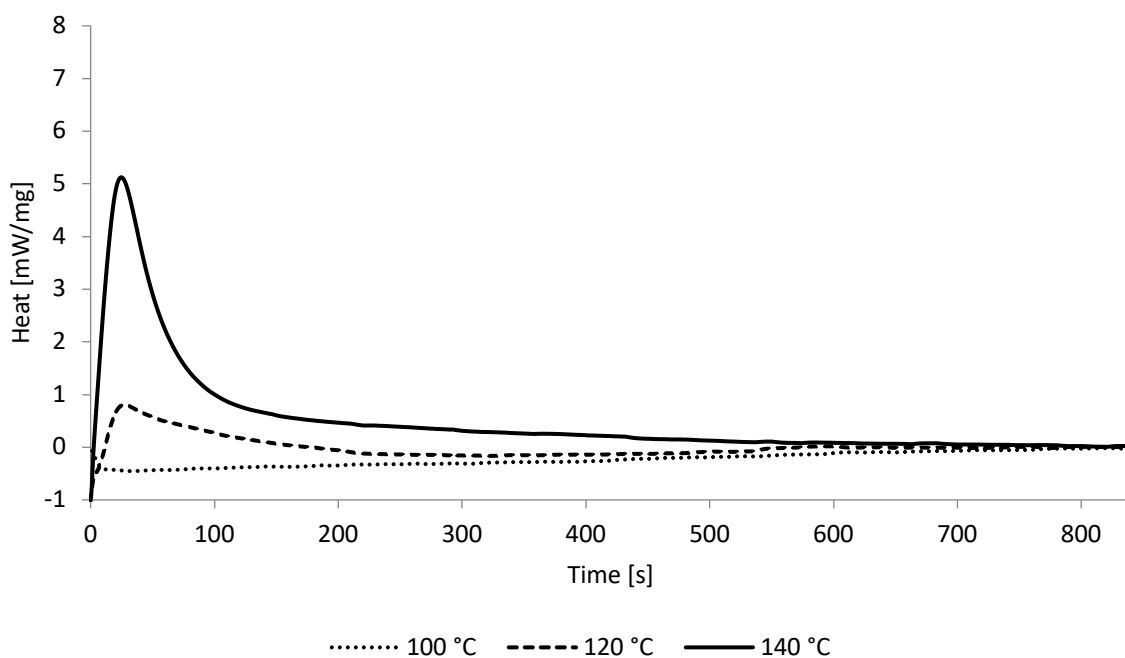
Figure 73: Photo-DSC analysis of a formulation of BisOx/OctOx/PhOx 20:40:40 (0.5 mol% S-B per reactive group) at temperatures of 100, 120 and 140 °C

For comparative reasons, the sole components BisOx, OctOx and PhOx with the corresponding PAG concentration were also included in this measurement series. The comparative analysis at 140 °C is depicted in Figure 74.
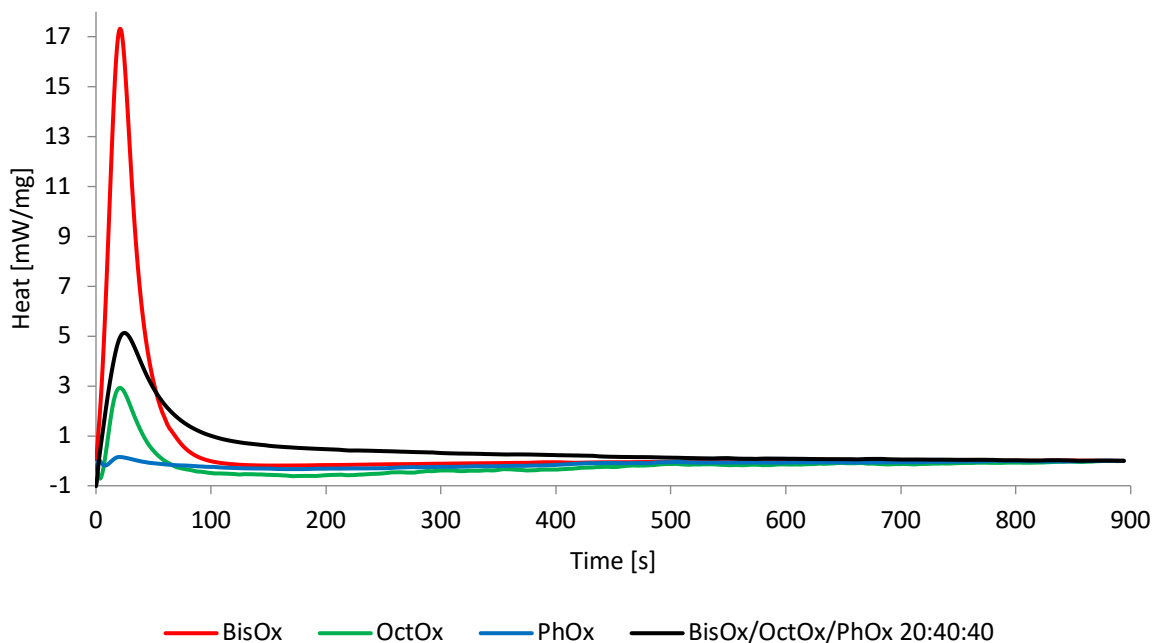
Figure 74: Comparative photo-DSC analysis of BisOx, OctOx, PhOx and the formulation BisOx/OctOx/PhOx 20:40:40 (all with 0.5 mol% S-B per reactive group) at 140 °C and 3 W/cm² irradiation intensity

As seen from above analyses in comparative display, the ternary formulation of BisOx/OctOx/PhOx reflects on the combined reactivities of its single components. On the one hand, rapid photopolymerization occurs with high exothermicity similar to BisOx in homopolymerization. On the other hand, long polymerization times are observed representing the low polymerization rates of monofunctional OctOx and PhOx included in the mixture, which substantiate the irradiation times of 900 s. In order to evaluate the photo-DSC analysis of a formulation containing multiple monomers, the equations introduced in section 1.4 are modified. The conversion of an *i*-component system calculates by the following Equation 4.

Equation 4: Calculation of conversion by photo-DSC of a mixture of multiple monomers

$$C = \frac{\Delta H}{\frac{\sum m_i}{m_{tot}}} * \sum \frac{M_i * x_i}{\Delta H_{0,i}}$$

C	Conversion by photo-DSC [%]
ΔH	Heat of polymerization by photo-DSC (area) [J/g]
$\frac{\sum m_i}{m_{tot}}$	Ratio of the sum of monomer masses to total mass [ ]
M_i	Molecular weight of monomer *i* [g/mol]
$\Delta H_{0,i}$	Theoretical heat of polymerization of monomer *i* [J/mol]
x_i	Molar ratio of monomer *i* [ ]

Furthermore, the rate of polymerization of a mixture of multiple monomers is calculated according to Equation 5.

Equation 5: Calculation of the rate of polymerization of a mixture of multiple monomers

$$R_p = h * \sum \frac{\rho_i * x_i}{\Delta H_{0,i}}$$

h	Height of photo-DSC peak [W/g]
ρ_i	Density of monomer *i* [g/L]
R_p	Rate of polymerization [mol·L^{-1}·s^{-1}]

Following the evaluation of photo-DSC curves and calculation by above equations, the result parameters are depicted in Table 18.

Table 18: Results of photo-DSC analyses of a formulation of BisOx/OctOx/PhOx 20:40:40 at 100, 120 and 140 °C

Formulation	T [°C]	C [%]	t_{max} [s]	R_P [mmol L^{-1} s^{-1}]	t_{95} [s]
BisOx/OctOx/PhOx 20:40:40	100	-*	-*	-*	-*
	120	18	32.1	11.8	182
	140	95	29.8	63.6	508

* no exothermicity detected in DSC

As seen from the photo-DSC results, the conversion of a formulation of BisOx/OctOx/PhOx 20:40:40 is highly dependent on heat input to the

photopolymerization. At 140 °C nearly full conversion is observed, whereas at 120 °C the conversion decreases to below 20 %.

To confirm the final conversions calculated from photo-DSC analysis, further characterization of the 2-oxazoline-based system was conducted using ATR-IR spectroscopy.

2.9.4 ATR-IR spectroscopy of a 2-oxazoline-based photopolymer

In the preparation of 2-oxazoline-based photopolymers by UV-Curing in the described method (2.9.1), no monitoring of the polymerization is possible. Photo-DSC showed the curing behavior and enabled to derive the conversion by calculation from the exothermicity of the cationic photopolymerization.

In further characterizations, the final conversion was analyzed by ATR-IR spectroscopy by determination of the amount of unreacted monomer in the photopolymer sample of a formulation of BisOx/OctOx/PhOx 20:40:40, as this formulation was designated for further examinations of thermomechanical properties. According to literature, the 2-oxazoline imine (C=N) vibrational band is expected at 1667 cm^{-1}, whereas the poly(2-oxazoline) carbonyl (C=O) band occurs at 1634 cm^{-1}. Clearly the deconvolution of signals would limit the sensitivity of the analysis, as seen in RT-MIR-photorheology in section 2.8.2 before. To evaluate the exact MIR bands of the 2-oxazoline monomer components in the mixture, the pristine monomers BisOx, OctOx and PhOx were measured. Furthermore, the formulation of BisOx/OctOx/PhOx 20:40:40 containing 0.5 mol% of S-B per reactive group was investigated. The samples of liquid (OctOx, PhOx) and solid (BisOx) monomers, as well as the unreacted formulation were applied on the ATR-IR crystal, whereas the photopolymerized sample thereof was cryomilled to yield a fine powder for analysis.

Figure 75 depicts the normalized MIR bands of the monomers OctOx, BisOx and PhOx in comparative display.
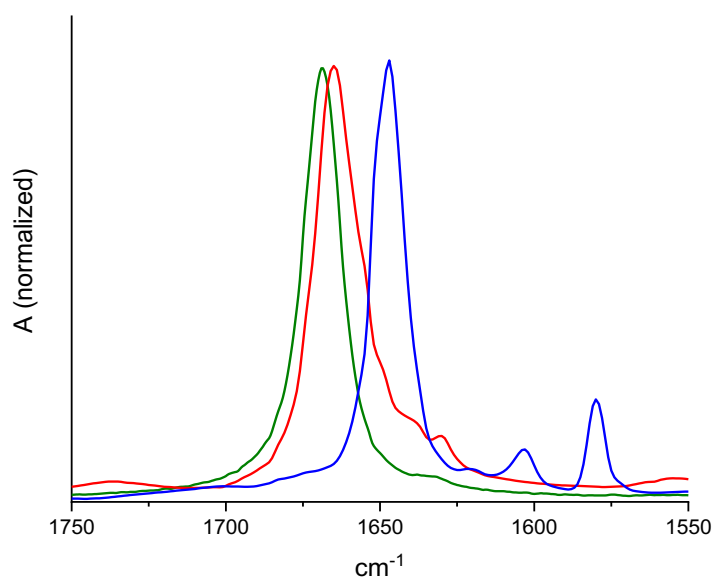
Figure 75: C=N vibrational bands of monomers OctOx (green, 1668 cm^{-1}), BisOx (red, 1665 cm^{-1}) and PhOx (blue, 1647 cm^{-1}); normalized to respective signals

Evidently, the aliphatic components OctOx and BisOx show signals according to literature around 1667 cm^{-1}, whereas the aromatic PhOx gives a shifted signal at 1647 cm^{-1} due to the different molecular surrounding of the imine bond. The formulation of these three components is thus expected to give a combination of these signals.

In order to evaluate the conversion of the photoreactive formulation BisOx/OctOx/PhOx 20:40:40 including triarylsulfonium PAG S-B, Figure 76 shows the measurement before and after photopolymerization. The spectra were normalized to the unchanged C-H vibrational signal of the aliphatic substituent around 2930 cm^{-1} to set the strong carbonyl band in relation to the monomer imine signals.
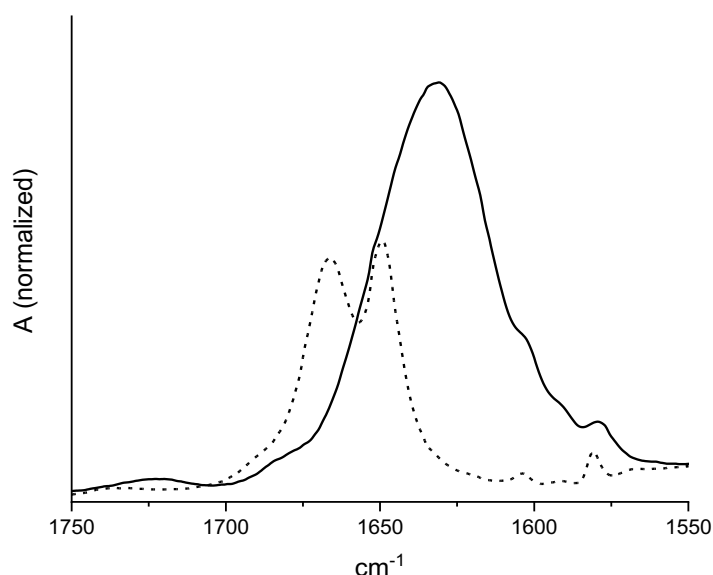
Figure 76: C=N bands of formulation BisOx/OctOx/PhOx 20:40:40 containing 0.5 mol% of S-B per reactive group (- - dashed, 1666 cm^{-1} and 1649 cm^{-1}), and C=O bands of photopolymer thereof (— solid, 1630 cm^{-1}); normalized to 2927 cm^{-1}

The photoreactive formulation shows two bands representing the combination of aliphatic and aromatic monomers in the formulation. After photopolymerization at 140 °C, the distinct shift towards the poly(2-oxazoline) carbonyl band is evident. In prior RT-MIR-photorheology analysis it was observed that the high intensity of the resulting carbonyl band and low deconvolution of peaks impeded the evaluation of conversion. In the here presented analysis, the absence of residual monomer signals can be confirmed. Using analytical software for peak deconvolution (PeakFit), no traces of monomers were found in the spectrum of cryomilled photopolymer. In summary, a conversion over 95 % was evaluated by photo-DSC and confirmed by ATR-IR spectroscopy. On this basis, the mechanical testing of 2-oxazoline-based photopolymers was conducted.

2.10 Comparative thermomechanical testing of poly(2-oxazoline) and poly(methacrylate) materials

The photoreactivity studies by photorheology showed the general characteristic differences of 2-oxazoline-, glycidyl ether- and methacrylate-based photopolymers. In

analogy, the comparative study of 2-oxazoline with epoxy and methacrylate monomers should be conducted in mechanical testing of photopolymer materials. However, no extended mechanical testing in terms of standardized tensile testing and impact resistance testing was applicable with the homopolymer networks arising from purely difunctional monomer formulations. However, in prior investigations on thermomechanical properties of 2-oxazolines it was found that a mixture of 20 mol% difunctional BisOx with 40 mol% OctOx and 40 mol% PhOx gave materials with suitable material properties for comparative mechanical testing with reference formulations.

Comparable cationically photopolymerizable 2-oxazoline and epoxy monomers expressed the distinctly higher reactivity of BDDGE. Experience of earlier experiments showed, however, that the aliphatic diglycidyl ether monomer BDDGE gives polymers with undesired material properties, such as low glass transition temperatures and intensive dark discoloration during UV-curing, which complicates the subsequent investigation of the material. In contrast, the comparable 2-oxazoline monomer BisOx gives photopolymers with high glass transition temperature, high storage modulus and low discoloration upon cationic photopolymerization.

During the preparation of epoxy-based specimen via cationic photopolymerization in silicon molds it was noted that the photopolymer showed strong deformation and intense discoloration. Similar to the observations in photorheology, the strong discoloration led to very limited light penetration and allowed only for curing of the formulation surface. Subsequently, the rapid curing reaction in this thin layer led to polymerization shrinkage and to a curling effect which caused dramatic deformations throughout the UV-curing process. The use of monofunctional reactive diluents such as phenyl glycidyl ether did not solve the observed issue in UV-curing of the epoxy monomers. Samples containing more than 50 mol% of the crosslinker BDDGE could not be recovered undamaged, whereas samples containing less than 50 mol% BDDGE gave complete samples but were not stressable in mechanical testing due to a severe lack of rigidity. After several approaches of optimization of curing conditions and analysis of purity it is concluded that the observed unsuitable material properties of BDDGE are of intrinsic nature and occur upon highly exothermic cationic photopolymerization even at room temperature. High temperatures up to 170 °C are reported for of aliphatic and aromatic glycidyl ethers cationically photopolymerized at

room temperature, which demonstrates the excessive exothermicity and UV-curing behavior of BDDGE. [41] In consequence, no further attempts using the diglycidyl ether BDDGE were performed.

Due to the unsuitability of the epoxy reference system, a corresponding methacrylate-based material consisting of BDDMA, hexyl methacrylate (HexMA) and benzyl methacrylate (BMA) in equal molar ratio of 20:40:40 served as a reference system for extended comparative studies of mechanical properties. In analogy to the 2-oxazoline-based system, reference compounds of similar molecular structure were selected for the formulation to obtain equal impact on the resulting photopolymer network. Within these comparative studies, 0.5 mol% per reactive group of the radical photoinitiator BMDG was used in the methacrylate-based reference formulation.

Clearly, the methacrylate network obtained by free radical photopolymerization follows a fundamentally different chain growth mechanism than cationically polymerized systems. Nevertheless, methacrylate systems represent the current state-of-the-art approach for rapid photopolymerization in stereolithography in high abundance. Due to their inherently fast polymerization, methacrylate monomers are also considered as benchmark for the production of materials by SLA and the here emphasized Hot Lithography. The introduced 2-oxazoline systems is intended to show fundamental advantages of 2-oxazoline-based photopolymers over poly(methacrylate) materials with respect to their potential application in the toughening of photopolymer products in Hot Lithography. The monomer components of the formulations used for comparative mechanical testing are depicted in Figure 77.

mol%

20

40

40

S-B

0.5 mol%
per reactive group

BMDG
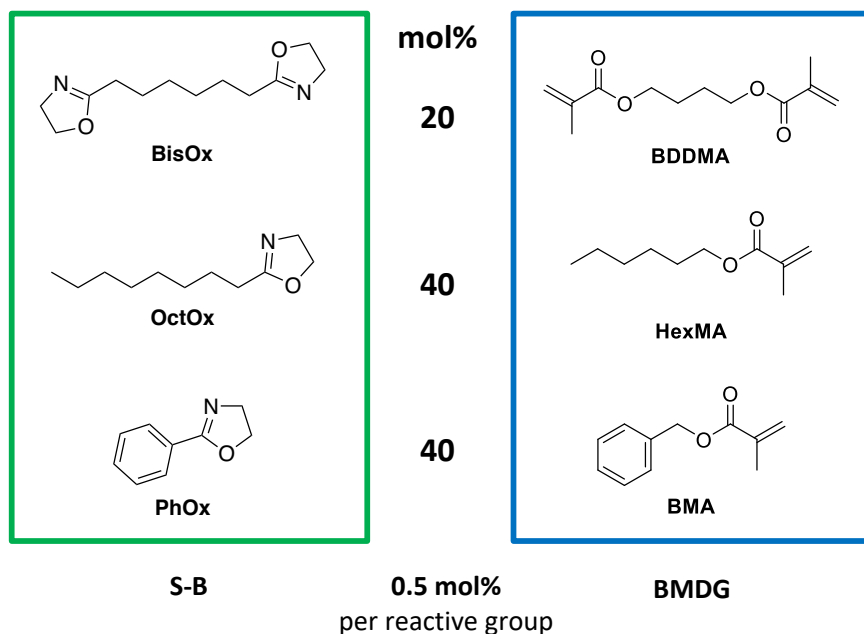
Figure 77: Monomer systems for comparative studies of 2-oxazoline and methacrylate materials

The methacrylate-based formulation BDDMA/HexMA/BMA 20:40:40 was photopolymerized for 2 times 10 min in a Lumamat UV-oven (400-500 nm) at 25 °C. Hence, the significant temperature difference in the UV-curing of comparative systems must be considered. The methacrylate formulation was photopolymerized at room temperature, thus below the T_g of the resulting photopolymer, whereas the 2-oxazoline formulation is only fully curable at temperatures above 120 °C, thus above its T_g. This might have a distinct influence on the polymer network and its morphology. As poly(methacrylate) photopolymers cannot be produced at high temperature due to thermal instability, this difference in photopolymerization condition is inherent in the respective reactive moieties and a general precondition of the conducted comparative studies.

2.10.1 DMTA

The 2-oxazoline- and methacrylate-based formulations, BisOx/OctOx/PhOx 20:40:40 and BDDMA/HexMA/BMA 20:40:40, were cured by described methods and examined via DMTA analysis in a range from -20 to 200 °C. Figure 78 shows the DMTA analysis of photopolymer of BisOx/OctOx/PhOx 20:40:40 in comparison to BDDMA/HexMA/BMA 20:40:40.
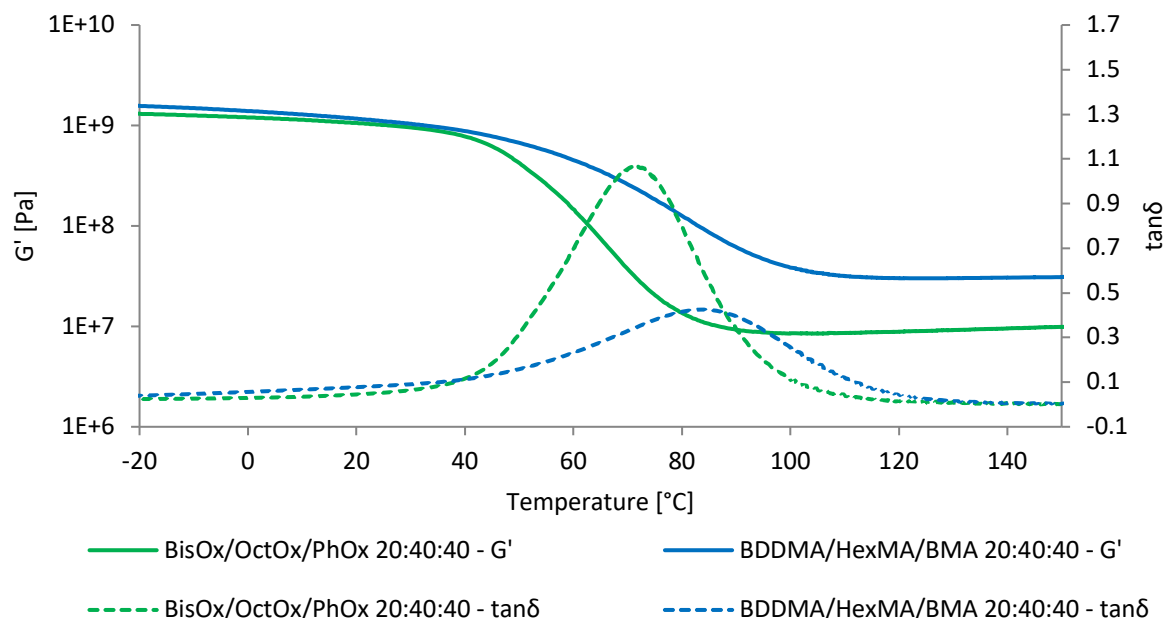
Figure 78: Comparative DMTA analysis of 2-oxazoline- and methacrylate-based materials

As seen, comparable storage moduli at G'_{20} are observed for the 2-oxazoline and methacrylate-based system. The 2-oxazoline-based material exhibits a T_g of 73 °C, whereas the methacrylate reference material shows an increased T_g of 84 °C. A distinctly broader glass transition is characteristic for the unregulated free radical polymerization of methacrylates, whereas the cationic polymerization gives a sharper transition, which is reasoned by the lack of termination processes and a more homogeneous polymer network. G'_r is significantly higher for the poly(methacrylate) photopolymer presumably due to higher crosslink density of radically polymerized networks, which tend to exhibit chain transfer and branching throughout the chain growth reaction. The results of the comparative DMTA analysis are displayed in Table 19.

Table 19: Glass transition temperatures (T_g) and storage moduli (G'_{20} and G'_r) of 2-oxazoline- and methacrylate-based materials

Formulation	T_g [°C]	G'_{20} [MPa]	G'_r [MPa]
BisOx/OctOx/PhOx 20:40:40	73	1100	8.5
BDDMA/HexMA/BMA 20:40:40	84	1200	35

2.10.2 Tensile strength

The described materials of 2-oxazoline and methacrylate-based formulations were subsequently investigated by tensile testing. The analysis was conducted from equally photopolymerized materials as in prior analyses. The measurements were conducted according to ISO SO 527 by applying axial stress to the specimens until break. The measurements were performed in 5-fold repetition for each material. Exemplary curves which most accurately represent the average are depicted in Figure 79 to give an impression of the tensile behavior of the compared materials.
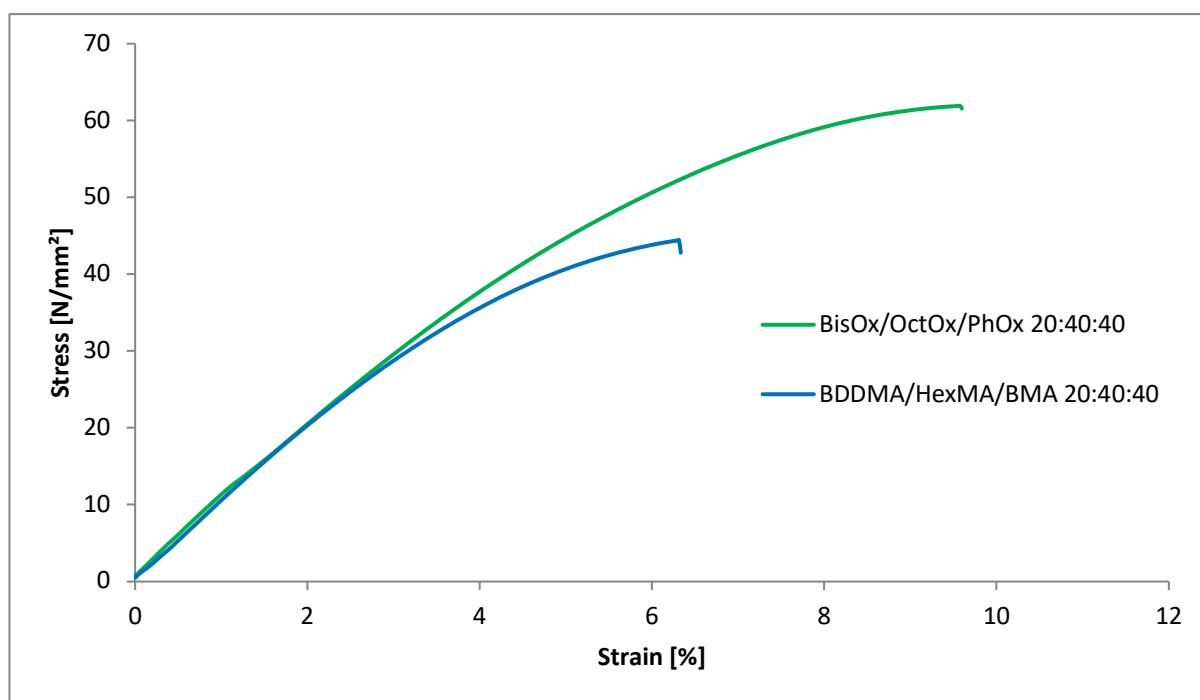
Figure 79: Comparative tensile testing of 2-oxazoline- and methacrylate-based materials

It is seen that the 2-oxazoline-based material shows a generally better tensile behavior with increased stress and strain at break. With initially equal slope in the stress-strain curves, the materials show comparable stiffness.

Table 20: Maximum stress (σ_B) and strain at break (ε_B) of 2-oxazoline- and methacrylate-based materials

Formulation	σ_B [Nmm^{-2}]	ε_B [%]
BisOx/OctOx/PhOx 20:40:40	59 ± 1.7	9.5 ± 2.2
BDDMA/HexMA/BMA 20:40:40	42 ± 1.0	6.2 ± 0.6

Taking the maximum stress and strain values into consideration, the 2-oxazoline based material reaches values of σ_B = 59 Nmm^{-2} and ε_B = 9.5 %, whereas the methacrylate-based material reaches σ_B = 42 Nmm^{-2} and ε_B = 6.2 %. Evidently, the 2-oxazoline material shows greater resistance to mechanical stress under axial load in tensile testing. Despite higher crosslink density was presumed for the methacrylate-based material in foregoing DMTA analyses, the 2-oxazoline-based material seem to exhibit higher intrinsic strength and toughness.

2.10.3 Impact resistance

The standardized DynStat impact resistance tests were conducted in 4-fold repetition for each formulation using a 10 kpcm (1 J) tool. Figure 80 shows the results of the comparative impact resistance measurements for the 2-oxazoline- and methacrylate-based materials.
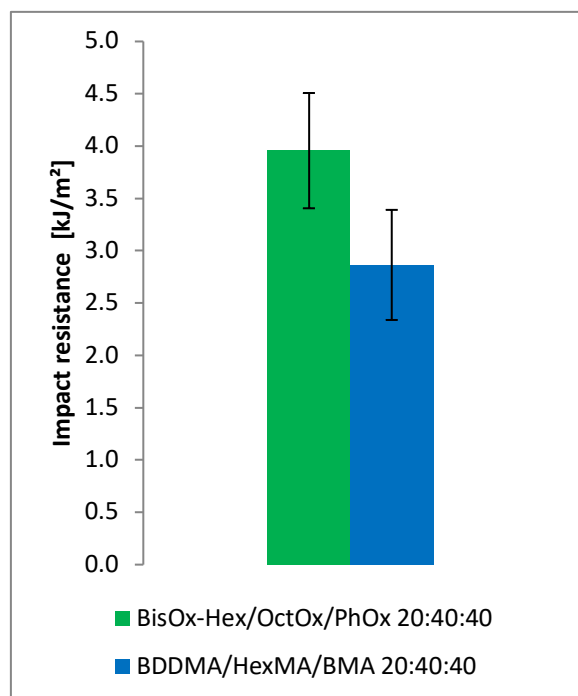
Figure 80: Comparative DynStat impact resistance of 2-oxazoline- and methacrylate-based materials

The results above show impact resistance values of 4.0 kJ m^{-2} for the 2-oxazoline material, and 2.9 kJ m^{-2} for the methacrylate reference material. Evidently, the lower results in impact resistance arise from the comparably high brittleness of the poly(methacrylate) material.

Table 21: Dynstat impact resistance of 2-oxazoline- and methacrylate-based materials

Formulation	Impact resistance [kJ m^{-2}]
BisOx/OctOx/PhOx 20:40:40	4.0 ± 0.6
BDDMA/HexMA/BMA 20:40:40	2.9 ± 0.5

In summary, the comparison between BisOx/OctOx/PhOx 20:40:40 and BDDMA/HexMA/BMA 20:40:40 allows for the interpretation that the different reactive moiety has a significantly advantageous impact on the mechanical properties of the 2-oxazoline-based material. Despite the different polymerization mechanisms, the

beneficial properties are attributed to the poly(2-oxazoline) structure and its intramolecular interaction in the polymer.

2.10.4 Thermal analysis of poly(2-oxazoline) and poly(methacrylate) materials

The photopolymers obtained from mixtures of 2-oxazoline model compounds give poly(amide) structures, which reportedly exhibit high thermal stability.[128] Therefore, the photopolymer samples of BisOx/OctOx/PhOx 20:40:40 were examined by TGA to determine the thermogravimetric loss in comparison to a corresponding methacrylate-based reference material of BDDMA/HexMA/BMA 20:40:40. The photopolymers were cryomilled and the powders were analyzed by TGA in a temperature range from 25 – 500 °C with a heating rate of 10 K/min under nitrogen atmosphere. The resulting curves of thermogravimetric mass loss are depicted in Figure 81.
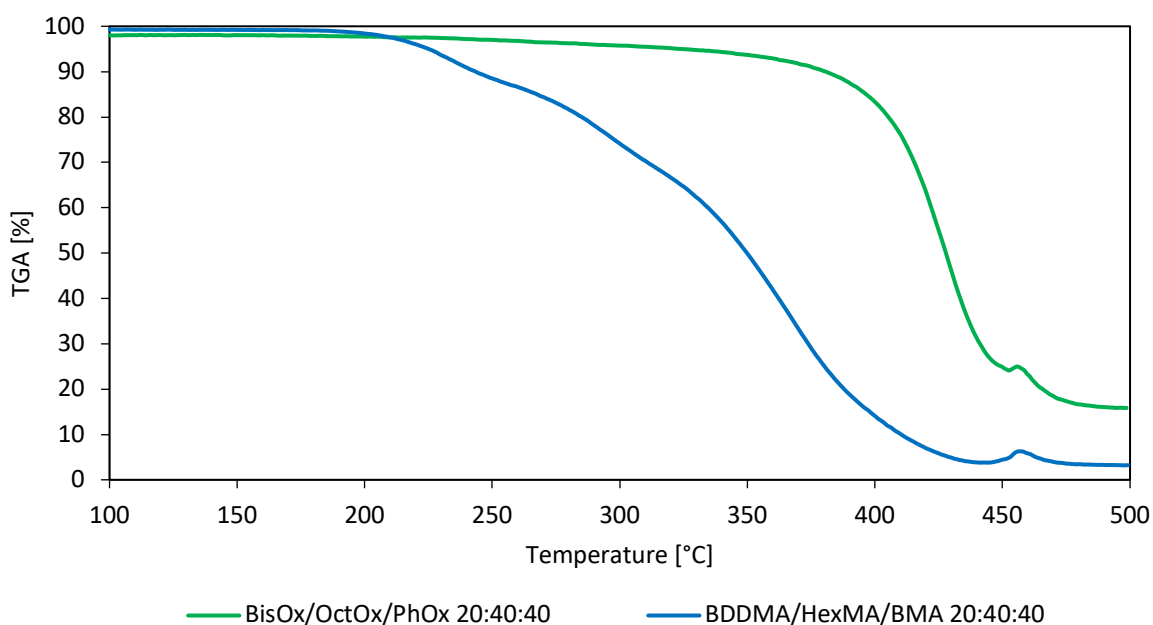
Figure 81: Thermogravimetric analysis (TGA) for thermal stability of comparative photopolymers of 2-oxazoline (PAOx) and methacrylate (polyMA) formulations

As expected, the 2-oxazoline-based photopolymer shows high thermal stability over 300 °C. As a parameter for the resistance to thermal degradation, the temperature of 5 % mass loss by degradation (T_D) is extracted. The results are displayed in Table 22.

Table 22: Temperatures of 5 % mass loss by degradation (T_D) by thermal analysis (TGA)

Formulation	T_D [°C]
BisOx/OctOx/PhOx 20:40:40	324
BDDMA/HexMA/BMA 20:40:40	225

As seen from above results for T_D, the poly(2-oxazoline) exhibits about 100 °C higher thermal stability than the comparable poly(methacrylate) material. The found results are in good agreement with literature data of comparable thermally cured difunctional poly(2-oxazolines), which show T_D around 350 °C.[128]

2.11 Hot Lithography of 2-oxazolines

Classically, photopolymerization is based on the rapid polymerization reaction at room temperature triggered solely by a light stimulus and without the need for further thermal input. Nevertheless, the lack of toughness and structural strength represents a problem of photopolymers, which remains part of ongoing developments. With innovative additive manufacturing technologies on the rise, the development of corresponding materials is facing this challenge with novel approaches. Especially in Hot Lithography, the heated SLA instrumentation offers a way to overcome these limitations by applying formulations of macromolecular building blocks, which exhibit excellent toughness and impact resistance, however, also very high viscosity. Inevitably, these formulations can only be processed when heated.

Alternatively, the here presented work introduces a yet uninvestigated approach to photopolymer products with enhanced mechanical properties from low molecular weight 2-oxazoline monomers. In foregoing studies, the input of external heat was found to be crucial for the cationic photopolymerization of 2-oxazolines. With the Hot Lithography setup being able to fit these demands, preliminary irradiation testing was conducted as a proof of concept for the printability of 2-oxazolines.

The Hot Lithography instrumentation comprises an SLA system with 375 nm laser irradiation and a maximum output power of 140 mW. Given the small area of irradiation by the laser beam and a hatching distance of 10-20 µm, the irradiation intensity is outstandingly high in comparison to prior investigations of cationic photopolymerization of 2-oxazolines. Although the short irradiation times represent a strong limitation, the high irradiation intensity is expected to efficiently generate solidification of the formulation upon the passing of the laser beam. Furthermore, light-induced SLA methods are based on the production of green bodies from the 3D printing process and rely on further post-curing to reach final product properties. Therefore, the spatially selective, layer-by-layer photopolymerization of a part with sufficient green strength is the dominant aim.

The rapid polymerization at elevated temperatures is crucial for the application of 2-oxazoline systems, whereas Hot Lithography is limited to temperatures of 140 °C. Within this temperature range it was seen before that only the difunctional 2-oxazoline model compound BisOx is polymerized in suitable rates in order to solidify upon the swift passing of the laser beam. The difunctional monomer BisOx also provides sufficiently low volatility throughout the printing process at high temperatures.

After detailed studies on temperature stability, photoreactivity, thermomechanical properties and further features of this novel cationically photopolymerizable monomer class, the testing of 2-oxazoline formulations for compatibility with the printing conditions was conducted.

2.11.1 Photorheology pretests using 365 and 385 nm LED irradiation

In order to determine the gel point as a measure for solidification of the monomer BisOx in SLA printing, photorheology pretests were conducted with a formulation of BisOx containing 2 mol% S-B. LED spotlight sources of 365 nm and 385 nm wavelength were applied to test the wavelength sensitivity of the 2-oxazoline formulation. Irradiation intensities of 8.3 mW/cm² for 365 nm, and 7.0 mW/cm² for 385 nm were measured at the sample position in the photorheology instrument. It must be mentioned that in Hot Lithography a distinctly higher laser output power of 70 mW or 140 mW is applied, thus the here performed pretest serve as a simulation of polymerization behavior. In consequence to prior observations on the influence of layer thickness, a lower gap size

is preferable in photorheology analyses. Furthermore, the layer-by-layer 3D printing in Hot Lithography is mostly conducted with layer thickness below 100 µm to ensure sufficient solidification of each layer without delamination of the printed part. Thus, the photorheology analyses were conducted at a gap size of 50 µm. Accordingly, 50 µL sample volume was used. The analysis was conducted at the highest applicable temperature of 100 °C and the irradiation time was set to 300 s to observe the gel point based on prior observations in the cationic photopolymerization of BisOx. The measurements using 365 and 385 nm LEDs are depicted in Figure 82 in comparative display.
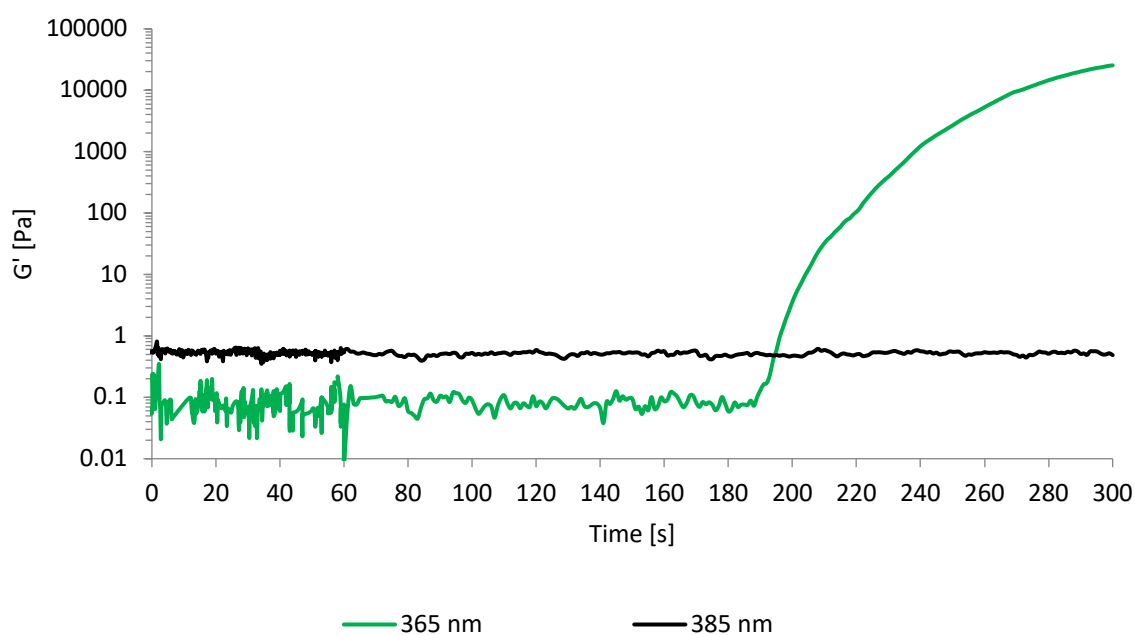
Figure 82: Photorheology measurements of a photoreactive formulation of BisOx at 100 °C using 365 and 385 nm LED irradiation

The clear wavelength sensitivity using the triarylsulfonium PAG S-B in BisOx is evident, as no solidification is observed at 385 nm irradiation within 300 s. In contrast, irradiation at 365 nm leads to gelation within 194 s, as seen from the gel point of the respective measurement. From these analyses, the wavelength sensitivity in the cationic photopolymerization of BisOx using triarylsulfonium PAG S-B is seen. Clearly, also the reduced irradiation intensity influences the retardation of gelation, which might be overcome by high intensity laser irradiation. Nevertheless, the use of compatible photosensitizer must be considered for the printing process at 375 nm in Hot Lithography to enhance the spectral sensitivity in the processing of S-B based

formulations. To test the photopolymerization behavior in printing conditions, laser exposure tests of photoreactive BisOx formulations were conducted in Hot Lithography setups.

2.11.2 Pretests of photoreactive 2-oxazoline formulations for Hot Lithography

2.11.2.1 *Laser exposure tests using Hot Lithography prototype at 100 °C*

The first laser exposure tests for the potential application of a 2-oxazoline system in Hot Lithography was conducted using a prototype device with a maximum applicable temperature of 100 °C. This device is equipped with a 375 nm laser with a maximum laser output power of 70 mW. The testing was conducted to prove the general applicability of the cationic photopolymerization system of the monomer BisOx and PAG S-B.

As the intended Hot Lithography printing is preferably conducted using a layer thickness of 100 µm, the desired layer thickness in laser exposure pretests lies at a minimum of 300 µm. Layer thickness lower than 100 µm lead to incomplete layer build-up during the printing process, whereas photopolymerization with excessive layer thickness over 1000 µm diminishes the number of reactive groups on contact area between the irradiated and the consecutive layer. The lack of chemical bonding to the consecutively applied material in the additive manufacturing process leads to delamination in the object.

As the printing prolongs crucially with each exposure in the layer-by-layer approach, no more than 4 exposures were used as a framework condition of 3D printing. For the laser exposure test using the Hot Lithography prototype system at 100 °C, a circular area of 15 mm diameter was irradiated with a writing speed between 50 and 500 mm/s. In each irradiation run, 2 exposures with orthogonal laser writing directions and a hatching distance of 15 µm were performed to cover the whole area in bottom-up exposure. The laser output power was set to 100 % corresponding to 70 mW. As low reactivity was expected at 100 °C, low writing speeds of 50 mm/s were initially tested and increased until no platelet was formed.

At laser speeds higher than 200 mm/s the number of exposures was doubled to four exposures, as no complete layer was achieved in a single run. Subsequently, the

writing speed was increased to 350 and 500 mm/s and irradiated using 4 exposures. After laser exposure, the polymer films were removed from the vat and washed with acetone to separate unreacted formulation from the samples.

Table 23 displays the layer thicknesses obtained with different laser speeds and numbers of laser exposure.

Table 23: Layer thicknesses in Hot Lithography irradiation pretests at 100 °C using 70 mW laser power

Laser speed [mm/s]	Nr. of exposures	Layer thickness [µm]
50	2	250
100	2	130
200	2	70
	4	180
350	4	110
500	4	-

Evidently, the increase of laser writing speed leads to significantly lower layer thicknesses due to shorter dwell time of the laser beam on the formulation. Finally, no polymer film was obtained with a laser speed of 500 mm/s with 4 sequential exposures. It is seen, that even at lowest writing speed of 50 mm/s, the layer thickness remains below 300 µm after 2 exposures. As this is insufficient for effective layer build-up and an increase of exposures leads to excessive printing times and decreased resolution of the printed parts, further proceedings were performed on a Hot Lithography printer with increased temperature range and enhanced laser output power.

2.11.2.2   *Laser exposure tests using Hot Lithography at 120 and 140 °C*

The decisive laser exposure tests were conducted using a Caligma 200 UV Hot Lithography printer developed by Cubicure GmbH. This device differs from prior pretests by its extended temperature range up to 140 °C and the double laser output power of 140 mW.

Within these laser exposure tests the optimization of conditions for Hot Lithography was conducted. Therefore, the photoreactive formulation and the Hot Lithography conditions were improved by variation of the following parameters:

- PAG concentration: 0.5 - 2 mol%
- Temperature: 120 °C, 140 °C
- Laser speed: 50 - 12000 mm/s
- Number of exposures per layer: 1 - 4

The optimization process clearly showed the limitations by each parameter, thus, gave a great number of unsuccessful laser exposure tests. The following Table 24 provides an overview of conditions, which gave successfully cured photopolymer platelets in laser exposure tests.

Table 24: Layer thicknesses in Hot Lithography irradiation pretests at 120 and 140 °C using 140 mW laser power

T [°C]	Laser speed [mm/s]	Nr. of exposures	Layer thickness [µm]
140	500	4	370
	250	4	740
	100	2	370
	50	2	670
120	50	2	670

From foregoing analyses of the cationic photopolymerization of 2-oxazoline BisOx it was expected that a temperature of 140 °C would provide advantageous conditions for the rapid solidification in Hot Lithography. In fact, the difunctional 2-oxazoline monomers generated photopolymer platelets with 2 laser exposures up to a writing speed of 100 mm/s. Reducing the writing speed to 50 mm/s resulted in significantly higher dwell time on the sample. In consequence, the layer thickness increases from 370 to 670 µm, which is considered as a more viable value to use in a proof of concept 3D printing process. It was found that equal layer thickness of 670 µm was obtained in laser exposure tests at 120 °C. Clearly, the use of lower temperatures is advantageous, as excessive heat influences the spatial selectivity of photopolymerization by higher

diffusion of reactive species. In fact, less diffusional overpolymerization was observed on the objects after irradiation at 120 °C in comparison to 140 °C.

In further investigations it was found that samples already irradiated in laser exposure tests at 120 °C showed reduced reactivity upon repetitive irradiation. It was assumed that the formulation containing triarylsulfonium PAG S-B does not withstand repetitive irradiation and is prone to inactivation of the PAG. The depletion of photoreactivity of WCA-based S-B was tested by comparison to an alternative PAG. Therefore, a commercially available solution of triarylsulfonium hexafluoroantimonate compounds (S-Sb; 50 wt% in propylene carbonate) was tested as PAG in laser exposure tests of a corresponding formulation. The photoinitiating components of S-Sb are depicted in Figure 83.
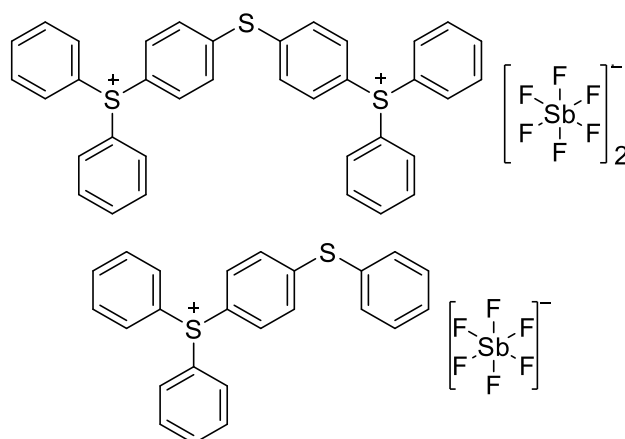
Figure 83: Structure of PAG components in the photoinitiating mixture of S-Sb (50 wt% in propylene carbonate)

The formulations containing S-B or S-Sb were compared in repetitive laser exposure tests at 120 °C after 0, 2 and 4 hours to examine their thermal stability by the ability to generate polymer films under irradiation. Over this time, the sample were kept at 120 °C inside the vat. The resulting layer thicknesses are displayed in the Table 25.

Table 25: Layer thicknesses in Hot Lithography laser exposure tests after 0, 2 and 4 hours at 120 °C

Heat exposure [h]	PAG	Layer thickness [µm]
0	S-B	670
	S-Sb	670
2	S-B	-
	S-Sb	610
4	S-B	-
	S-Sb	600

The results of irradiation tests showed that S-Sb provided better thermal stability than S-B in experimental laser exposure tests. As seen, no photopolymer platelets were obtained from laser exposure tests after 2 hours using a formulation based on S-B, whereas BisOx containing S-Sb still gave a layer thickness of 600 µm even after 4 hours at 120 °C. Hence, the observed difference in thermal stability and photoinitiation ability at elevated temperatures was analyzed in STA measurements and photo-DSC analysis of BisOx formulations containing S-B and S-Sb.

2.11.2.3   STA of S-Sb in BisOx for application in Hot Lithography

In analogy to the STA measurement of a BisOx formulation containing S-B, the corresponding formulation containing the 1 mol% hexafluoroantimonate-based PAG S-Sb was analyzed. 14 ± 1 mg of the melted solution were weighed into a DSC crucible and closed using a pierced lid. The analysis was conducted by heating the sample to 300 °C under nitrogen atmosphere using a heating rate of 10 K/min. Figure 84 shows the STA of S-B and S-Sb in BisOx formulations in comparative display.
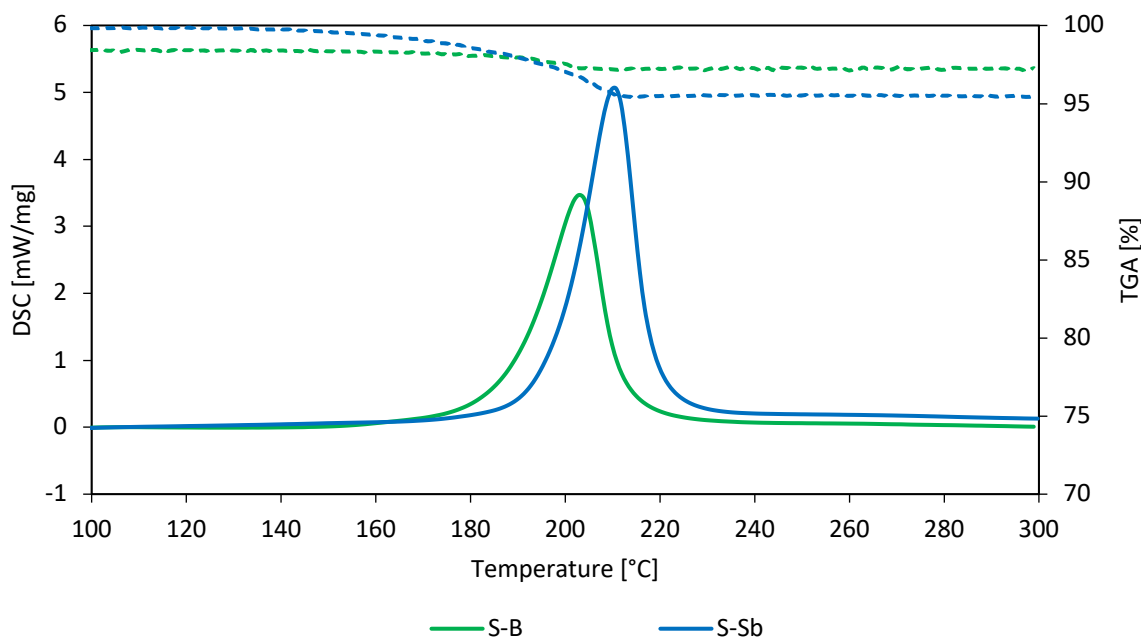
Figure 84: STA analyses of BisOx with 1 mol% PAG (S-B or S-Sb); TGA dashed

The mixture of triarylsulfonium hexafluoroantimonate salts S-Sb evidently exhibits higher thermal stability than S-B. As the thermal stability is solely determined by the cation structure, the discrepancy is clearly arising from the different triarylsulfonium structures of the PAGs. The highly conjugated structure of S-B is designed for highest light absorption and quantum yields for efficient photodecomposition, however, shows lower thermal stability than the less advanced mixture of triarylsulfonium species of S-Sb at elevated temperatures. This causes the premature depletion of photoinitiation ability of S-B in laser exposure tests, whereas S-Sb enables the photopolymerization efficiently even after 4 hours at elevated temperatures.

For determination of potential differences in photoreactivity, the PAGs S-B and S-Sb were examined in photo-DSC analysis. These measurements should provide further information, whether the less favored hexafluoroantimonate-based PAG exhibits reduced initiation ability in photopolymerizations.

2.11.2.4   Photo-DSC of S-Sb in BisOx for application in Hot Lithography

As the PAG S-Sb not only showed higher thermal stability, but also better performance in irradiation tests, the photoinitiation ability was evaluated in photo-DSC measurements. The analyses were conducted using formulations of BisOx containing 1 mol% of the PAGs S-B or S-Sb, respectively. Standard conditions of 130 mW/cm^2 irradiation intensity, two irradiation periods of 900 s and temperatures of 100, 120 and 140 °C were applied. Figure 85 shows the measurements of both formulations at 100, 120 and 140 °C in comparative display.
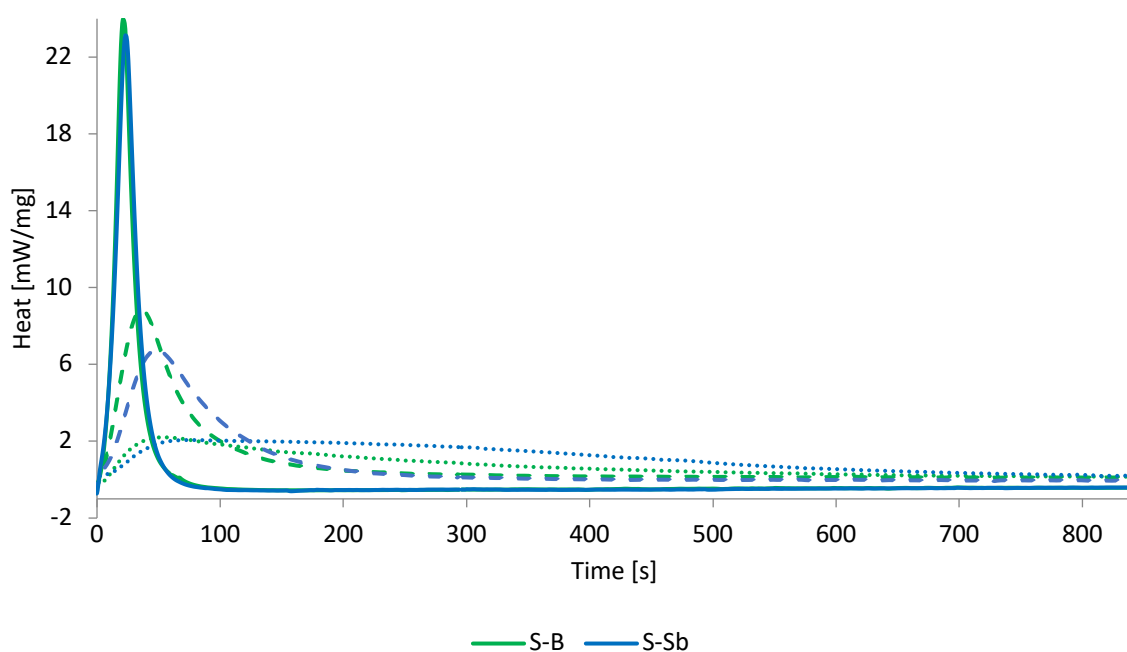
Figure 85: Photo-DSC analysis for comparison of formulations of BisOx containing the PAGs S-B or S-Sb (100 °C dotted; 120 °C dashed; 140 °C solid)

As seen from the depicted measurements of formulations containing S-B and S-Sb, respectively, only marginal differences in photoinitiation ability are observed. This reasons the comparable photoreactivity of the formulations in laser exposure tests. The results of respective photo-DSC measurements are displayed in Table 26.

Table 26: Photo-DSC results of BisOx formulations containing 1 mol% PAG (S-Al, S-B, S-C) at 100, 120 and 140 °C

Temperature (°C)	Formulation	C [%]	t_{max} [s]	R_p [mmol L^{-1} s^{-1}]	t_{95} [s]
100	S-B	80	53	14	533
	S-Sb	-	76	13	603
120	S-B	98	36	60	271
	S-Sb	>99	48	47	228
140	S-B	>99	21	165	50
	S-Sb	>99	23	163	46

As seen from the result parameters, the WCA-based S-B induced the cationic photopolymerization in marginally higher rates than the antimonate-based S-Sb. The results for t_{max} and R_p are considered as most representative for application as photoinitiators to obtain rapid solidification in Hot Lithography. It is assumed that the determined differences do not significantly affect the applicability in stereolithography.

It can be concluded that advantageous thermal stability and comparably high photoreactivity arises from the use of S-Sb as PAG for the cationic photopolymerization of BisOx. Due to the better performance in laser exposure tests without signs of diffusional overpolymerization or depletion of initiation ability upon repetitive exposure at high temperatures, S-Sb it is a suitable cationic photoinitiator for the described application in 3D-printing of 2-oxazoline based materials.

2.11.3 3D printing of a 2-oxazoline-based formulation

As the laser exposure tests and resulting layer thicknesses showed promising photopolymerization behavior, the Caligma 200 UV Hot Lithography printer was used for the 3D printing of 2-oxazoline BisOx

Following an optimization process to find a suitable formulation for Hot Lithography, BisOx containing 1.5 mol% of S-Sb (corresponding to 12 wt% of S-Sb solution in propylene carbonate 50:50 wt%) was used. In order to enhance the selectivity of photopolymerization and for better compatibility of the photoinitiation system with the 375 nm UV-laser, the common photosensitizer 9,10-dibutoxyanthracene was used.
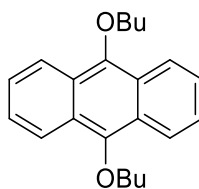
9,10-dibutoxyanthracene

This sensitizer is literature-known for high reactivity and solubility in photopolymerizable systems comprising triarylsulfonium PAGs.[92] In an iterative optimization a concentration of 0.05 wt% of 9,10-dibutoxyanthracene was suitable for the sensitization of a formulation consisting of BisOx and 1.5 mol% S-Sb.

In a simultaneous printing job at 120 °C, the structures depicted in Figure 86 and Figure 87 were 3D structured.
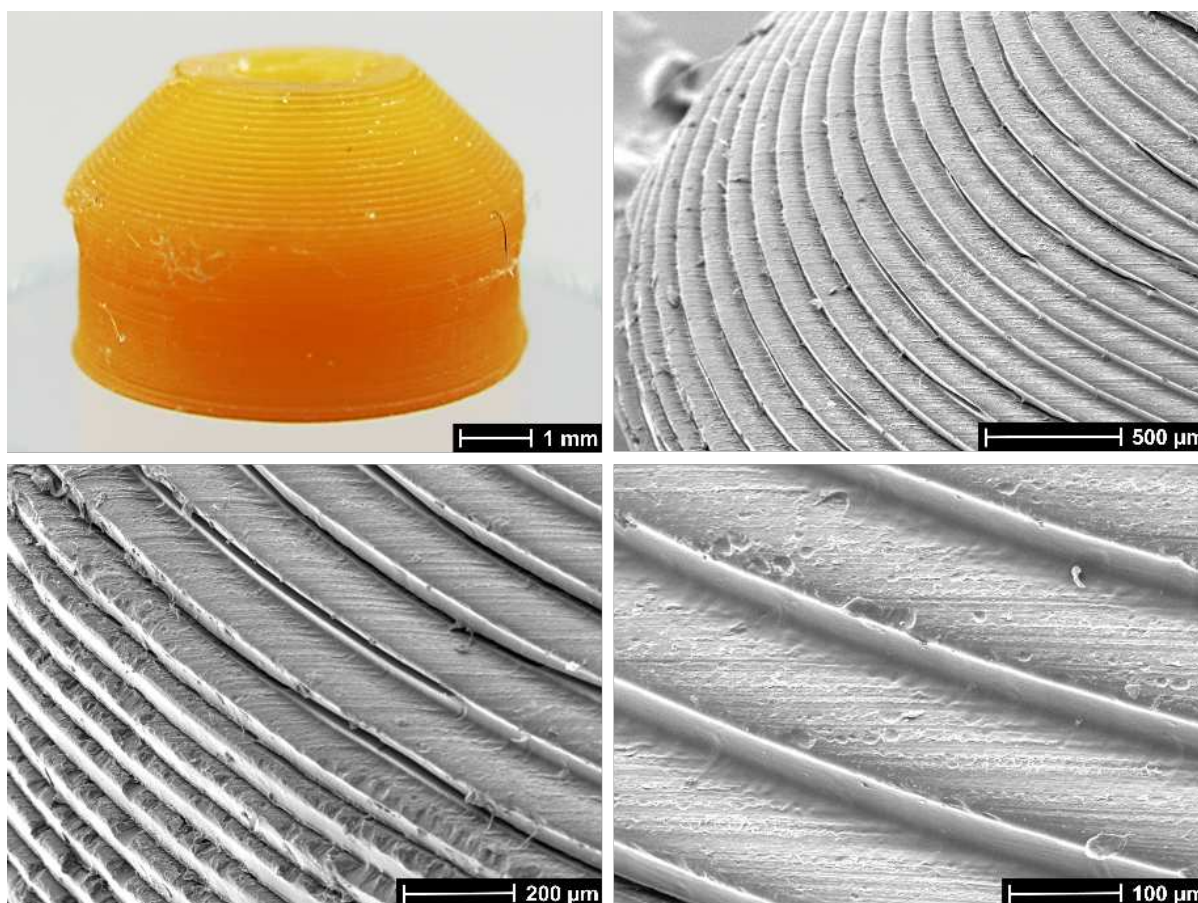
Figure 86: Photography and SEM images of poly(BisOx) 3D-printed by Hot Lithography (100 μm layer thickness)
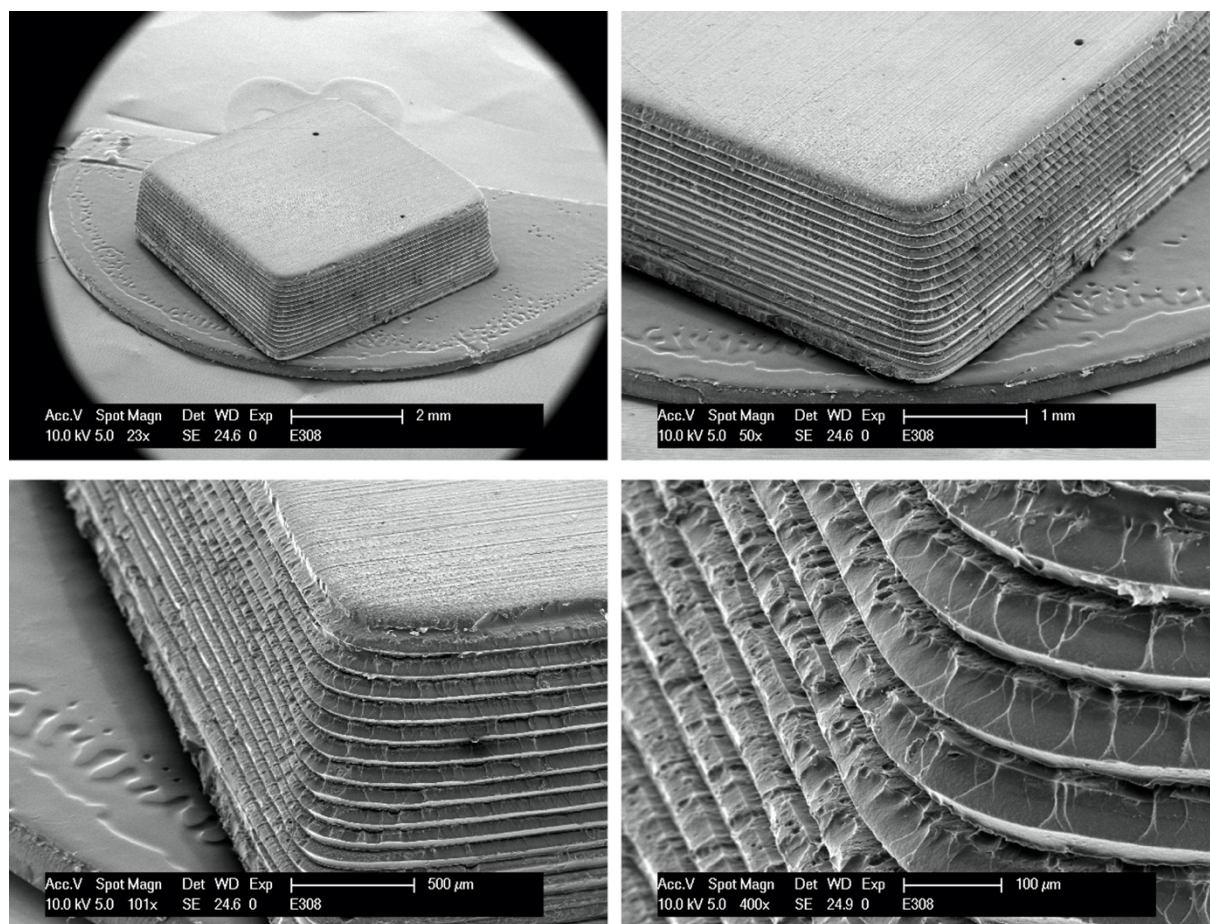
Figure 87: Photography and SEM images of poly(BisOx) 3D-printed by Hot Lithography (100 µm layer thickness)

As seen from the photography and SEM images, the successful structuring of defined 3D-parts confirms the efficient application of UV-induced CROP of 2-oxazolines in Hot Lithography. The nozzle-type cylindrical-conical object was structured in a layer-by-layer approach via laser at 120 °C. The high resolution of the printed layers confirms the selectivity of the photopolymerization reaction, whereas the high lateral precision is expressed by the accurate layer thickness without light-induced or diffusional overpolymerization.

EXPERIMENTAL PART

1   Initiation systems for cationic photopolymerization in Hot Lithography

1.2   Synthesis of alkoxyaluminate-based PAGs

1.2.1   Synthesis of diphenyliodonium tetrakis(perfluoro-t-butyloxy)aluminate (I-Al)

Prior to synthesis, the starting material $LiAlH_4$ was purified by extraction with absolute diethyl ether.

Compound	m [g]	V [mL]
lithium aluminum hydride (techn.)	2.0	
diethyl ether (abs.)		100

Under dry conditions the grey powder was placed in the upper part of an extraction frit and subsequently the solvent was added in small portions and sucked into a vessel below using Schlenk technique. 50 mL of absolute diethyl ether was used per gram of $LiAlH_4$. The solvent was evaporated under magnetic stirring at 80 °C and the pure white powder was dried under high vacuum until weight constant. The purified $LiAlH_4$ was ground as fine as possible using an agate mortar in a glove box to enhance the surface area of the solid for subsequent synthesis of the desired WCA.

The synthesis of lithium tetrakis(perfluoro-t-butyloxy)aluminate was conducted according to Krossing et al.[68]
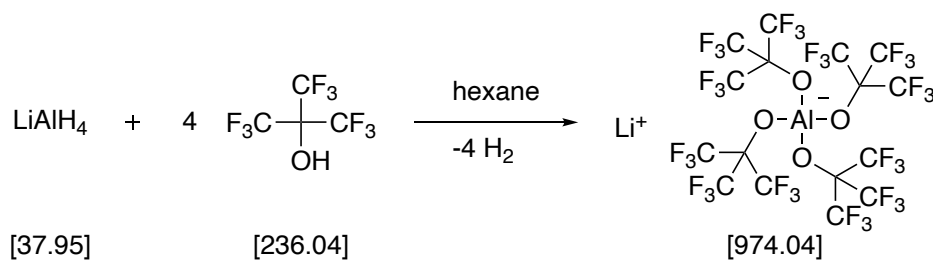
Compound	Equivalents	n [mmol]	m [g]	V [mL]
lithium aluminum hydride	1	6.6	0.252	
perfluoro-t-butanol	4.1	27.1	6.39	3.77
n-hexane (abs.)				35

The reaction was conducted under argon protective atmosphere to ensure moisture-free environment (LiAlH$_4$). All glassware was dried in a hot drying oven at 140 °C overnight.

In a 2-necked Schlenk flask equipped with a gas cooler, a septum and a magnetic stirring bar purified lithium aluminum hydride was mixed with 35 mL n-hexane (abs.). The gas cooler was cooled to -25 °C using a cryostat. Under stirring perfluoro-t-butanol was added dropwise via syringe and septum. After complete addition of the alcohol, the reaction mixture was heated to reflux for 3 hours. The completion of the reaction was tested by taking a small amount of the precipitate out of the flask and dipping it carefully into water. The absence of violent hydrolysis of residual Al-H bonds indicated the completion of conversion. Precipitation of product was completed by cooling the flask to -20 °C. The supernatant solvent was decanted off and the product dried under high-vacuum until weight-constant resulting in a white solid (5.84 g, 90 % of theory).

m.p. 143 - 153 °C (lit. 145 - 150 °C)

^{13}C-NMR (100 MHz, CDCl$_3$) δ (ppm): 121.3 (q, J=292.9 Hz, C(CF$_3$)$_3$)

^{27}Al-NMR (104 MHz, DMSO-d$_6$) δ (ppm): 75.42

ATR-IR (cm^{-1}): 725, 834, 966, 1174, 1203, 1241, 1265, 1296, 1353, 1629

Diphenyliodonium tetrakis(perfluoro-t-butyloxy)aluminate (I-Al) was synthesized in a procedure similar to Höfer.[169]

[316.57]	[974.04]		**I-Al** [1248.21]
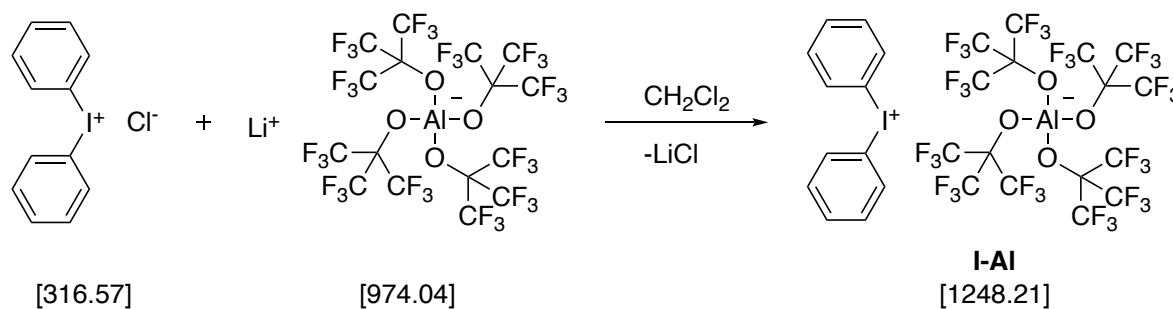
Compound	Equivalents	n [mmol]	m [g]	V [mL]
lithium tetrakis(perfluoro-t-butyloxy)aluminate	1	0.90	0.87	
diphenyliodonium chloride	1.05	0.95	0.30	
dichloromethane (abs.)				20

The synthesis was conducted in the orange light room and under argon atmosphere. In a 20 mL test tube equipped with a septum and a magnetic stirring bar and closed by a metal lid lithium tetrakis(perfluoro-t-butyloxy)aluminate was dissolved in 10 mL of absolute dichloromethane. No homogenous solution could be achieved. A solution of of diphenyliodonium chloride in 5 mL of absolute dichloromethane was added dropwise. The immediate precipitation of a white solid was observed. Another 5 mL of absolute dichloromethane were added, and the reaction stirred overnight at room temperature. After 24 hours reaction control by TLC showed full conversion of the lithium salt and excess of diphenyliodonium chloride. The reaction mixture was extracted three-times with 50 ml deionized water. To separate residual starting materials from the product the combined organic phases were filtered through a short plug of silica. The solvent was evaporated in vacuo and the residue dried under high vacuum resulting in a white solid. (1.12 g, 85 % of theory)

m.p.: 172 - 174 °C

TLC (CH_2Cl_2): R_f = 0.41

^{1}H-NMR (400 MHz, CD$_2$Cl$_2$) δ (ppm): 7.94-8.03 (m, 4H, *o*-Ar), 7.79-7.89 (m, 2H, *p*-Ar), 7.58-7.70 (m, 4H, *m*-Ar)

^{13}C-NMR (100 MHz, CD$_2$Cl$_2$) δ (ppm): 111.8 (>C-I), 121.7 (q, J=291.5 Hz, C(CF$_3$)), 134.4 (*m*), 135.1 (*p*), 135.5 (*o*).

^{27}Al-NMR (104 MHz, CD$_2$Cl$_2$) δ (ppm): 34.7

ATR-IR (cm^{-1}): 1470, 1449, 1351, 1296, 1273, 1239, 1205, 1165, 966, 831, 735, 724, 673, 548, 571, 560, 536 cm^{-1}

Elementary analysis	%C	%H	%N	%S	%F	%I
calculated	26.94	0.81	0.00	0.00	54.79	10.17
found	27.19	0.82	0.15	0.19	53.04	9.86

1.2.2 Synthesis of diphenyliodonium tetrakis(hexafluoroisopropoxy)aluminate

The synthesis of the WCA-based precursor lithium tetrakis(hexafluoroisopropoxy)-aluminate was conducted according to Krossing et al.[68]
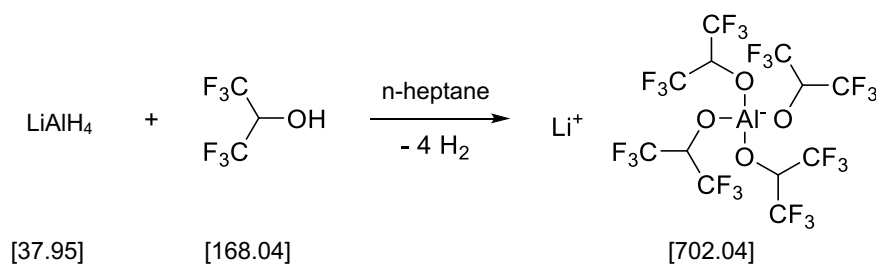
Compound	Equivalents	n [mmol]	m [g]	V [mL]
lithium aluminum hydride	1	10	0.380	
hexafluoroisopropanol (abs.)	10	100	16.8	10.5
n-heptane (abs.)				20

The reaction was conducted under Schlenk conditions to ensure moisture-free environment. All glassware was dried in a hot drying oven at 140 °C overnight. Lithium aluminium hydride was purified according to the above described method.

Hexafluoroisopropanol was distilled prior usage to reach a water content below 20 ppm (Karl-Fischer titration).

In a 2-necked Schlenk flask equipped with a gas cooler, a dropping funnel and a magnetic stirring bar purified lithium aluminum hydride was mixed with 20 mL n-heptane (abs.). The gas cooler was cooled to -25 °C using a cryostat. Under intensive stirring hexafluoroisopropanol was added dropwise to the milky suspension, resulting in a vigorous reaction and the precipitation of a white solid. After complete addition of the alcohol, the precipitate dissolved in the 2-phased mixture, which was heated to reflux at 80 °C overnight. After cooling to room temperature, the completion of the reaction was tested by dipping a small amount of the precipitate carefully into water. The absence of violent hydrolysis of residual Al-H bonds indicated the completion of conversion. Precipitation of product was completed by cooling the flask to -20 °C. The supernatant solution of n-heptane was removed by decantation and the residual HFIP was evaporated. The white solid was dried in high vacuum until constant weight. The product was purified by sublimation at 150 °C at 5×10^{-2} mbar under Schlenk conditions (6.55 g, 90 % of theory).

m.p. 120 - 128 °C (lit. 120 - 125 °C)

^{1}H-NMR (250 MHz, DMSO-d_6) δ (ppm): 4.60 (sept, J_{HF}=6.69 Hz, CH)

^{13}C-NMR (150 MHz, DMSO-d_6) δ (ppm): 70.7 (sept, J=31.4 Hz, C-O), 123.4 (q, J=286.3 Hz, $C(CF_3)_3$)

^{27}Al-NMR (65 MHz, DMSO-d_6) δ (ppm): 52.3

ATR-IR (cm^{-1}): 688, 751, 767, 855, 866, 885, 895, 926, 1087, 1159, 1171, 1217, 1285, 1376

1.3 Thermal stability of cationic photoinitiation systems

STA measurements were conducted using a STA 449 F1 Jupiter from Netzsch. Photoreactive formulations of bisphenol-A diglycidyl ether (BADGE) containing 1 mol% I-Al, 1 mol% I-Al in combination with 0.1 mol% bis(4-methoxybenzoyl)-diethylgermanium (BMDG), or 1 mol% tris(4-((4-acetylphenyl)thio)phenyl)sulfonium

tetrakis(pentafluorophenyl)borate (S-B), respectively, were weighed into 3 ml brown glass vials and stirred magnetically for 1 hour at 50 °C until all photoinitiator solids were dissolved. About 14 ± 0.5 mg of the respective formulations were weighed into standard aluminum DSC crucibles. The crucibles were closed with appropriate aluminum lids that were pierced by a syringe needle before application.

The thermal stabilities of photoreactive formulations in temperature gradient mode (1.3.1) were determined with a heating rate of 10 K/min from 25 °C to 300 °C under nitrogen atmosphere.

The thermal stabilities of photoreactive formulations with constant temperature (1.3.2) were determined by heating the samples to the designated temperatures with a heating rate of 10 K/min and keeping the samples for 120 min at high temperature to follow their thermal behavior in DSC and TGA signals.

The evaluation was done with the Netzsch Proteus Thermal Analysis software. The plot was transformed to a temperature ordinate to show the TGA curve for thermogravimetric loss and DSC for thermal decomposition processes. Also deviations in the heating rate were considered during the measurement.

1.4   Photo-DSC studies of cationic photoinitiation systems in BADGE at elevated temperatures

Photo-DSC studies were conducted using a photo-DSC 204 F1 Phoenix from Netzsch. All measurements were conducted under inert atmosphere (Nitrogen flow of 20 mL min^{-1}). A 4 min conditioning time at the respective measurement temperature was run before two-fold irradiation of the samples as the second period indicates the baseline signal for subsequent calculative subtraction. For photo-DSC of BADGE formulations, two irradiation periods of 300 s were applied for each measurement. The heat flow of the reaction was recorded as a function of time. The sample mass in the aluminum crucibles was 14 ± 0.5 mg. The aluminum crucibles were closed by a glass lid to reduce evaporation. The evaluated results represented the overall polymerization enthalpy by the peak area (ΔH_P [J/g]), the time to reach the peak maximum (t_{max} [s]), the time to reach 95 % of conversion (by peak area) (t_{95} [s]), and the peak height (h [W/g]). The calculation of conversion (C [%]) and rate of polymerization (R_p [mol·L^{-1}·s$^-$

[1]) from photo-DSC analyses were accessible after determination of the theoretical functional group enthalpy (ΔH_{0P}) of the reactive moiety.

For glycidyl ether monomers, such as the diglycidyl ether BADGE, the theoretical functional group enthalpy (ΔH_{0P}) was literature known and amounted 80.6 kJ/mol per reactive group.[56]

1.4.1 Photo-DSC studies using broadband irradiation

The formulations formerly used for STA measurement measurements were used for photo-DSC measurements of BADGE monomer formulations in 320-500 nm broadband irradiation. Hence, the formulations consisted of BADGE containing 1 mol% I-Al, 1 mol% S-B, or 1 mol% I-Al in combination with 0.1 mol% BMDG, respectively. Photo-DSC measurements were conducted at 80, 100 and 120 °C.

Filtered UV-Vis light (320-500 nm) was applied using an Exfo OmniCure 2000 with a glassfiber filled double-core lightguide (3 mm fiber diameter). The light intensity was calibrated by an Omnicure R2000 radiometer and set to 3 W/cm² at the tip of the light guide, corresponding to 130 mW/cm² irradiation intensity at the sample position, which was measured by an Ocean Optics USB 2000+ spectrometer.

1.4.2 Photo-DSC studies using LED irradiation

For photo-DSC experiments with 385 or 400 nm LED irradiation, an Omnicure LX400 LED UV Spot Curing System was used to control the UV-LED heads. To connect the photo-DSC to the LED UV Spot Curing System, an Arduino board was used as CPU to perform the translation of commands between the two devices. The UV-LED heads provide peak irradiance of 16 mW/cm^2 (385 nm) and 9 mW/cm^2 (400 nm), respectively.[170] Photo-DSC measurements were conducted at 80, 100 and 120 °C.

For these measurements with LED irradiation the commercial diaryliodonium photoinitiator (p-octyloxyphenyl)phenyliodonium hexafluoroantimonate (I-Sb) was used. Formulation of the monomer BADGE containing 1 mol% I-Sb with 0.1 mol% BMDG, I-Sb with 1 mol% BMDG, or 1 mol% S-B, respectively.

2 Cationic photopolymerization of 2-oxazolines

2.2 Synthesis of a triarylsulfonium alkoxyaluminate PAG

The alkoxyaluminate-based PAG tris(4-((4-acetylphenyl)thio)phenyl)sulfonium tetrakis(perfluor-t-butyloxy)aluminate (S-Al) was synthesized in a similar procedure to Höfer.[56, 169]

Compound	Equivalents	n [mmol]	m [g]	V [mL]
lithium tetrakis(perfluoro-t-butyloxy)aluminate	1	0.08	0.077	
tris(4-((4-acetylphenyl)thio)phenyl)-sulfonium chloride	1	0.08	0.060	
dichloromethane abs.				15

The synthesis was conducted in the orange light room and under argon atmosphere.

In a 20 mL test tube equipped with a septum and a magnetic stirring bar and closed by a metal lid lithium tetrakis(perfluor-t-butyloxy)aluminate was dissolved in 10 mL of CH_2Cl_2. A solution of of tris(4-((4-acetylphenyl)thio)phenyl)sulfonium chloride in 5 mL of CH_2Cl_2 was added dropwise under vigorous stirring. The immediate precipitation of a white solid was observed. The reaction mixture was stirred overnight and the conversion controlled by TLC. 5 mL of deionized water were added to dissolve the solid. The phases were separated and the organic phase was extracted another two times with 5 mL each of deionized water. To separate residual starting materials from the product the combined organic phases were filtered through a short plug of silica in

a glass pipette. The solvent was evaporated in vacuo and the residue dried under high vacuum yielding a white solid (106 mg, 80 % of theory)

m.p.: 174.0 - 176.0 °C

TLC (CH$_2$Cl$_2$): R$_f$ = 0.15

^{1}H-NMR (200 MHz, CDCl$_3$) δ (ppm): 8.00 (d, 6H, J=8.60 Hz, Ar), 7.59 (d, 6H, J=8.60 Hz, Ar), 7.34 (d, 6H, J=8.56 Hz, Ar), 7.26 (d, 6H, J=9.00 Hz, Ar), 2.62 (s, 9H, CH$_3$).

ATR-IR (cm^{-1}): 1685, 1572, 1478, 1398, 1352, 1298, 1276, 1239, 1213, 1166, 1089, 1067, 972, 814, 727, 620

Elementary analysis	%C	%H	%N	%S
calculated	41.44	1.98	0.00	7.63
found	41.77	1.91	< 0.05	7.38

2.3 Preceding investigations of photoinitiation systems for CROP of 2-oxazolines

2.3.1 STA of diaryliodonium and triarylsulfonium PAGs in PhOx

The analysis was conducted according to 1.3.

Formulations of I-Al, I-Sb, S-Al, S-B and S-C in PhOx in a concentration of 1.67 mol% in PhOx were used.

2.3.2 Photo-DSC of triarylsulfonium PAG S-B in PhOx at elevated temperatures

The analysis was conducted according to 1.4 using 320-500 nm irradiation with 130 mW/cm^2 intensity.

Irradiation periods of 900 s were applied at temperatures of 120, 130 and 140 °C.

Formulations of S-Al, S-B and S-C in PhOx in a concentration of 1.67 mol% in PhOx were used.

2.4　Synthesis of 2-oxazoline monomers for cationic photopolymerization

2.4.1　Synthesis of 2-octyl-2-oxazoline (OctOx)

The synthesis of 2-octyl-2-oxazoline (OctOx) was conducted according to reported Witte et al. from the corresponding nitrile.[164] [156]

[139.24]　　　　　　　　[61.08]　　　　　　　　　　OctOx
　　　　　　　　　　　　　　　　　　　　　　　　　[183.30]
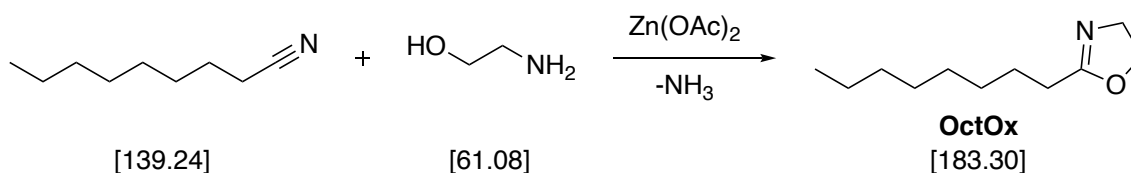
Compound	Equivalents	n [mmol]	m [g]	V [mL]
nonanenitrile	1	250	34.8	
ethanolamine	1.2	300	18.3	18.1
zinc acetate dihydrate	0.025	6.3	1.37	

The synthesis was conducted under argon atmosphere. In a 100 mL 3-necked round bottom flask equipped with a reflux condenser, a septum, an inert gas inlet and a magnetic stirring bar, zinc acetate dihydrate was dispersed in nonanenitrile and heated to 130 °C. Ethanolamine was added dropwise under vigorous stirring. The solution was stirred at 130 °C overnight and the conversion controlled via TLC. After cooling to room temperature, 200 mL of deionized water was added to the reaction mixture. The phases were separated, and the aqueous phase extracted three-times with 200 mL CH_2Cl_2. The combined organic phases were dried over Na_2SO_4 and the solvent evaporated *in vacuo*. The crude product was purified by distillation yielding a colorless liquid (25.2 g, 55 % of theory).

b.p.: 110 °C / 7.5 Torr

TLC (PE/EA 2:1): R_f = 0.27

¹H-NMR (400 MHz, CDCl$_3$) δ (ppm): 4.21 (2H, t, J=9.54 Hz), 3.81 (t, 2H, J=9.54 Hz), 2.26 (t, 2H, J=7.80 Hz), 1.62 (q, 2H, J=7.51 Hz), 1.16-1.39 (m, 10H), 0.87 (t, 3H, J=6.82 Hz)

¹³C-NMR (100 MHz, CDCl$_3$) δ (ppm): 168.8 (C=N), 67.2 (CH$_2$-O), 54.5 (CH$_2$-N=), 31.9 (CH$_2$-C=N), 29.4 (CH$_2$), 29.3 (CH$_2$), 29.2 (CH$_2$), 28.1 (CH$_2$), 26.1 (CH$_2$-CH$_3$), 22.7 (CH$_2$-CH$_2$-C=N), 14.2 (CH$_3$)

GC-MS: rt 9.78 min, > 99 %; m/z: 184.21 (3) [M +H]$^+$, 154.20 (13) [M – C$_2$H$_5$]$^+$, 140.13 (19) [M – C$_3$H$_7$]$^+$, 112.09 (13) [M – C$_5$H$_{11}$]$^+$, 98.07 (69) [M – C$_6$H$_{13}$]$^+$, 85.09 (100) [C$_6$H$_{13}$]$^+$

2.4.2 Synthesis of 1,6-bis(4,5-dihydrooxazol-2-yl)hexane (BisOx)

The synthesis of (BisOx) was conducted according to Witte et al. from the corresponding nitrile. [164]

Compound	Equivalents	n [mmol]	m [g]	V [mL]
1,6-dicyanohexane	1	320	43.6	45.7
ethanolamine	3	960	58.6	58.0
zinc acetate dihydrate	0.05	16	3.52	

The synthesis was conducted under argon atmosphere. In a 250 mL 3-necked round bottom flask equipped with a reflux condenser, a septum, an inert gas inlet and a magnetic stirring bar, zinc acetate dihydrate was dispersed in 1,6-dicyanohexane and heated to 100 °C. Ethanolamine was added dropwise under vigorous stirring. The solution was stirred at 100 °C for 48 hours and the conversion controlled via ¹H-NMR. After cooling to room temperature, 200 mL of deionized water was added to the reaction mixture and extracted three-times with 250 mL dichloromethane. The

combined organic phases were dried over Na_2SO_4 and the solvent evaporated *in vacuo*. The crude product was purified by distillation (b.p. 132 °C/0.03 Torr) yielding 38.5 g of colorless solid (172 mmol, 54 %).

m.p.: 64-66 °C

b.p.: 132 °C / 0.03 Torr

TLC (CH_2Cl_2/MeOH 9:1): R_f = 0.59

^{1}H-NMR (400 MHz, $CDCl_3$) δ (ppm): 4.18 (t, 2H, J=9.36 Hz), 3.78 (t, 2H, J=9.56 Hz), 2.23 (t, 2H, J=7.61 Hz), 1.60 (m, 4H), 1.34 (m, 4H)

^{13}C-NMR (100 MHz, $CDCl_3$) δ (ppm): 168.6 (C=N), 67.2 (CH_2-O), 54.5 (CH_2-N=), 28.9 (CH_2-C=N), 28.0 (CH_2), 25.9 (CH_2)

GC-MS: rt 14.99 min, > 99 %; m/z: 223.06 (14) [M]$^+$, 140.08 (100) [M − C_4H_6NO]$^+$, 112.15 (29) [$C_6H_{10}NO$]$^+$, 98.07 (100) [C_5H_8NO]$^+$, 85.15 (38) [C_6H_{13}]$^+$

2.4.3 Synthesis of hydroxyl-terminated 2-alkyl-2-oxazolines

2.4.3.1 Synthesis of ε-hydroxypentyl-2-oxazoline
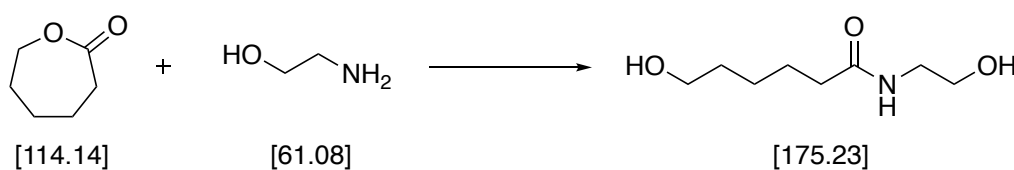
Compound	Equivalents	n [mmol]	m [g]	V [mL]
e-caprolactone	1	100	11.42	
ethanolamine abs.	1	100	6.14	

The synthesis was conducted under argon atmosphere. In a 50 mL 3-necked round bottom flask equipped with a reflux condenser, a dropping funnel, an inert gas inlet and a magnetic stirring bar, dry ethanolamine (1 eq) was added to ε-caprolactone (1 eq) at 80 °C under vigorous stirring. The reaction mixture was heated to 120 °C for 3 hours. The product precipitated at room temperature overnight and crystallization was

completed at -20 °C. The crude product was purified by recrystallization from acetone. The synthesis gave 7.3 g of white waxy solid in a yield of 42% of theory.

Purity was confirmed by TLC, ^{1}H-NMR and GC-MS.

m.p.: 72-74 °C

TLC (CHCl$_3$/MeOH 9:1): R$_f$ = 0.62

^{1}H-NMR (400 MHz, DMSO-d$_6$) δ (ppm): 7.74 (s, 1H), 4.62 (t, 1H, J=5.46 Hz), 4.33 (t, 1H, J=5.08 Hz), 3.36 (tt, 4H, J=6.24 Hz), 3.09 (q, 2H, J=5.85 Hz), 2.04 (t, 2H, J=7.42 Hz), 1.16-1.39 (m, 4H), 1.24 (m, 2H)

GC-MS: rt 9.9 min, > 90 %, m/z: 174.86 (2) [M]$^+$, 156.98 (2) [M − OH]$^+$, 145.15 (12) [M − CH$_2$-OH]$^+$, 132.03 (14) [M − C$_2$H$_4$-OH]$^+$, 115.02 (77) [M − C$_3$H$_6$-OH]$^+$, 103.04 (83) [M − C$_4$H$_8$-OH]$^+$

2.5 STA of photoreactive formulations of PhOx, OctOx and BisOx with S-B

The analysis was conducted according to 1.3.

Formulations of PhOx, OctOx and BisOx containing 0.5 mol% S-B per reactive group of monomer were used.

2.6 Photo-DSC studies of 2-oxazolines at elevated temperatures

2.6.1 Theoretical polymerization enthalpy of 2-oxazolines in photo-DSC

The determination of theoretical polymerization enthalpy of monofunctional monomers was conducted by photo-DSC and ^{1}H-NMR analysis.

The photo-DSC analysis was conducted according to 1.4 using 320-500 nm irradiation with 130 mW/cm^2 intensity.

Irradiation periods of 900 s were applied at temperatures of 120 and 140 °C. A formulation of OctOx containing 0.5 mol% of S-B was prepared. As the triarylsulfonium photoacid generator S-B is not soluble in OctOx, it was dispersed in propylene carbonate (PAG/propylene carbonate 50:50 wt%), before adding the monomer. Subsequently, the formulation was treated in an ultrasonic bath for 30 min at room temperature.

Different to standard photo-DSC measurements, the determination of theoretical polymerization enthalpy was conducted using one single irradiation period of 900 s. After one irradiation period the measurement, the polymer samples were added to 0.7 mL of deuterated chloroform and quenched with a drop of pyridine. After dissolution of the polymer samples, ^{1}H-NMR measurements gave the conversion by the amount of residual monomer from the integrals of 2-oxazoline's 4- and 5-positioned proton signals in relation to the octyl substituent's methyl protons as internal standard. The overall enthalpy detected in photo-DSC analysis ΔH_P was set in relation to the conversion determined from ^{1}H-NMR analysis of the soluble linear-chained polymer (C_{NMR}). All measurements were carried out in triplicates.

2.6.2 Photo-DSC of PhOx, OctOx and BisOx

The photo-DSC analysis was conducted according to 1.4 using 320-500 nm irradiation with 130 mW/cm^2 intensity. Irradiation periods of 900 s were applied at temperatures of 100, 120 and 140 °C.

Formulations of the respective monomer and 0.5 mol% of S-B per reactive group of 2-oxazoline were prepared. The formulations were weighed into 3 mL brown glass vials and subsequently stirred magnetically for 30 min at room temperature, or at 80 °C above the melting point of the monomer BisOx, respectively. As the triarylsulfonium photoacid generator S-B is not soluble in OctOx, it was dispersed in propylene carbonate (PAG/propylene carbonate 50:50 wt%), before adding the monomer.

For evaluation of the rate of polymerization, the density of 2-oxazoline monomers was not accessible by literature and therefore determined by pycnometry in triplicate measurements. For 2-octyl-2-oxazoline density of d^{25} = 896.5 g/L was determined, whereas the density of melted BisOx at 100 °C was determined by conditioning of the

filled pycnometer in a 100 °C drying oven (d^{100} = 1004.8 g/L). A 1 mL pycnometer was used and calibrated with deionized water at 25 °C to determine the exact volume.

2.6.3 Photo-DSC of triarylsulfonium PAGs in BisOx

The photo-DSC analysis was conducted according to 1.4 using 320-500 nm irradiation with 130 mW/cm^2 intensity. Irradiation periods of 900 s were applied at temperatures of 100, 120 and 140 °C.

Formulations of S-Al, S-B and S-C in a concentration of 1 mol% in BisOx were prepared. The formulations were weighed into 3 mL brown glass vials and stirred magnetically for 30 min at 80 °C. The heated formulation of BisOx was pipetted into the crucibles on an 80 °C heating block and subsequently weighed to contain 14 ± 0.5 mg of formulation.

2.6.4 Variation of PAG concentration in PhOx, OctOx and BisOx

The photo-DSC analysis was conducted according to 1.4 using 320-500 nm irradiation with 130 mW/cm^2 intensity. Irradiation periods of 900 s were applied at 120 °C.

Formulations of the monomer PhOx, OctOx and BisOx containing 0.5, 1 and 1.5 mol% of S-B per reactive group of 2-oxazoline were prepared.

2.7 GPC studies of poly(OctOx)

Samples of poly(OctOx) from separately conducted photopolymerization experiments by photo-DSC at temperatures of 100, 120 and 140 °C were analyzed by gel permeation chromatography (GPC).

The polymerizations by photo-DSC were conducted according to 1.4 using 320-500 nm irradiation with 130 mW/cm^2 intensity. Irradiation periods of 900 s were applied at temperatures of 100, 120 and 140 °C.

Formulations of 2-octyl-2-oxazoline (OctOx) containing 0.5, 1.0 and 1.5 mol% S-B and propylene carbonate (PAG/propylene carbonate 50:50 wt%) were used.

The polymer samples were analyzed by GPC on a Viscotek GPCmax VE2001 instrument equipped with three columns (Styragel HR 0.5 THF, Styragel HR 3 THF, Styragel HR 4 THF) and a Viscotek VE3580 RI detector. Dry THF was used as the mobile phase (1.0 mL min^{-1} flow rate) at 40 °C. Polystyrene standards (in the range between M_n = 0.370 and 177 kDa) were used for standard calibration. The photopolymers were dissolved in dry THF, and these solutions were filtered with a 200 nm poly(tetrafluoroethylene) syringe filter. Portions of 100 µL of the samples were injected. Empower Pro software was used for the evaluation of the elugrams and to calculate the number- and weight-average molecular weight (M_n and M_w) and the polydispersity Đ (M_w/M_n) of the polymers.

2.8 Photoreactivity studies of 2-oxazoline, epoxy and methacrylate formulations

2.8.1 STA of photoreactive formulations of BisOx, BDDGE and BDDMA

The analysis was conducted according to 1.3.

Formulations of BisOx and BDDGE containing 1 mol% S-B, as well as BDDMA containing 1 mol% of BMDG were used.

2.8.2 RT-NIR/MIR-Photorheology of BisOx, BDDGE and BDDMA formulations at 100 °C

For RT-NIR/MIR-photorheology analyses an Anton Paar MCR 302 WESP rheometer with a P-PTD 200/GL Peltier plate, an H-PTD 200 heating hood, and a disposable PP25 measuring system was used.

For analyses in NIR, a quartz glass window was used as lower plate for UV and NIR transmission. It was covered with PE tape for subsequent removal of cross-linked polymer samples. Coupled to the rheometer, a Bruker Vertex 80 FTIR spectrometer was used to analyze the real-time conversion of the sample.

The measurements were conducted at 25 °C or 100 °C. A 5 min conditioning time was conducted before starting the measurement. The formulations were sheered with a

strain of 1% and a frequency of 1 Hz. UV-irradiation was applied by an Exfo OmniCure 2000 device with a broadband Hg lamp (320-500 nm, 80 mW cm^{-2} on the sample position, measured with an Ocean Optics USB 2000+ spectrometer). The methacrylate double-bond conversion (DBC) and epoxy conversion (EC) were determined by recording a set of single spectra (time interval ~0.26 s) with an OPUS 7.0 software and then integrating the respective bands at ~6160 cm^{-1} (double bond) and 4530 cm^{-1} (epoxy). The ratio of the peak area at the start and after a certain irradiation period gave the respective conversion value. All measurements were performed in duplicates for confirmation of reproducibility.

In the photorheologic measurement the samples reach their gel point in the cross-section of storage and loss modulus, G' and G'', respectively. As most representative parameters, the time to reach the gel point (t_g), the conversion at gel point (C_g), the time of 95 % conversion (t_{95}) and the final conversion (C_{final}) are defined and were accessible by evaluation using corresponding analytic software.

Formulations of BisOx with 2 mol% S-B, BDDGE with 2 mol% S-B and BDDMA with 2 mol% BMDG were used. For each measurement at 200 µm gap size, 150 µL of formulation were applied. Formulations of BDDGE and BDDMA were measured using 300 s irradiation time, whereas the formulation of BisOx was measured using 900 s irradiation time.

RT-MIR-photorheology measurements of BisOx with 2 mol% S-B were conducted using a calcium fluoride window as lower plate to allow for transmission of MIR radiation. The calcium fluoride plate was analogously covered with PE tape. Furthermore, due to the high intensity of signals in MIR, the gap size was reduced to the minimum applicable distance of 50 µm. 50 µL of formulation were applied.

2.8.2.1 Influence of gap size and discoloration on the photorheology analysis of BDDGE

The RT-NIR-photorheology analysis was conducted according to 2.8.2.

The measurements were conducted at 100 °C using gap sizes of 50, 100 and 200 µm.

A formulation of BDDGE containing 2 mol% S-B was used.

2.8.2.2 DSC of poly(BisOx), poly(BDDGE) and poly(BDDMA)

Thermal differential scanning calorimetry (DSC) of polymers was conducted using a DSC TA Q2000 system in a temperature range from -50 to 250 °C. The photopolymer specimen of poly(BisOx), poly(BDDGE) and poly(BDDMA) were obtained from prior RT-NIR-photorheology measurements (2.8.2). Pieces of photopolymer were cut in circular shape of 3-4 mm diameter to fit the size of aluminum crucibles used in DSC measurements. The measurements were conducted in two consecutive heating cycles in a range from -80 to 250 °C in nitrogen atmosphere to ensure full thermal post-curing of the polymers. The glass transition temperatures (T_g) were evaluated by corresponding software to detect the inflection point in the curve of the DSC signal.

2.8.2.3 DMTA of poly(BisOx) and poly(BDDGE)

Thin layer dynamic mechanical-thermal analysis (DMTA) was performed in tension mode using a Dynamic Mechanical Analyzer (TA Instruments 2980) from −100 to 200 °C with a heating rate of 3 °C min^{-1}. The test was done with a frequency of 1 Hz, an amplitude of 20 µm and a preload force of 0.1 N. The tanδ peak was used as an indicator for the glass transition temperature (T_g).

The photopolymer specimen of poly(BisOx) and poly(BDDGE) were obtained from prior RT-NIR-photorheology measurements (2.8.2). Pieces of photopolymer film were cut in rectangular geometry of about 8 x 2.2 mm^2 and their dimension measured via optical microscope.

2.8.3 Shrinkage of BisOx, BDDGE and BDDMA formulations in photorheology

The RT-NIR-photorheology analysis was conducted according to 2.8.2.

The measurements were conducted using 200 µm gap size. 100 °C were applied for BisOx with 2 mol% S-B, and 25 °C for BDDGE with 2 mol% S-B and BDDMA with 2 mol% BMDG.

The normal force on the PP25 measuring system was evaluated as a measure of shrinkage force during photopolymerization of cross-linking formulations.

2.9 Thermomechanical properties of poly(2-oxazoline)s

For comparative thermomechanical studies photoreactive formulations of methacrylates and 2-oxazolines were photopolymerized under respective conditions.

A methacrylate formulation of BDDMA, HexMA and BMA (20:40:40 molar ratio) containing 0.5 mol% BMDG per reactive group of monomer was used. The formulations were weighed into 3 mL brown glass vials and treated in an ultrasonic bath for 30 min to dissolve the photoinitiator.

The specimens for mechanical testing were prepared by photopolymerization of the formulations in silicon molds (for DMTA: 5 x 2 x 40 mm³; for Dynstat impact test: 4 × 10 × 15 mm^3; for tensile tests: dumbbell-shaped according ISO527-2:2012 geometry 5B, total length of 35 mm, thickness 2 mm).

The methacrylate reference specimens were cured using a Lumamat 100 light chamber (Ivoclar Vivadent, 25 °C, 400–580 nm, 20 mW cm^{-2}) for 420 s on both sides of the specimens. All samples were polished with sandpaper to reach uniform geometries and to remove defects from the photopolymer surface.

2.9.1 UV-Curing of 2-oxazoline-based photopolymers at elevated temperatures

Photoreactive formulations of BisOx, OctOx and PhOx in different compositions were used. The formulations were weighed into 3 mL brown glass vials and treated in an ultrasonic bath for 30 min to dissolve the photoinitiator.

In accordance to 2.9, specimens for thermomechanical testing in specific dimensions for DMTA, Dynstat impact testing and tensile test were prepared.

The respective 2-oxazoline formulations were preheated to 100 °C and filled into a preheated silicon-mold (140 °C). The mold was attached to a custom-made heating plate (140 °C) and the setup was placed in an Uvitron UV 1080 Flood Curing System with Uvitron Intelliray 600 halide lamps (600 W, 120 mW cm^{-2}, 320-580 nm). The samples were cured for 900 s on both sides of the specimens. Equally heated samples without irradiation confirmed the thermal stability of the formulations in parallel.

2.9.2 DMTA screening of 2-oxazoline-based photopolymers

Dynamic Mechanical Thermal Analysis (DMTA) was performed using an Anton Paar MCR 301 device with a CTD 450 oven and an SRF 12 measuring system. The prepared DMTA samples were tested in torsion mode with a frequency of 1 Hz and a strain of 0.1%. The temperature was increased from −20 to 200 °C with a heating rate of 2 °C min^{-1}. The glass transition temperature was determined from the temperature at the maximum loss factor (tanδ). Formulations of BisOx, OctOx and PhOx in different ratios containing 1 mol% S-B per reactive group of monomer were applied.

The glass transition temperature was determined from the temperature at the maximum loss factor (tanδ). The storage modulus at 20 °C (G´$_{20}$), as well as the storage modulus in the rubbery region 30 °C above respective T$_g$ (G´$_r$) were determined.

The measurement of a composition of BisOx/PhOx 10:90 was conducted in two consecutive heating cycles of -20 to 250 °C to evaluate the influence of thermal post-curing on the poly(2-oxazoline) photopolymer.

2.9.3 Photo-DSC of a formulation for 2-oxazoline-based photopolymers

The photo-DSC analysis was conducted according to 1.4 using 320-500 nm irradiation with 130 mW/cm^2 intensity. Irradiation periods of 900 s were applied at temperatures of 100, 120 and 140 °C.

A formulation of the BisOx/OctOx/PhOx (20:40:40) containing 0.5 mol% of S-B per reactive group of 2-oxazoline was used and compared to corresponding formulations of the single monomers BisOx, OctOx and PhOx.

2.9.4 ATR-IR spectroscopy of a 2-oxazoline-based photopolymer

For determination of conversion in poly(2-oxazoline) samples, FTIR-ATR was measured on a Spectrum 65 FTIR-ATR spectroscope from Perkin-Elmer.

The measurement of reference spectra was conducted using the pristine monomers BisOx, OctOx and PhOx, as well as the pristine photoreactive formulation of

BisOx/OctOx/PhOx (20:40:40) containing 0.5 mol% of S-B per reactive group of 2-oxazoline.

The full conversion of monomers was confirmed from the measurement of the cryomilled photopolymer powder of BisOx/OctOx/PhOx (20:40:40). In the direct comparison of the ternary photoreactive mixture of BisOx, OctOx and PhOx before and after photopolymerization, the spectra were normalized to the unchanged signal at 2927 cm^{-1}.The absence of monomer signals in the spectrum was controlled by the disappearance of the monomer signals of BisOx and OctOx (both around 1667 cm^{-1}) and PhOx (1647 cm^{-1}). Peak deconvolution by the software PeakFit was applied, to confirm the absence of residual unreacted monomer.

2.10 Comparative thermomechanical testing of poly(2-oxazoline) and poly(methacrylate) materials

2.10.1 DMTA

The analysis was conducted according to 2.9.2.

Photopolymers of compositions of BisOx/OctOx/PhOx (20:40:40) and BDDMA/HexMA/BMA (20:40:40) were measured in one heating cycle from -20 to 200 °C.

2.10.2 Tensile strength

Tensile tests were performed using a Zwick Z050 equipped with a 1 kN load cell (Zwick Roell, Ulm, Germany) according to ISO 527-1:2012 with a test speed of 5 mm min^{-1}. The dimensions of the specimens were measured with an accuracy of ± 0.02 mm according to ISO 16012:2015. The strain was recorded and analyzed via testXpert II testing software.

Photopolymers of compositions of BisOx/OctOx/PhOx (20:40:40) and BDDMA/HexMA/BMA (20:40:40) were measured. For each formulation five specimens were tested.

2.10.3 Impact resistance

Dynstat impact resistance testing was conducted using a Karl Frank GmbH Dynstat device (Type 573) with a 1 J hammer tool. The results were determined by conversion to kJ and divided by the respective cross-sectional area.

Photopolymers of compositions of BisOx/OctOx/PhOx (20:40:40) and BDDMA/ HexMA/BMA (20:40:40) were measured. For each formulation four specimens were tested.

2.10.4 Thermal analysis of poly(2-oxazoline) and poly(methacrylate) materials

The photopolymer samples of poly(2-oxazoline) and poly(methacrylate) used for tensile testing before (2.10.2) were cryomilled to yield fine powders.

The analysis by STA was conducted according to 1.3. using 12 ± 1 mg of photopolymer powders. Thermal stabilities of photopolymer samples were determined with a heating rate of 10 °C min^{-1} from 25 °C to 500 °C under nitrogen atmosphere. The decomposition temperatures T_D were determined as temperature of 5 % mass loss.

2.11 Hot Lithography of 2-oxazolines

2.11.1 Photorheology pretests using 365 and 385 nm LED irradiation

The photorheology analysis was conducted according to 2.8.2. An Omnicure LX400 LED UV Spot Curing System was used to control the 365 and 385 nm UV-LED heads. The UV-LED heads provide peak irradiance of 14 W/cm² (365 nm) and 16 mW/cm² (385 nm), respectively.[170] On the sample position 8.3 mW/cm² for 365 nm, and 7.0 mW/cm² for 385 nm were measured with an Ocean Optics USB 2000+ spectrometer.

A formulation of BisOx containing 2 mol% S-B was used at 100 °C with an irradiation time of 300 s. The gap size was 50 μm and a sample volume of 50 μL was used.

2.11.2 Pretests of photoreactive 2-oxazoline formulations for Hot Lithography

2.11.2.1 *Laser exposure tests using Hot Lithography prototype at 100 °C*

Laser exposure tests at 100 °C were conducted using a prototype heatable SLA setup developed at TU Wien. The setup comprises a 375 nm diode laser (Omicrometer) in combination with a galvanometer−scanner (IntelliSCAN 10, Scanlab). The laser provides a maximum irradiation intensity of 70 mW.

Formulations of 1 and 2 mol% S-B in BisOx were tested, whereas only the higher PAG concentration gave successful laser exposure tests at 100 °C.

The two-dimensional area for laser exposure was predefined by the software to yield a circular disc of 15 mm diameter, a laser hatching distance of 15 µm and two consecutive exposures in x- and y- writing direction, respectively, for each irradiation run.

Scan speeds between 50 and 500 mm/s were applied to determine the limits of polymerizability in laser exposure tests. After successful laser exposure tests, the polymer samples were carefully removed from the Teflon-coated vat surface and washed with distilled acetone to remove soluble material from the cross-linked polymer disc. After drying at room temperature overnight, the thickness of the samples was determined by a micrometer caliper.

2.11.2.2 *Laser exposure tests using Hot Lithography at 120 and 140 °C*

Laser exposure tests for Hot Lithography at 120 and 140 °C were conducted on a Caligma 200 UV developed by the company Cubicure GmbH. Irradiation was applied by two UV class 3B diode lasers with an irradiation wavelength of 375 nm and an optical output power of 140 mW. The irradiated geometry was a platelet of 1x3 cm^2.

Formulations of 1 and 2 mol% S-B in BisOx were tested. The photosensitizer (PS) 9,10-dibutoxyanthracene was added to the formulations in varying concentrations.

The formulations were magnetically stirred at 80 °C until dissolution of all monomer and photosensitizer solids. Subsequently, the melted solution was applied on the irradiation position in the material vat to cover the platelet size for laser exposure.

Table 27 summarizes the conducted laser exposure tests at 120 and 140 °C.

Table 27: Laser exposure tests of BisOx formulations with varied parameters

S-B [mol%]	T [°C]	Laser speed [mm/s]	Nr. of exposures	PS conc. [wt%]	Layer thickness [µm]
1	140	250	5	0	no polymer
		100	5	0	no polymer
		50	5	0	no polymer
	120	1000	5	0.1	no polymer
		500	5	0.1	no polymer
		100	5	0.1	no polymer
		50	4	0.1	no polymer
			4	0.25	no polymer
			4	0.5	no polymer
			4	1	no polymer
			4	3	no polymer
2	140	500	4	0	370
		250	4	0	740
		100	2	0	370
		50	2	0	670
	120	50	2	0	670

2.11.2.3   STA of S-Sb in BisOx for application in Hot Lithography

The analysis was conducted according to 1.3.

Formulations of BisOx containing 1 mol% S-B or 1 mol% S-Sb, respectively, were applied.

2.11.2.4   Photo-DSC of S-Sb in BisOx for application in Hot Lithography

The analysis was conducted according to 1.4 using 320-500 nm irradiation with 130 mW/cm^2 intensity.

Irradiation periods of 900 s were applied at temperatures of 100, 120 and 140 °C.

Formulations of BisOx containing 1 mol% S-B or 1 mol% S-Sb, respectively, were applied.

2.11.3 3D printing of a 2-oxazoline-based formulation

In analogy to foregoing laser exposure tests, the 3D printing was conducted on a Caligma 200 UV developed by the company Cubicure GmbH. All parts in contact with the formulation, including the vat, the building platform and the coating unit were heated to 120 °C. For printing, a formulation consisting of the monomer BisOx, 12 wt% of a mixture of triarylsulfonium hexafluoroantimonate salts (S-Sb) in propylene carbonate (50 wt%) was used and 0.05 wt% of the photosensitizer 9,10-dibutoxyanthracene were added to improve the spectral compliance with the 375 nm laser. The specimens were printed with a laser power of 100 %, a scan speed of 50 mm s^{-1} and a layer thickness of 100 µm, while the contours of each layer were scanned first, followed by scanning of the area within the contours with a hatching distance of 15 µm in x- and y-direction.

SUMMARY

Lithography-based additive manufacturing technologies (L-AMTs) have marked great developments in the 3D printing of polymer materials with outstanding precision and surface qualities. Especially the application of laser-based stereolithography (SLA) has established a benchmark for accuracy in 3D printing, however, it demands for fastest solidification of the liquid photopolymerizable formulation upon the swift passing of the laser beam. Therefore, the progress over the last decades relied on rapid free-radical photopolymerization of acrylate and methacrylate monomers for efficient layer-by-layer structuring. With the evolution of 3D printing from a rapid prototyping tool to a product manufacturing method, the poor mechanical properties of photopolymer products and the cytotoxicity of (meth)acrylate monomers became increasingly detrimental factors. Moreover, the oxygen sensitivity and polymerization shrinkage in free radical photopolymerization sets the limits for further improvements of additive manufacturing processes.

Hence, it has been the aim of ongoing research to enable SLA of a greater variety of monomer classes with advantageous polymerization chemistry, which is offered by cationic photopolymerization. Besides the oxygen insensitive cationic polymerization reaction and highest conversions, the benefits arise most dominantly from the great number of applicable monomer classes. Especially ring-opening monomers, such as epoxides, exhibit outstanding mechanical, chemical and electrical properties and are therefore abundantly applied in the coatings industries. Still the direct application of UV-induced cationic ring-opening polymerization (CROP) in L-AMTs was obstructed by the limited reactivity at room temperature. Over the last decades, the poor reactivity of ring-opening monomers was circumvented by the addition of vinyl ether or (meth)acrylate monomers to give dual cure or hybrid systems as a compromise. The factual direct 3D printing of e.g. epoxides thus remained an unachieved goal.

Just recently, innovative Hot Lithography enabled the 3D printing via SLA at temperatures up to 140 °C. Besides the reduction of the inherently high viscosity in methacrylate formulations for "thermoplast-like" photopolymers, the possibility to operate at elevated temperatures was expected to strongly reduce of activation energies of UV-induced CROP. Once initiated by a photoacid generator (PAG), the

ring-opening propagation is thermally driven to reach highest conversions in sufficient polymerization rates. In this context, innovative Hot Lithography sparked the here presented studies on thermally promoted cationic photopolymerization for direct 3D printing of epoxy monomers, but also the broadening to other heterocyclic monomers, which have not been considered for cationic UV-curing applications due to insufficient reactivity at room temperature.

In the first part of this thesis a suitable cationic photoinitiation system was determined to meet the requirements of highest reactivity and thermal stability, and to ensure the selectivity of the light-induced curing reaction at elevated temperatures. The investigations were conducted in photoreactive formulations of the most important epoxy monomer bisphenol-A diglycidyl ether (BADGE), which makes up for 75 % of epoxy monomer sales volume. For the evaluation of cationic photoinitiation systems in BADGE at elevated temperatures, recently developed state-of-the-art onium salt photoacid generators (PAGs) of Weakly Coordinating Anions (WCAs) were applied. Generally, the photoinitiation system is characterized by its absorption range, thermal stability and reactivity, which are determined by the cation and anion of the PAG salts Therefore, a novel, highly reactive diaryliodonium alkoxyaluminate PAG (I-Al) was prepared and used in direct comparison to the state-of-the-art triarylsulfonium tetraarylborate benchmark (S-B) with strongly extended absorption.

The spectral compatibility with the 375 nm laser is decisive for successful application in Hot Lithography but exceeds the absorption ranges of common diaryliodonium and triarylsulfonium PAGs. Therefore, the photosensitization of I-Al to wavelengths above 350 nm was facilitated by efficient Free Radical Promoted Cationic Polymerization (FRPCP). The outstanding ability of the free radical photoinitiator bis(4-methoxybenzoyl)diethylgermanium (BMDG) to serve as a redox sensitizer in the FRPCP reaction up to 420 nm has been reported earlier, yet never investigated for thermal stability and reactivity in consideration of a stereolithographic process.

I-Al

BMDG

S-B
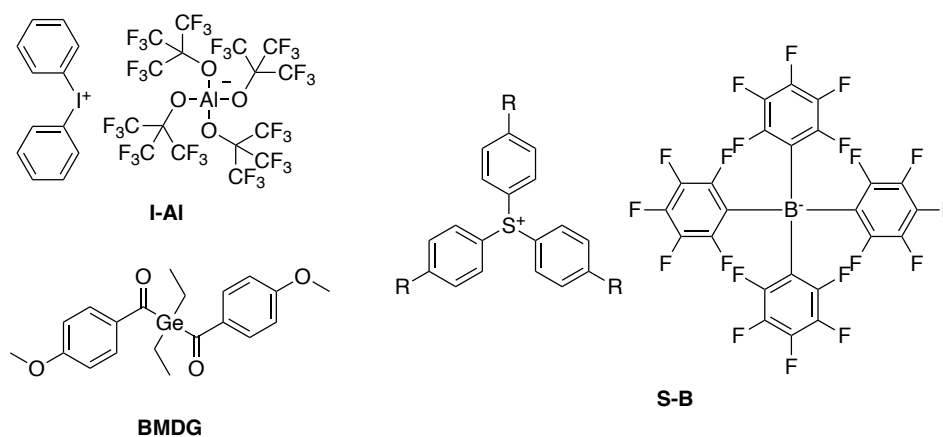
In comparative studies by simultaneous thermal analysis (STA) and photo-DSC, the thermal stability and photoreactivity of a diaryliodonium PAG, a triarylsulfonium PAG and a diaryliodonium salt FRPCP system containing BMDG was investigated. It was found that the thermal stability of the FRPCP system in BADGE was limited to 120 °C, whereas the formulations of diaryliodonium PAGs showed stability below 140 °C. Only the triarylsulfonium PAG gave extended thermal stability beyond 200 °C arising from the nature of the sulfonium cation. In consideration of this precondition, the photo-DSC analyses significantly confirmed the generally high versatility of the WCA-based triarylsulfonium PAG S-B under 320-500 nm broadband irradiation, as well as 385 and 400 nm LED irradiation. Although the FRPCP system showed beneficial photopolymerization behavior at low temperatures and broadband irradiation, a thermally stable triarylsulfonium PAGs, such as S-B, was found as the generally most suitable photoinitiator for efficient cationic photopolymerization at elevated temperatures and narrow wavelength distributions, such as in Hot Lithography.

Subsequently, the thermal promotion of UV-induced CROP of BADGE and the determination of an efficient and stable cationic photoinitiator led to the consideration of further heterocyclic monomers for cationic photopolymerization at elevated temperatures.

The second part of this thesis describes the studies of a cationically polymerizable ring-opening monomer class with outstanding structural versatility and promising applicability, namely 2-oxazolines. The particularities of poly(2-alkyl/aryl-2-oxazoline)s (PAOx) raised tremendous interest in surface modification, copolymer architecture, drug delivery, protein conjugation and various fields of biomedical research. Still PAOx were only accessible by inefficient thermal CROP of 2-oxazolines in classical thermal preparations or small batch microwave-assisted methods. This reasons the dominating

studies on the protein-related characteristics of PAOx in living systems, whereas hardly any research focused on the polyamide backbone structure for application in materials with promising thermomechanical properties. Therefore, by using WCA-based onium salt PAGs as initiators with lowest nucleophilicity, not only an increase in polymerization efficiency was expected, but also the yet unreported UV-induced CROP of 2-oxazolines.

Within the here presented studies, successful experiments firstly confirmed the hypothesis of efficient and selective UV-induced CROP of 2-oxazoline monomers by onium salt PAGs at elevated temperatures. After the synthesis of monofunctional and difunctional 2-oxazoline model compounds and the determination of thermal stability of photoreactive formulations below 140 °C, the complex influence of the substituents in 2-position on the polymerization rates were evaluated in photo-DSC measurements between 100 and 140 °C.
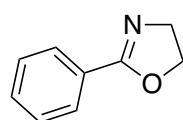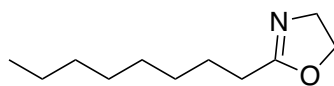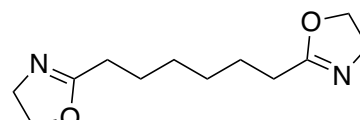
PhOx **OctOx** **BisOx**

It is concluded that the photoacid-initiated polymerization by direct protonation of the imine moiety follows the same kinetic trends as reported for thermal CROP of 2-oxazolines by initial alkylation from e.g. methyl tosylate. The significantly higher reactivity of aliphatic (OctOx) compared to aromatic 2-oxazolines (PhOx) was evident from more than two-fold polymerization rates at 140 °C. The living character of the UV-induced CROP was confirmed by GPC, showing the correlation of molecular weights with variation of PAG concentration and temperatures of photopolymerization.

With the aim being the generation of crosslinked 2-oxazoline-based photopolymer materials for Hot Lithography, the difunctional aliphatic 2-oxazoline model compound (BisOx) showed high reactivity in photo-DSC and the generation of a glassy thermoset. The promising behavior of the crosslinker BisOx was further investigated by RT-NIR/MIR-photorheology in comparison to a corresponding epoxy monomer as cationically polymerizable reference and a comparable methacrylate monomer as radically polymerizable benchmark for Hot Lithography. The comparative studies showed the reactivity limitations of the photopolymerizable 2-oxazoline system on the one hand and confirmed the superior polymer characteristics of UV-cured poly(2-

oxazoline) materials on the other hand. The investigations of tertiary mixtures of PhOx, OctOx and BisOx expressed the structure-property relationship of 2-oxazoline photopolymers in DMTA, tensile testing, impact resistance and thermal stability analysis of the novel photopolymers. In comparison to a corresponding tertiary methacrylate reference system, the poly(2-oxazoline) material withstands 40 % higher stress and 53 % higher strain at break in tensile testing, 38 % higher impact resistance and significantly higher thermal resistance up to 320 °C.

As the difunctional model compound not only showed highest reactivity, but also no volatility in photopolymerizations at high temperatures, the experimental 3D printing by Hot Lithography was successfully conducted following the elaborate pretesting of printing conditions. The applied photopolymerizable system of the 2-oxazoline monomer BisOx was selectively cured by a 375 nm laser, which enabled the 3D structuring of objects with highest precision and resolution of details in the micrometer scale.

In conclusion, this project enlightened the innovative approach of thermally promoted cationic photopolymerization and established a novel class of photopolymers with unique characteristics and superior material properties. The Hot Lithography of low reactive 2-oxazolines demonstrated the direct stereolithography of cationically ring-opening monomers, which may promote the development of lithography-based additive manufacturing technologies.

MATERIALS AND METHODS

Chemicals	Distributor
Bisphenol-A-diglycidyl ether (BADGE)	Huntsman
(Bis(4-methoxybenzoyl)diethylgermanium (BMDG, Ivocerin)	Ivoclar
Chloroform-d	Eurisotop
Dichloromethane	Donau Chemie
Dichloromethane-d_2	Eurisotop
Diethyl ether	Donau Chemie
Diphenyliodonium chloride	Sigma-Aldrich
Dodecylvinylether (DVE)	Sigma-Aldrich
DMSO-d_6	Eurisotop
ε-Caprolacton	Aldrich
3,4-Epoxycyclohexylmethyl 3,4-epoxycyclohexanecarboxylate (CE)	Sigma-Aldrich
Ethanol amine	Aldrich
Lithium aluminum hydride	Fluka
Methanol	Donau Chemie
n-Hexane (abs)	Merck
Nonafluoro-t-butanol	Apollo Scientific
Nonane nitrile	Fluka
Phenyl glycidyl ether	Fluka
2-Phenyl-2-oxazoline (PhOx)	Aldrich
p-(Octyloxyphenyl)phenyliodonium hexafluoroantimonate (I-Sb)	ABCR
Perylene	Fluka
Propylene carbonate	Acros
Pyridine	ABCR
Tris(4-((4-acetylphenyl)thio)phenyl)sulfonium chloride	BASF
Tris(4-((4-acetylphenyl)thio)phenyl)sulfonium tetrakis(pentafluorophenyl)borate (S-B)	BASF
Tris(4-((4-acetylphenyl)thio)phenyl)sulfonium tris((trifluoromethyl)sulfonyl)methanide (S-C)	BASF
Zinc acetate dihydrate	Fluka

Thin-layer-chromatography was done on aluminum TLC-plates from Merck (Silicagel 60, F254).

Column-Chromatography was carried out on a Buechi Sepacore Flash System (Buechi pump module C-605, Buechi control unit C-620, Buechi UV-Photometer C-635, Buechi fraction collector C-660). Glass and polyethylene columns were used, packed with Silicagel 60 (Merck, 40-64-μm). The used eluents are mentioned at the purification section of the preparation procedures.

NMR spectra were recorded on a Bruker DPX-200 Fourier transform spectrometer at 200 MHz for ^{1}H and 50 MHz for ^{13}C. Furthermore some measurements have been recorded on a Bruker Avance at 400 MHz for ^{1}H and 100 MHz for ^{13}C and 104 MHz for ^{27}Al. The signals are noted according to their shifts in comparison to tetramethylsilane (d = 0 ppm) and were always referenced on the used NMR-solvent:

^{1}H: CDCl$_3$: 7.26 ppm, D$_2$O: 4.79 ppm, DMSO-d$_6$: 2.50 ppm, CD$_2$Cl$_2$: 5.32 ppm, d$_6$-Acetone: 2.05 ppm

^{13}C: CDCl$_3$: 77.16 ppm, DMSO-d$_6$: 39.52 ppm, CD$_2$Cl$_2$: 53.84 ppm, d$_6$-Acetone: 29.84 ppm

In case of ^{27}Al-NMR 1 drop of a saturated solution of Al(acac)$_3$ in deuterated benzene (C$_6$D$_6$) was added. The signal of Al(acac)$_3$ was set to 0 ppm.

The chemical shifts were reported in ppm (s = singlet, d = doublet, t = triplet, q = quartet, qn = quintet, sep = septet, m = multiplet, bs = broad singlet).

Analysis of the spectra was carried out with the program TopSpin (Version 2.1) by Bruker.

ATR-FTIR was measured on a Spectrum 65 spectroscope from Perkin-Ellmer. For the analysis of the results the software Spectrum from Perkin-Ellmer in version 10.03.07.0112 was used.

Simultaneous thermal analysis was performed using a STA 449 F1 Jupiter from Netzsch. Nitrogen was used as protection and purge gas. Calibration was done in Nitrogen with the elements bismuth, indium, tin and zinc. Proteus - Thermal Analysis in version 5.2.1 from Netzsch Geraetebau was used for the data analysis.

For the determination of **melting points** an OptiMelt automated melting point system from SRS Stanford Research Systems was used. A typical measurement was conducted with a heating rate of 5 °C/min. All melting points have not been corrected and reported usually as melting interval.

For all **photo-DSC and STA** measurements 25 µ aluminium pans (DSC-crucible Order-No: 6.239.2-64.5.01) were used.

The preparation of photoreactive formulations and substances was carried out in a **yellow light laboratory**. The laboratory had adhesive foils of the company IFOHA attached to all windows and the fluorescent lamps were type Osram lumilux with chip control light colour 62 (wavelengths below 480 nm are filtered).

Photo-DSC measurements were performed using Omnicure 2000 from Lumen Dynamics with glass fibre light wave guides. The UV source was calibrated at least once a day with an Omnicure R2000 radiometer.

Photo-DSC studies were conducted on a Photo-DSC 204 F1 from Netzsch. As light source an Omnicure 2000 was used in combination with a glassfiber filled double-core lightguide (3 mm fiber diameter). All measurements were conducted under inert atmosphere (N_2 flow of 20 mL/min). The heat flow of the reaction was recorded as a function of time. Proteus - Thermal Analysis in version 5.2.1 from Netzsch Geraetebau was used for the data analysis.

For photo-DSC experiments with LED irradiation an Omnicure LX400 LED UV Spot Curing System was used to control LED heads. To connect the photo-DSC to the LED-source an Arduino board was used as CPU to perform the translation of commands between the two devices.

GPC measurements were performed with a Waters GPC using three columns connected in series (Styragel HR 0.5, Styragel HR 3 and a Styragel HR 4) and a Waters 2410 RI detector.

For **RT-NIR/MIR-photorheology** analyses an Anton Paar MCR 302 WESP rheometer with a P-PTD 200/GL Peltier plate, an H-PTD 200 heating hood, and a disposable PP25 measuring system was used. The rheometer was coupled with a Bruker Vertex 80 FTIR spectrometer. The irradiation intensity was calibrated using an Ocean Optics USB 2000+ spectrometer.

DSC of polymers was conducted using a DSC TA Q2000 system in a temperature range from -50 to 250 °C.

Polymer specimen were cured using a Uvitron UV 1080 Flood Curing System with Uvitron Intelliray 600 halide lamps (600 W, 120 mW cm^{-2}, 320-580 nm) or a Lumamat 100 light chamber (Ivoclar Vivadent, 400–580 nm, 20 mW cm^{-2}).

Thin layer DMTA was performed in tension mode using a Dynamic Mechanical Analyzer (TA Instruments 2980).

DMTA measurements of molded photopolymers were performed with an Anton Paar MCR 301 with a CTD 450 oven.

Tensile tests were performed by means of a Zwick Z050 with Zwick Z050 with a maximum test force of 50 kN. TestXpert II software was used to process and evaluate the recorded

Dynstat impact tests were performed on a Karl Frank GmbH Dynstat device, Type 573 using a 1 J hammer.

Hot Lithography 3D printing was conducted on a heated SLA prototype by TU Wien and a Caligma 200 UV developed by the company Cubicure GmbH.

ABBREVIATIONS

A	Absorption
abs.	absolute
AM	Additive manufacturing
AMT	Additive manufacturing technology
ATR-IR	Attenuated total reflection infrared spectroscopy
BADGE	Bisphenol-A-diglycidyl ether
BAPO	Bisacylphosphineoxide
BDDGE	Butanediol diglycidyl ether
BDDMA	Butanediol dimethacrylate
BisOx	1,6-bis(4,5-dihydrooxazol-2-yl)hexane
BMA	Benzyl methacrylate
BMDG	(Bis(4-methoxybenzoyl)diethylgermanium (Ivocerin)
b.p.	boiling point
CAD	Computer-aided design
C_g	Conversion at gel point
C_{final}	Final conversion
C_{NMR}	Conversion determined by NMR
conc.	concentration
$C_{photo-DSC}$	Conversion determined by photo-DSC
CROP	Cationic ring-opening polymerization
Đ	Polydispersity index
DBC	Double bond conversion
DLP	Digital light processing
DMD	Digital micromirror device
DMTA	Dynamic-mechanical thermal analysis
DSC	Differential scanning calorimetry
EA	ethyl acetate
EC	Epoxy group conversion
ECC	3,4-epoxycyclohexylmethyl 3,4-epoxycyclohexanecarboxylate
EtOx	2-Ethyl-2-oxazoline

eq	equivalents
FDM	Fused deposition modeling
FRPCP	Free radical promoted cationic polymerization
G'	Storage modulus
G''	Loss modulus
GC-MS	Gas chromatography – mass spectroscopy
GPC	Gel permeation chromatography
G'_r	Storage modulus in rubbery state
G'_{20}	Storage modulus at 20 °C
HexMA	Hexyl methacrylate
HexOx	2-Hexyl-2-oxazoline
HO-PentOx	ε-Hydroxypentyl-2-oxazoline
HO-EtOx	β-Hydroxyethyl-2-oxazoline
I-Al	Diphenyliodonium tetrakis(perfluoro-t-butyloxy)aluminate
iPrOx	2-Isopropyl-2-oxazoline
I-Sb	p-(Octyloxyphenyl)phenyliodonium hexafluoroantimonate
IR	Infrared
I-Sb	p-(Octyloxyphenyl)phenyliodonium hexafluoroantimonate
L-AMT	Lithography-based additive manufacturing technology
λ_{max}	Absorption maximum
LED	Light emitting diode
M	molecular weight
MeOx	2-Methyl-2-oxazoline
M_n	Number average molecular weight
M_w	Weight average molecular weight
mol%	Molar percent
m.p.	Melting point
MW	Microwave
NMR	Nuclear magnetic resonance
OctOx	2-Octyl-2-oxazoline
PAG	Photoacid generator
PAOx	Poly(2-alkyl/aryl-2-oxazoline)
PE	petrol ether
pH	Potentia hydrogenii

photo-DSC	photo differential scanning calorimetry
PhOx	2-Phenyl-2-oxazoline
PGE	Phenyl glycidyl ether
pKa	Logarithmic acid dissociation constant
PI	Photoinitiator
PS	Photosensitizer
R_P	Rate of polymerization
RT-FTIR	Real-time Fourier-transform infrared spectroscopy
SLA	Stereolithography (apparatus)
SLS	Selective laser sintering
STA	Simultaneous thermal analysis
T_g	Glass transition temperature
t_g	gel point
t_{95}	Time of 95 % conversion
S-Al	Tris(4-((4-acetylphenyl)thio)phenyl)sulfonium tetrakis(perfluoro-t-butyloxy)aluminate
S-B	Tris(4-((4-acetylphenyl)thio)phenyl)sulfonium Tetrakis(pentafluorophenyl)borate
S-C	Tris(4-((4-acetylphenyl)thio)phenyl)sulfonium Tris((trifluoromethyl)sulfonyl)methanide
S-Sb	Triarylsulfonium hexafluoroantimonate
tButOx	2-Tert-butyl-2-oxazoline
techn.	technical grade
T_g	Glass transition temperature
TGA	Thermogravimetric analysis
TLC	Thinlayer chromatography
t_{max}	Time of polymerization maximum
UV	Ultraviolet
WCA	Weakly coordinating anion
wt%	Weight percent
3D	3-dimensional

BIBLIOGRAPHY

1.   Srivatsan, T. S.; Sudarshan, T. S., *Additive Manufacturing: Innovations, Advances, and Applications*. Taylor & Francis: 2015.
2.   Gebhardt, A.; Hötter, J.-S., Characteristics of the Additive Manufacturing Process. In *Additive Manufacturing*, Carl Hanser Verlag GmbH & Co. KG: 2016; pp 21-91.
3.   Ligon, S. C.; Liska, R.; Stampfl, J.; Gurr, M.; Mülhaupt, R., Polymers for 3D Printing and Customized Additive Manufacturing. *Chem. Rev.* **2017,** *117* (15), 10212-10290.
4.   Associates, W., *Wohlers Report 2018, 3D Printing and Additive Manufacturing State of the Industry, Annual Worldwide Progress Report*. USA, 2018.
5.   Wohlers, T.; Caffrey, T., Wohlers Report: Additive manufacturing and 3D printing state of the industry. *Fort Collins. Wohlers Associates Inc.. ICED15* **2013,** *12*.
6.   https://www.sonova.com/en/story/innovation/3d-printing-technology-improved-hearing. (accessed 03/29/2020).
7.   Bullis, K. A More Efficient Jet Engine Is Made from Lighter Parts, Some 3-D Printed. https://www.technologyreview.com/s/514656/a-more-efficient-jet-engine-is-made-from-lighter-parts-some-3-d-printed/ (accessed 03/29/2020).
8.   Fox, S., Third Wave Do-It-Yourself (DIY): Potential for prosumption, innovation, and entrepreneurship by local populations in regions without industrial manufacturing infrastructure. *Technology in Society* **2014,** *39*, 18-30.
9.   Swetly, T.; Stampfl, J.; Kempf, G.; Hucke, R.-M., Capabilities of additive manufacturing technologies (AMT) in the validation of the automotive cockpit. *RTejournal - Forum für Rapid Technologie* **2014,** *2014* (1).
10.   Ligon-Auer, S. C.; Schwentenwein, M.; Gorsche, C.; Stampfl, J.; Liska, R., Toughening of photo-curable polymer networks: a review. *Polym. Chem.* **2016,** *7* (2), 257-286.
11.   Hull Charles, W. Apparatus For Production Of Three-dimensional Objects By Stereolithography. US 4575330 A, 1984/08/08, 1986.
12.   Bártolo, P. J., *Stereolithography: materials, processes and applications*. Springer Science & Business Media: 2011.
13.   https://www.zare.it/de/stereolithographie. (accessed 03/30/2020).
14.   Bayer, H. Photo-curable resin with low shrinkage and its use in a stereolithography process. DE19541075C1, 1995.
15.   Stampfl, J.; Baudis, S.; Heller, C.; Liska, R.; Neumeister, A.; Kling, R.; Ostendorf, A.; Spitzbart, M., Photopolymers with tunable mechanical properties processed by laser-based high-resolution stereolithography. *Journal of Micromechanics and Microengineering* **2008,** *18* (12), 125014.
16.   Gmeiner, R.; Mitteramskogler, G.; Stampfl, J.; Boccaccini, A. R., Stereolithographic Ceramic Manufacturing of High Strength Bioactive Glass. *International Journal of Applied Ceramic Technology* **2015,** *12* (1), 38-45.
17.   Homa, J.; Schwentenwein, M., A Novel Additive Manufacturing Technology for High-Performance Ceramics. In *Advanced Processing and Manufacturing Technologies for Nanostructured and Multifunctional Materials*, 2015; pp 33-40.
18.   Zanchetta, E.; Cattaldo, M.; Franchin, G.; Schwentenwein, M.; Homa, J.; Brusatin, G.; Colombo, P., Stereolithography of SiOC Ceramic Microcomponents. *Adv. Mater.* **2016,** *28* (2), 370-376.
19.   Fouassier, J.-P., *Photoinitiation, Photopolymerization, and Photocuring: Fundamentals and Applications*. Hanser: 1995.
20.   Fouassier, J. P.; Allonas, X.; Burget, D., Photopolymerization reactions under visible lights: principle, mechanisms and examples of applications. *Prog. Org. Coat.* **2003,** *47* (1), 16-36.
21.   Peiffer, R. W., Applications of Photopolymer Technology. In *Photopolymerization*, American Chemical Society: 1997; Vol. 673, pp 1-14.
22.   Green, W. A., *Industrial Photoinitiators: A Technical Guide*. Taylor & Francis: 2010.
23.   Ganster, B.; Fischer, U. K.; Moszner, N.; Liska, R., New Photocleavable Structures. Diacylgermane-Based Photoinitiators for Visible Light Curing. *Macromolecules* **2008,** *41* (7), 2394-2400.
24.   Kim, L. U.; Kim, J. W.; Kim, C. K., Effects of Molecular Structure of the Resins on the Volumetric Shrinkage and the Mechanical Strength of Dental Restorative Composites. *Biomacromolecules* **2006,** *7* (9), 2680-2687.

25.   Gorsche, C.; Seidler, K.; Knaack, P.; Dorfinger, P.; Koch, T.; Stampfl, J.; Moszner, N.; Liska, R., Rapid formation of regulated methacrylate networks yielding tough materials for lithography-based 3D printing. *Polym. Chem.* **2016,** *7* (11), 2009-2014.

26.   Crivello, J. V.; Dietliker, K.; Bradley, G., *Photoinitiators for Free Radical Cationic & Anionic Photopolymerisation*. Wiley: 1999.

27.   Bulut, U.; Crivello, J. V., Investigation of the Reactivity of Epoxide Monomers in Photoinitiated Cationic Polymerization. *Macromolecules* **2005,** *38* (9), 3584-3595.

28.   Sipani, V.; Scranton, A. B., Dark-cure studies of cationic photopolymerizations of epoxides: Characterization of the active center lifetime and kinetic rate constants. *J. Polym. Sci., Part A: Polym. Chem.* **2003,** *41* (13), 2064-2072.

29.   Decker, C.; Moussa, K., Kinetic study of the cationic photopolymerization of epoxy monomers. *J. Polym. Sci., Part A: Polym. Chem.* **1990,** *28* (12), 3429-3443.

30.   Ito, H.; Kidokoro, N.; Ishikawa, H., DIFFERENTIAL PHOTOCALORIMETRIC STUDY OF CATIONIC PHOTOPOLYMERIZATION. *J. Photopolym. Sci. Technol.* **1992,** *5* (2), 235-246.

31.   Sangermano, M., Advances in cationic photopolymerization. *Pure and Applied Chemistry* **2012,** *84* (10), 2089.

32.   Crivello, J. V.; Falk, B.; Zonca, M. R., Photoinduced cationic ring-opening frontal polymerizations of oxetanes and oxiranes. *J. Polym. Sci., Part A: Polym. Chem.* **2004,** *42* (7), 1630-1646.

33.   Pham, H. Q.; Marks, M. J., Epoxy Resins. In *Ullmann's Encyclopedia of Industrial Chemistry*, Wiley-VCH Verlag GmbH & Co. KGaA: 2000.

34.   Lapin, S. C. Stereolithography using vinyl ether-epoxide polymers. US5437964A, 1995.

35.   O'Connor, J. C.; Chapin, R. E., Critical evaluation of observed adverse effects of endocrine active substances on reproduction and development, the immune system, and the nervous system. In *Pure and Applied Chemistry*, 2003; Vol. 75, p 2099.

36.   Lawrence, W. H.; Malik, M.; Turner, J. E.; Autian, J., Toxicity profile of epichlorohydrin. *J. Pharm. Sci.* **1972,** *61* (11), 1712-1717.

37.   Crivello, J. V., Advances in the design of photoinitiators, photosensitizers and monomers for photoinitiated cationic polymerization. *Des. Monomers Polym.* **2002,** *5* (2-3), 141-154.

38.   Searles, S.; Tamres, M.; Lippincott, E. R., Hydrogen Bonding Ability and Structure of Ethylene Oxides. *Journal of the American Chemical Society* **1953,** *75* (11), 2775-2777.

39.   Pell, A. S.; Pilcher, G., Measurements of heats of combustion by flame calorimetry. Part 3.-Ethylene oxide, trimethylene oxide, tetrahydrofuran and tetrahydropy. *Transactions of the Faraday Society* **1965,** *61* (0), 71-77.

40.   Yamashita, Y.; Tsuda, T.; Okada, M.; Iwatsuki, S., Correlation of cationic copolymerization parameters of cyclic ethers, formals, and esters. *Journal of Polymer Science Part A-1: Polymer Chemistry* **1966,** *4* (9), 2121-2135.

41.   Crivello, J. V., Effect of Temperature on the Cationic Photopolymerization of Epoxides. *Journal of Macromolecular Science, Part A* **2008,** *45* (8), 591-598.

42.   Crivello, J. V., "Kick-Starting" oxetane photopolymerizations. *J. Polym. Sci., Part A: Polym. Chem.* **2014,** *52* (20), 2934-2946.

43.   Sangermano, M.; Malucelli, G.; Bongiovanni, R.; Priola, A., Photopolymerization of oxetane based systems. *European Polymer Journal* **2004,** *40* (2), 353-358.

44.   Sasaki, H.; Rudzinński, J. M.; Kakuchi, T., Photoinitiated cationic polymerization of oxetane formulated with oxirane. *J. Polym. Sci., Part A: Polym. Chem.* **1995,** *33* (11), 1807-1816.

45.   Crivello, J. V.; Sasaki, H., Structure and Reactivity Relationships in the Photoinitiated Cationic Polymerization of Oxetane Monomers. *J. Macromol. Sci., Part A: Pure Appl.Chem.* **1993,** *30* (2-3), 189-206.

46.   Bulut, U.; Crivello, J. V., Reactivity of oxetane monomers in photoinitiated cationic polymerization. *J. Polym. Sci., Part A: Polym. Chem.* **2005,** *43* (15), 3205-3220.

47.   Sangermano, M.; Malucelli, G.; Morel, F.; Decker, C.; Priola, A., Cationic photopolymerization of vinyl ether systems: influence of the presence of hydrogen donor additives. *Eur. Polym. J.* **1999,** *35* (4), 639-645.

48.   Hoyle, C. E.; Kinstle, J. F., *Radiation curing of polymeric materials*. ACS Publications: 1990.

49.   Crivello, J. V.; Lam, J. H. W., Diaryliodonium Salts. A New Class of Photoinitiators for Cationic Polymerization. *Macromolecules* **1977,** *10* (6), 1307-1315.

50.   Pappas, S. P., *Radiation Curing: Science and Technology*. Springer US: 2013.

51.   Decker, C., Photoinitiated crosslinking polymerisation. *Progress in Polymer Science* **1996,** *21* (4), 593-650.

52.   Crivello, J. V., The discovery and development of onium salt cationic photoinitiators. *J. Polym. Sci., Part A: Polym. Chem.* **1999,** *37* (23), 4241-4254.

53.   Schlesinger, S. I., Epoxy photopolymers in photoimaging and photofabrication. *Polym. Eng. Sci.* **1974,** *14* (7), 513-515.

54.   Bachofner, H. E.; Beringer, F. M.; Meites, L., Diaryliodonium Salts. V. The Electroreduction of Diphenyliodonium Salts1,2. *Journal of the American Chemical Society* **1958,** *80* (16), 4269-4274.

55.   McKinney, P. S.; Rosenthal, S., The electrochemical reduction of the triphenylsulfonium ion. *Journal of Electroanalytical Chemistry and Interfacial Electrochemistry* **1968,** *16* (2), 261-270.

56.   Klikovits, N.; Knaack, P.; Bomze, D.; Krossing, I.; Liska, R., Novel photoacid generators for cationic photopolymerization. *Polym. Chem.* **2017,** *8* (30), 4414-4421.

57.   Gillespie, R. J.; Peel, T. E., Superacid Systems. In *Adv. Phys. Org. Chem.*, Gold, V., Ed. Academic Press: 1971; Vol. Volume 9, pp 1-24.

58.   Dickert, F., G. A. Olah, G. K. S. Prakash, J. Sommer: Superacids, John Wiley & Sons, New York, Chichester, Brisbane, Toronto, Singapore 1985. 371 Seiten, Preis: £ 67. *Ber. Bunsenges. Phys. Chem.* **1987,** *91* (10), 1073-1074.

59.   Castellanos, F.; Fouassier, J. P.; Priou, C.; Cavezzan, J., Synthesis, reactivity, and properties of new diaryliodonium salts as photoinitiators for the cationic polymerization of epoxy silicones. *J. Appl. Polym. Sci.* **1996,** *60* (5), 705-713.

60.   Castellanos, F.; Cavezzan, J.; Fouassier, J. P.; Priou, C., Onium borates/borates of organometallic complexes and cationic initiation of polymerization therewith. Google Patents: 1997.

61.   Massey, A. G.; Park, A. J., Perfluorophenyl derivatives of the elements : I. Tris(pentafluorophenyl)boron. *J. Organomet. Chem.* **1964,** *2* (3), 245-250.

62.   Ikeda, Y.; Yamane, T.; Kaji, E.; Ishimaru, K. Method of producing tetrakis (pentafluorophenyl) borate derivatives using pentafluorophenyl alkali metal salt prepared from pentafluorobenzene. US5493056 (A), 1996.

63.   Krossing, I., 1.23 - Weakly Coordinating Anions: Fluorinated Alkoxyaluminates A2 - Reedijk, Jan. In *Comprehensive Inorganic Chemistry II (Second Edition)*, Poeppelmeier, K., Ed. Elsevier: Amsterdam, 2013; pp 681-705.

64.   Krossing, I.; Raabe, I., Noncoordinating Anions—Fact or Fiction? A Survey of Likely Candidates. *Angew. Chem. Int. Ed.* **2004,** *43* (16), 2066-2090.

65.   Strauss, S. H.; Nolan, B. G.; Barbarich, T. J.; Rockwell, J. J., Weakly coordinating anions containing polyfluoroalkoxide ligands. Google Patents: 1999.

66.   Strauss, S. H., The search for larger and more weakly coordinating anions. *Chem. Rev.* **1993,** *93* (3), 927-942.

67.   Ivanova, S. M.; Nolan, B. G.; Kobayashi, Y.; Miller, S. M.; Anderson, O. P.; Strauss, S. H., Relative Lewis basicities of six Al(ORF)4- superweak anions and the structures of LiA. *Chem. - Eur. J.* **2001,** *7* (2), 503-10.

68.   Krossing, I., The Facile Preparation of Weakly Coordinating Anions: Structure and Characterisation of Silverpolyfluoroalkoxyaluminates AgAl(ORF)4, Calculation of the Alkoxide Ion Affinity. *Chem. - Eur. J.* **2001,** *7* (2), 490-502.

69.   Kocaarslan, A.; Kütahya, C.; Keil, D.; Yagci, Y.; Strehmel, B., Near-IR and UV-LED Sensitized Photopolymerization with Onium Salts Comprising Anions of Different Nucleophilicities. *ChemPhotoChem* **2019,** *3* (11), 1127-1132.

70.   Kütahya, C.; Wang, P.; Li, S.; Liu, S.; Li, J.; Chen, Z.; Strehmel, B., Carbon Dots as a Promising Green Photocatalyst for Free Radical and ATRP-Based Radical Photopolymerization with Blue LEDs. *Angew. Chem. Int. Ed.* **2020,** *59* (8), 3166-3171.

71.   Knaack, P.; Klikovits, N.; Tran, A. D.; Bomze, D.; Liska, R., Radical induced cationic frontal polymerization in thin layers. *J. Polym. Sci., Part A: Polym. Chem.* **2019,** *57* (11), 1155-1159.

72.   Tran, A. D.; Koch, T.; Knaack, P.; Liska, R., Radical induced cationic frontal polymerization for preparation of epoxy composites. *Composites Part A: Applied Science and Manufacturing* **2020,** *132*, 105855.

73.   Moraes, R. R.; Garcia, J. W.; Barros, M. D.; Lewis, S. H.; Pfeifer, C. S.; Liu, J.; Stansbury, J. W., Control of polymerization shrinkage and stress in nanogel-modified monomer and composite materials. *Dent. Mater.* **2011,** *27* (6), 509-519.

74.   Fouassier, J.-P., Photochemistry and UV curing : a brief survey of the latest trends. In *Photochemistry & UV Curing: New Trends*, J.P, F., Ed. Research Signpost Trivandrum: 2006; p 1.

75.   Gmeiner, R. Method and device for lithography-based additive production of three-dimensional shaped bodies. WO2018032022A1, 2018.

76.   Steyrer, B.; Busetti, B.; Harakály, G.; Liska, R.; Stampfl, J., Hot Lithography vs. room temperature DLP 3D-printing of a dimethacrylate. *Additive Manufacturing* **2018,** *21*, 209-214.

77.   Peer, G.; Dorfinger, P.; Koch, T.; Stampfl, J.; Gorsche, C.; Liska, R., Photopolymerization of Cyclopolymerizable Monomers and Their Application in Hot Lithography. *Macromolecules* **2018,** *51* (22), 9344-9353.

78.   Steyrer, B.; Liska, R.; Stampfl, J., *Thermoplasts as Toughening Agent for 3D-Printable Photopolymers*. 2017.

79.   Noren, G. K.; Krajewski, J. J.; Murphy, E. J. Cationically curable polyurethane compositions having vinyl ether functionality. US4996282A, 1991.

80.   Steinmann, B.; Wolf, J.-P.; Schulthess, A.; Hunziker, M. Photosensitive compositions. US Patent 5,476,748, 1995.

81.   Steinmann, B. Liquid, radiation-curable composition, especially for stereolithography. US5972563A, 1999.

82.   Yamamura, T. Photo-curable resin composition used for photo fabication of three-dimensional objects. US5981616A, 1999.

83.   Xu, J. PHOTO-CURABLE RESIN COMPOSITION. US9090020, 2014.

84.   Cai, Y.; Jessop, J. L. P., Decreased oxygen inhibition in photopolymerized acrylate/epoxide hybrid polymer coatings as demonstrated by Raman spectroscopy. *Polymer* **2006,** *47* (19), 6560-6566.

85.   Crivello, J. V., Hybrid acrylate-oxetane photopolymerizable systems. *J. Polym. Sci., Part A: Polym. Chem.* **2015,** *53* (4), 594-601.

86.   Decker, C.; Nguyen Thi Viet, T.; Decker, D.; Weber-Koehl, E., UV-radiation curing of acrylate/epoxide systems. *Polymer* **2001,** *42* (13), 5531-5541.

87.   Steinmann, B. (Meth)acrylates containing urethane groups. US5658712, 1997.

88.   Gorsche, C.; Harikrishna, R.; Baudis, S.; Knaack, P.; Husar, B.; Laeuger, J.; Hoffmann, H.; Liska, R., Real Time-NIR/MIR-Photorheology: A Versatile Tool for the in Situ Characterization of Photopolymerization Reactions. *Anal. Chem.* **2017,** *89* (9), 4958-4968.

89.   Shi, S.; Croutxé-Barghorn, C.; Allonas, X., Photoinitiating systems for cationic photopolymerization: Ongoing push toward long wavelengths and low light intensities. *Prog. Polym. Sci.* **2017,** *65*, 1-41.

90.   Dadashi-Silab, S.; Doran, S.; Yagci, Y., Photoinduced Electron Transfer Reactions for Macromolecular Syntheses. *Chemical Reviews* **2016,** *116* (17), 10212-10275.

91.   Crivello, J. V.; Lam, J. H. W., Dye-sensitized photoinitiated cationic polymerization. The system: Perylene–triarylsulfonium salts. *J. Polym. Sci., Polym. Chem. Ed.* **1979,** *17* (4), 1059-1065.

92.   Crivello, J.; Jang, M., Anthracene electron-transfer photosensitizers for onium salt induced cationic photopolymerizations. *J. Photochem. Photobiol. A: Chem.* **2003,** *159*, 173-188.

93.   Abdul-Rasoul, F. A. M.; Ledwith, A.; Yaḡci, Y., Photochemical and thermal cationic polymerizations promoted by free radical initiators. *Polymer* **1978,** *19* (10), 1219-1222.

94.   Yagci, Y.; Schnabel, W., Acylphosphine oxides as free radical promoters in cationic polymerizations. *Die Makromolekulare Chemie, Rapid Communications* **1987,** *8* (4), 209-213.

95.   Yagci, Y.; Denizligil, S., Photoinitiated cationic polymerization using o-phthaldehyde and pyridinium salt. *J. Polym. Sci., Part A: Polym. Chem.* **1995,** *33* (9), 1461-1464.

96.   Johnen, N.; Kobayashi, S.; Yagci, Y.; Schnabel, W., Substituted vinyl bromides as photoinitiators for cationic polymerizations. *Polym. Bull.* **1993,** *30* (3), 279-284.

97.   Yagci, Y.; Kminek, I.; Schnabel, W., Photochemical cationic polymerization of cyclohexene oxide in solution containing pyridinium salt and polysilane. *Eur. Polym. J.* **1992,** *28* (4), 387-390.

98.   Yagci, Y.; Schnabel, W., New aspects on the photoinitiated free radical promoted cationic polymerization. *Makromolekulare Chemie. Macromolecular Symposia* **1992,** *60* (1), 133-143.

99.   Yagci, Y.; Borbely, J.; Schnabel, W., On the mechanism of acylphosphine oxide promoted cationic polymerization. *Eur. Polym. J.* **1989,** *25* (2), 129-131.

100.   Yilmaz, G.; Beyazit, S.; Yagci, Y., Visible light induced free radical promoted cationic polymerization using thioxanthone derivatives. *J. Polym. Sci., Part A: Polym. Chem.* **2011,** *49* (7), 1591-1596.

101.   Baumann, H.; Müller, U.; Pfeifer, D.; Timpe, H.-J., Lichtinitiierte Polymer- und Polymerisationsreaktionen. III. Photoinduzierte Zersetzung von Aryldiazoniumsalzen durch Benzoinderivate. *Journal für Praktische Chemie* **1982,** *324* (2), 217-226.

102.   Dursun, C.; Degirmenci, M.; Yagci, Y.; Jockusch, S.; Turro, N. J., Free radical promoted cationic polymerization by using bisacylphosphine oxide photoinitiators: substituent effect on the reactivity of phosphinoyl radicals. *Polymer* **2003,** *44* (24), 7389-7396.

103.   Durmaz, Y. Y.; Moszner, N.; Yagci, Y., Visible Light Initiated Free Radical Promoted Cationic Polymerization Using Acylgermane Based Photoinitiator in the Presence of Onium Salts. *Macromolecules* **2008,** *41* (18), 6714-6718.

104.   Lalevée, J.; Dirani, A.; El-Roz, M.; Allonas, X.; Fouassier, J. P., Germanes as efficient coinitiators in radical and cationic photopolymerizations. *J. Polym. Sci., Part A: Polym. Chem.* **2008,** *46* (9), 3042-3047.

105.   Eibel, A.; Radebner, J.; Haas, M.; Fast, D. E.; Freißmuth, H.; Stadler, E.; Faschauner, P.; Torvisco, A.; Lamparth, I.; Moszner, N.; Stueger, H.; Gescheidt, G., From mono- to

tetraacylgermanes: extending the scope of visible light photoinitiators. *Polym. Chem.* **2018,** *9* (1), 38-47.

106.   Bassiri, T. G.; Levy, A.; Litt, M., Polymerization of cyclic imino ethers. I. Oxazolines. *Journal of Polymer Science Part B: Polymer Letters* **1967,** *5* (9), 871-879.

107.   Tomalia, D. A.; Sheetz, D. P., Homopolymerization of 2-alkyl- and 2-aryl-2-oxazolines. *Journal of Polymer Science Part A-1: Polymer Chemistry* **1966,** *4* (9), 2253-2265.

108.   Kagiya, T.; Narisawa, S.; Maeda, T.; Fukui, K., Ring-opening polymerization of 2-substituted 2-oxazolines. *Journal of Polymer Science Part B: Polymer Letters* **1966,** *4* (7), 441-445.

109.   Kobayashi, S.; Uyama, H., Polymerization of cyclic imino ethers: From its discovery to the present state of the art. *J. Polym. Sci., Part A: Polym. Chem.* **2002,** *40* (2), 192-209.

110.   Aoi, K.; Okada, M., Polymerization of oxazolines. *Prog. Polym. Sci.* **1996,** *21* (1), 151-208.

111.   Hoogenboom, R., Poly(2-oxazoline)s: A Polymer Class with Numerous Potential Applications. *Angew. Chem. Int. Ed.* **2009,** *48* (43), 7978-7994.

112.   Hoogenboom, R., Poly(2-oxazoline)s: Alive and Kicking. *Macromolecular Chemistry and Physics* **2007,** *208* (1), 18-25.

113.   Adams, N.; Schubert, U. S., Poly(2-oxazolines) in biological and biomedical application contexts. *Adv. Drug Del. Rev.* **2007,** *59* (15), 1504-1520.

114.   Kobayashi, S.; Igarashi, T.; Moriuchi, Y.; Saegusa, T., Block copolymers from cyclic imino ethers: a new class of nonionic polymer surfactant. *Macromolecules* **1986,** *19* (3), 535-541.

115.   Persigehl, P.; Jordan, R.; Nuyken, O., Functionalization of Amphiphilic Poly(2-oxazoline) Block Copolymers: A Novel Class of Macroligands for Micellar Catalysis. *Macromolecules* **2000,** *33* (19), 6977-6981.

116.   Litt, M.; Chen, T.-T.; Hsieh, B. R., Low surface energy polymers and surface active block polymers. I. t-butylphenyl containing polymers. *J. Polym. Sci., Part A: Polym. Chem.* **1986,** *24* (12), 3407-3422.

117.   Shoda, S.-I.; Masuda, E.; Furukawa, M.; Kobayashi, S., Synthesis and surfactant property of copolymers having a poly(2-oxazoline) graft chain. *J. Polym. Sci., Part A: Polym. Chem.* **1992,** *30* (7), 1489-1494.

118.   Wiesbrock, F.; Hoogenboom, R.; Abeln, C. H.; Schubert, U. S., Single-Mode Microwave Ovens as New Reaction Devices: Accelerating the Living Polymerization of 2-Ethyl-2-Oxazoline. *Macromol. Rapid Commun.* **2004,** *25* (22), 1895-1899.

119.   de la Rosa, V. R., Poly(2-oxazoline)s as materials for biomedical applications. *J. Mater. Sci. Mater. Med.* **2014,** *25* (5), 1211-1225.

120.   Luxenhofer, R.; Han, Y.; Schulz, A.; Tong, J.; He, Z.; Kabanov, A. V.; Jordan, R., Poly(2-oxazoline)s as Polymer Therapeutics. *Macromol. Rapid Commun.* **2012,** *33* (19), 1613-1631.

121.   Sedlacek, O.; Monnery, B. D.; Filippov, S. K.; Hoogenboom, R.; Hruby, M., Poly(2-Oxazoline)s – Are They More Advantageous for Biomedical Applications Than Other Polymers? *Macromol. Rapid Commun.* **2012,** *33* (19), 1648-1662.

122.   Woodle, M. C.; Engbers, C. M.; Zalipsky, S., New Amphipatic Polymer-Lipid Conjugates Forming Long-Circulating Reticuloendothelial System-Evading Liposomes. *Bioconjugate Chemistry* **1994,** *5* (6), 493-496.

123.   Zalipsky, S.; Hansen, C. B.; Oaks, J. M.; Allen, T. M., Evaluation of blood clearance rates and biodistribution of poly(2-oxazoline)-grafted liposomes. *J. Pharm. Sci.* **1996,** *85* (2), 133-137.

124.   Konradi, R.; Acikgoz, C.; Textor, M., Polyoxazolines for Nonfouling Surface Coatings — A Direct Comparison to the Gold Standard PEG. *Macromol. Rapid Commun.* **2012,** *33* (19), 1663-1676.

125.   Mero, A.; Pasut, G.; Via, L. D.; Fijten, M. W. M.; Schubert, U. S.; Hoogenboom, R.; Veronese, F. M., Synthesis and characterization of poly(2-ethyl 2-oxazoline)-conjugates with proteins and drugs: Suitable alternatives to PEG-conjugates? *Journal of Controlled Release* **2008,** *125* (2), 87-95.

126.   Knop, K.; Hoogenboom, R.; Fischer, D.; Schubert, U. S., Poly(ethylene glycol) in Drug Delivery: Pros and Cons as Well as Potential Alternatives. *Angew. Chem. Int. Ed.* **2010,** *49* (36), 6288-6308.

127.   Barz, M.; Luxenhofer, R.; Zentel, R.; Vicent, M. J., Overcoming the PEG-addiction: well-defined alternatives to PEG, from structure–property relationships to better defined therapeutics. *Polym. Chem.* **2011,** *2* (9), 1900-1918.

128.   Steinhauser, N.; Mülhaupt, R., Preparation, cure behavior and properties of bis(2-oxazoline)s containing well-defined oligo(tetrafluoroethylene) segments. *Macromol. Rapid Commun.* **1994,** *15* (4), 365-372.

129.   Wiesbrock, F.; Hoogenboom, R.; Leenen, M.; van Nispen, S. F. G. M.; van der Loop, M.; Abeln, C. H.; van den Berg, A. M. J.; Schubert, U. S., Microwave-Assisted Synthesis of a 42-Membered Library of Diblock Copoly(2-oxazoline)s and Chain-Extended Homo Poly(2-oxazoline)s and Their Thermal Characterization. *Macromolecules* **2005,** *38* (19), 7957-7966.

130.   Jerca, V. V.; Lava, K.; Verbraeken, B.; Hoogenboom, R., Poly(2-cycloalkyl-2-oxazoline)s: high melting temperature polymers solely based on Debye and Keesom van der Waals interactions. *Polym. Chem.* **2016,** *7* (6), 1309-1322.

131.   Glassner, M.; Vergaelen, M.; Hoogenboom, R., Poly(2-oxazoline)s: A comprehensive overview of polymer structures and their physical properties. *Polym. Int.* **2018,** *67* (1), 32-45.

132.   Luef, K. P.; Hoogenboom, R.; Schubert, U. S.; Wiesbrock, F., Microwave-Assisted Cationic Ring-Opening Polymerization of 2-Oxazolines. In *Microwave-assisted Polymer Synthesis*, Hoogenboom, R.; Schubert, U. S.; Wiesbrock, F., Eds. Springer International Publishing: Cham, 2016; pp 183-208.

133.   Acetyl Halide Initiator Screening for the Cationic Ring-Opening Polymerization of 2-Ethyl-2-Oxazoline. *Macromolecular Chemistry and Physics* **2008,** *209* (8), 794-800.

134.   Dworak, A., Polymerization of methyl and phenyl oxazoline initiated with carboxylic acid chlorides. *Polym. Bull.* **1997,** *38* (1), 7-13.

135.   Hrkach, J. S.; Matyjaszewski, K., Reaction of 2-methyl-2-oxazoline with trimethylsilyl initiators: an unusual mode of ring opening. *Macromolecules* **1992,** *25* (8), 2070-2075.

136.   Jerca, V. V.; Nicolescu, F. A.; Vasilescu, D. S.; Vuluga, D. M., Synthesis of a new oxazoline macromonomer for dispersion polymerization. *Polym. Bull.* **2011,** *66* (6), 785-796.

137.   Dworak, A.; Schulz, R. C., Star polymers and block copolymers of 2-oxazolines using chloroformates as initiators. *Die Makromolekulare Chemie* **1991,** *192* (2), 437-445.

138.   Guillerm, B.; Monge, S.; Lapinte, V.; Robin, J.-J., Novel Investigations on Kinetics and Polymerization Mechanism of Oxazolines Initiated by Iodine. *Macromolecules* **2010,** *43* (14), 5964-5970.

139.   W., S.; E., A.; W., D.; R., F.; R., N.; W., T.; H., H., Neuere Synthesen und Reaktionen cyclischer Imidsäureester. *Angew. Chem.* **1966,** *78* (20), 913-927.

140.   Correia, V. G.; Bonifácio, V. D. B.; Raje, V. P.; Casimiro, T.; Moutinho, G.; da Silva, C. L.; Pinho, M. G.; Aguiar-Ricardo, A., Oxazoline-Based Antimicrobial Oligomers: Synthesis by CROP Using Supercritical CO2. *Macromol. Biosci.* **2011,** *11* (8), 1128-1137.

141.   Bonifácio, V. D. B.; Correia, V. G.; Pinho, M. G.; Lima, J. C.; Aguiar-Ricardo, A., Blue emission of carbamic acid oligooxazoline biotags. *Mater. Lett.* **2012,** *81*, 205-208.

142.   Saegusa, T.; Ikeda, H.; Fujii, H., Isomerization Polymerization of 2-Oxazoline. IV. Kinetic Study of 2-Methyl-2-oxazoline Polymerization. *Macromolecules* **1972,** *5* (4), 359-362.

143.   Müller, P.; Wörner, C.; Mülhaupt, R., 1,3-Oxazoline intermediates in reactive processing applications, 2.multiphase polymer blends via in-situ cationic melt phase polymerization of 2-phenyl-1,3-oxazoline. *Macromolecular Chemistry and Physics* **1995,** *196* (6), 1929-1936.

144.   Hoogenboom, R.; Fijten, M. W. M.; Schubert, U. S., Parallel Kinetic Investigation of 2-Oxazoline Polymerizations with Different Initiators as Basis for Designed Copolymer Synthesis. *Journal of Polymer Science, Part A: Polymer Chemistry* **2004,** *42* (8), 1830-1840.

145.   Verbraeken, B.; Monnery, B. D.; Lava, K.; Hoogenboom, R., The chemistry of poly(2-oxazoline)s. *Eur. Polym. J.* **2017,** *88*, 451-469.

146.   Glassner, M.; D'hooge, D. R.; Young Park, J.; Van Steenberge, P. H. M.; Monnery, B. D.; Reyniers, M.-F.; Hoogenboom, R., Systematic investigation of alkyl sulfonate initiators for the cationic ring-opening polymerization of 2-oxazolines revealing optimal combinations of monomers and initiators. *Eur. Polym. J.* **2015,** *65*, 298-304.

147.   Dworak, A., The role of cationic and covalent active centers in the polymerization of 2-methyl-2-oxazoline initiated with benzyl bromide. *Macromolecular Chemistry and Physics* **1998,** *199* (9), 1843-1849.

148.   Kobayashi, S.; Tokuzawa, T.; Saegusa, T., Cationic ring-opening isomerization polymerization of 2-[p-(substituted)phenyl]-2-oxazolines. Effects of the substituent on the reactivities. *Macromolecules* **1982,** *15* (3), 707-710.

149.   Miyamoto, M.; Aoi, K.; Saegusa, T., Mechanisms of ring-opening polymerization of 2-(perfluoroalkyl)-2-oxazolines initiated by sulfonates: a novel covalent-type electrophilic polymerization. *Macromolecules* **1988,** *21* (6), 1880-1883.

150.   Hoogenboom, R.; Fijten, M. W. M.; Thijs, H. M. L.; van Lankvelt, B. M.; Schubert, U. S., Microwave-assisted synthesis and properties of a series of poly(2-alkyl-2-oxazoline)s. *Des. Monomers Polym.* **2005,** *8* (6), 659-671.

151.   Lobert, M.; Thijs, H. M. L.; Erdmenger, T.; Eckardt, R.; Ulbricht, C.; Hoogenboom, R.; Schubert, U. S., Synthesis, Microwave-Assisted Polymerization, and Polymer Properties of Fluorinated 2-Phenyl-2-oxazolines: A Systematic Study. *Chemistry – A European Journal* **2008,** *14* (33), 10396-10407.

152.   Lobert, M.; Kohn, U.; Hoogenboom, R.; Schubert, U. S., Synthesis and microwave assisted polymerization of fluorinated 2-phenyl-2-oxazolines: the fastest 2-oxazoline monomer to date. *Chem. Commun.* **2008,** (12), 1458-1460.

153.   Hoogenboom, R.; Leenen, M. A. M.; Wiesbrock, F.; Schubert, U. S., Microwave Accelerated Polymerization of 2-Phenyl-2-oxazoline: Microwave or Temperature Effects? *Macromol. Rapid Commun.* **2005,** *26* (22), 1773-1778.

154.   Vergaelen, M.; Verbraeken, B.; Monnery, B. D.; Hoogenboom, R., Sulfolane as Common Rate Accelerating Solvent for the Cationic Ring-Opening Polymerization of 2-Oxazolines. *ACS Macro Letters* **2015,** *4* (8), 825-828.

155.   Tauhardt, L.; Kempe, K.; Knop, K.; Altuntaş, E.; Jäger, M.; Schubert, S.; Fischer, D.; Schubert, U. S., Linear Polyethyleneimine: Optimized Synthesis and Characterization – On the Way to "Pharmagrade" Batches. *Macromolecular Chemistry and Physics* **2011,** *212* (17), 1918-1924.

156.   Kempe, K.; Lobert, M.; Hoogenboom, R.; Schubert, U. S., Synthesis and characterization of a series of diverse poly(2-oxazoline)s. *J. Polym. Sci., Part A: Polym. Chem.* **2009,** *47* (15), 3829-3838.

157.   Wu, W.; Cui, S.; Li, Z.; Liu, J.; Wang, H.; Wang, X.; Zhang, Q.; Wu, H.; Guo, K., Mild Bronsted acid initiated controlled polymerizations of 2-oxazoline towards one-pot synthesis of novel double-hydrophilic poly(2-ethyl-2-oxazoline)-block-poly(sarcosine). *Polym. Chem.* **2015,** *6* (15), 2970-2976.

158.   Shiro, K.; Hidenori, D.; Takeo, S., Kinetic Studies on the Cationic Ring-Opening Polymerization of Tetrahydrofuran Initiated by Superacid Esters. *Bull. Chem. Soc. Jpn.* **1973,** *46* (10), 3214-3220.

159.   Rudolph, T.; Kempe, K.; Crotty, S.; Paulus, R. M.; Schubert, U. S.; Krossing, I.; Schacher, F. H., A strong cationic Bronsted acid, [H(OEt2)2][Al{OC(CF3)3}4], as an efficient initiator for the cationic ring-opening polymerization of 2-alkyl-2-oxazolines. *Polym. Chem.* **2013,** *4* (3), 495-505.

160.   Hoogenboom, R.; Fijten, M. W. M.; Schubert, U. S., The Effect of Temperature on the Living Cationic Polymerization of 2-Phenyl-2-oxazoline Explored Utilizing an Automated Synthesizer. *Macromol. Rapid Commun.* **2004,** *25* (1), 339-343.

161.   Wiesbrock, F.; Hoogenboom, R.; Leenen, M. A. M.; Meier, M. A. R.; Schubert, U. S., Investigation of the Living Cationic Ring-Opening Polymerization of 2-Methyl-, 2-Ethyl-, 2-Nonyl-, and 2-Phenyl-2-oxazoline in a Single-Mode Microwave Reactor. *Macromolecules* **2005,** *38* (12), 5025-5034.

162.   Beck, M.; Birnbrich, P.; Eicken, U.; Fischer, H.; Fristad, W. E.; Hase, B.; Krause, H. J., Polyoxazoline auf fettchemischer Basis. *Die Angewandte Makromolekulare Chemie* **1994,** *223* (1), 217-233.

163.   Kempe, K.; Lobert, M.; Hoogenboom, R.; Schubert, U. S., Screening the Synthesis of 2-Substituted-2-oxazolines. *J. Comb. Chem.* **2009,** *11* (2), 274-280.

164.   Witte, H.; Seeliger, W., Cyclische Imidsäureester aus Nitrilen und Aminoalkoholen. *Justus Liebigs Ann. Chem.* **1974,** *1974* (6), 996-1009.

165.   <US2001020050A1.pdf>.

166.   <EP0970945A1.pdf>.

167.   Crivello, J. V., Cationic photopolymerization of alkyl glycidyl ethers. *J. Polym. Sci., Part A: Polym. Chem.* **2006,** *44* (9), 3036-3052.

168.   Shijian, L.; Wong, C. P. In *Thermo-mechanical properties of epoxy formulations with low glass transition temperatures*, 2002 Proceedings. 8th International Advanced Packaging Materials Symposium (Cat. No.02TH8617), 3-6 March 2002; 2002; pp 226-231.

169.   Höfer, M., *Components for visible curable formulations with low oxygen inhibition. Ph.D. thesis.* Institut für Angewandte Synthesechemie, Technische Universität Wien, Hötzendorfstraße 9, 2231 Strasshof, 2009.

170.   https://www.excelitas.com/product/omnicure-lx500-led-uv-max-heads. (accessed 04/02/2020).